

NASA
Technical
Paper
2785

February 1988

Shock Structure and Noise of Supersonic Jets in Simulated Flight to Mach 0.4

Thomas D. Norum
and John G. Shearin

NASA

**NASA
Technical
Paper
2785**

1988

Shock Structure and Noise of Supersonic Jets in Simulated Flight to Mach 0.4

Thomas D. Norum
and John G. Shearin

*Langley Research Center
Hampton, Virginia*

NASA

National Aeronautics
and Space Administration

Scientific and Technical
Information Division

Abstract

Measured jet plume static pressure distributions and far-field acoustic spectra are presented for under-expanded jets in simulated flight up to a Mach number of 0.4. A gradual stretching of the downstream shock cells is found as the Mach number increases, with no perceptible change in the shock strength. There appears to be little effect of flight on the amplitude of the broadband shock noise, and the small changes in its peak frequency for the same emission angle are correlated with the slightly longer shock cells in flight. The larger changes in the broadband peak frequency found at the same angle in wind-tunnel coordinates are attributable to convection. Jet mixing noise production decreases significantly with increasing flight speed.

Introduction

The noise generated by supersonic jets containing shock cells has been of interest for some time. The development of the Concorde and research conducted on other supersonic cruise aircraft led to concerns for the effect of this noise on communities near airports. The increase in the power of military engines has resulted in higher dynamic loads on aircraft structures because of this noise. An additional current interest for the application of supersonic jet noise data is the detection of military aircraft from their noise signatures.

In addition to the noise created by the mixing of any turbulent jet, shocks in the jet plume result in two additional well-known noise sources. The first of these is jet screech, which consists of discrete tones and their harmonics. Screech was first investigated by Powell (ref. 1), who proposed a model based on a feedback mechanism between the nozzle exit and the shocks. Subsequent research has shown this model to be essentially correct, although some of the details of the interaction processes are still unknown. The other shock-associated noise component is called broadband shock noise because of the wide frequency range it encompasses. It was first studied in detail by Harper-Bourne and Fisher (ref. 2), who proposed a turbulence-shock interaction model similar to that proposed by Powell for the screech process. The apparent nonstationary nature of the source of broadband shock noise, indicated by its frequency changes with observation angle, was accounted for by phase differences between the noise emitted at different shocks. A different model of the broadband shock noise process, consisting of the interaction of the large-scale jet structures with the shock cell system, has been proposed by Tam and Tanna (ref. 3) and extended to flight conditions by Tam (ref. 4).

Previous studies using a scale-model nozzle and a free jet to investigate flight effects on supersonic jet noise were performed by Bryce and Pinker (ref. 5) and by Yamamoto et al. (ref. 6). In the current study, the objective was to relate changes in the radiated sound field of an underexpanded jet in simulated flight to changes in the mean flow field. Some of the data generated in this investigation have been analyzed previously and the results reported in references 7 and 8.

The change in screech frequency with forward speed has been predicted by extending Powell's theory to flight (ref. 7). The amplitude and directivity of screech were seen to be essentially unchanged by flight so as to maintain the necessary feedback cycle (ref. 8). The main effect of flight on screech is a change in the dominant screech mode as flight speed increases (ref. 7) and the introduction of screech modes not present in the static condition (ref. 8).

In reference 7 the change to the peak frequency of broadband shock noise in flight could not be predicted from the model of Harper-Bourne and Fisher (ref. 2). Application of Tam's model (ref. 4) at higher flight speeds in reference 8 showed good agreement between measurement and prediction of this peak frequency. Very little change to the amplitude of the broadband noise was found with increasing flight speed (ref. 8).

The purpose of the current report is to present the detailed measured far-field noise spectra and plume static pressure distributions and to supplement and refine the analyses presented in references 7 and 8.

Symbols

a	ambient speed of sound
c	position for correction to ray angle
d	nozzle diameter, 1 in.
e	position for correction to phase angle
L	average shock cell length
L_0	average shock cell length at static condition
m	microphone position
M	simulated flight free jet Mach number, u/c
M_j	Mach number for fully expanded jet
n	number of shock cells

p	static pressure in jet plume
p_a	ambient static pressure
p_t	total pressure
SPL	sound pressure level
u	free jet velocity
x	axial distance from nozzle exit
β	shock noise parameter related to jet total pressure
λ	broadband shock noise peak wavelength
λ_0	broadband shock noise peak wavelength at static condition
ψ	far-field microphone angle measured from upstream direction
ψ_c	convected, or ray, angle
ψ_e	emission, or phase, angle

Experimental Details

Detailed mean static pressure measurements along the centerline of a supersonic jet and far-field acoustic measurements of the noise produced by the jet were made over a wide range of nozzle pressure ratios, from the static condition up to a simulated flight Mach number of 0.4. The experiment was performed in the Quiet Flow Facility in the Langley Aircraft Noise Reduction Laboratory. This anechoic chamber is approximately 20 ft by 24 ft by 30 ft and is lined with acoustic wedges to provide a cutoff frequency of 70 Hz. The experiment was conducted in two phases. The first phase used a low-pressure fan to provide the free jet. Its Mach number was limited to 0.15, and it exhausted vertically. The orientation was changed to horizontal and a centrifugal compressor was used in the second phase; this allowed an increase in the free jet Mach number to 0.4. The free jet exhausted from an 18-in.-diameter nozzle.

The same high-pressure air supply system was used in both phases to supply the supersonic jet. This jet exhausted from a contoured convergent nozzle of 1 in. exit diameter. The nozzle exit was located 14 in. downstream from the exit of the coaxial 18-in.-diameter nozzle. This configuration provided an unobstructed line of sight between the small nozzle exit and the measurement microphones. Twelve quarter-inch microphones were located on an arc of 72-in. radius centered on the axis of the nozzles and 4 in. downstream of the exit of the small nozzle. A photograph of the nozzle installed for the first

phase tests is shown in figure 1, and a sketch showing the relevant dimensions during the acoustic tests is given in figure 2. The plume static pressure measurements were performed with the floor wedges removed and a three-dimensional traverse installed. Details of the supersonic static pressure probe can be found in reference 9.

The operating condition of the small jet is represented by the shock parameter β , originally introduced by Harper-Bourne and Fisher (ref. 2) to correlate broadband shock noise. This parameter is related to the fully expanded jet Mach number M_j and nozzle pressure ratio by

$$\beta^2 = M_j^2 - 1 = 5(p_t/p_a)^{2/7} - 6$$

Results are given herein for β varying from 0.4 to 1.7, corresponding to fully expanded jet Mach numbers from 1.08 to 1.97 and nozzle pressure ratios from 2.1 to 7.5.

The total pressures of both streams were continuously monitored during the experiments. The free jet was very stable, having total pressure fluctuations less than $\pm 0.1\%$ of the set pressure. No account is taken in this report for entrainment effects that result in an effective external stream for the nominal $M = 0$ condition, or for the boundary-layer buildup that reduces the effective external velocity near the supersonic jet nozzle exit (see ref. 8). The supply pressure of the supersonic jet was less stable than the free jet pressure, giving cyclic variations during a run. The variations were generally within $\pm 1.0\%$, although sometimes they were as high as $\pm 1.8\%$ of the set pressure.

Plume Static Pressure Measurements

A depiction of the shock cell structure within the supersonic plume was obtained through measurements of static pressure along the jet centerline. The results of these measurements for β ranging from 0.6 to 1.7 at selected free jet Mach numbers are given in appendix A. Shown is the ratio of static pressure to ambient pressure versus the distance from the exit of the small nozzle. The probe was traversed in increments of $0.05d$ during the first phase tests and $0.1d$ during the second phase. Although not shown, the repeatability between repeat runs and between the two phases was excellent for all cases in which a smooth pressure distribution was obtained. The uneven distributions obtained at β less than 0.9 are due to the aforementioned variations in total pressure. Discontinuities occur at $\beta = 1.1$ and 1.2 and are likely due to changes in the dominant screech mode of the jet, as documented in reference 7. The

smoothness of the distributions at $\beta = 0.9$ and higher permits an average shock cell spacing to be obtained. This cell length is defined as the distance between the first and the last (or perhaps the next to last) peak in the static pressure distributions divided by the number of shock cells in between. The non-dimensionalized average shock cell length is given versus the free jet Mach number in figure 3, where n is the number of shock cells over which the average was computed and is chosen to be constant for a given value of β . There is an increase in cell length with forward speed that is more predominant at the higher β values. This increase is mainly due to a stretching of the downstream shock cells with increasing free-stream velocity.

The strength of the shocks within the jet plume is represented by the difference between the maximum and minimum static pressures within a shock cell. Comparison of the static pressure distributions at a given β in appendix A shows that, except for changes in the downstream shock cells that may be associated with screech mode changes, no effect of Mach number on shock strength is discernible. This was shown quantitatively up to a Mach number of 0.15 in reference 7.

Far-Field Acoustic Measurements

Far-field acoustic measurements were obtained for most operating conditions of $\beta = 0.4$ to 1.6 in steps of 0.1, and $M = 0$ to 0.4 in steps of 0.05. Narrowband sound pressure levels (SPL's) for frequencies between 0.3 kHz and 40 kHz with a bandwidth of 60 Hz are presented in appendix B. For the higher free jet Mach numbers, the spectral data were compared with the background noise (measured for the same external flow with no supersonic jet). A horizontal line is drawn under the portions of each spectrum in appendix B for all frequencies at which the signal-to-noise ratio is less than 6 dB.

After the tests were completed, it was discovered that the digital output of the amplifier on 2 of the 12 microphone systems failed to lock before reading, resulting in an occasional error in the amplitudes recorded for the microphones at the measurement angles $\psi = 40^\circ$ and 70° . Hence, although the frequency distribution and relative amplitudes are correct, the absolute amplitudes at these two angles may not always be accurate.

To study the effects of nozzle pressure ratio and free-stream velocity on only the jet mixing noise and broadband shock noise, all screech tones were digitally removed from each spectrum. The resulting spectrum was then integrated to obtain an overall sound pressure level representative of a combination of jet mixing noise and broadband shock noise. These

screech-removed SPL's are given in figures 4 through 6. Figure 4 shows the variation in the screech-removed SPL versus β for each value of free jet Mach number and the 10 good microphone angles. Since Harper-Bourne and Fisher (ref. 2) have shown that broadband shock noise in the static case is well represented by a β^4 dependence, a line representing this dependence is shown at all angles for $M = 0$. At the upstream angles where broadband shock noise dominates, the data follow the line up to a β of about 1.2. At higher nozzle pressure ratios the broadband shock noise no longer increases, corresponding to the growth of a Mach disc that reduces the strengths of the downstream shocks (see ref. 7).

The screech-removed SPL's were replotted in figure 5 versus measurement angle. The most striking conclusion drawn from figure 5 is the relative constancy of the SPL up to an angle of at least 120° . Since the spectra are dominated by broadband shock noise in all but the downstream directions, we conclude that the omnidirectionality of broadband shock noise known to exist at the static condition (see ref. 2) also exists in flight to at least $M = 0.4$.

The effects of flight Mach number on the overall SPL can best be seen in figure 6. Here the screech-removed SPL's are plotted versus M for a given β and measurement angle. At the furthestmost downstream angle, where the spectra are dominated by jet mixing noise, a consistent reduction in SPL with increasing flight speed is obvious. It was shown in reference 7 that up to at least $M = 0.15$ the reduction of jet mixing noise with increasing Mach number was very similar to that obtained for a subsonic jet. It appears from spectral comparisons in appendix B that this conclusion can be extended to higher Mach numbers. A quantitative demonstration of this is not possible, however, since even at this most downstream location broadband shock noise dominates a good portion of the spectra at higher flight Mach numbers. This dominance of the spectra by shock noise is due to the large reductions in mixing noise with increasing Mach number. It can be seen in appendix B near 20 kHz as an increasing spectral level with increasing frequency for most β at $\psi = 150^\circ$ and $M = 0.4$.

Figure 6 shows that the decrease in SPL with increasing Mach number occurs at all angles, although less so at the upstream angles. Since it is well known that broadband shock noise dominates the SPL in the upstream direction, we can conclude that the measured broadband shock noise decreases with increasing M . It must be remembered, however, that the measurements were obtained after the emitted noise was propagated through, and hence refracted by, the mixing layer of the 18-in. jet that was simulating the forward motion. If it is desirable to adjust these data

to equivalent wind-tunnel conditions, shear-layer refraction corrections as large as 3 dB in amplitude and 35° in angle would be applied at $M = 0.4$. Smaller corrections would be required if we desire instead to investigate the effects of simulated motion on the output of the acoustic source. A comparison with actual flight would require the usual Doppler corrections to frequency, as well as an additional amplitude correction to account for actual motion between source and observer.

Since the corrections to be applied to the data depend on the application, a review of the angles involved in the shear-layer refraction phenomenon is appropriate. A schematic depicting this phenomenon is given in figure 7. The sound emitted by the supersonic jet at an emission angle ψ_e is convected at the velocity u of the free jet so that its ray angle becomes ψ_c . Upon passing through the shear layer of the free jet (which for computational purposes can be successfully replaced by a vortex sheet), the sound ray is refracted in the upstream direction and is finally sensed on the far-field arc by the microphone at point m . If we wish to compare with the wind-tunnel condition (i.e., source and observer stationary with respect to each other but moving with velocity u with respect to the ground), the measured results at point m should be corrected to point c (i.e., constant ray angle), whereas if we wish to determine the effects of motion on the source emission characteristics only (i.e., the wind-tunnel condition minus the effects of convection by the external stream), corrections should be made to point e (i.e., constant emission angle).

In reference 7 no shear-layer refraction corrections were made because the free-stream Mach number was limited to 0.15, where the corrections are relatively small. If refraction effects had been applied to the analysis of the broadband noise, the wavelengths at right angles to the jet would have been slightly larger than reported. This reinforces the conclusion of reference 7 that predictions derived from a simple extension of the theory of Harper-Bourne and Fisher (ref. 2) to flight yield the incorrect direction of frequency change at the peak of the broadband shock noise spectrum. In reference 8 refraction corrections were applied to simulate the wind-tunnel condition (i.e., the data were corrected to point c in fig. 7). These corrections have been shown in reference 10 to be very accurate at the frequencies and free jet velocities of interest. It was concluded in reference 8 that there are no apparent changes in the amplitude of the broadband shock noise as the Mach number is increased to 0.4. The change with Mach number in the frequency of the peak of the broadband shock

noise spectrum was found to be predicted quite well by the theory of Tam (ref. 4).

The preceding conclusions regarding the broadband shock noise refer to the wind-tunnel condition, which includes changes due to convection as well as changes to the source emission. To isolate the effects of simulated motion on the acoustic source itself, the data should be corrected to constant emission angle (point e in fig. 7). The differences in the angle correction to be applied in the two correction schemes can be seen in figure 8. For the geometry of the experiment, both the ray angle within the free jet ψ_c (corresponding to the wind-tunnel point c) and the phase angle within the jet ψ_e (corresponding to the constant emission angle point e) are shown versus the microphone angle ψ . The ray angle correction increases continuously with Mach number at all microphone angles. The phase angle correction is much less, and is almost insignificant for microphone angles between 60° and 130° . In fact the phase angle is equal to the microphone angle for all Mach numbers at angles of about 70° and 113° (and hence no angle correction need be applied).

The wavelength corresponding to the frequency at the spectral peak of the broadband shock noise at an emission angle of $\psi_e = 90^\circ$ was determined by interpolating the measured frequency of the spectral peak at the three microphones closest to this angle. The result is very close to that obtained at the measurement angle of 90° , since the correction for constant phase angle is small. The variation of this wavelength with Mach number is given in figure 9. At the smaller β there is little change in peak broadband shock noise wavelength with Mach number. A change in the screech mode occurs between $M = 0.10$ and 0.15 that causes the discontinuity in the wavelength variation at $\beta = 1.2$ and has a large effect on the structure of the jet (ref. 7). Other than this, the largest changes with Mach number occur at the higher β , where a consistent increase in the wavelength occurs. This wavelength behavior is very similar to the behavior of the average shock cell spacing given in figure 3. The ratio of each of these lengths to their static value is given versus Mach number at $\beta = 1.4$ in figure 10. The agreement in the behavior of the two lengths indicates that the decreases in the emission frequency at the broadband spectral peak as the Mach number increases are due to the longer paths that the disturbances must travel between neighboring shocks.

There is no effect of refraction on the measurement of the screech frequency, since the acoustic sources of screech are stationary with respect to the nozzle exit. It was shown in reference 7 that except for the frequency jumps that occur with mode

changes the behavior of the screech frequency with changing Mach number is predicted well by an extension of Powell's theory of screech (ref. 1) to flight. In reference 8 it was shown that the directivity of the second harmonic of screech peaks at close to 90° to the jet axis in wind-tunnel coordinates for all external Mach numbers. This implies that the screech parameters are adjusted as the Mach number increases so that the fundamental screech tone remains directed towards the nozzle exit and the feedback loop is sustained.

Concluding Remarks

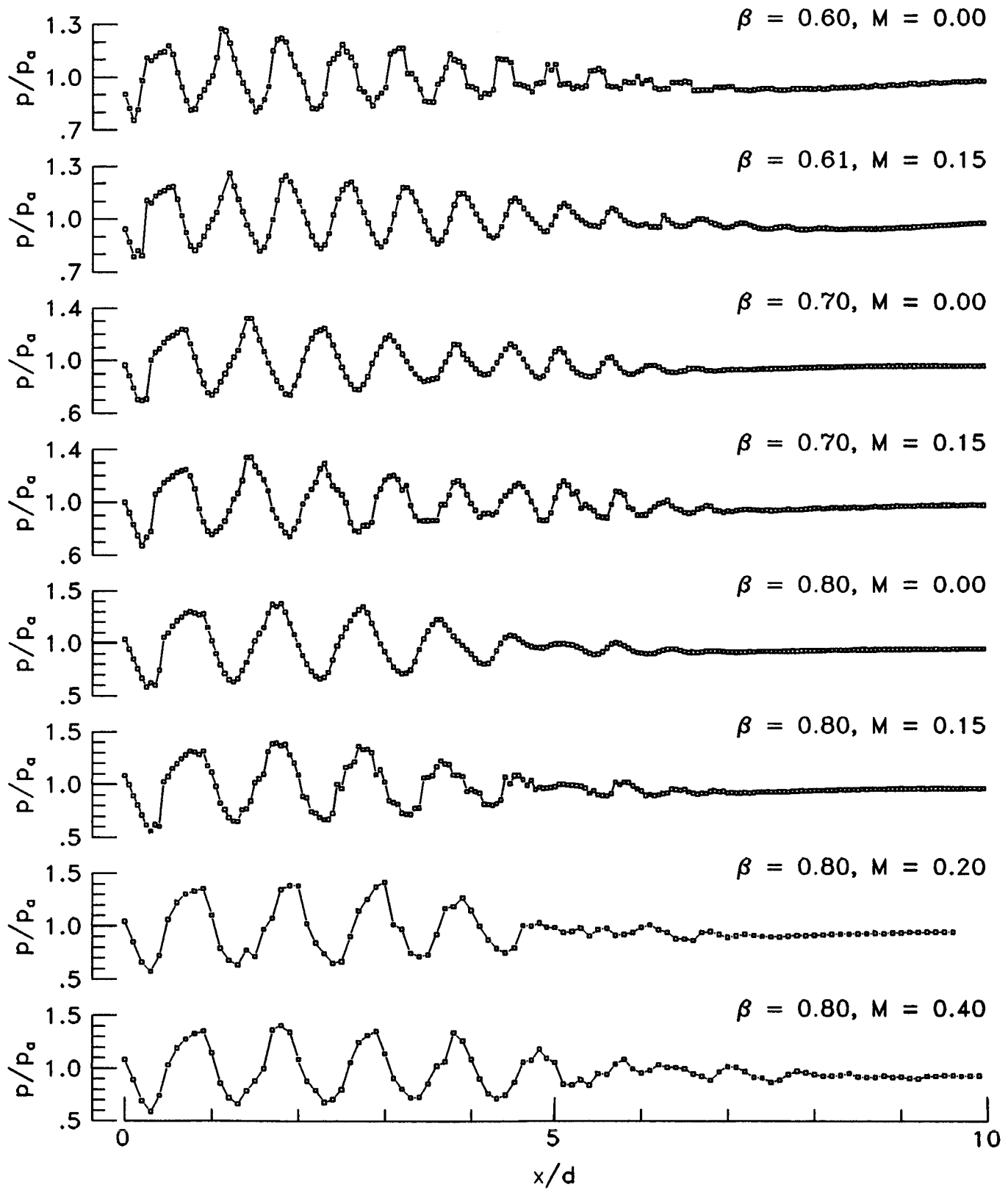
Detailed plume static pressure distributions and far-field acoustic spectra have been presented for underexpanded jets in simulated flight. There is a gradual stretching of the downstream shock cells with increasing flight Mach number but no

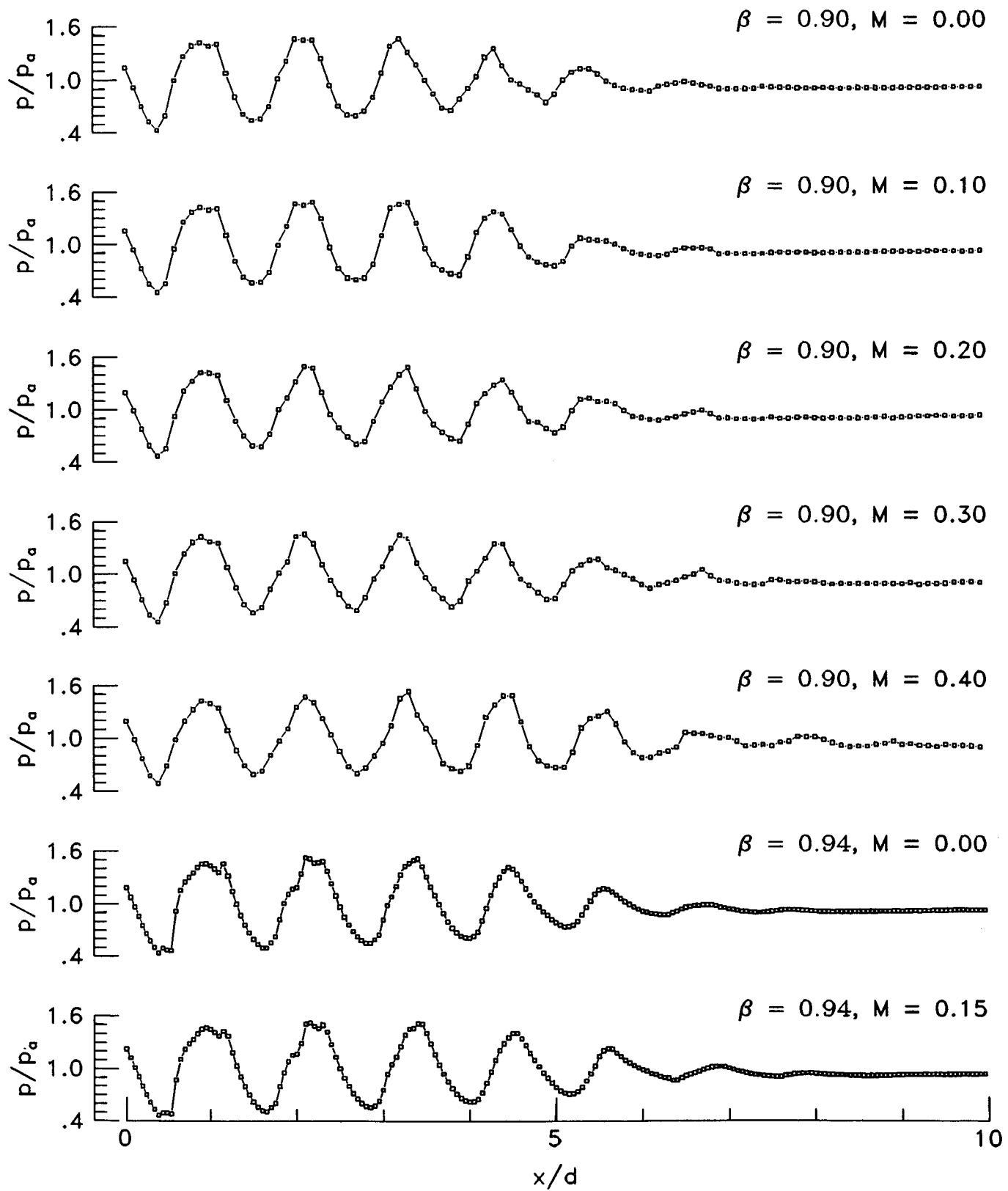
perceptible change in shock strength. The small changes that occur in the peak emission frequency of the broadband shock noise with simulated flight correlate with changes in the shock cell spacing. The larger changes that occur when the data are transformed to wind-tunnel coordinates are attributable to convection effects. Amplitude changes to the broadband shock noise in flight to Mach 0.4 are found to be insignificant, whereas the jet mixing noise decreases continuously with increasing Mach number.

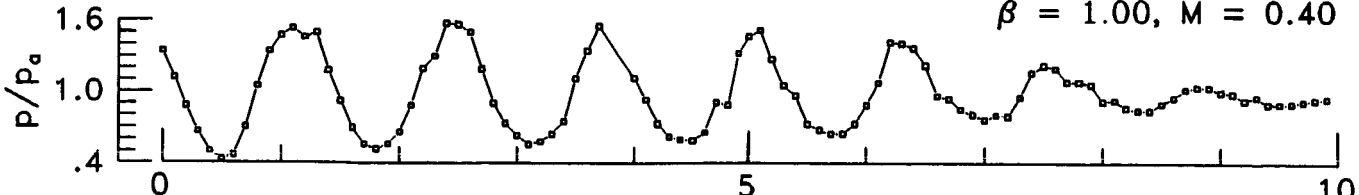
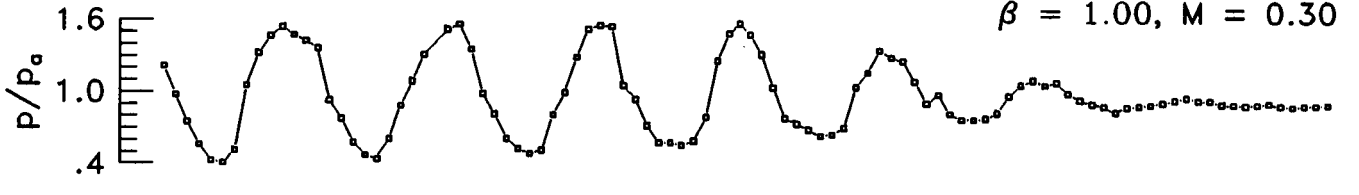
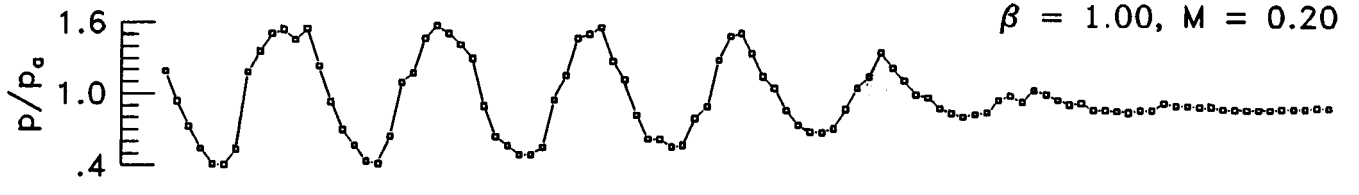
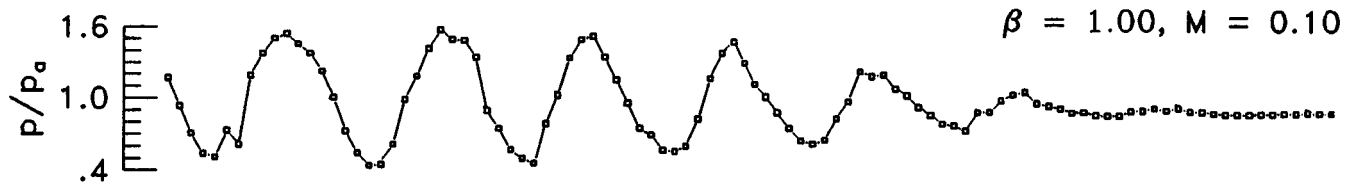
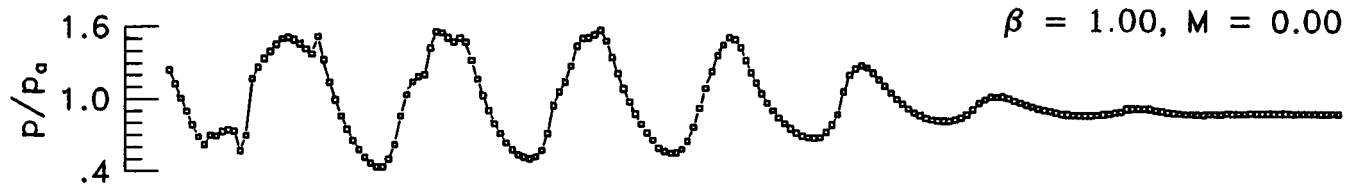
NASA Langley Research Center
Hampton, Virginia 23665-5225
December 10, 1987

Appendix A

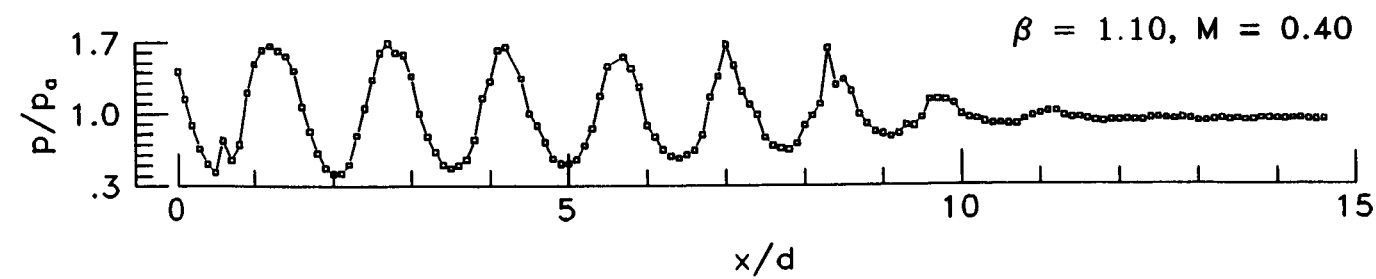
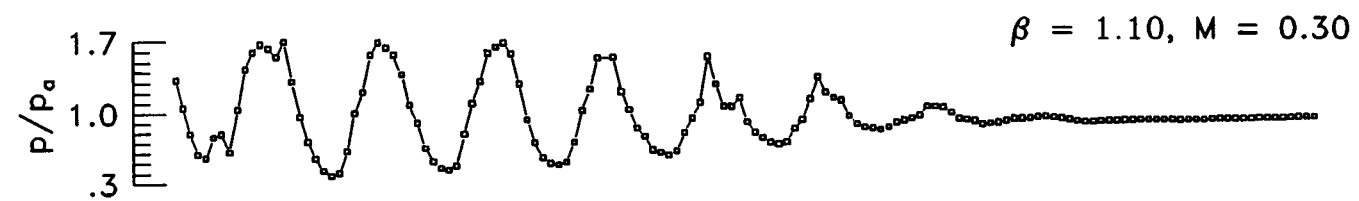
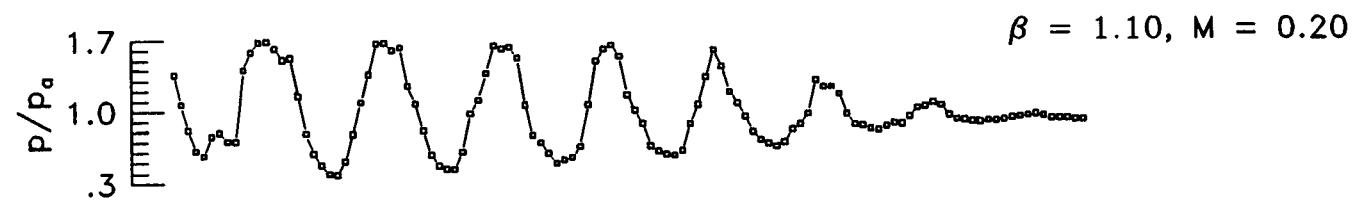
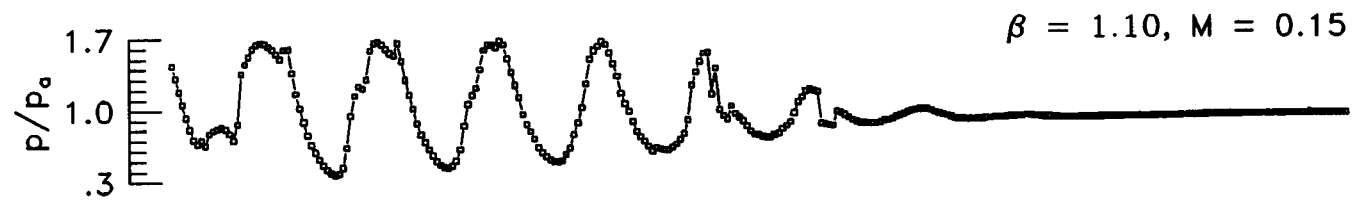
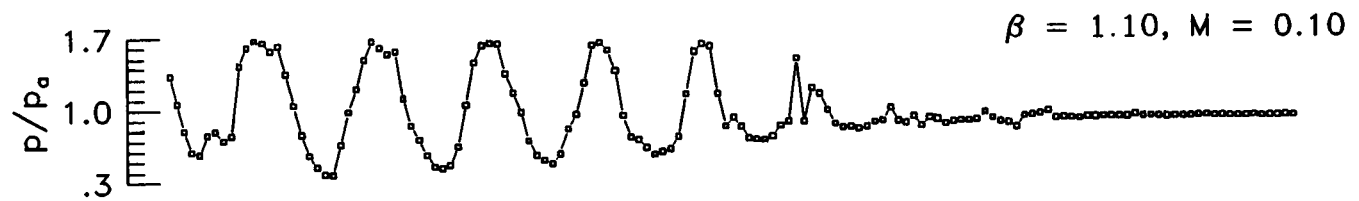
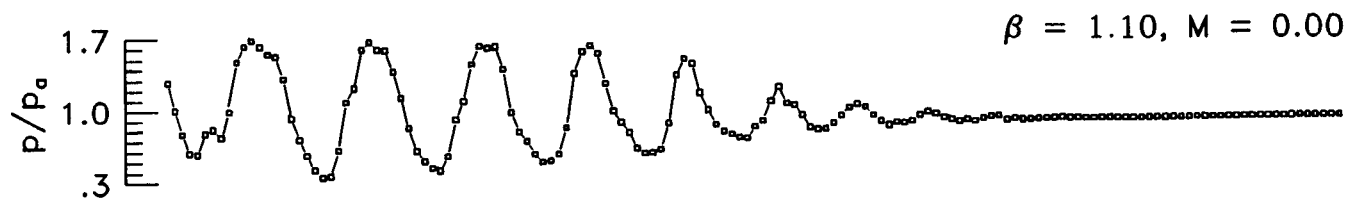
Static Pressure Distributions Along Plume Centerline

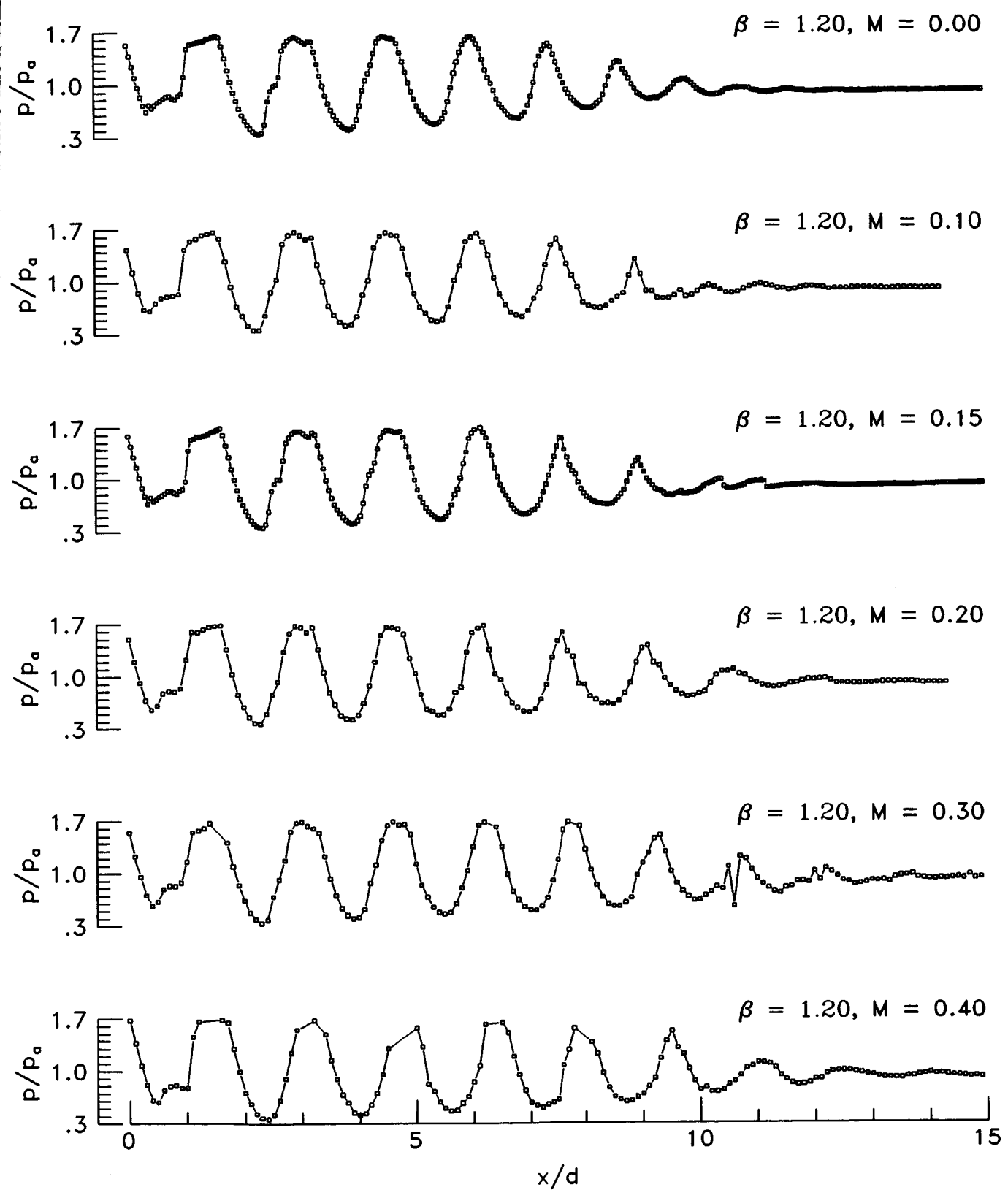


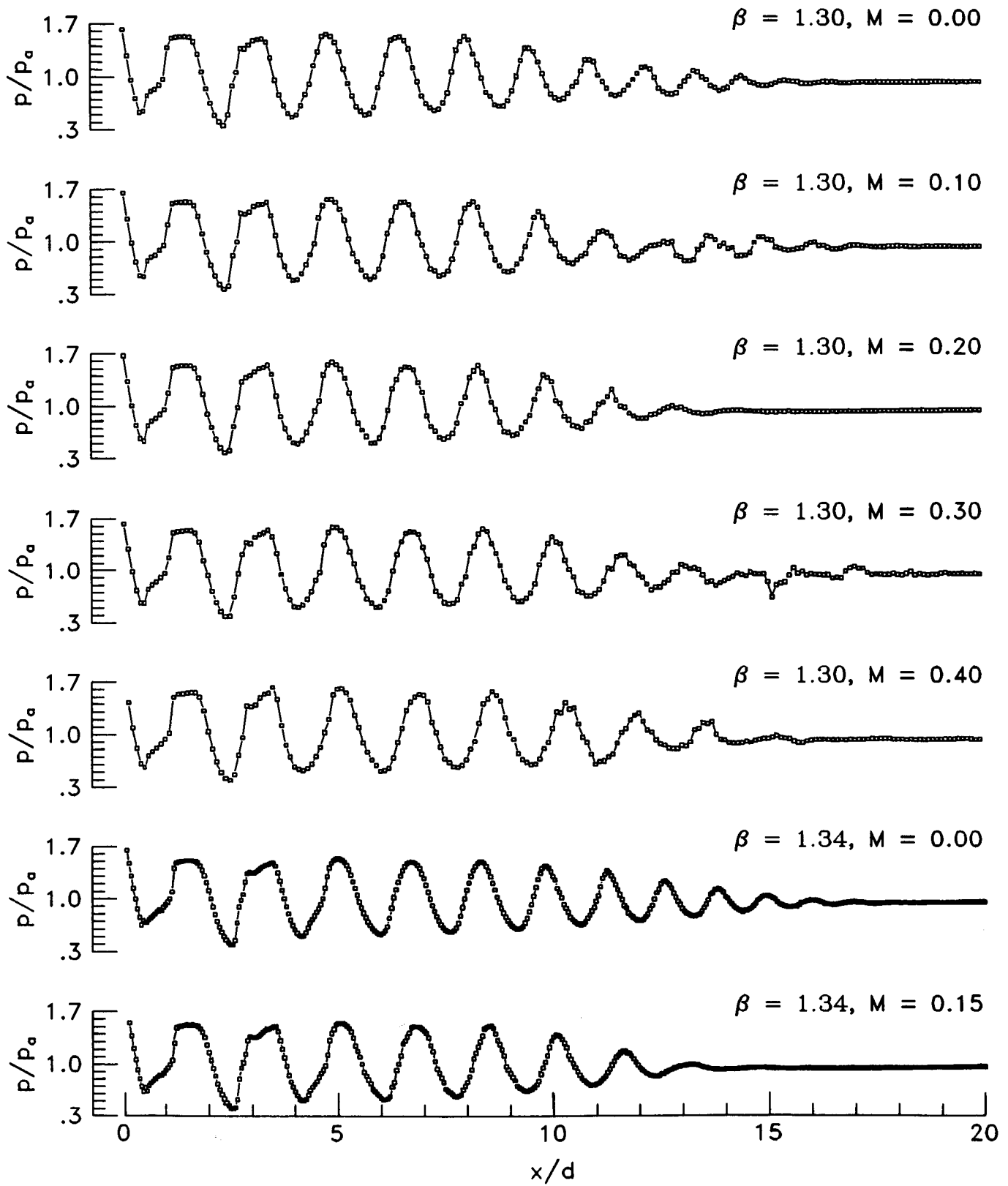


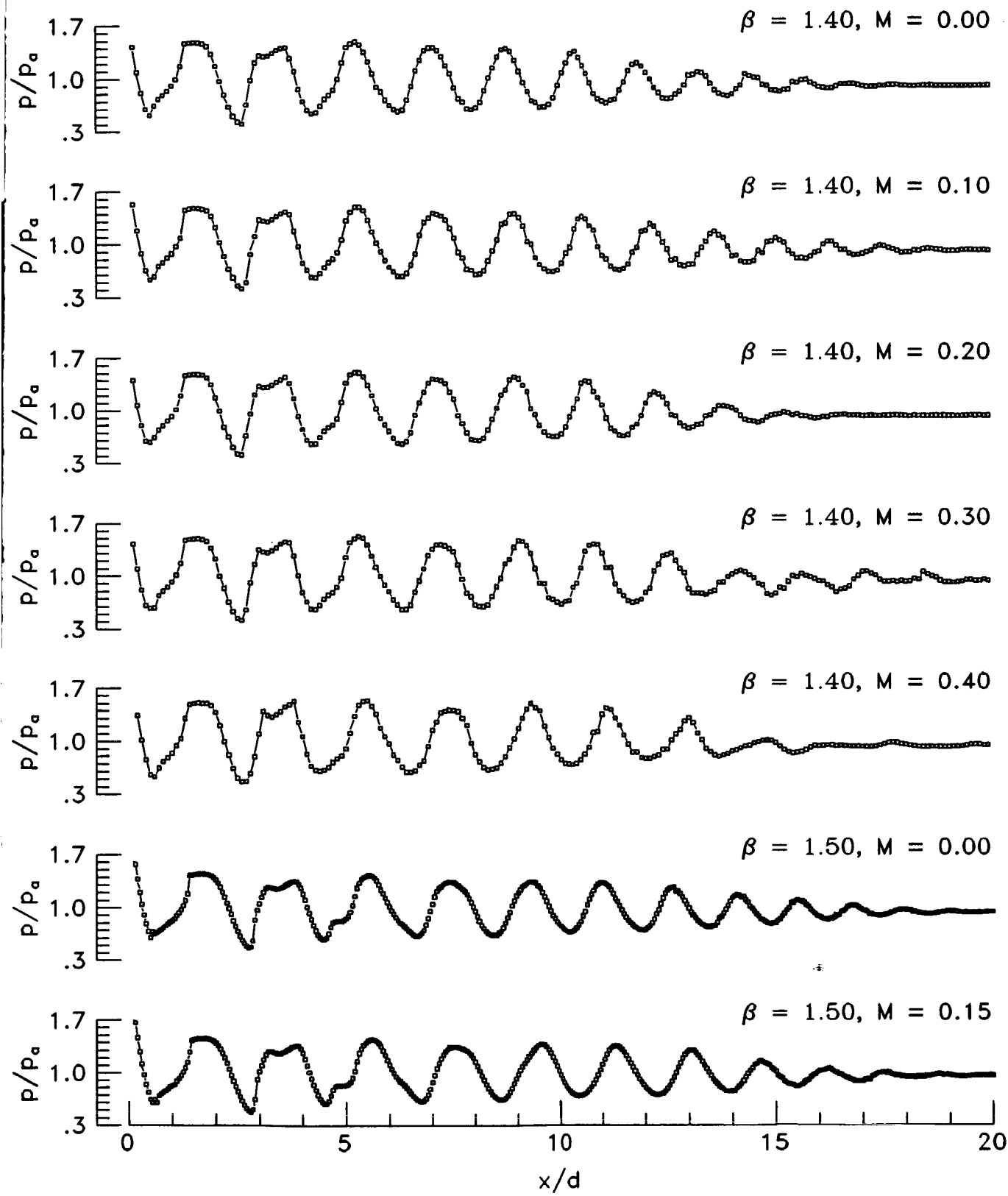


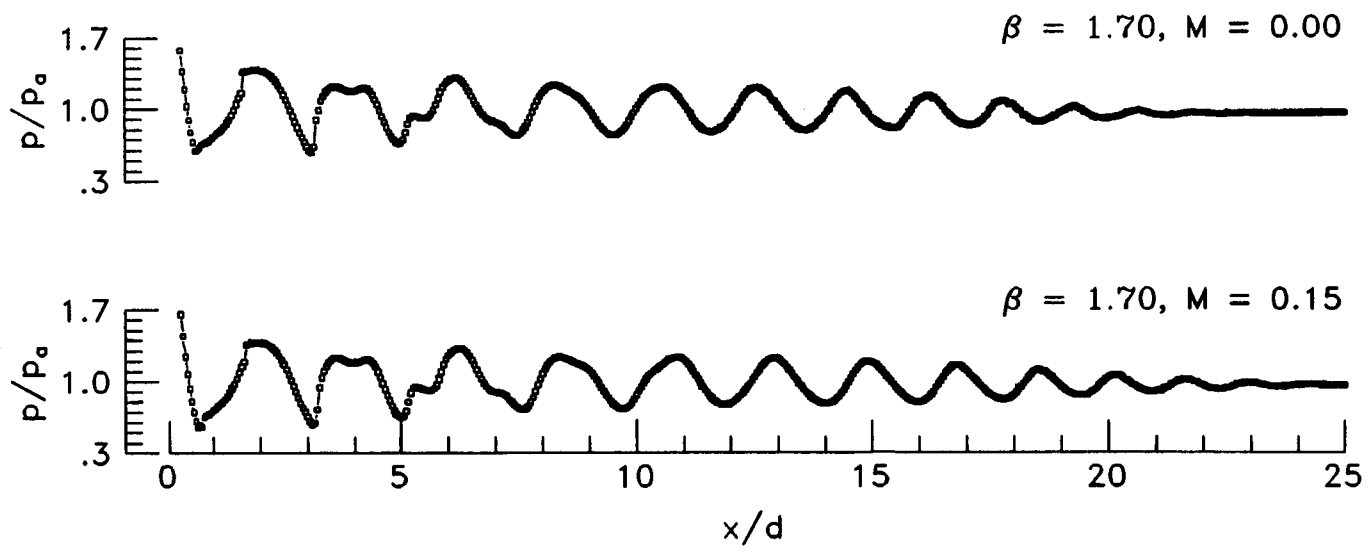
x/d







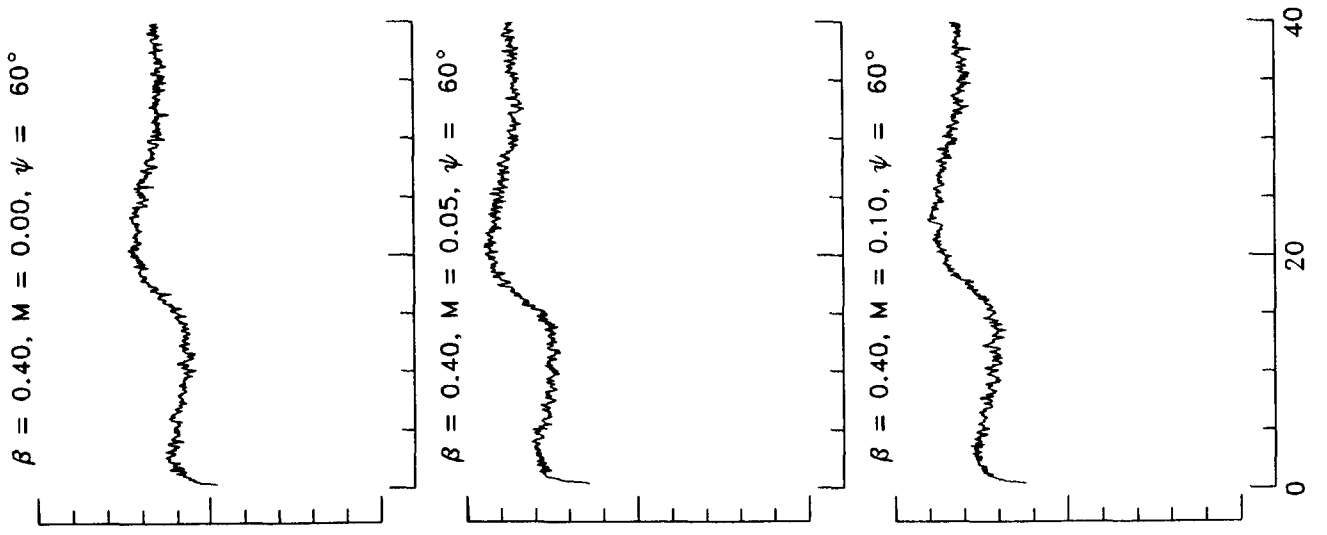
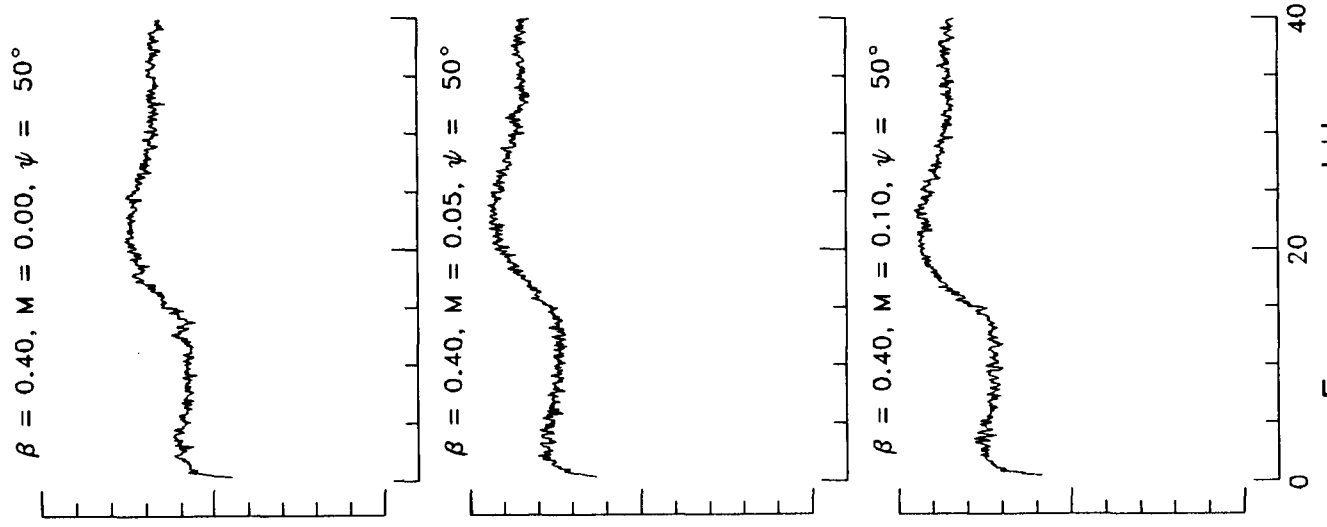
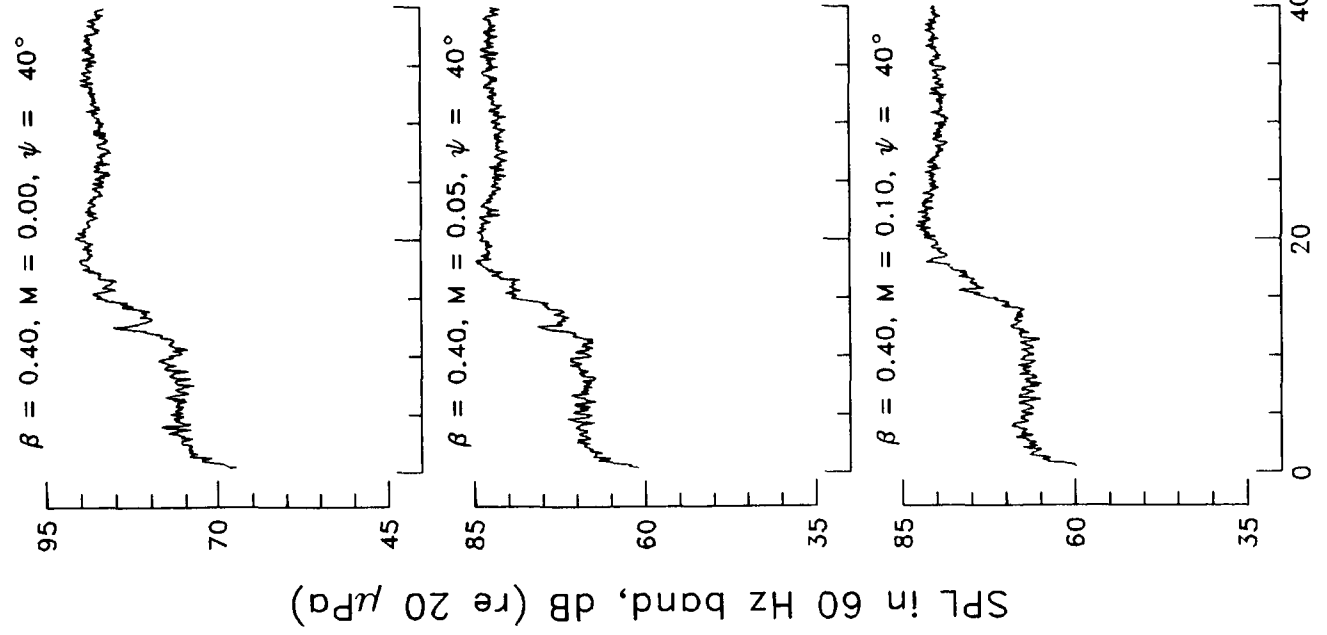




Appendix B

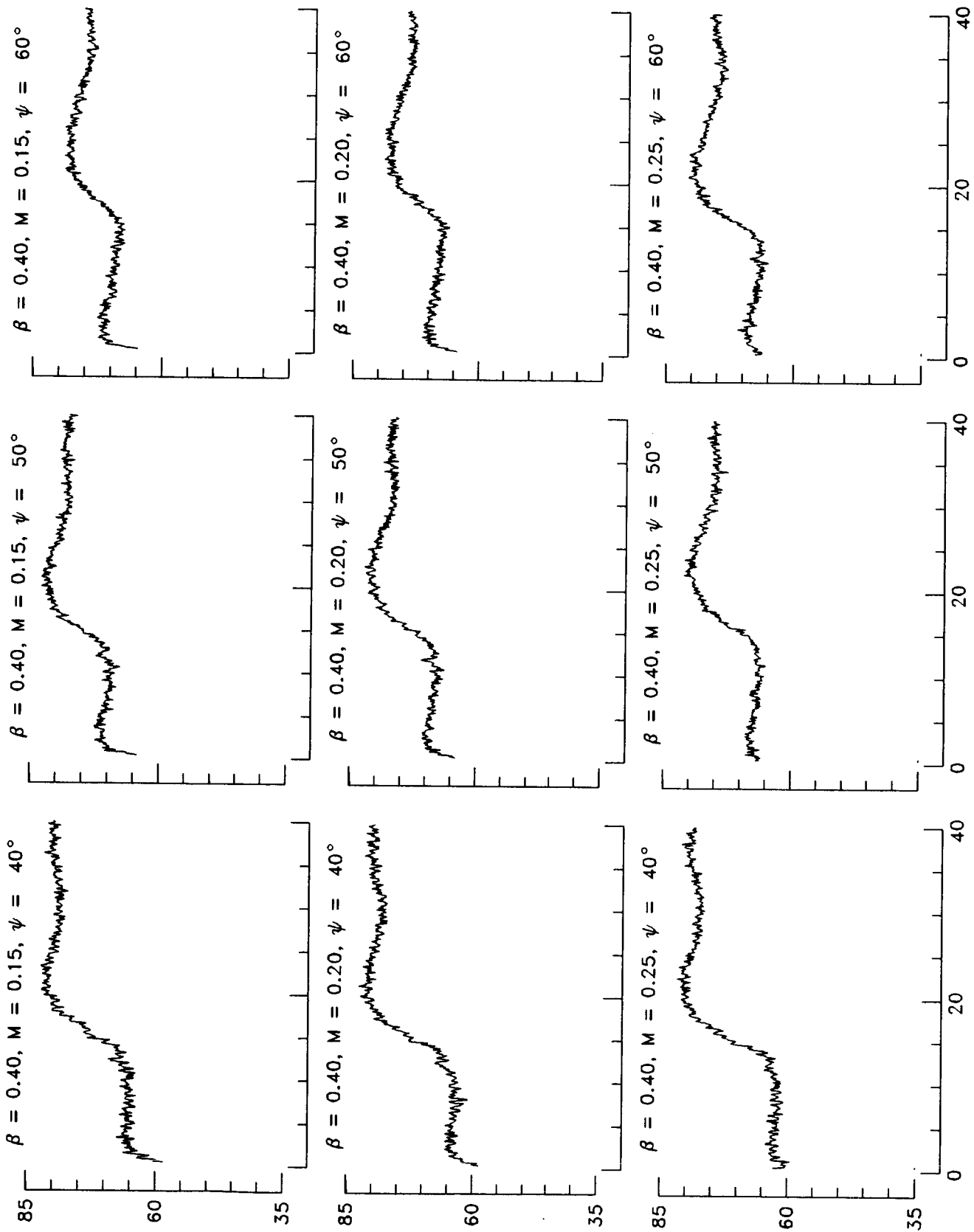
Power Spectra

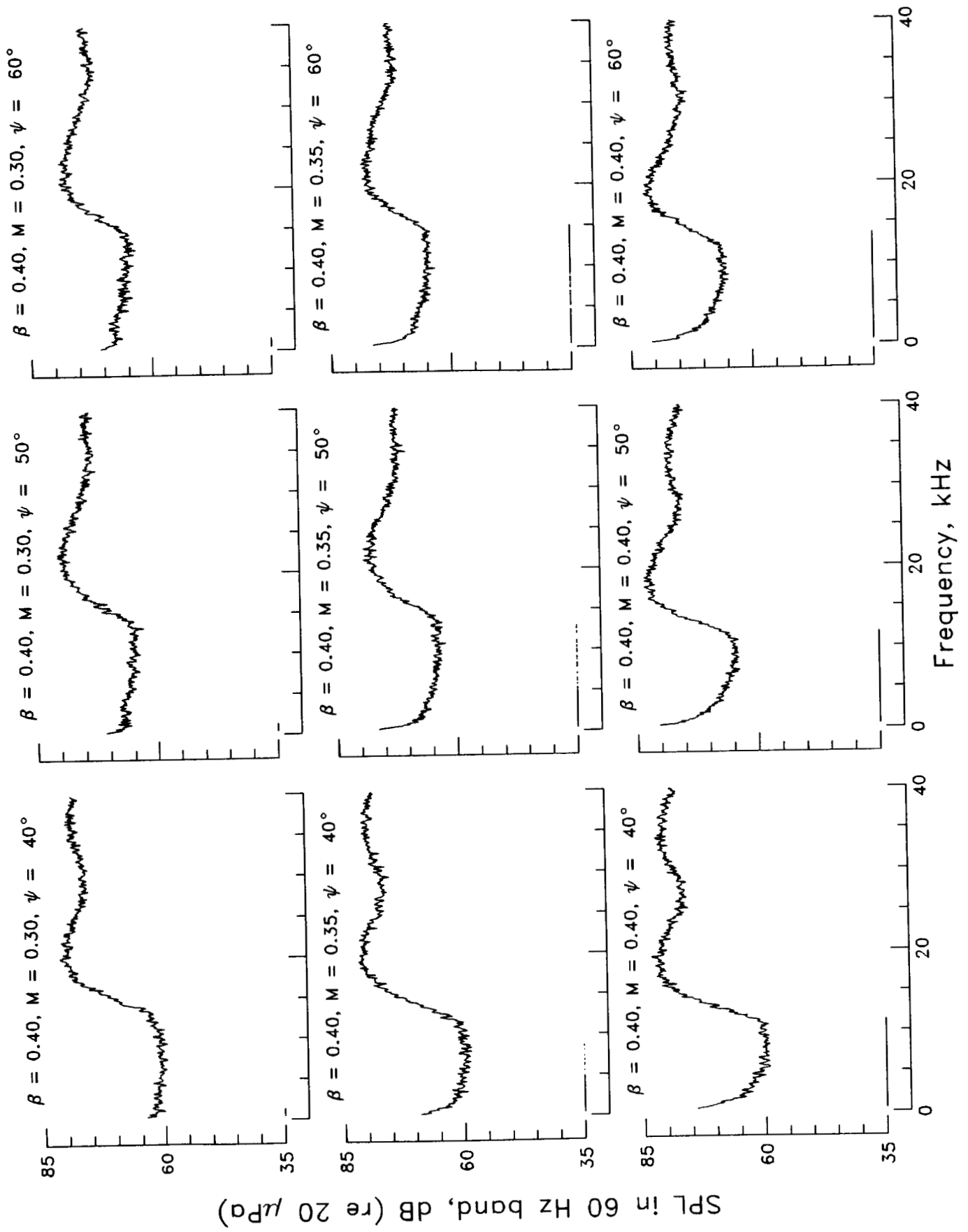
(Portions of the spectra for which the signal-to-noise ratio is less than 6 dB are underscored.)

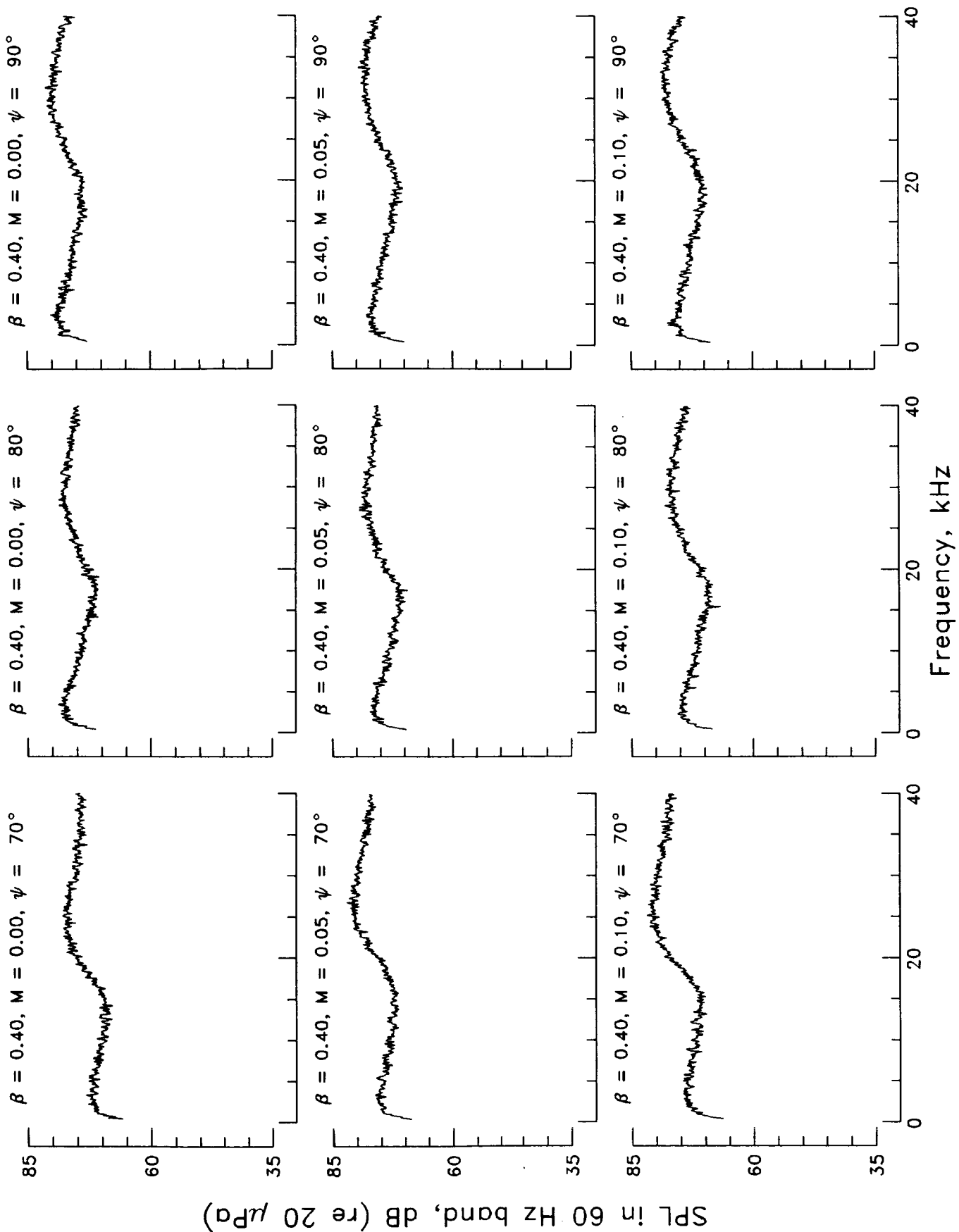


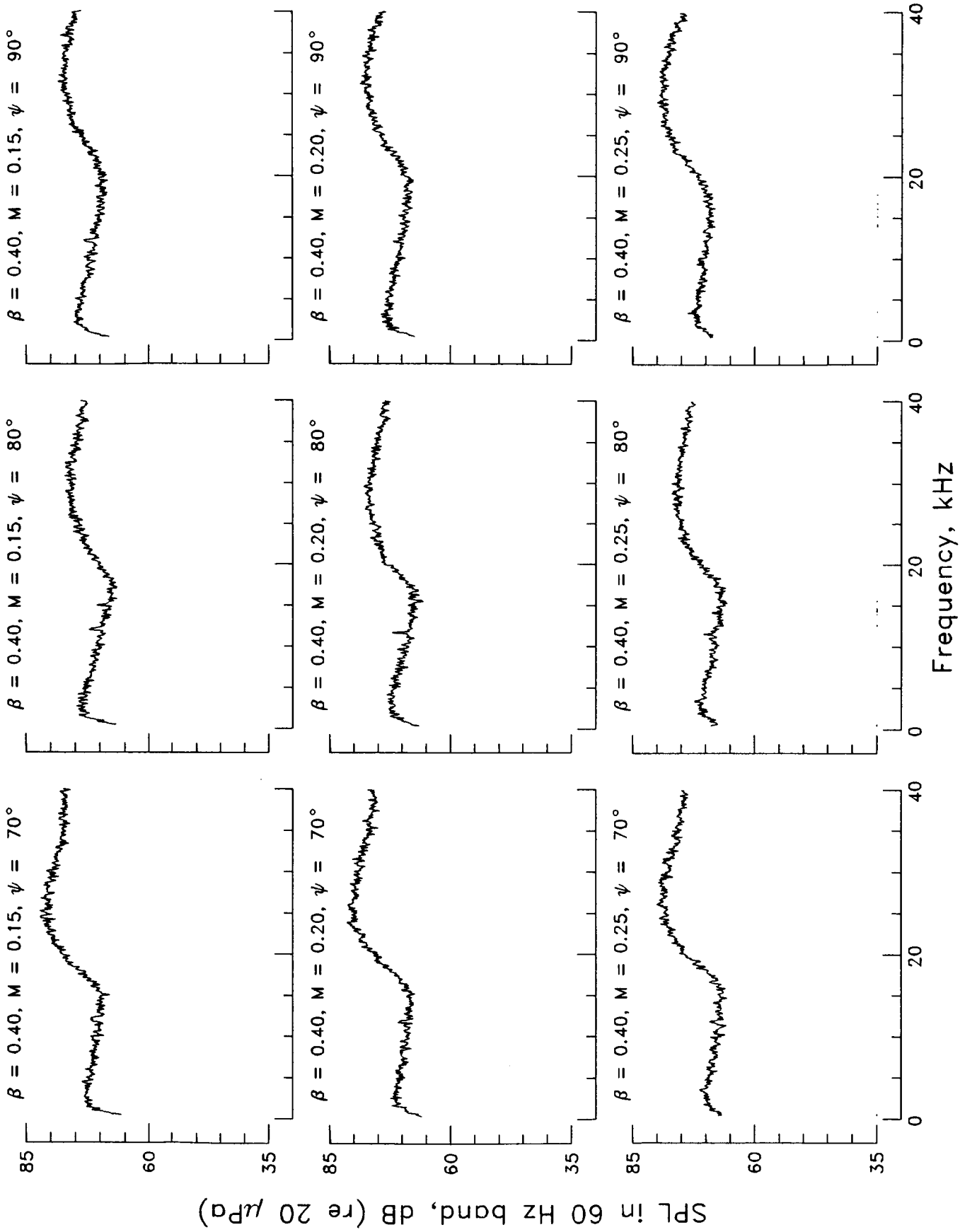
Frequency, kHz

SPL in 60 Hz band, dB (re 20 μ Pa)

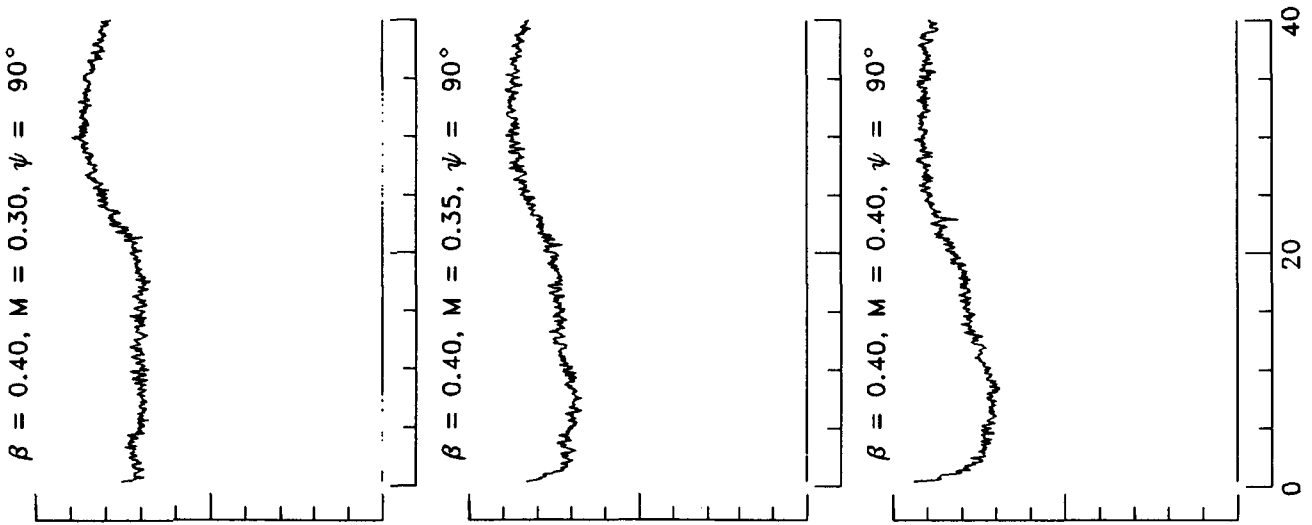
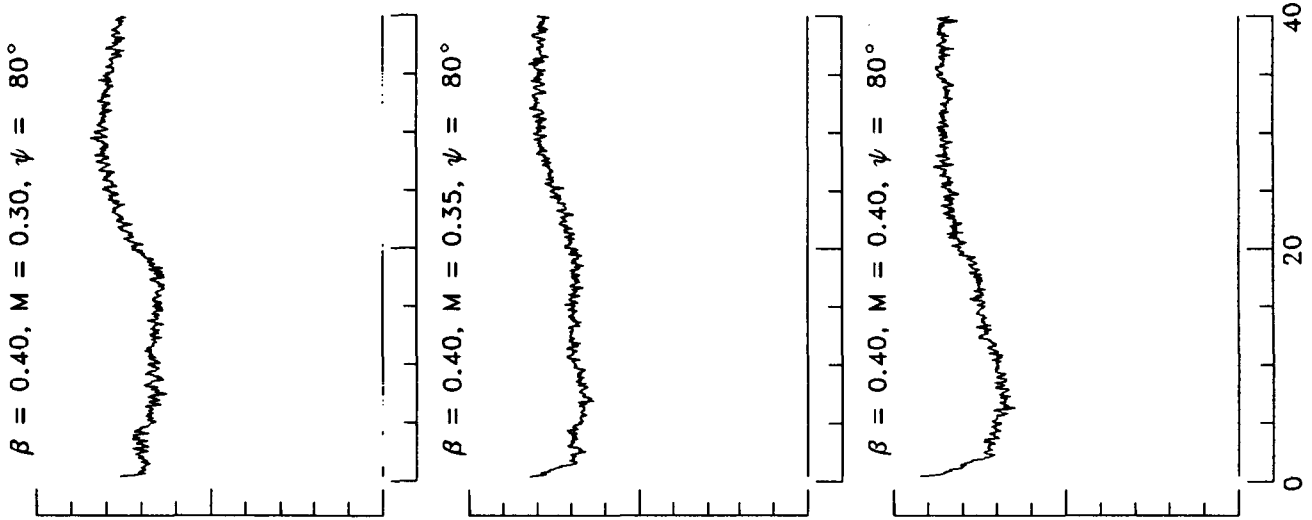
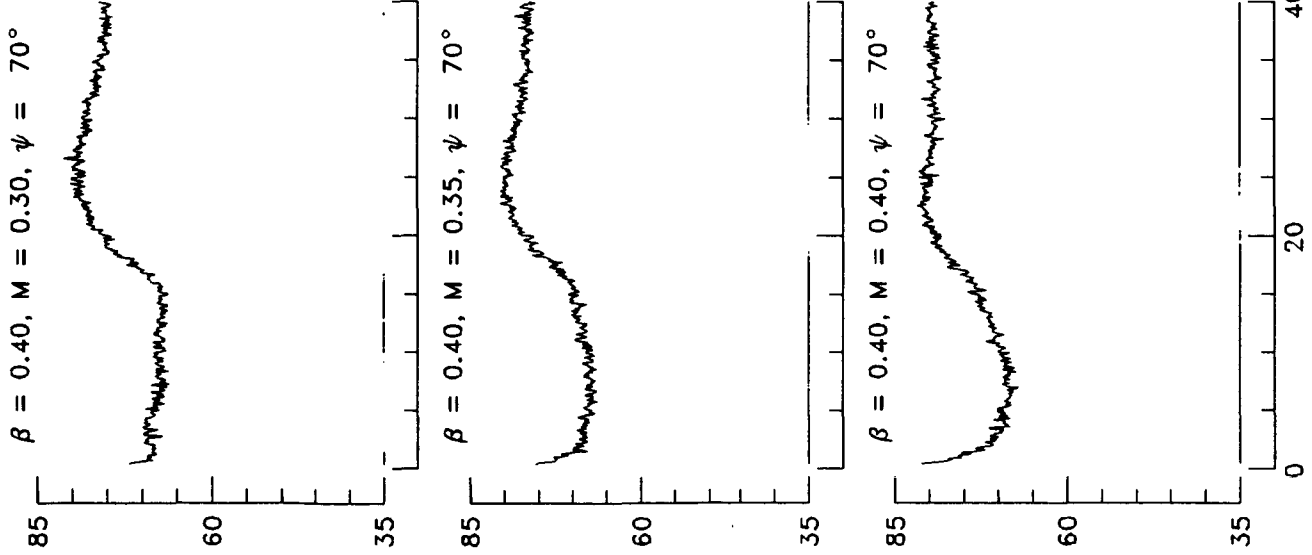




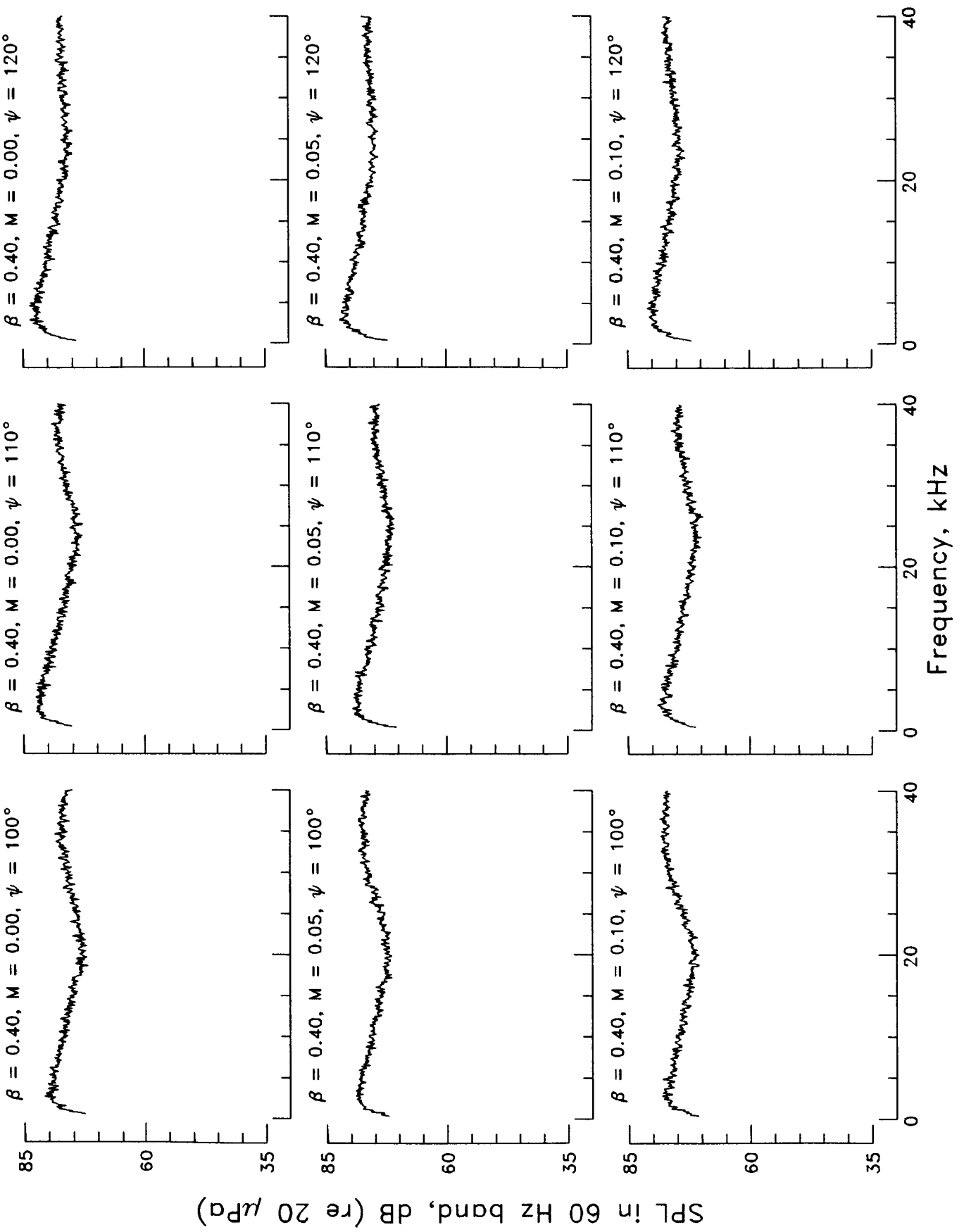


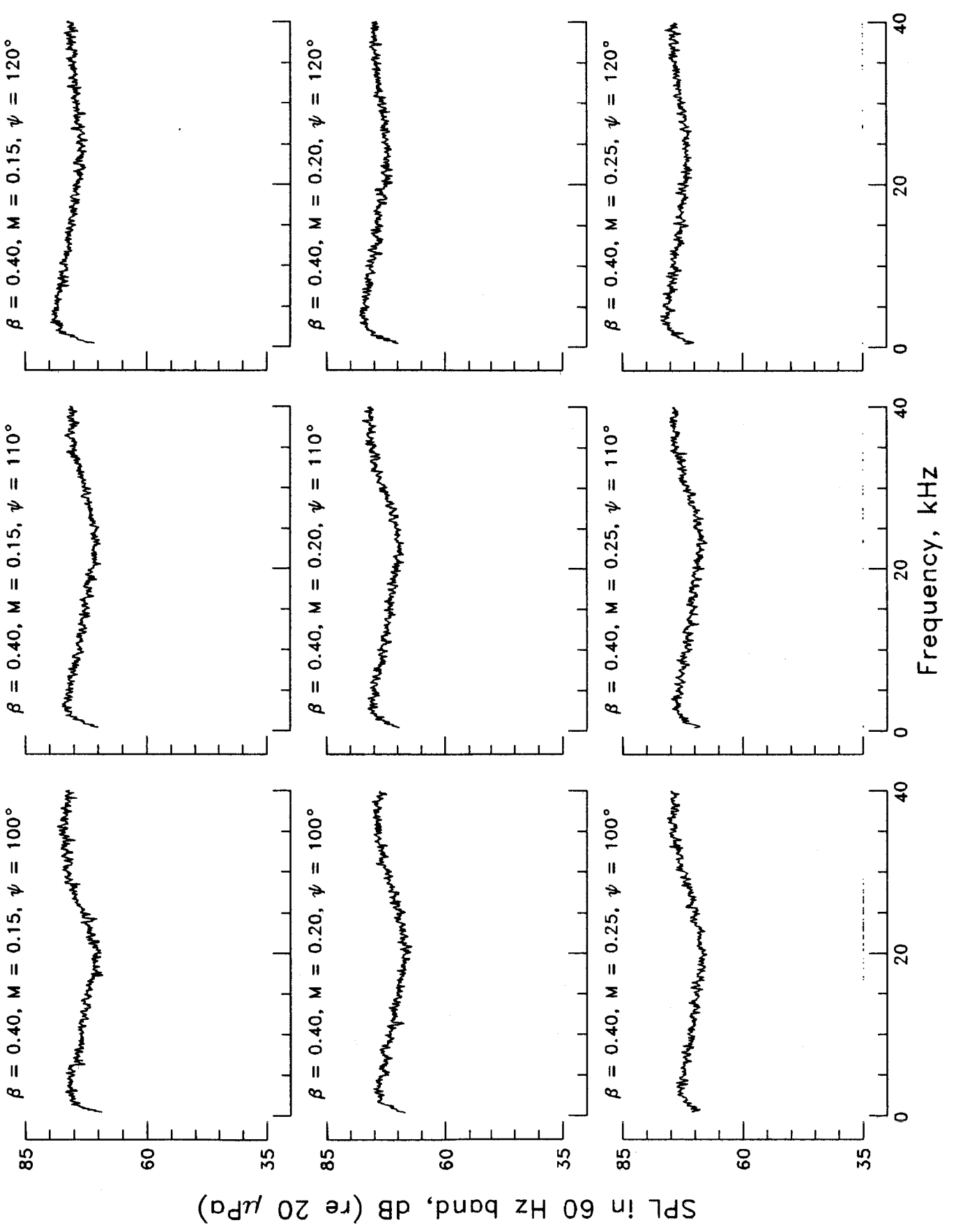


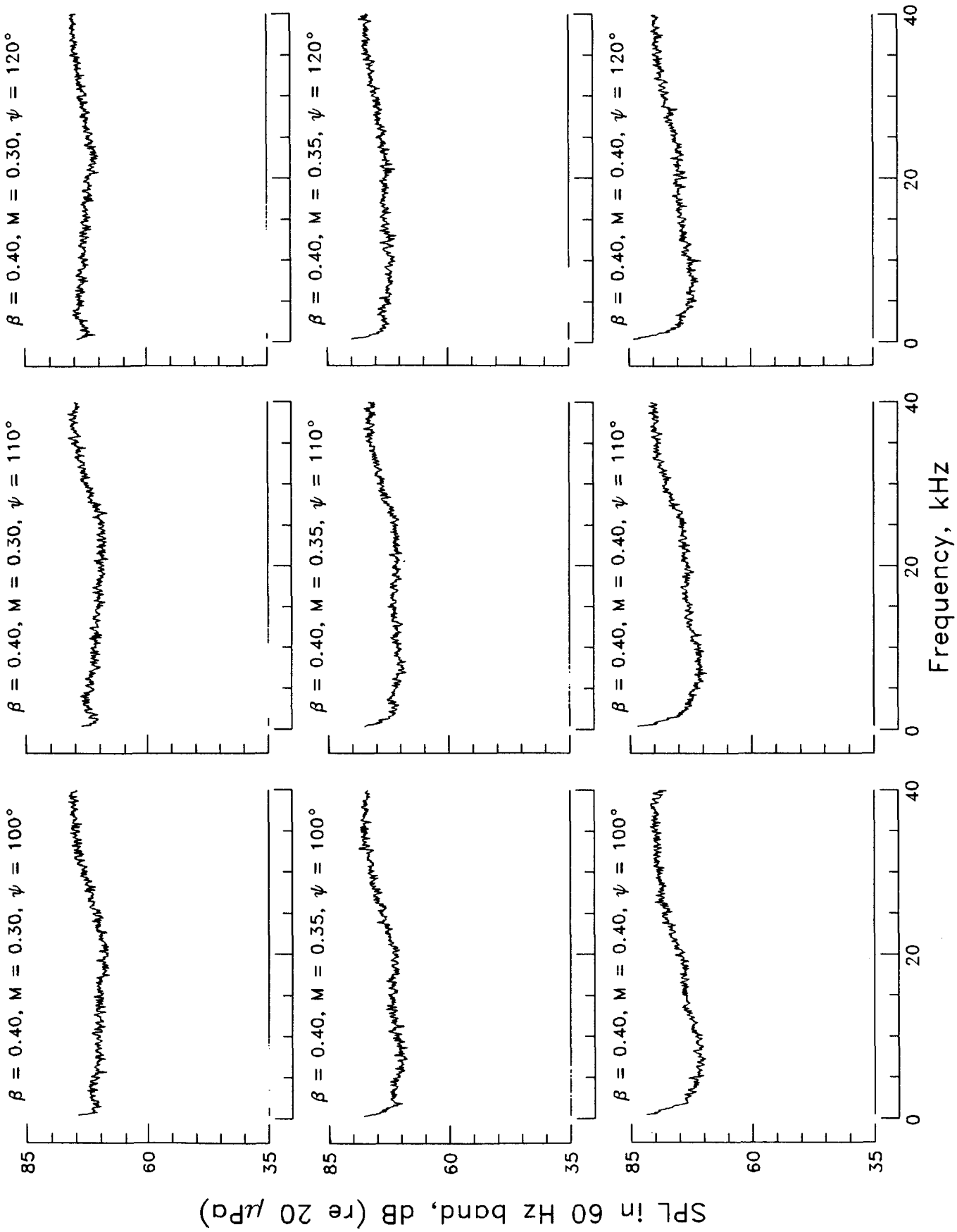
SPL in 60 Hz band, dB (re 20 μ Pa)



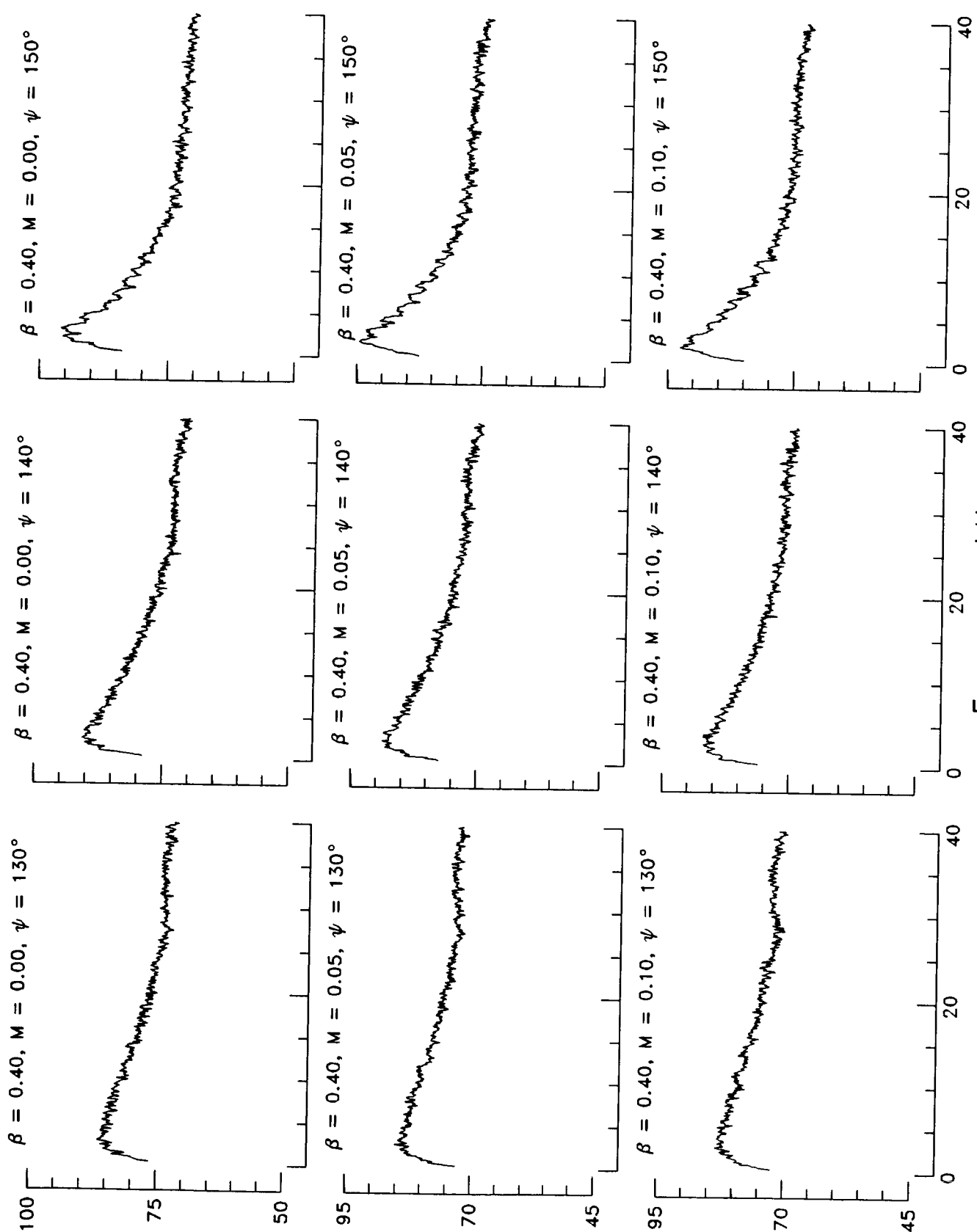
Frequency, kHz

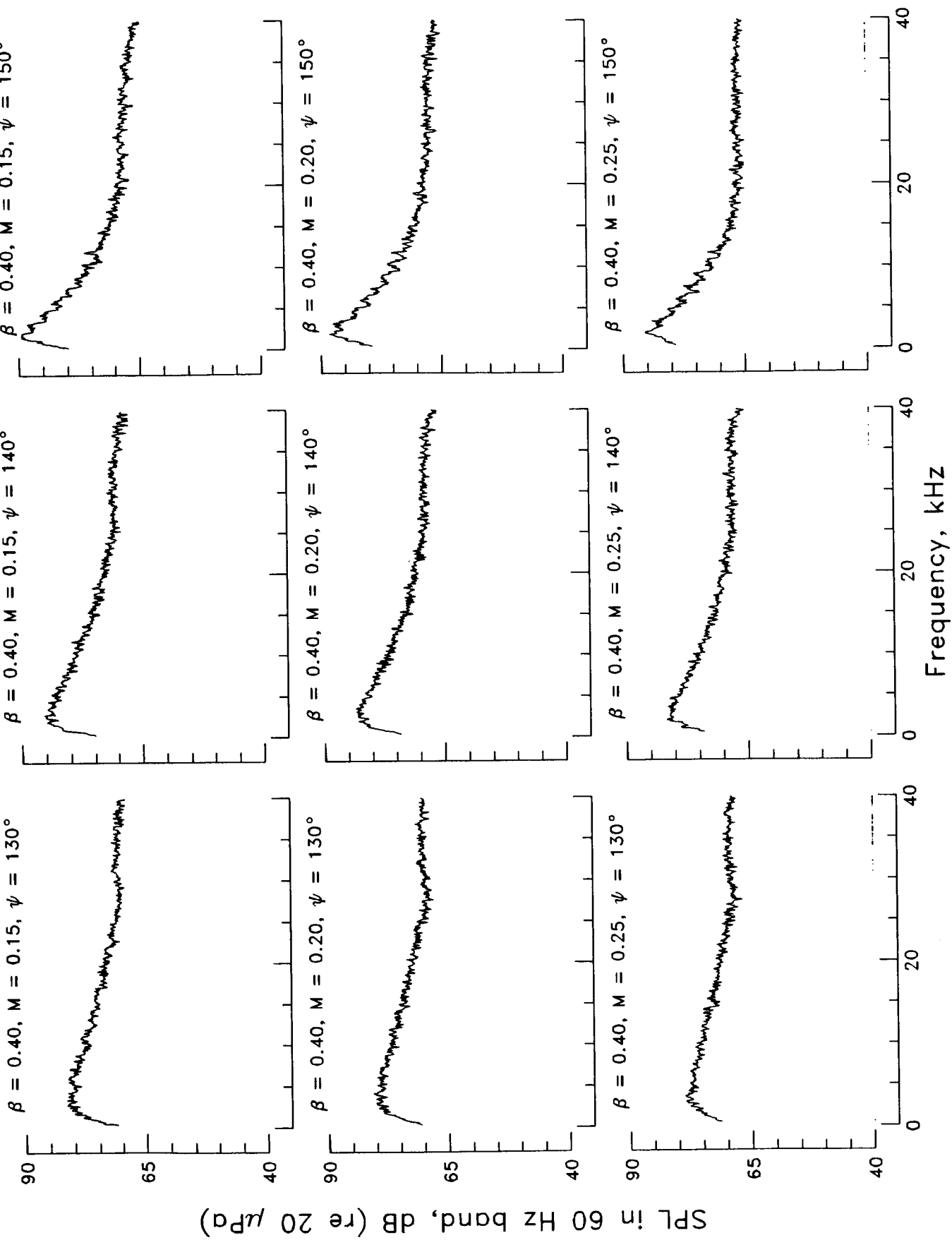


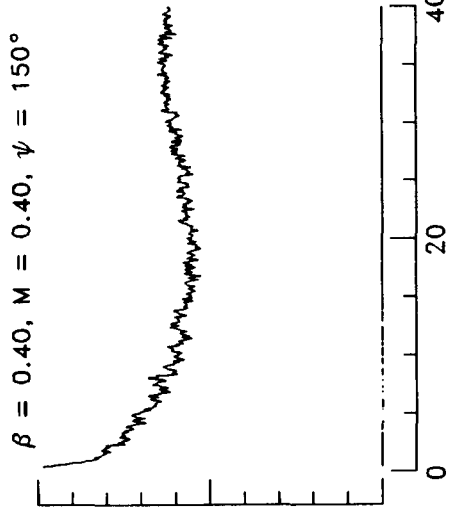
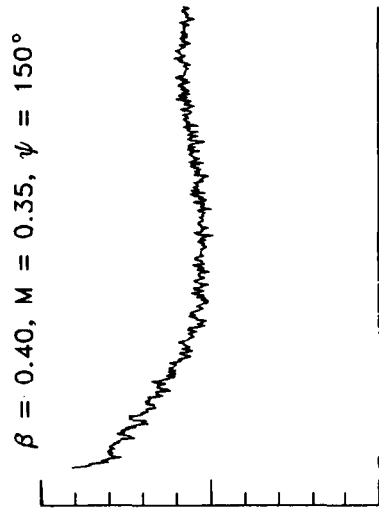
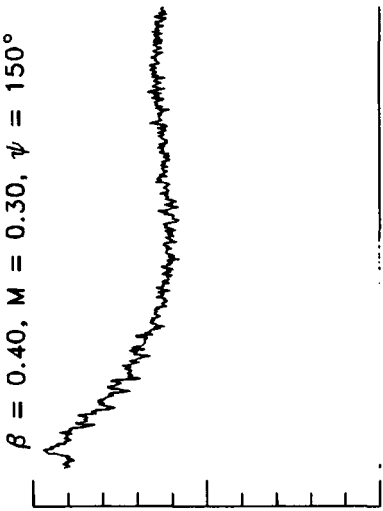
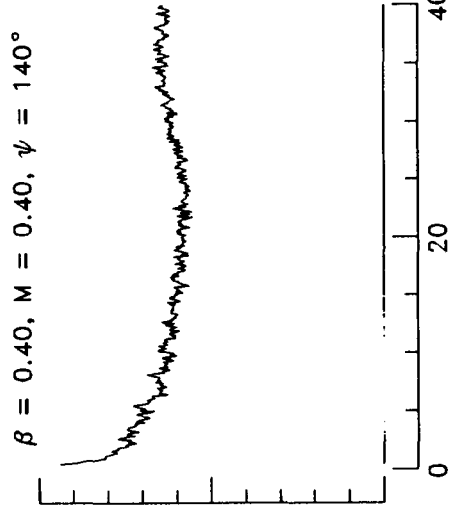
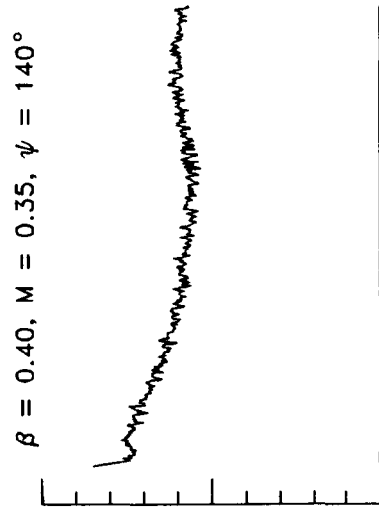
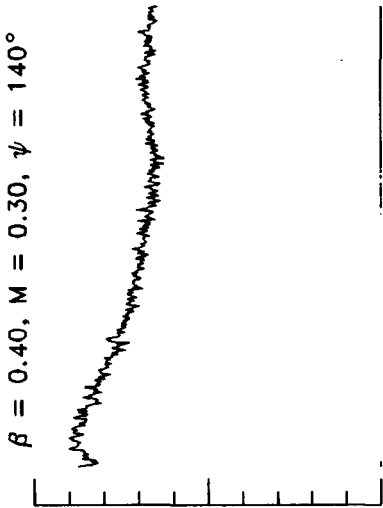
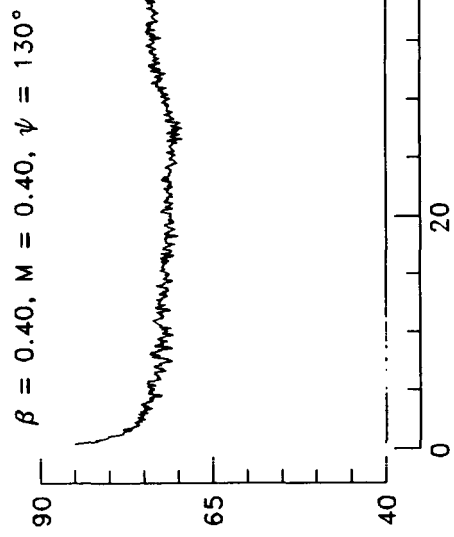
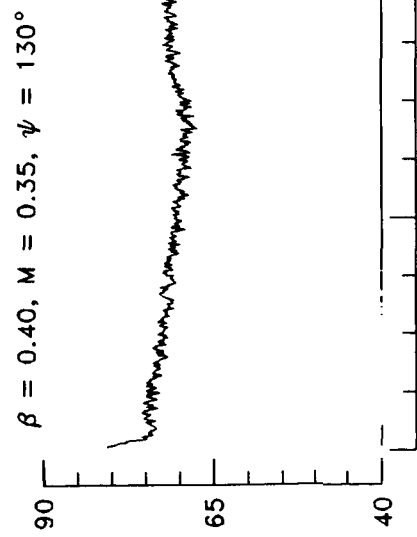
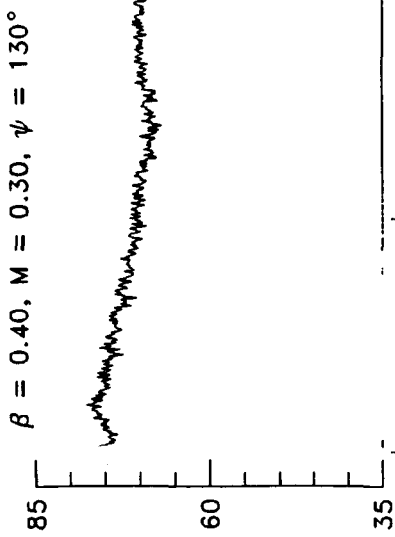




SPL in 60 Hz band, dB (re 20 μ Pa)

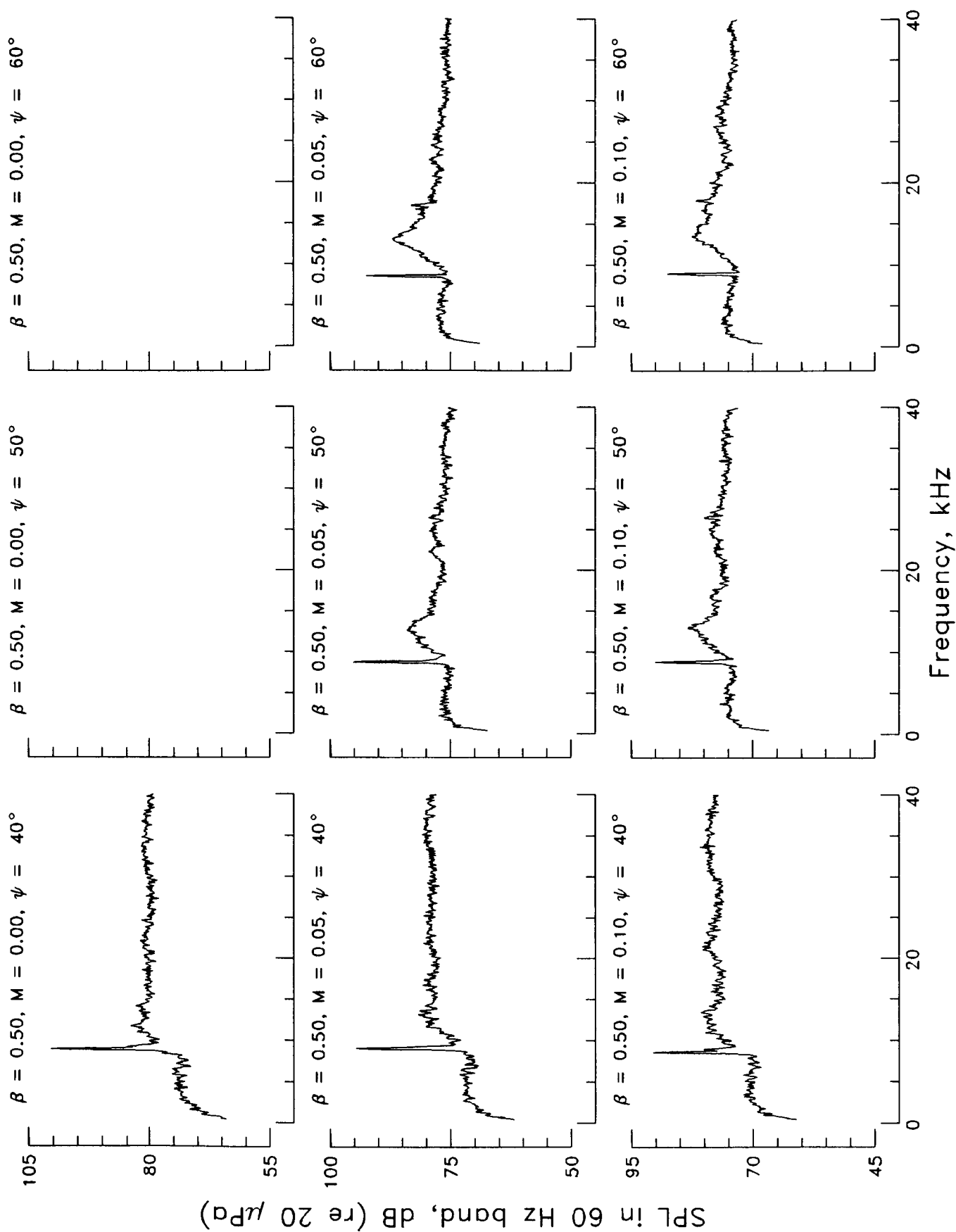


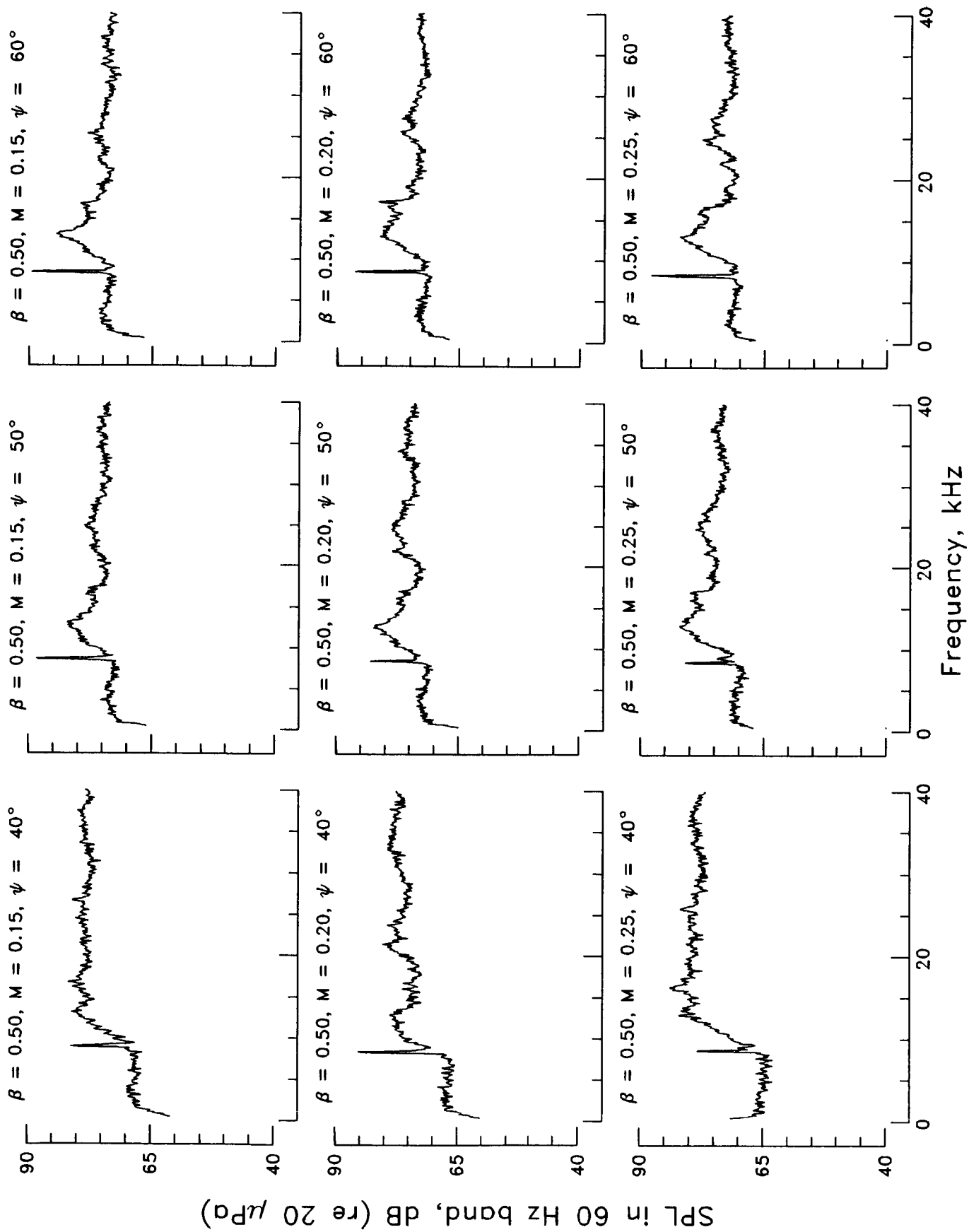


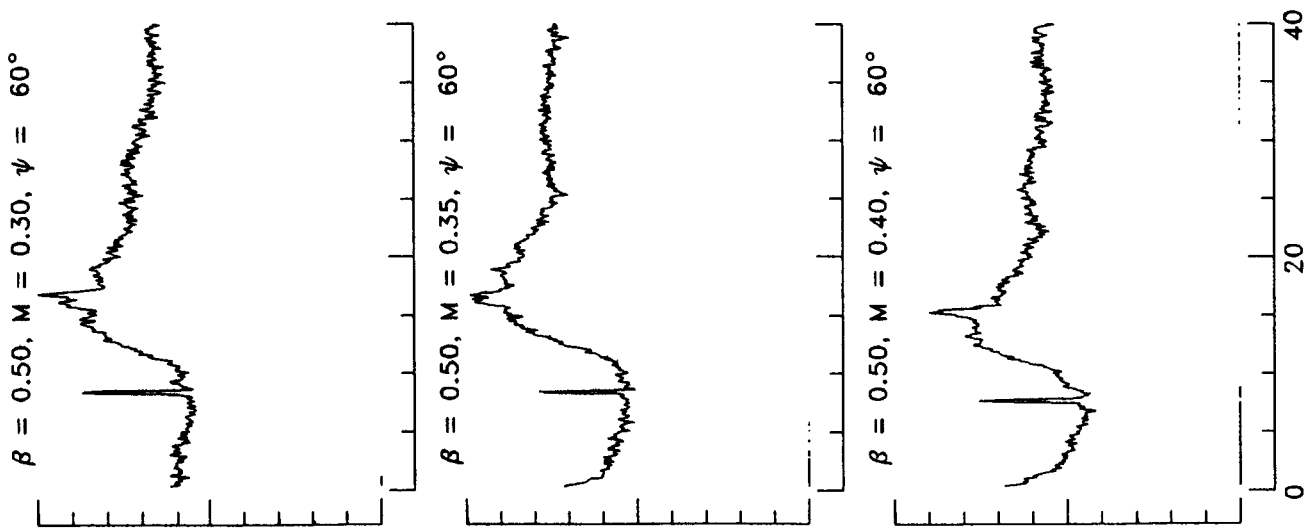
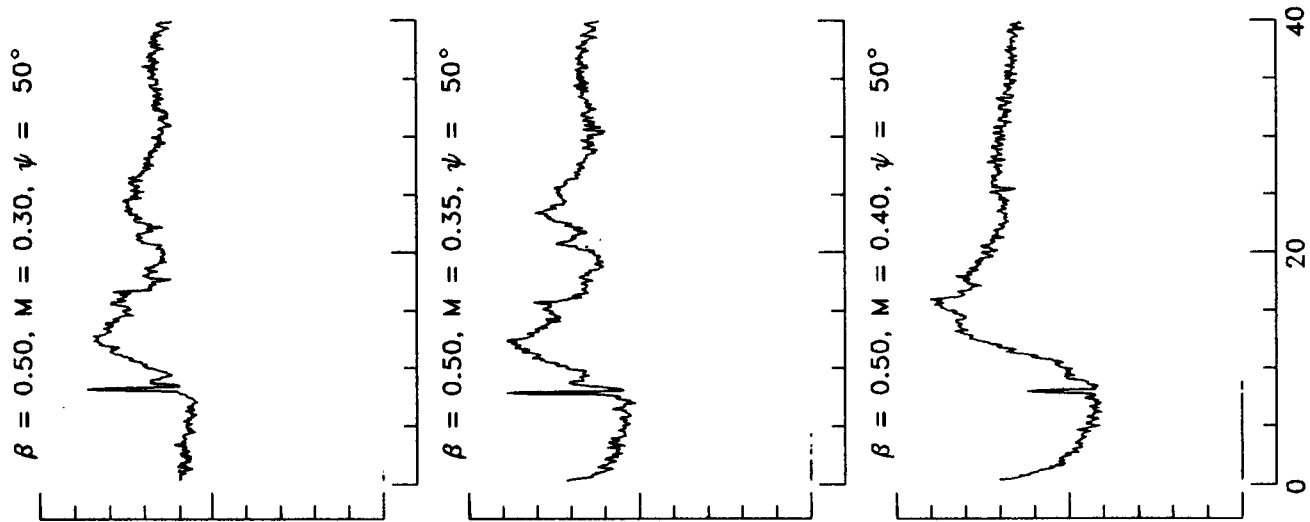
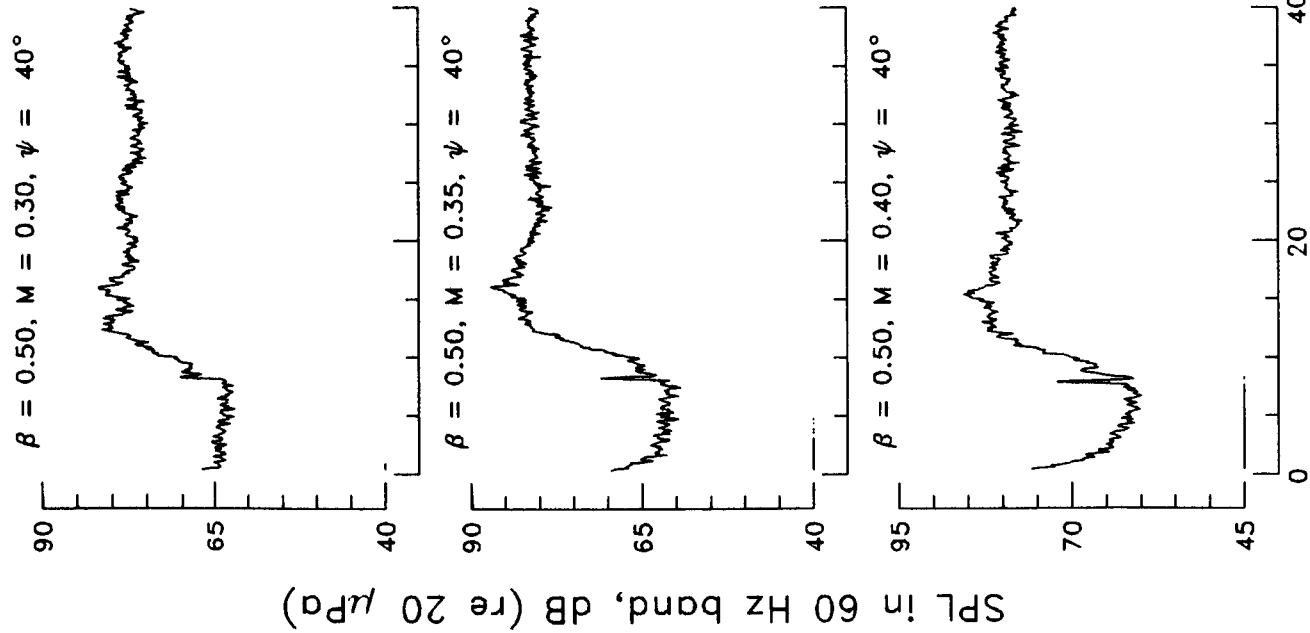


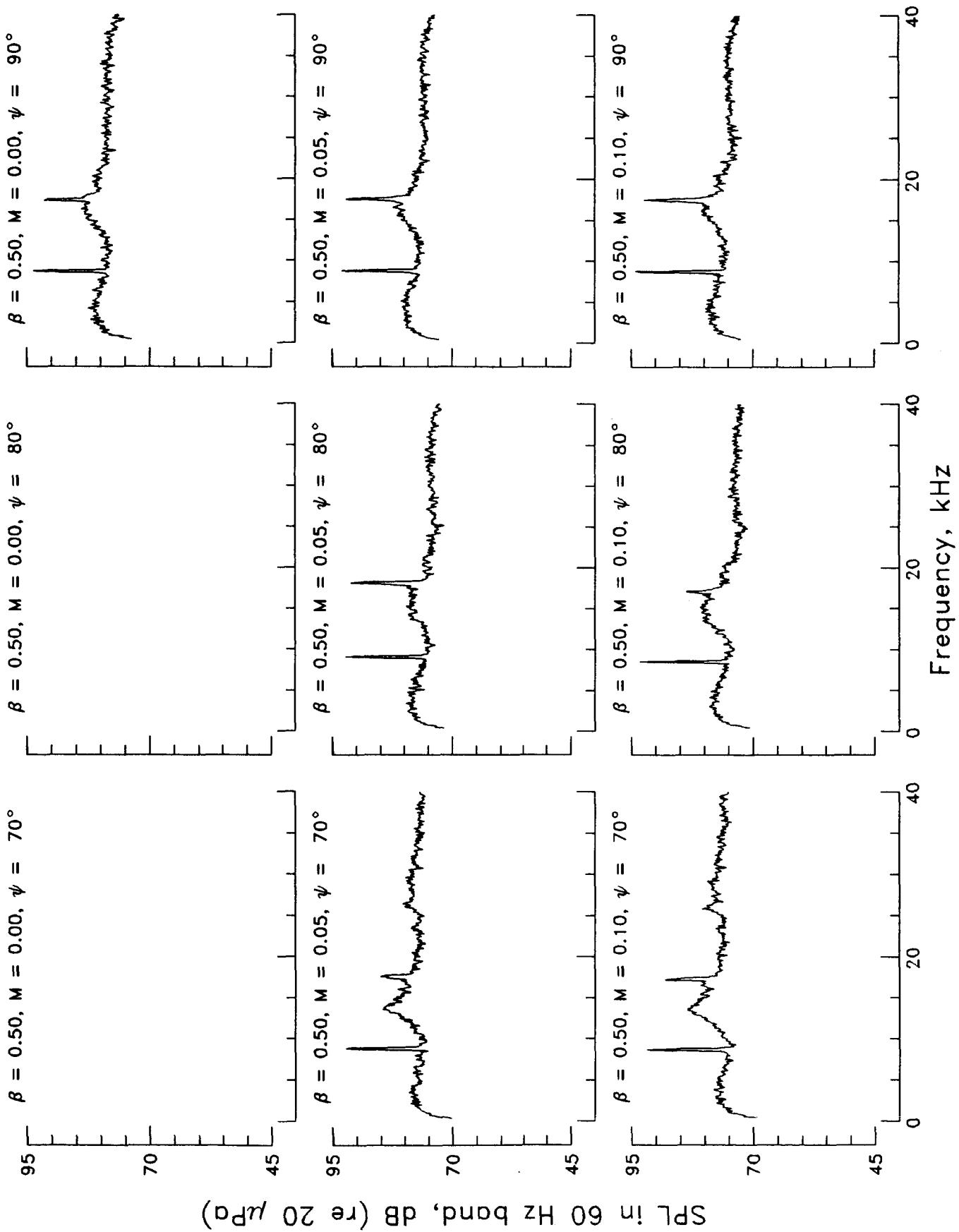
SPL in 60 Hz band, dB (re 20 μ Pa)

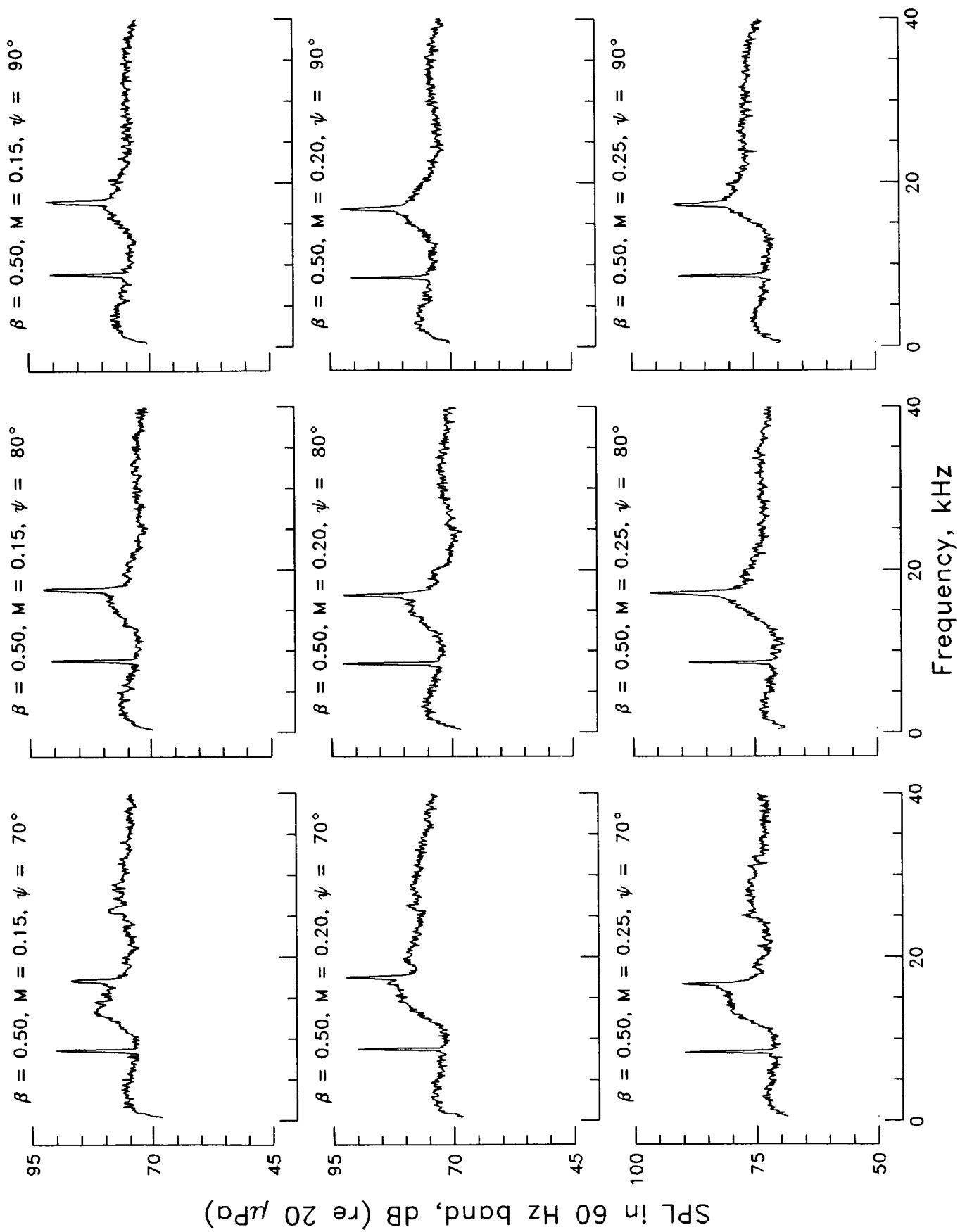
Frequency, kHz

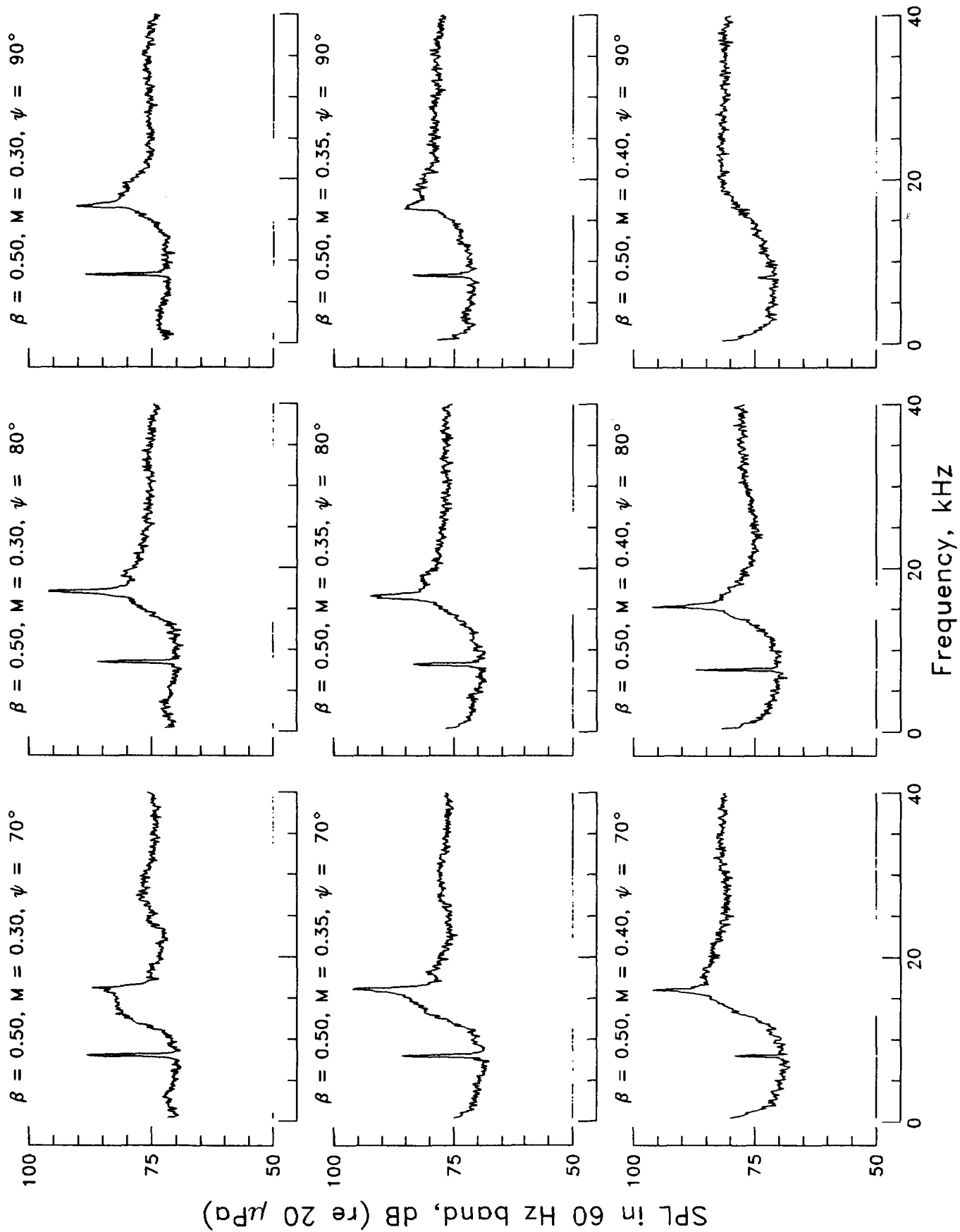


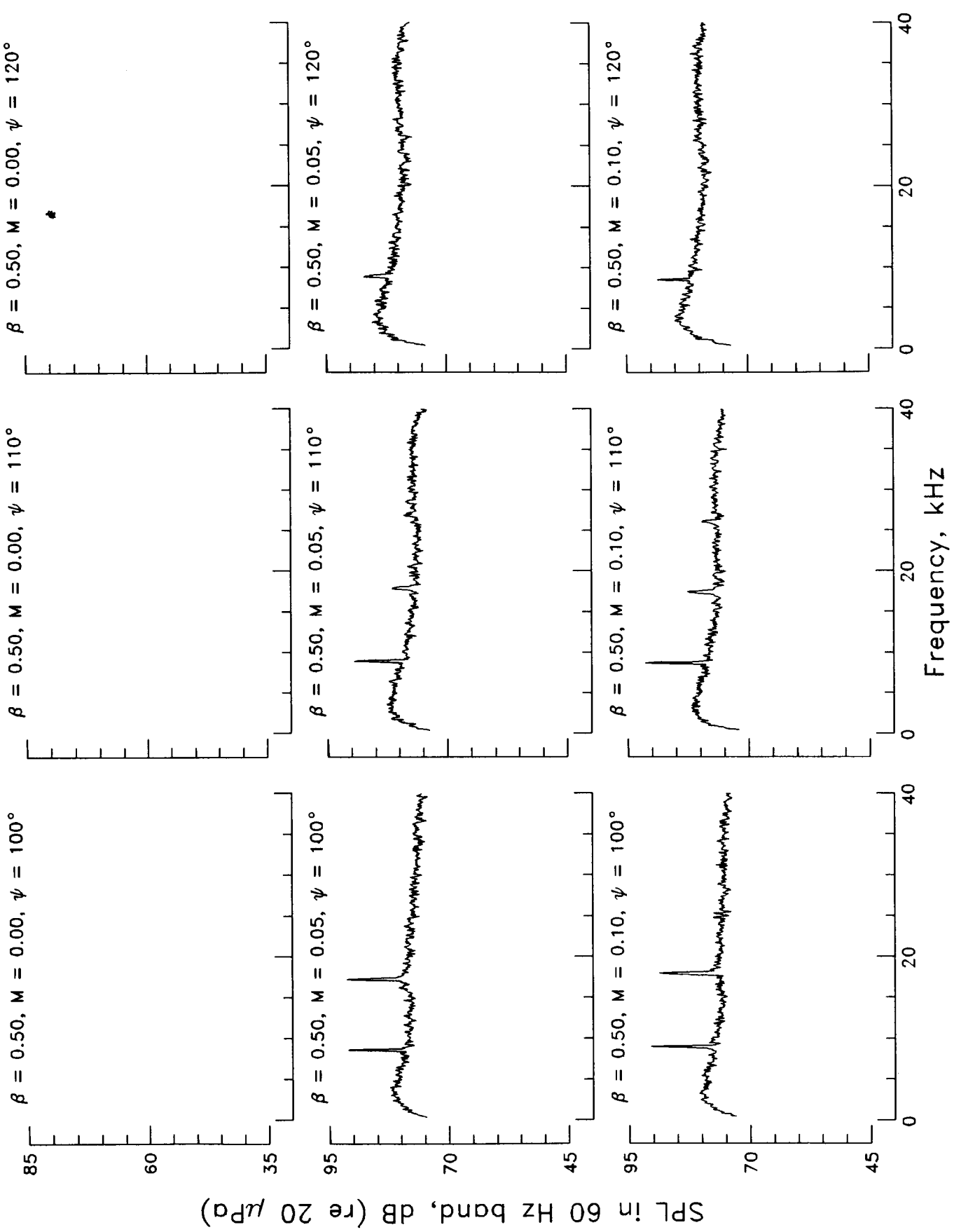


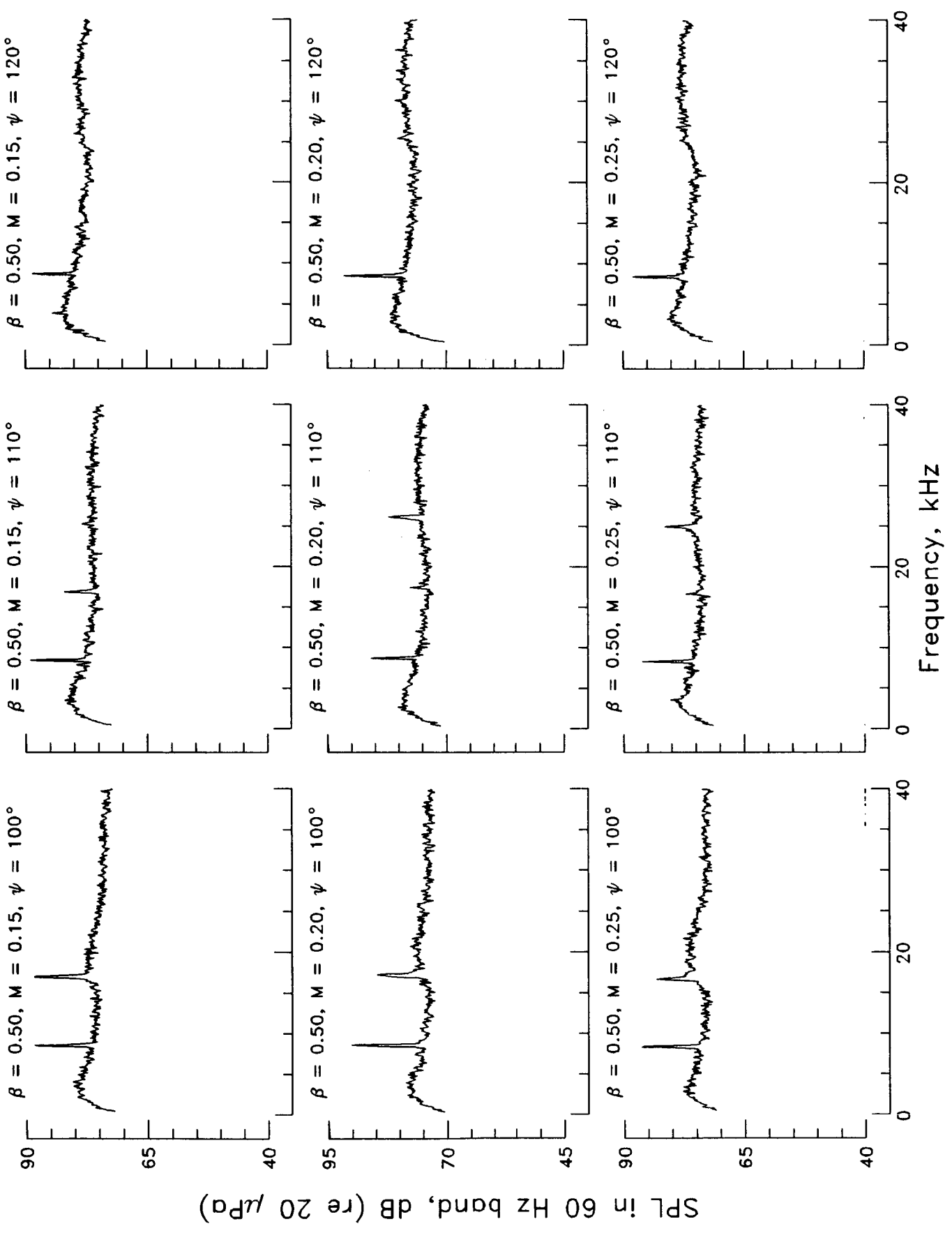


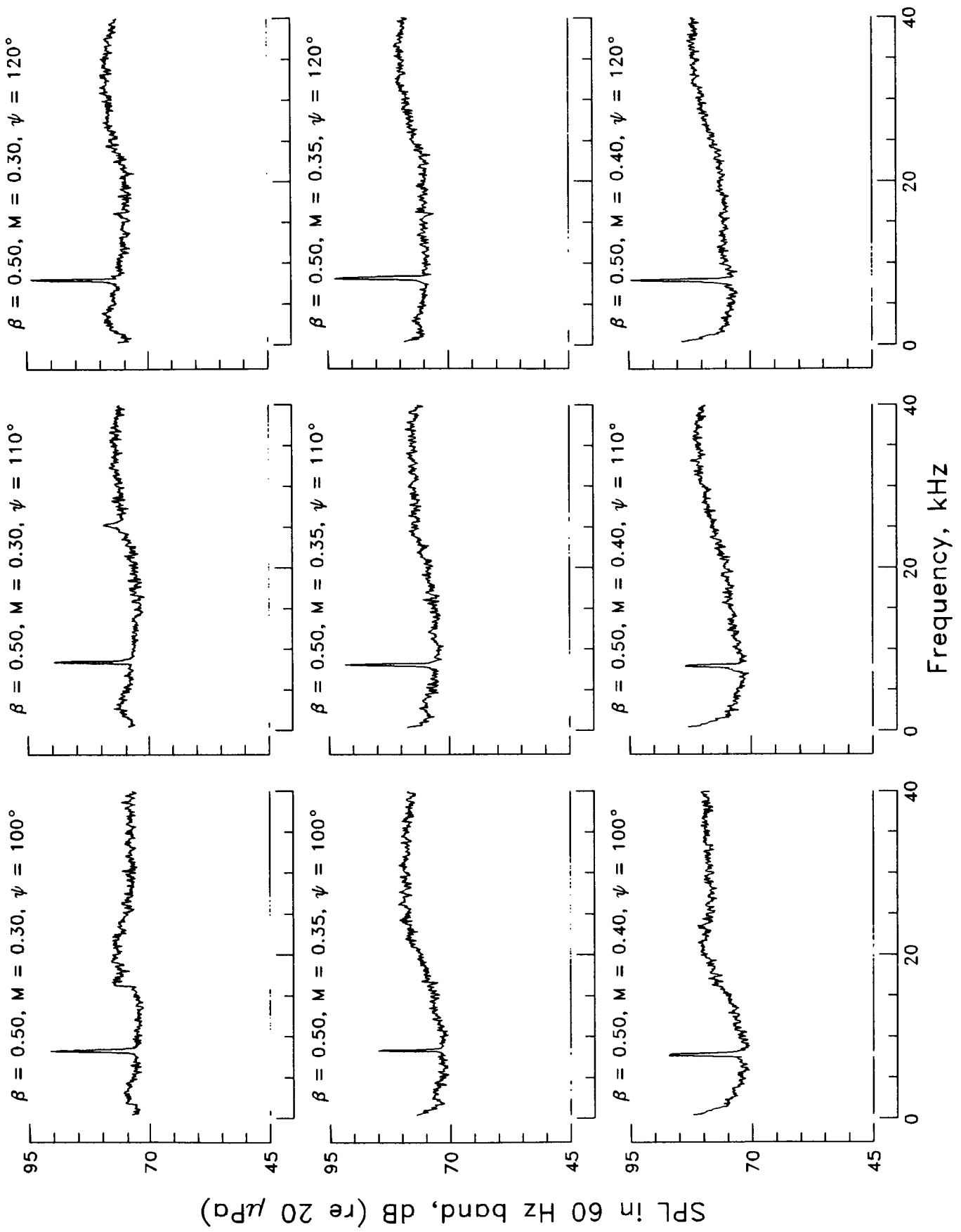


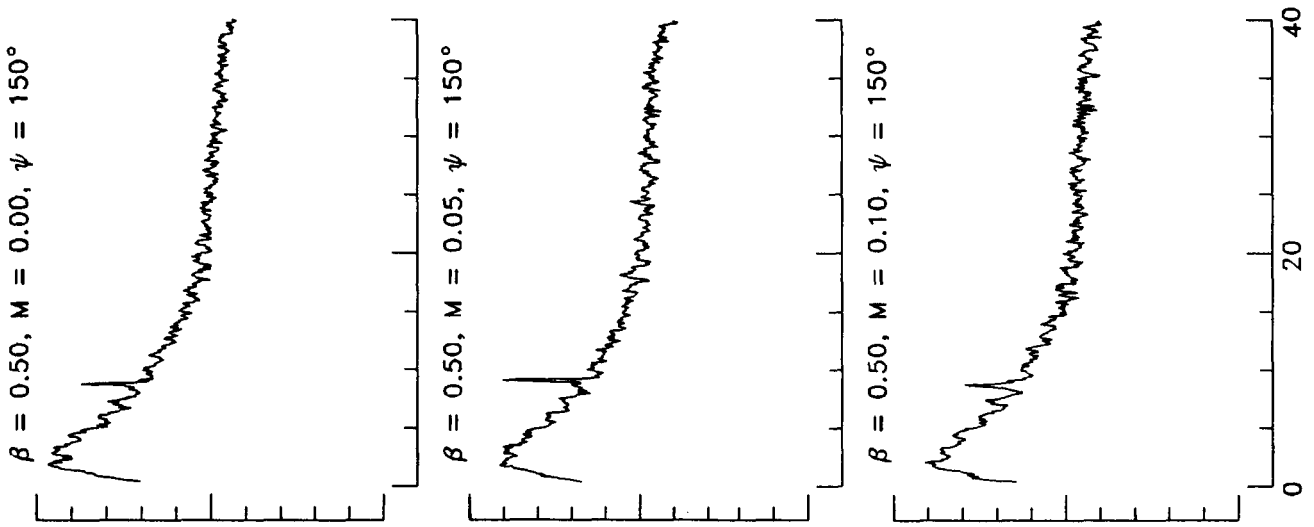
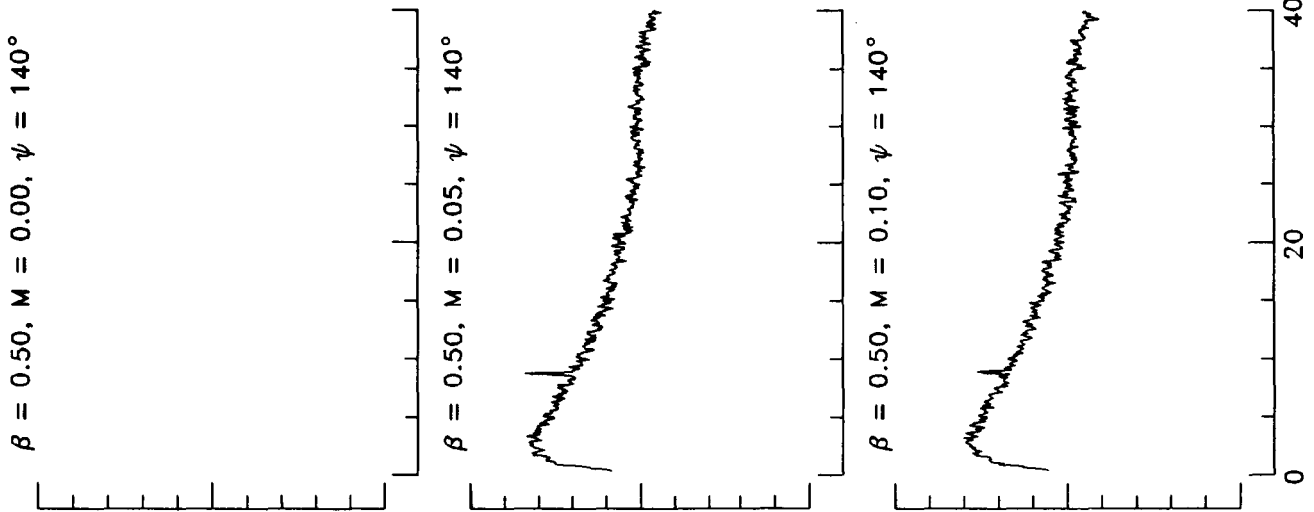
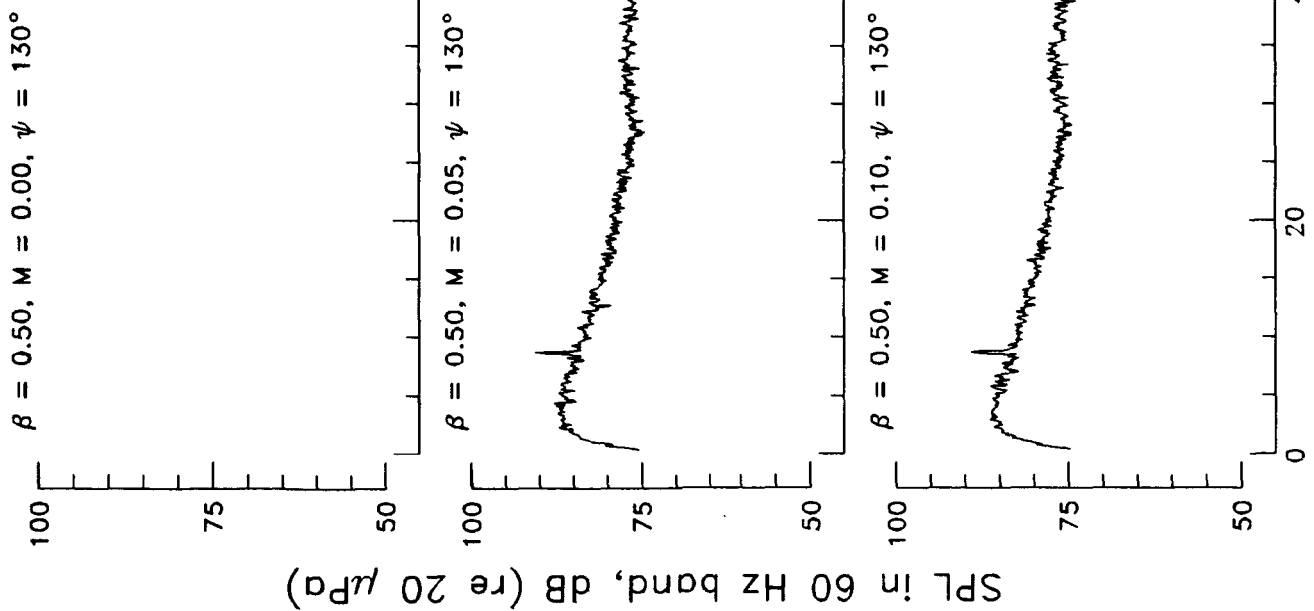






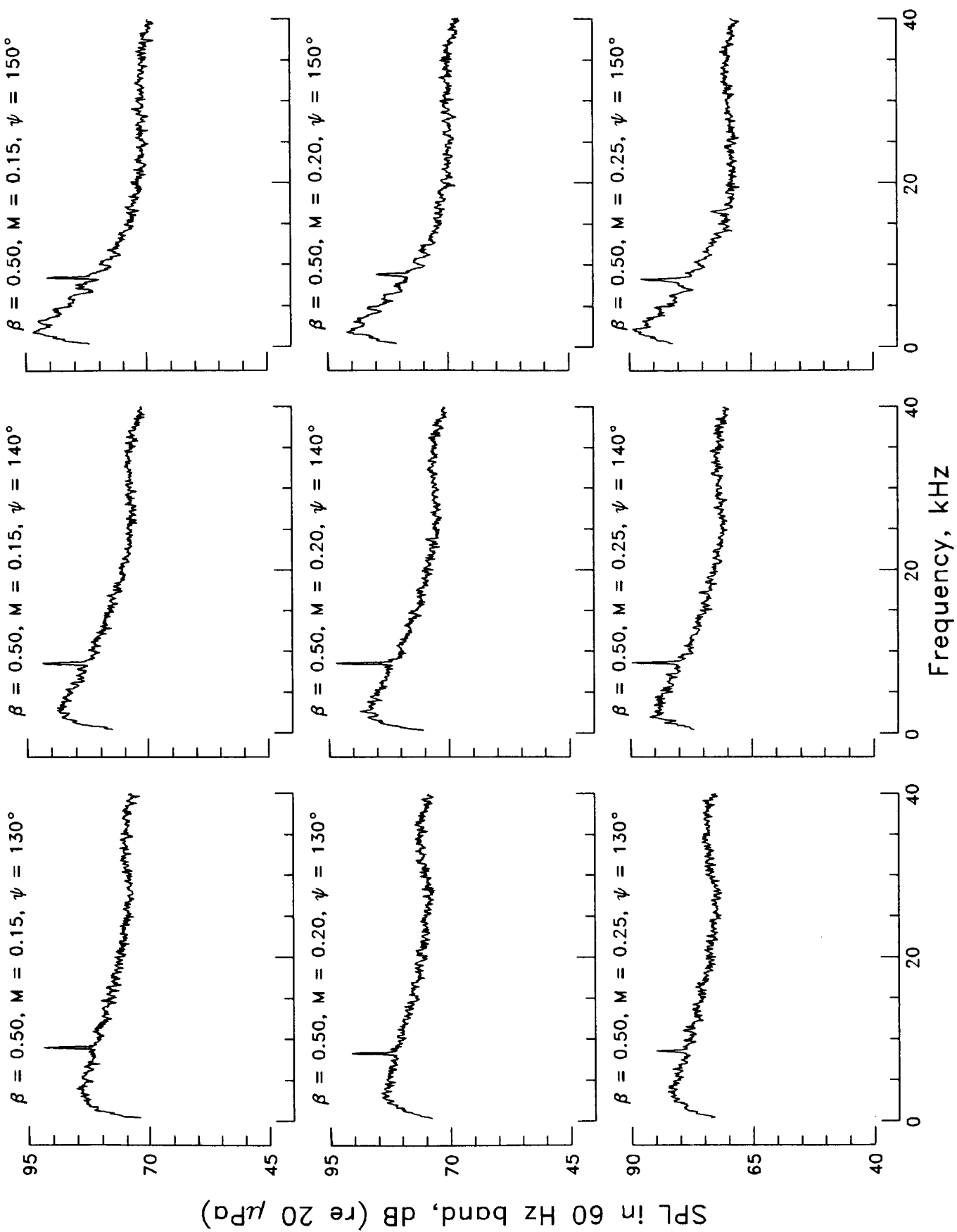


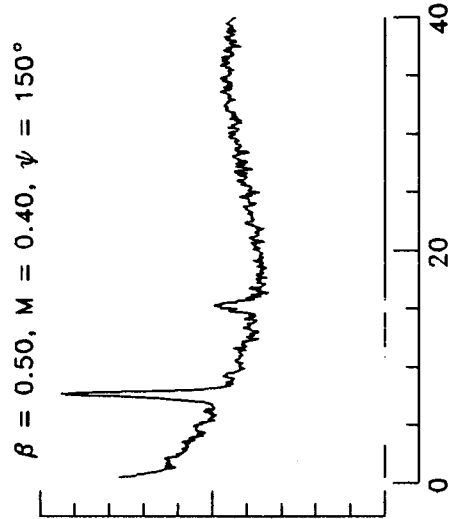
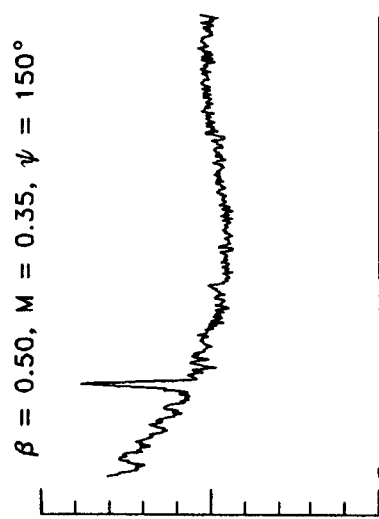
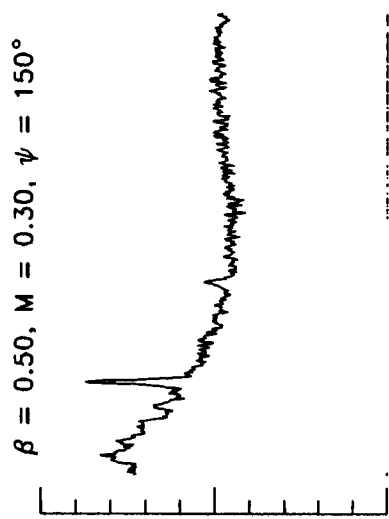
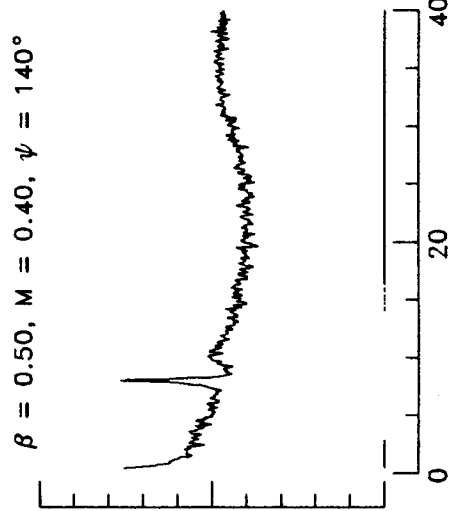
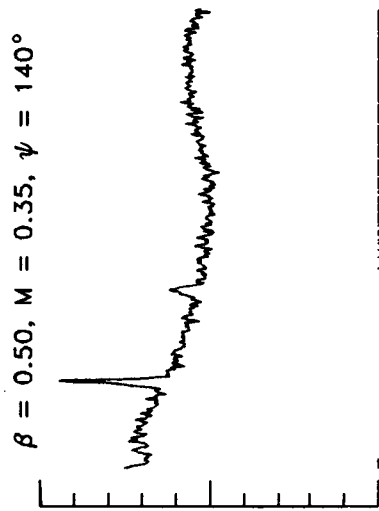
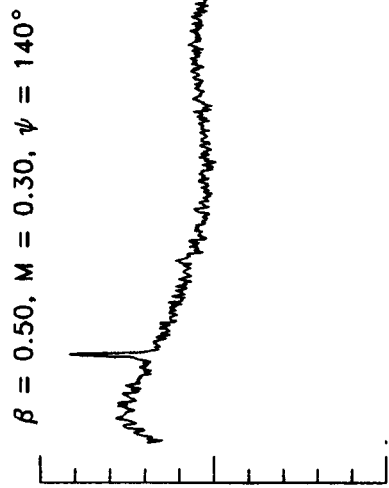
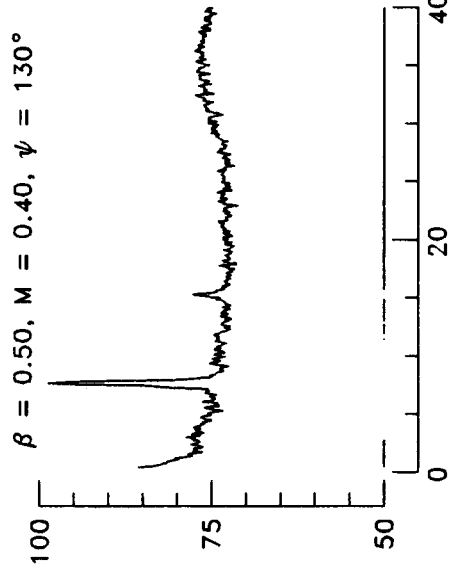
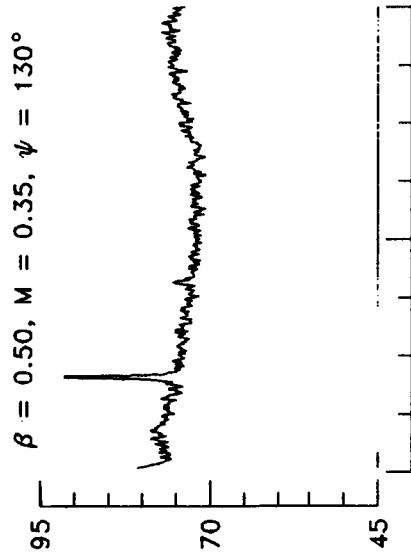
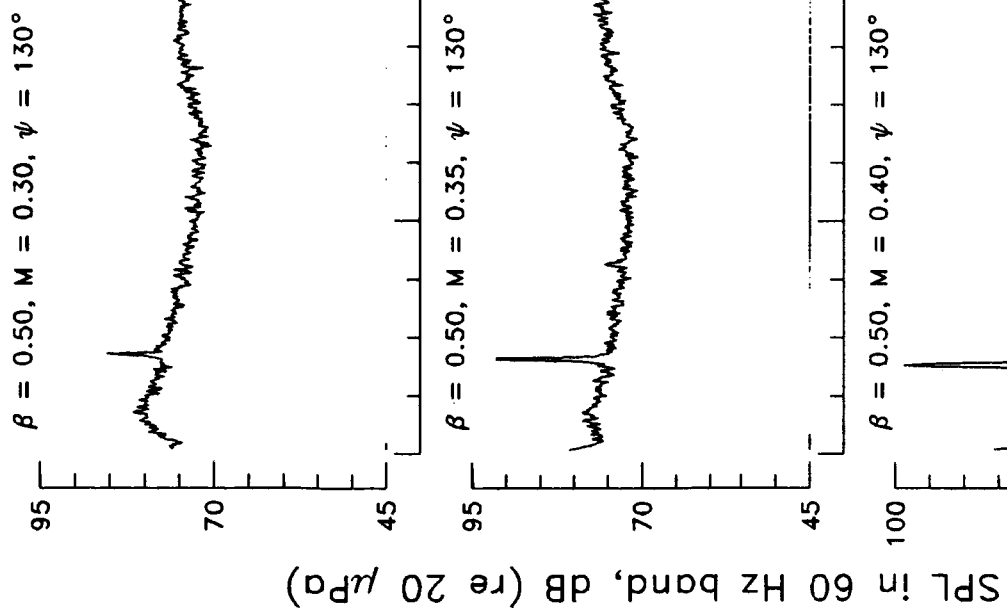




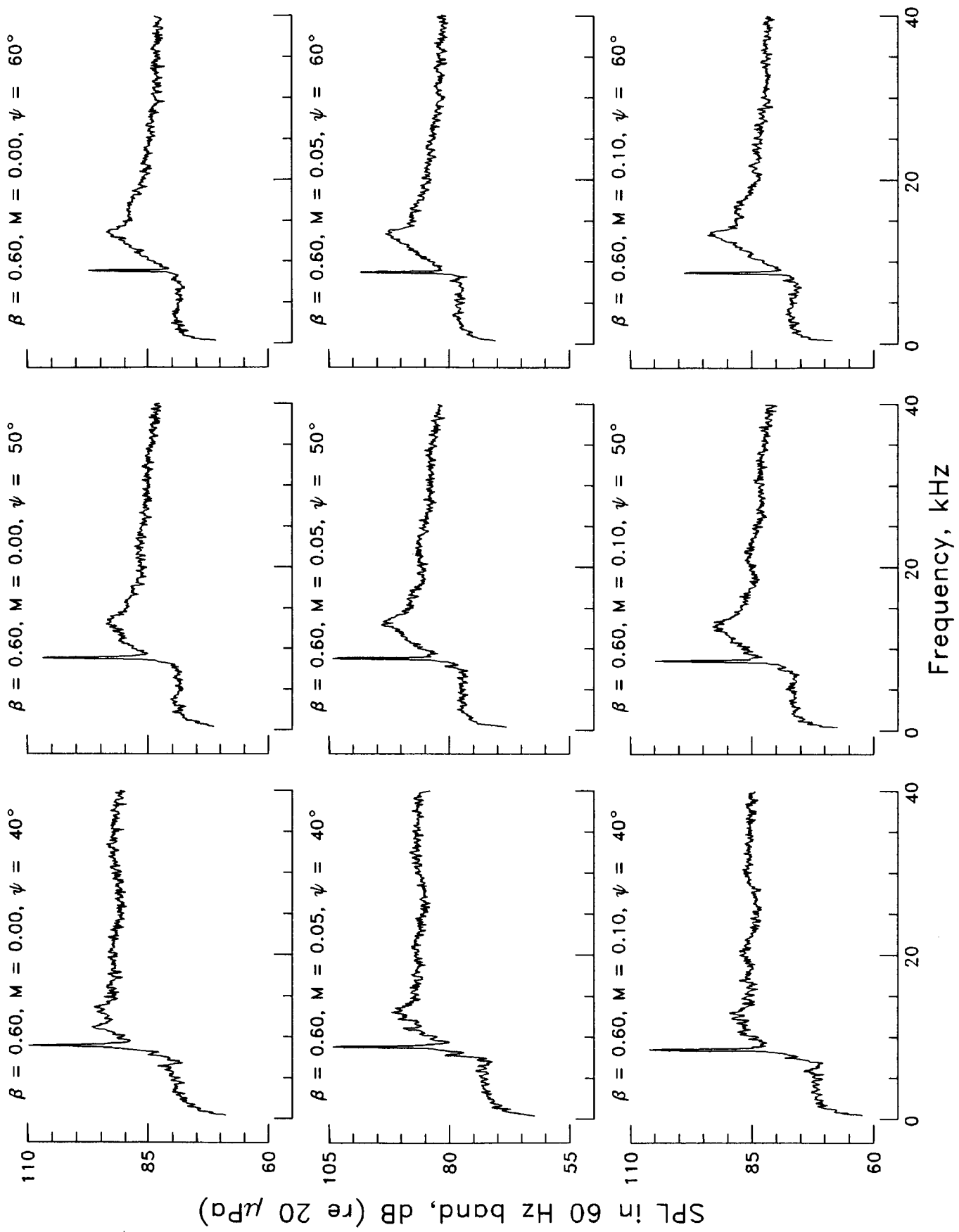
Frequency, kHz

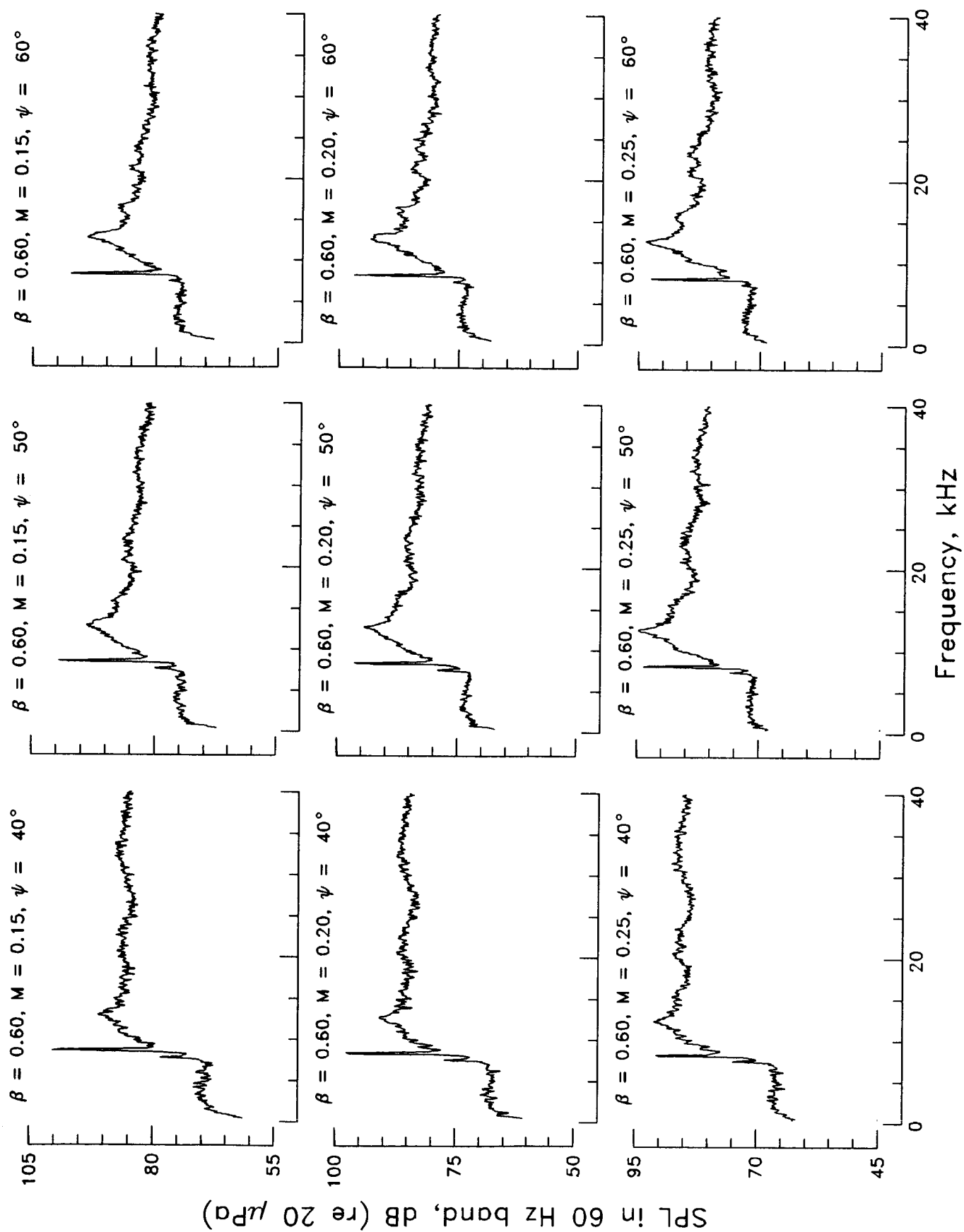
SPL in 60 Hz band, dB (re 20 μ Pa)

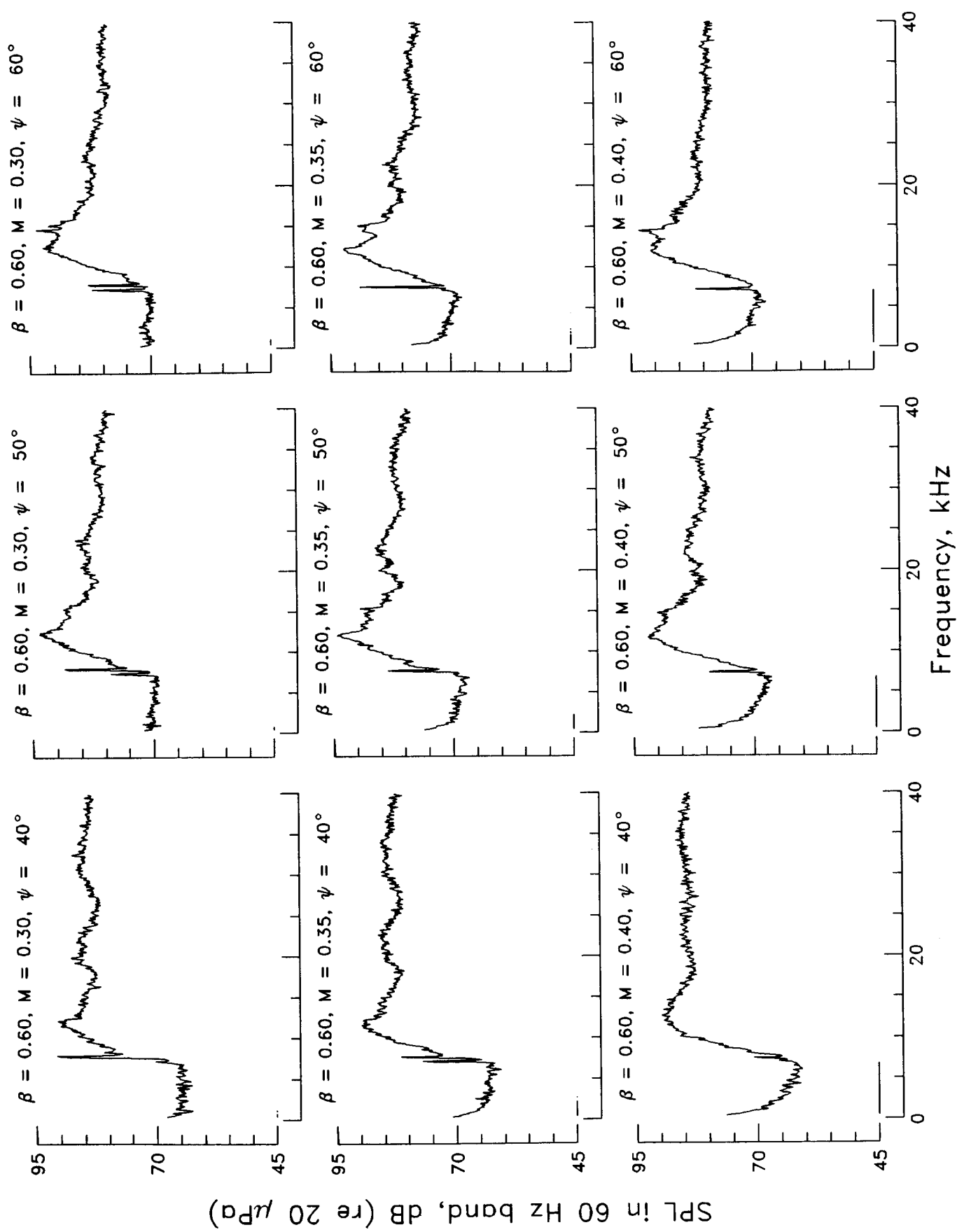


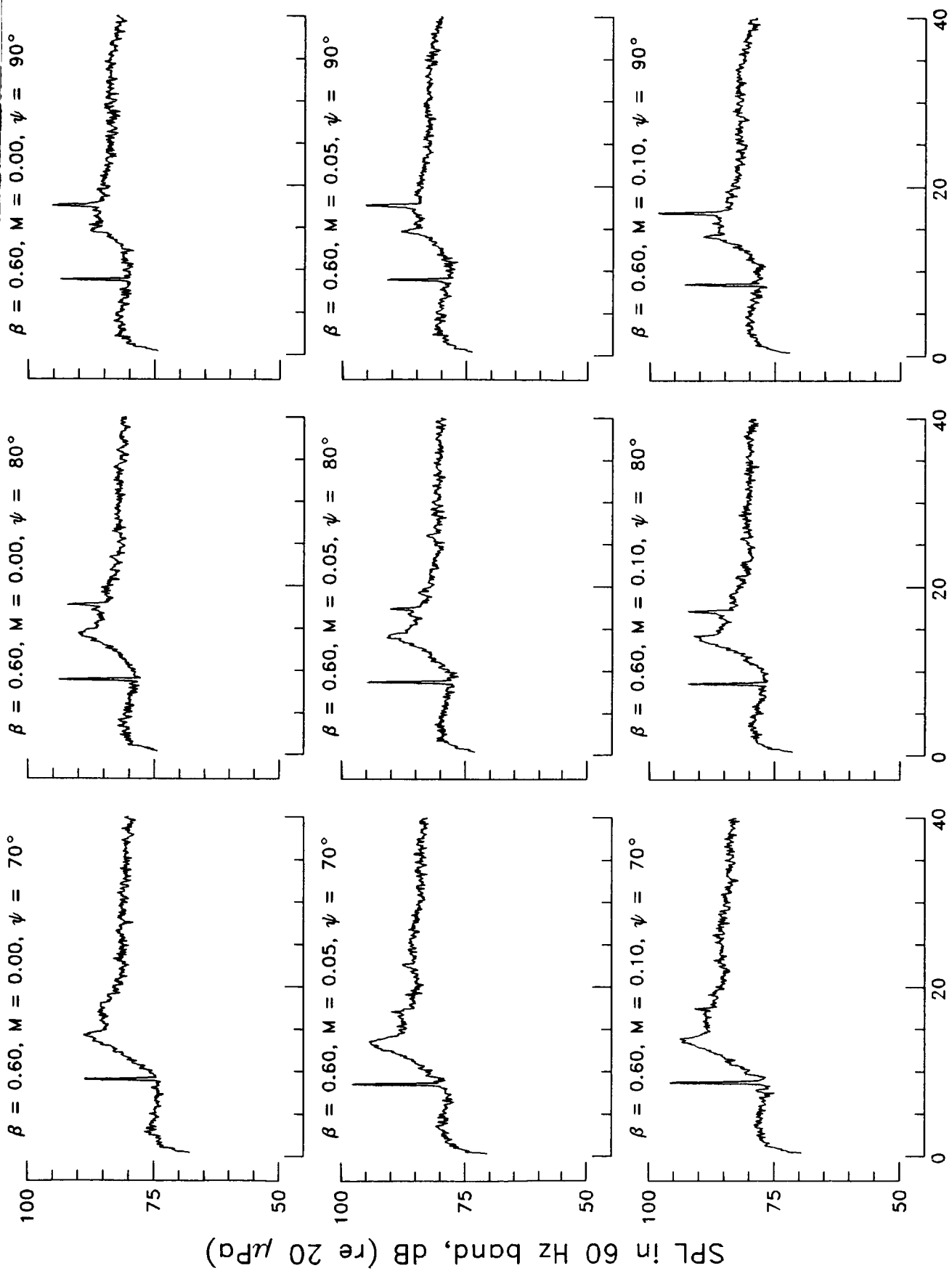


Frequency, kHz

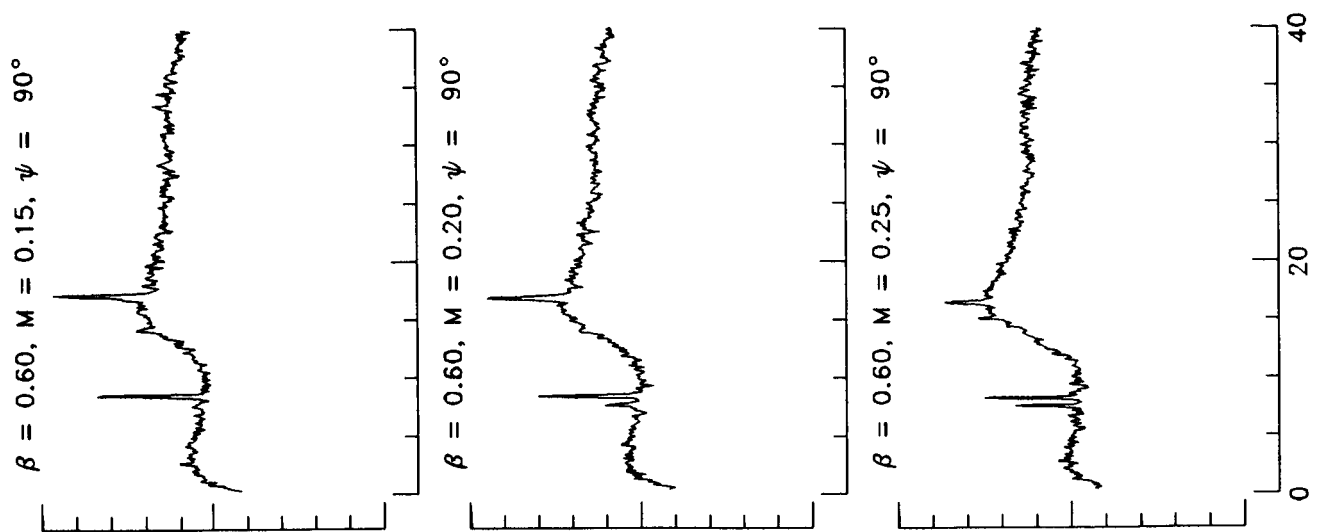
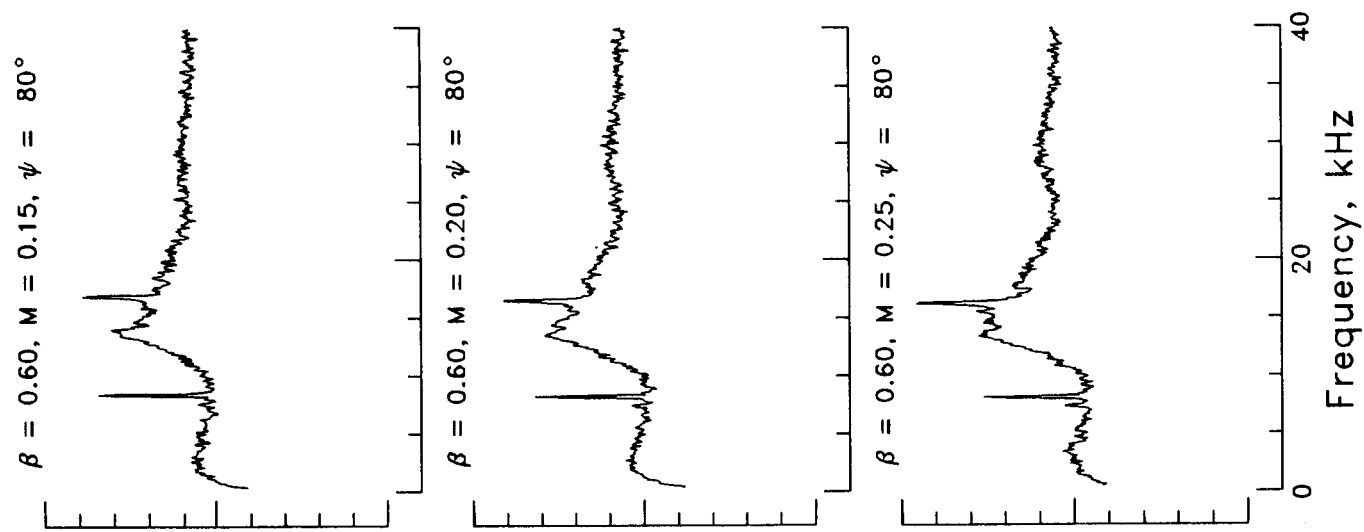
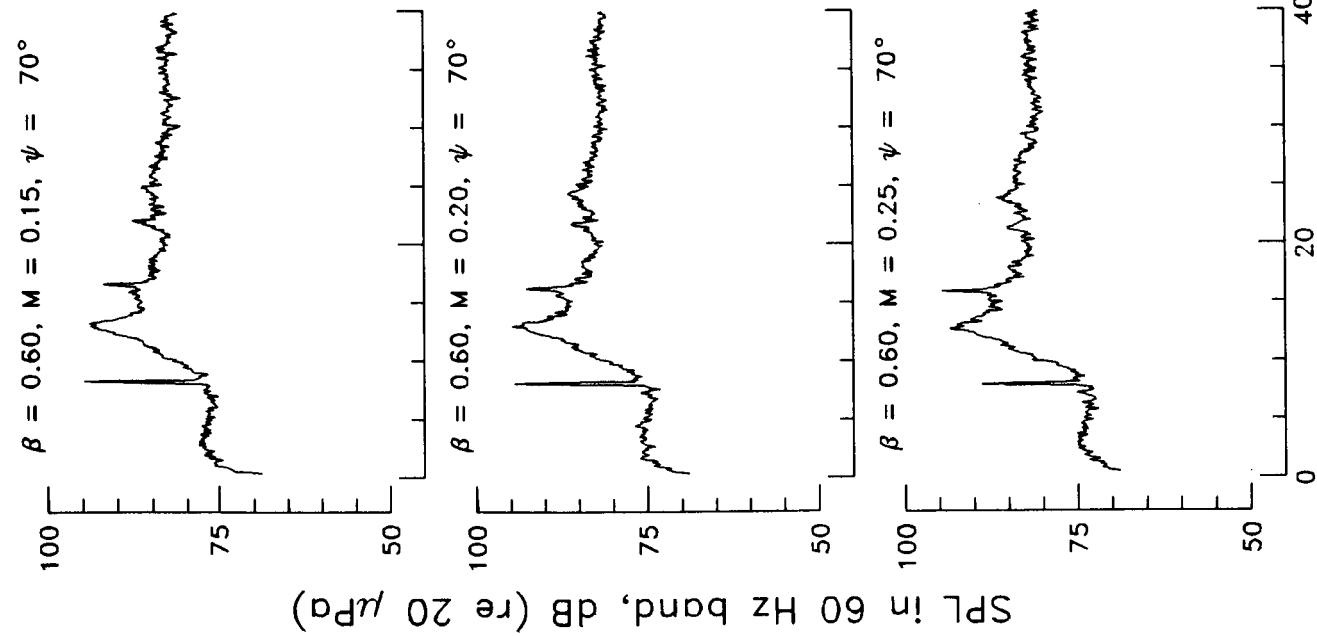


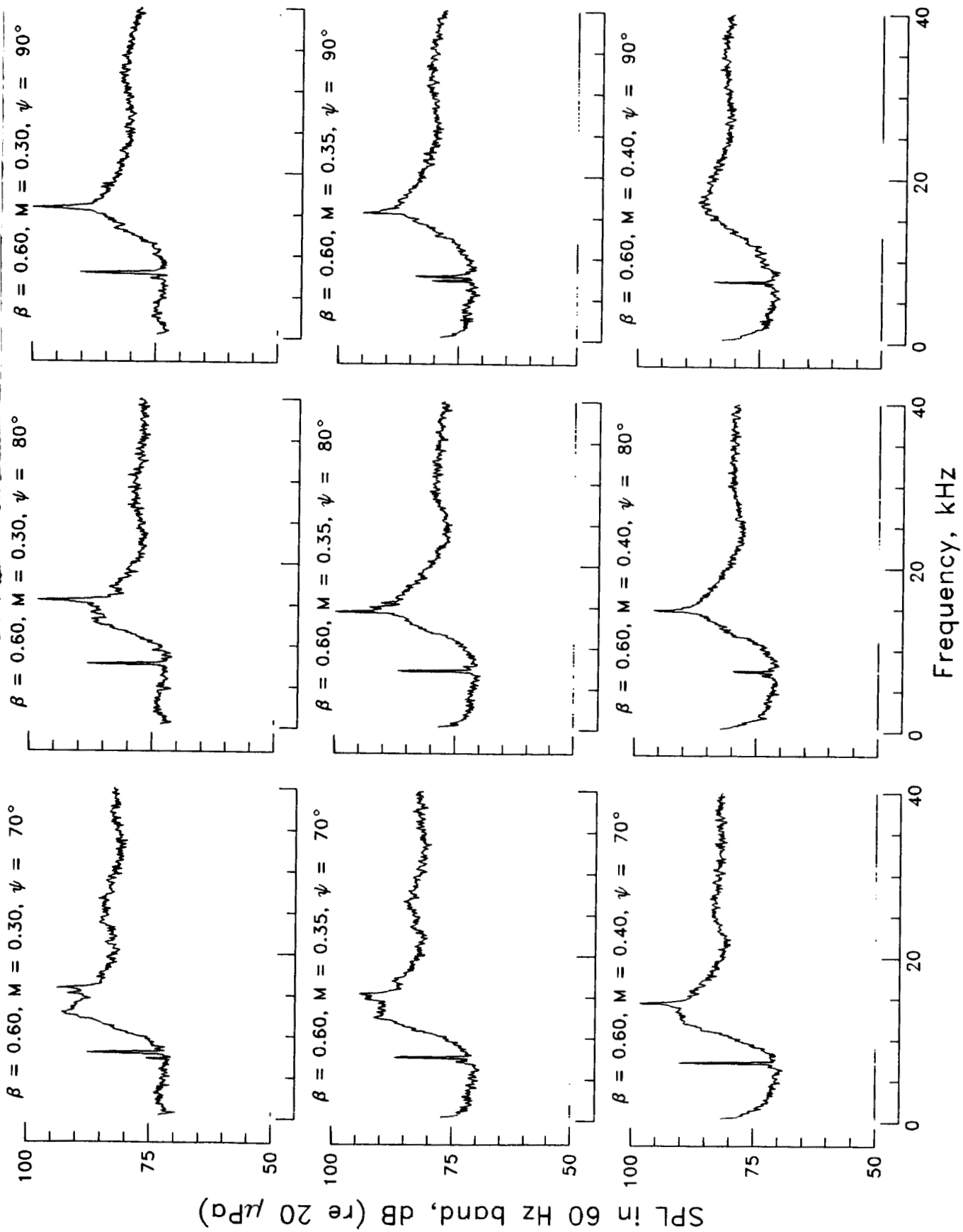




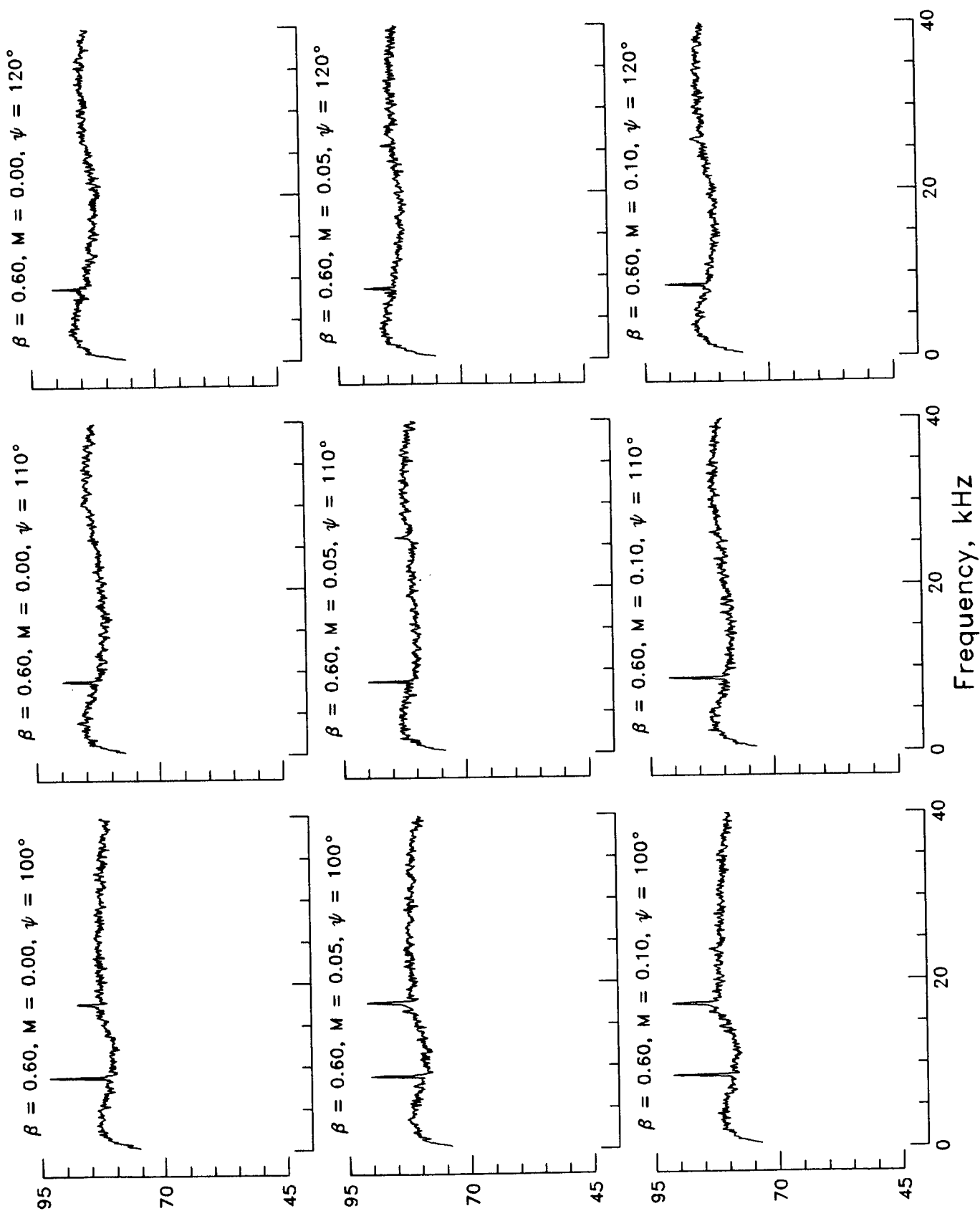


Frequency, kHz

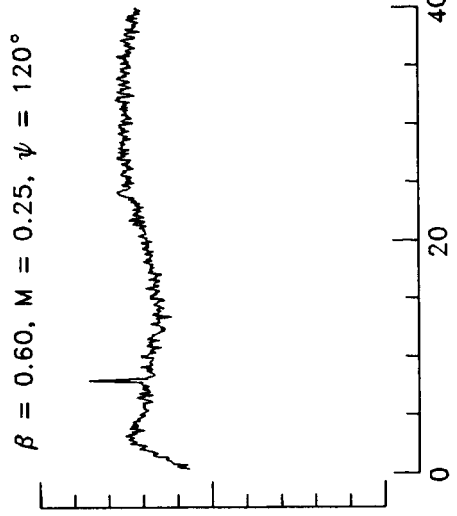
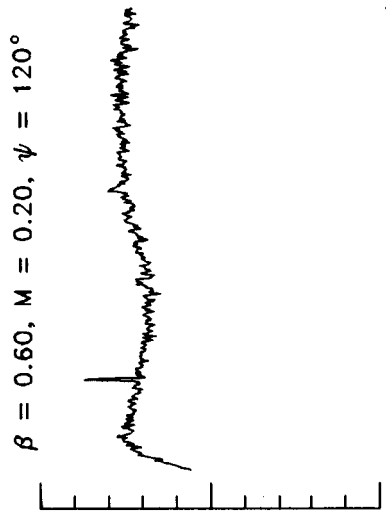
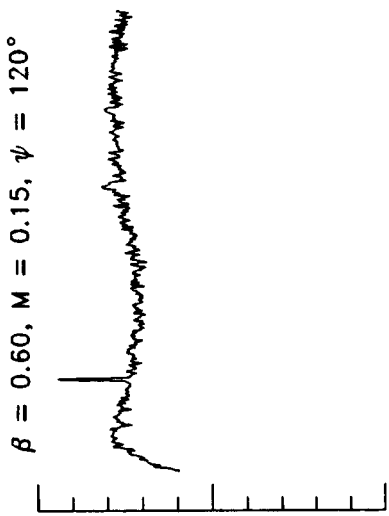
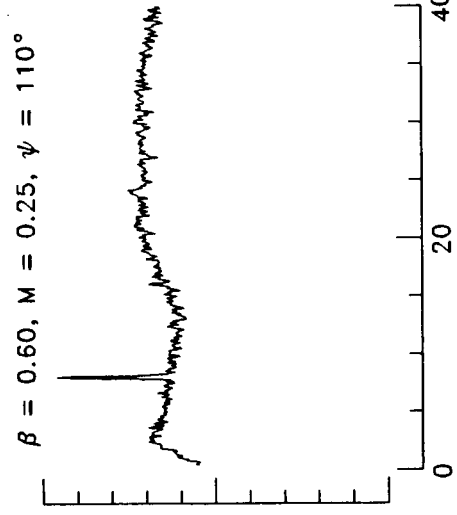
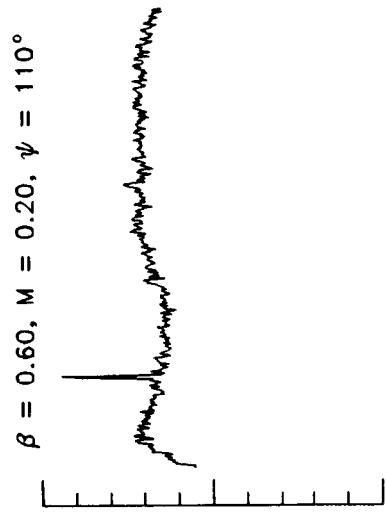
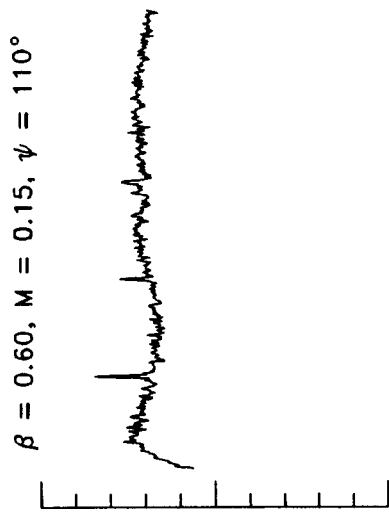
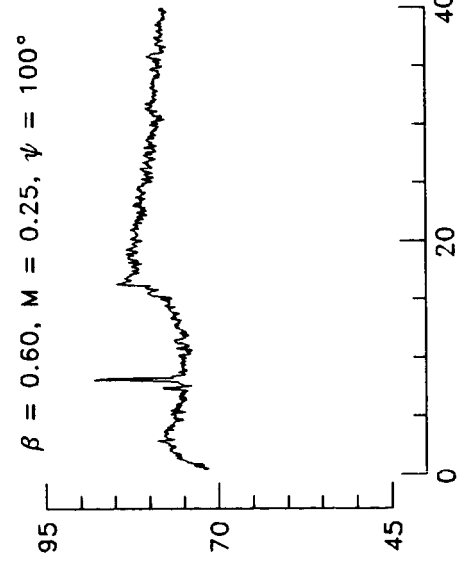
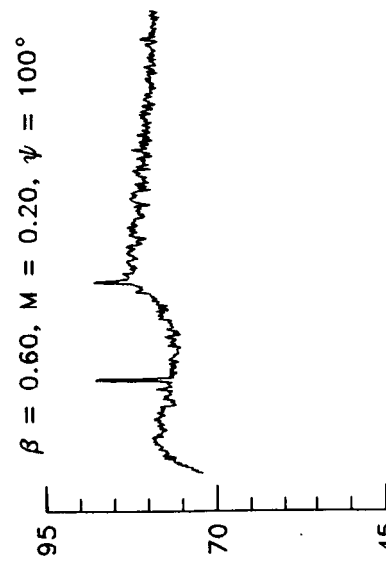
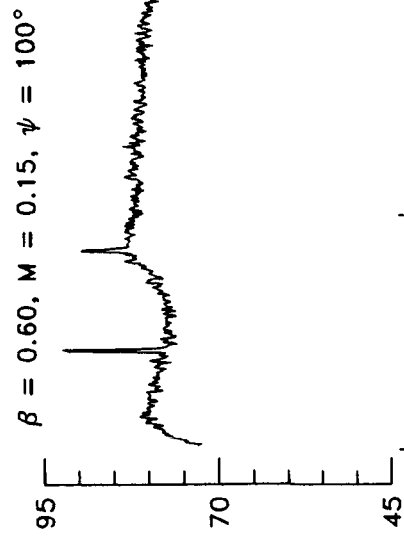




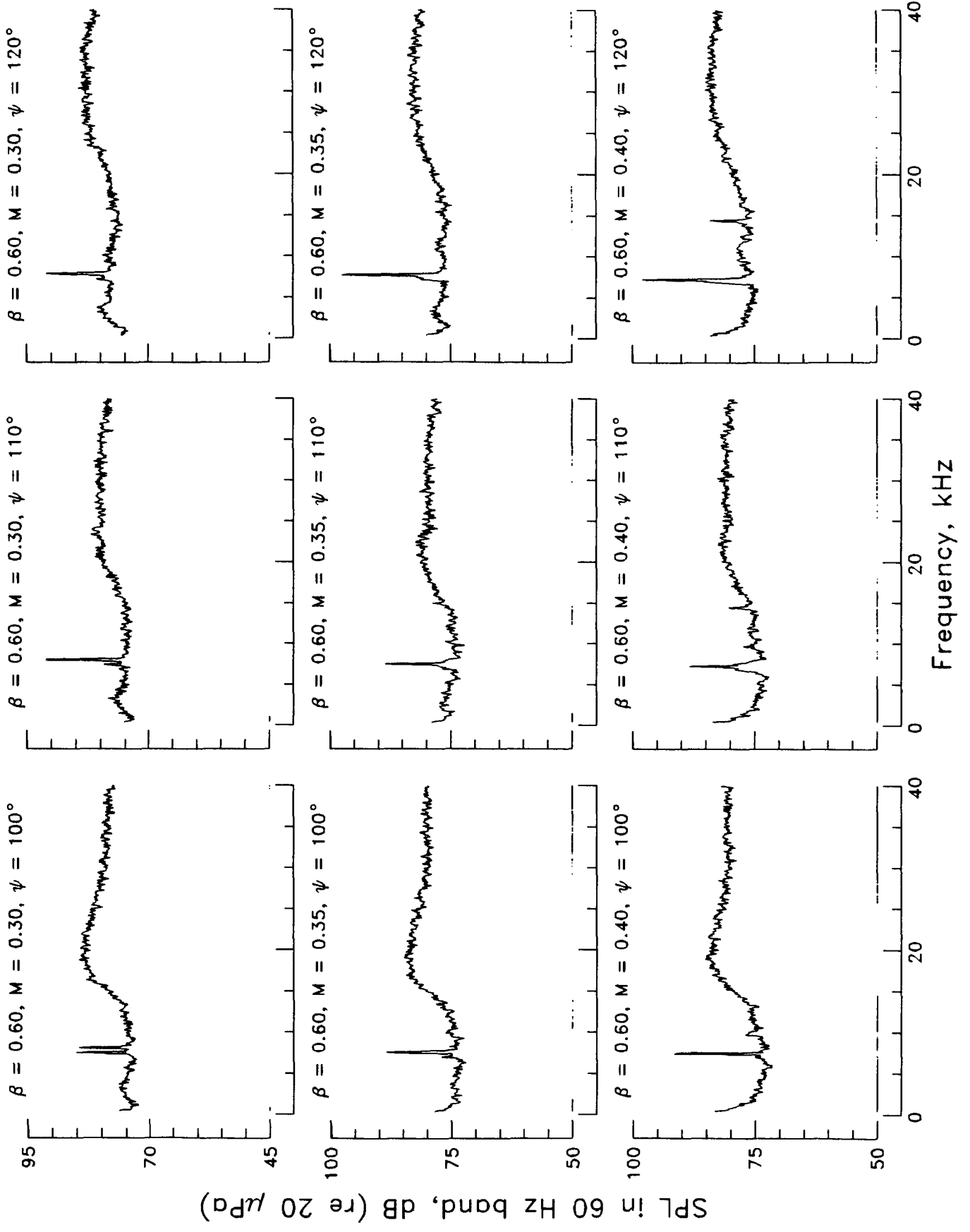
SPL in 60 Hz band, dB (re 20 μ Pd)

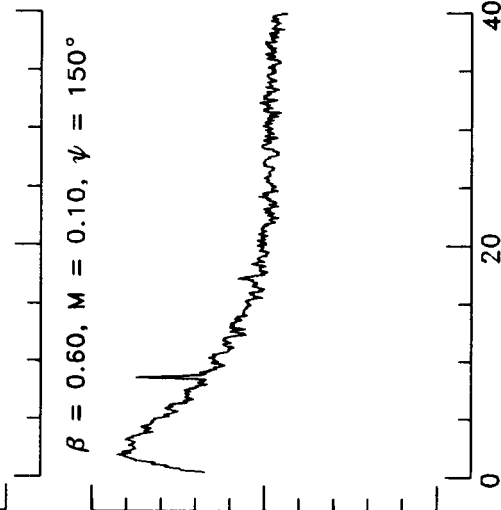
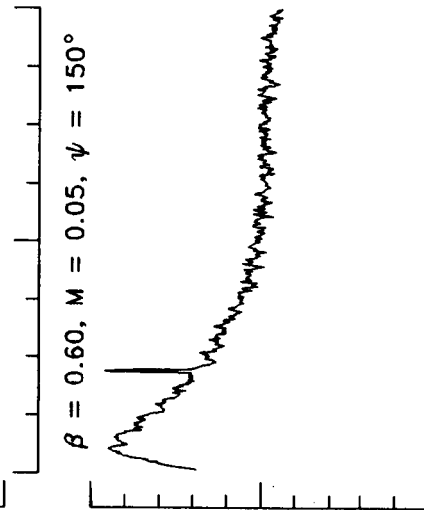
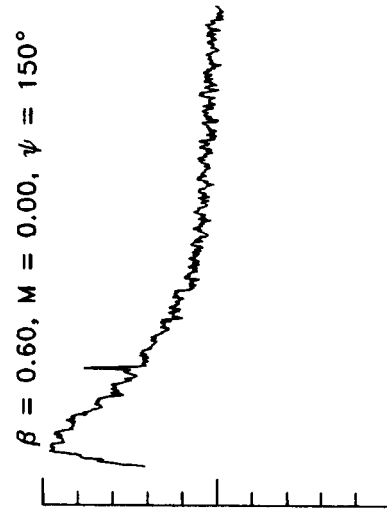
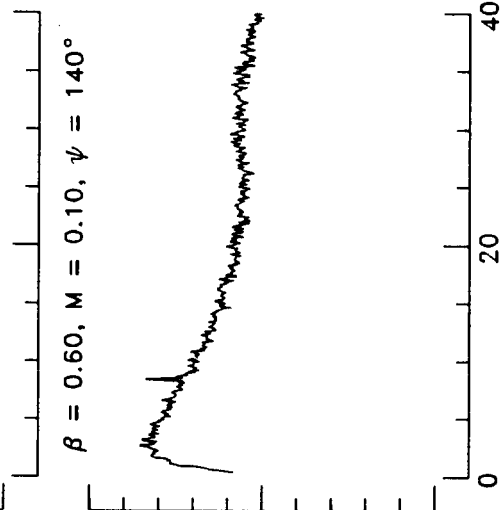
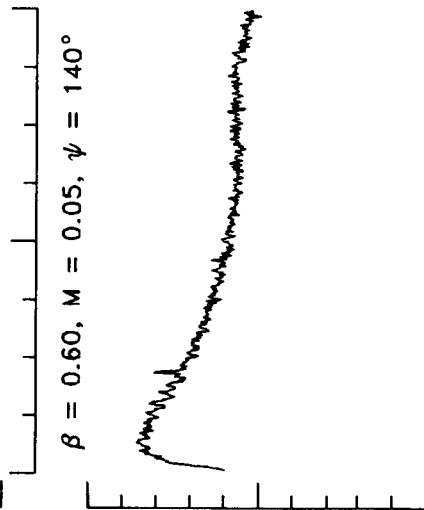
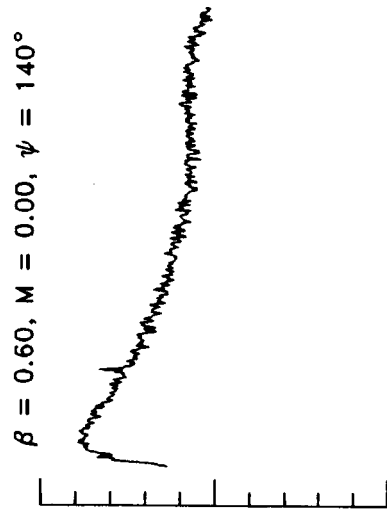
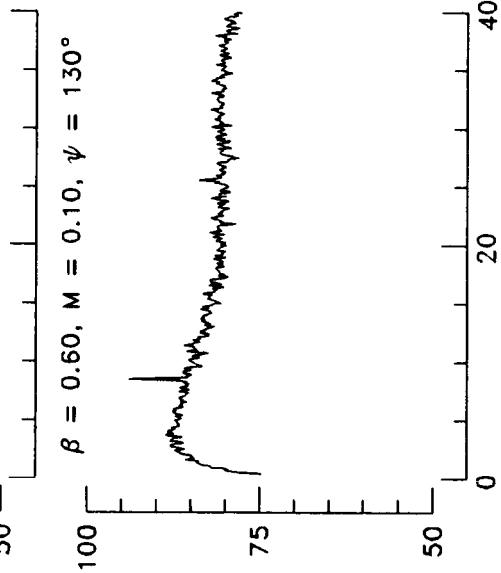
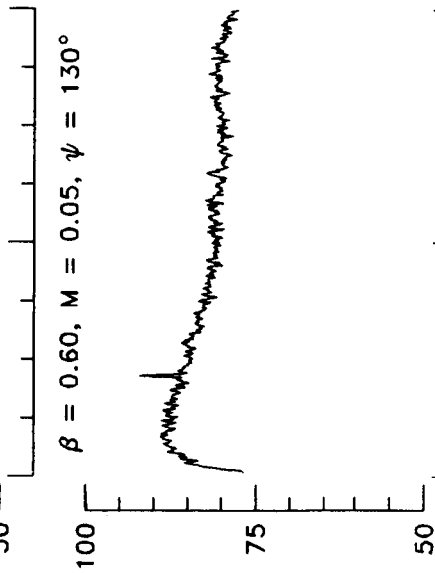
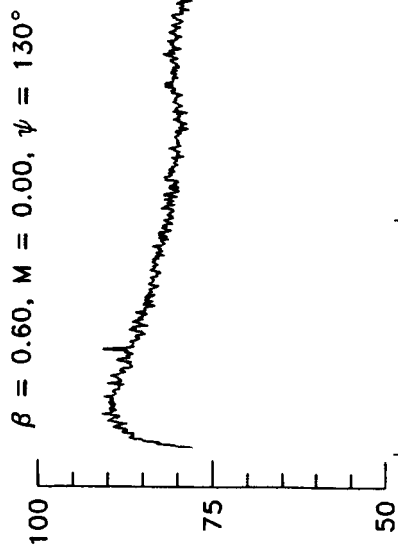


SPL in 60 Hz band, dB (re 20 μ Pa)



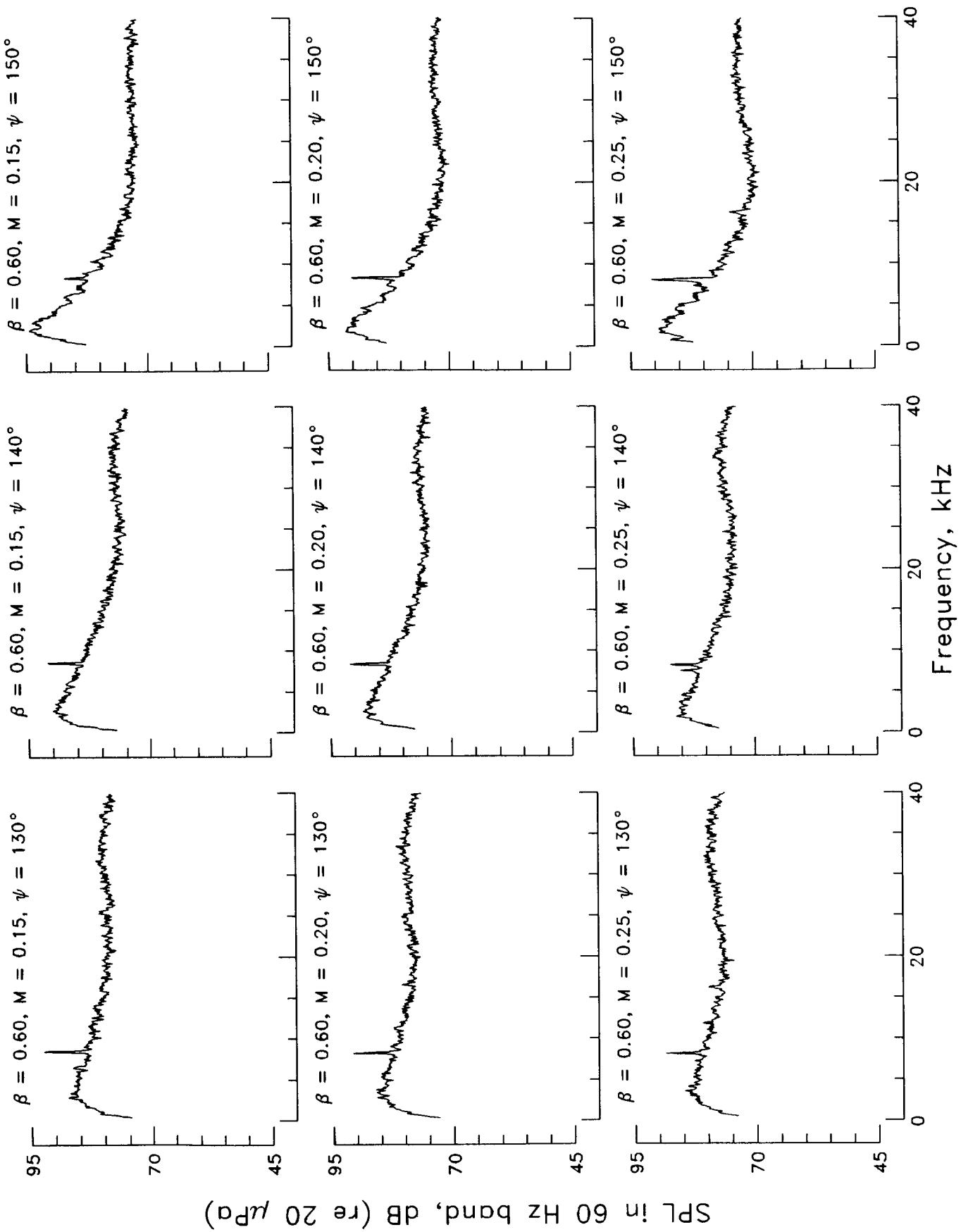
Frequency, kHz

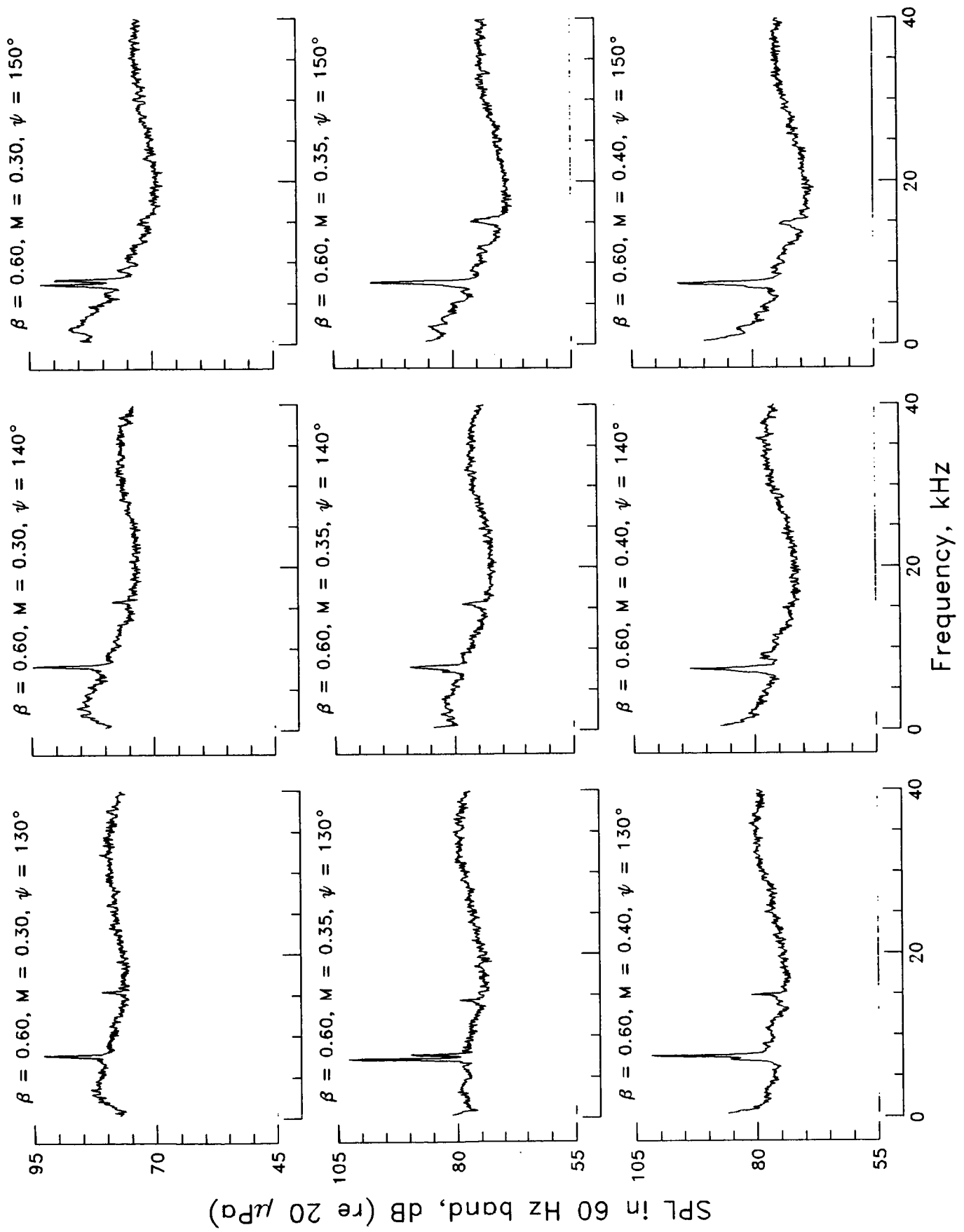


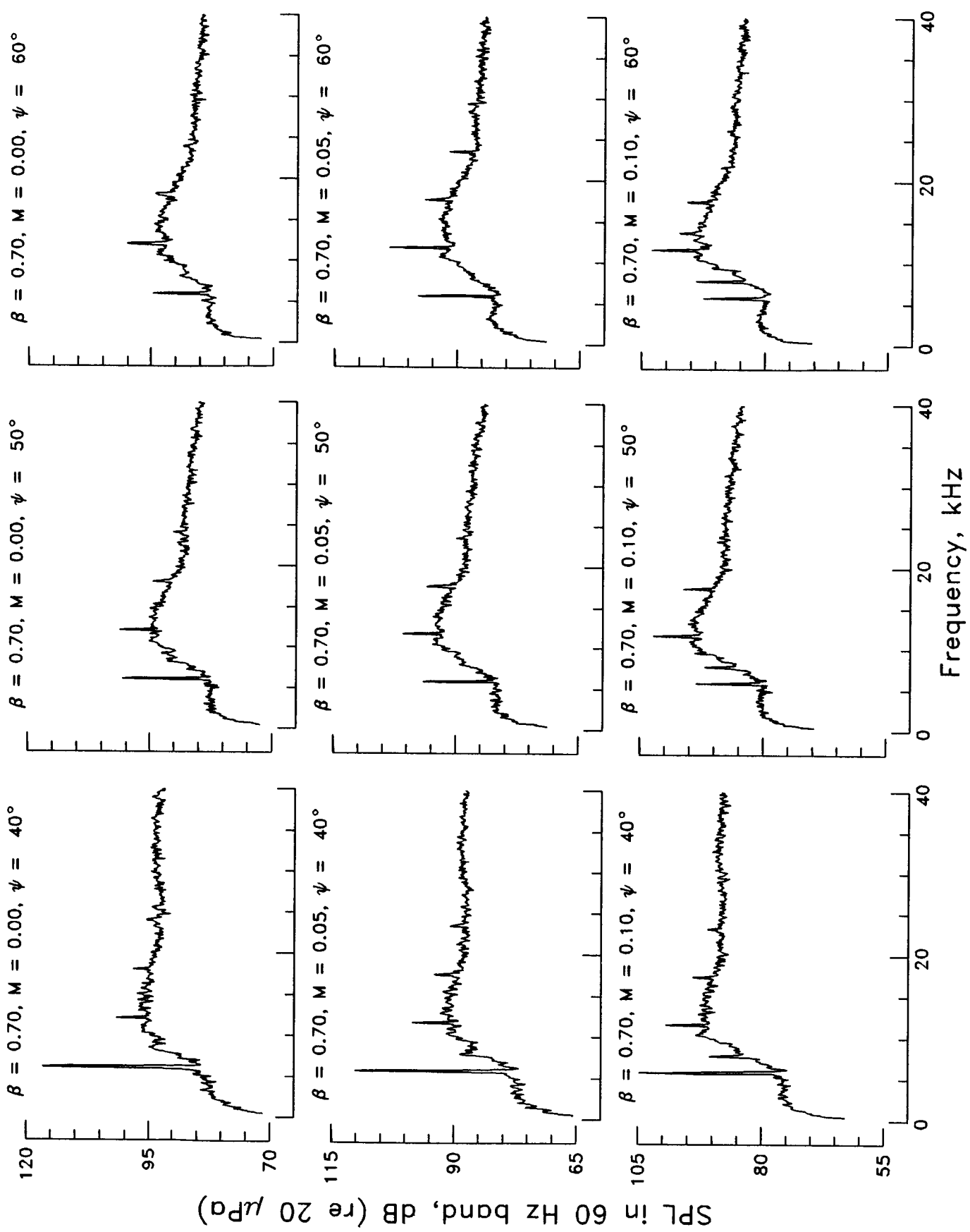


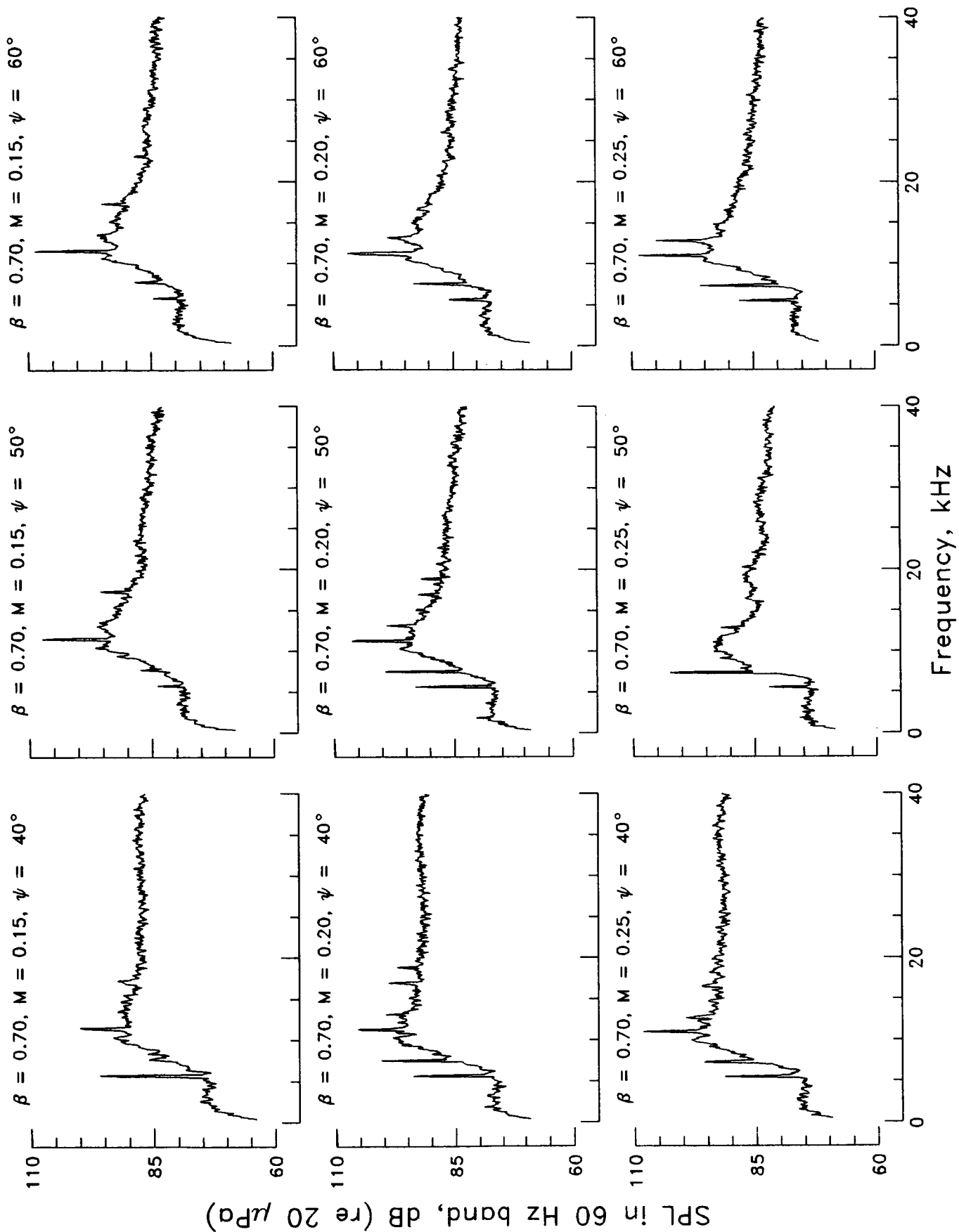
SPL in 60 Hz band, dB (re 20 μ Pa)

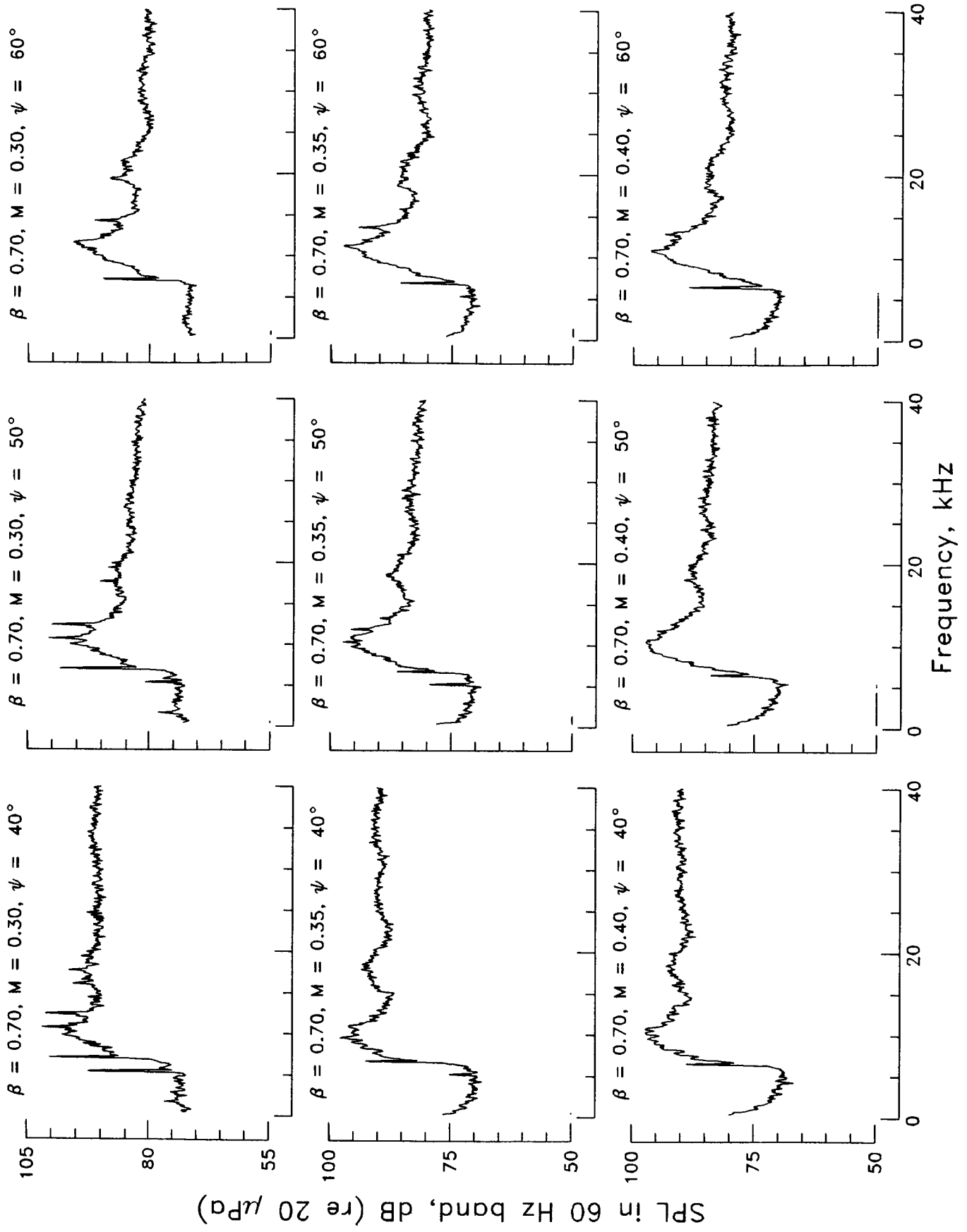
Frequency, kHz

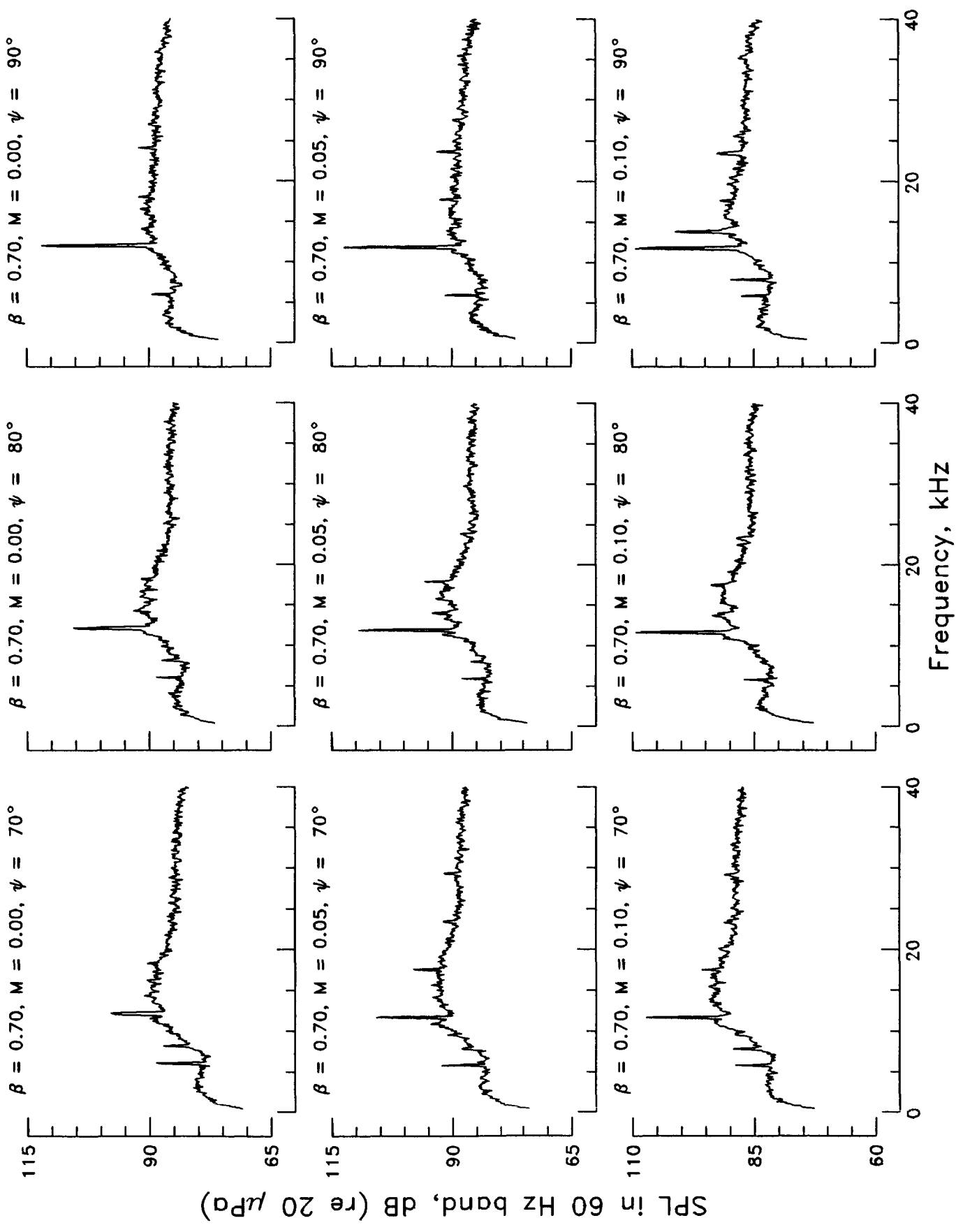


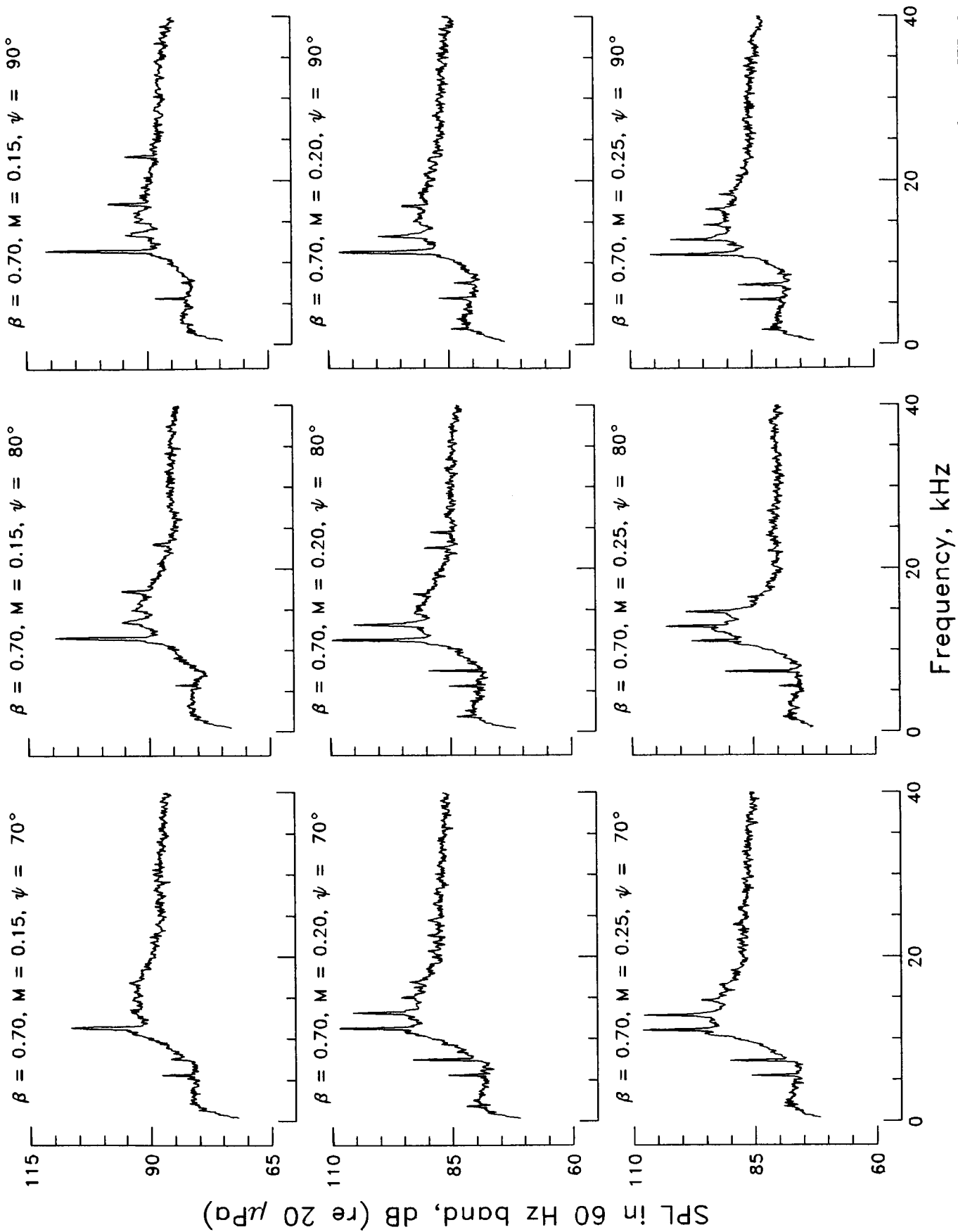


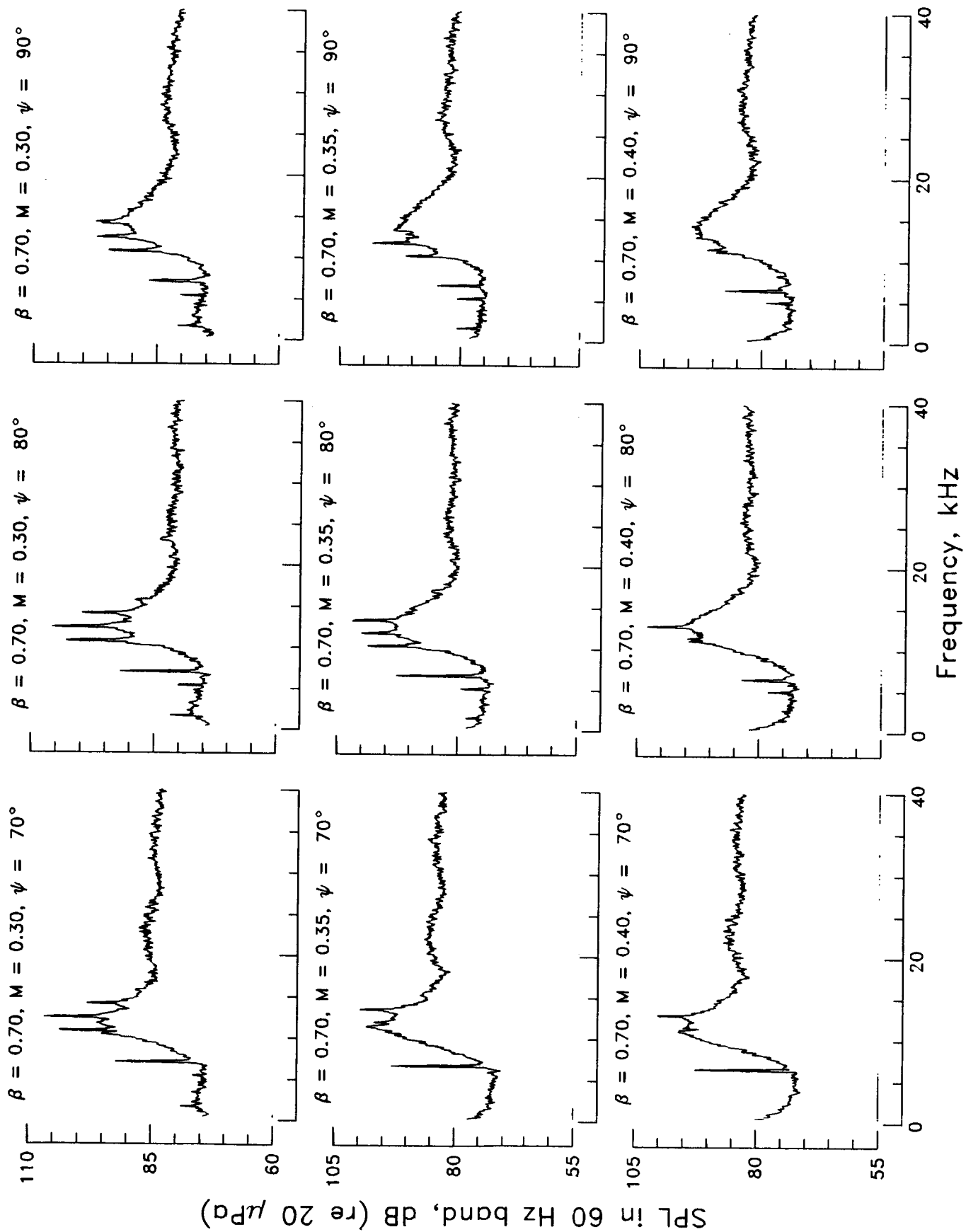


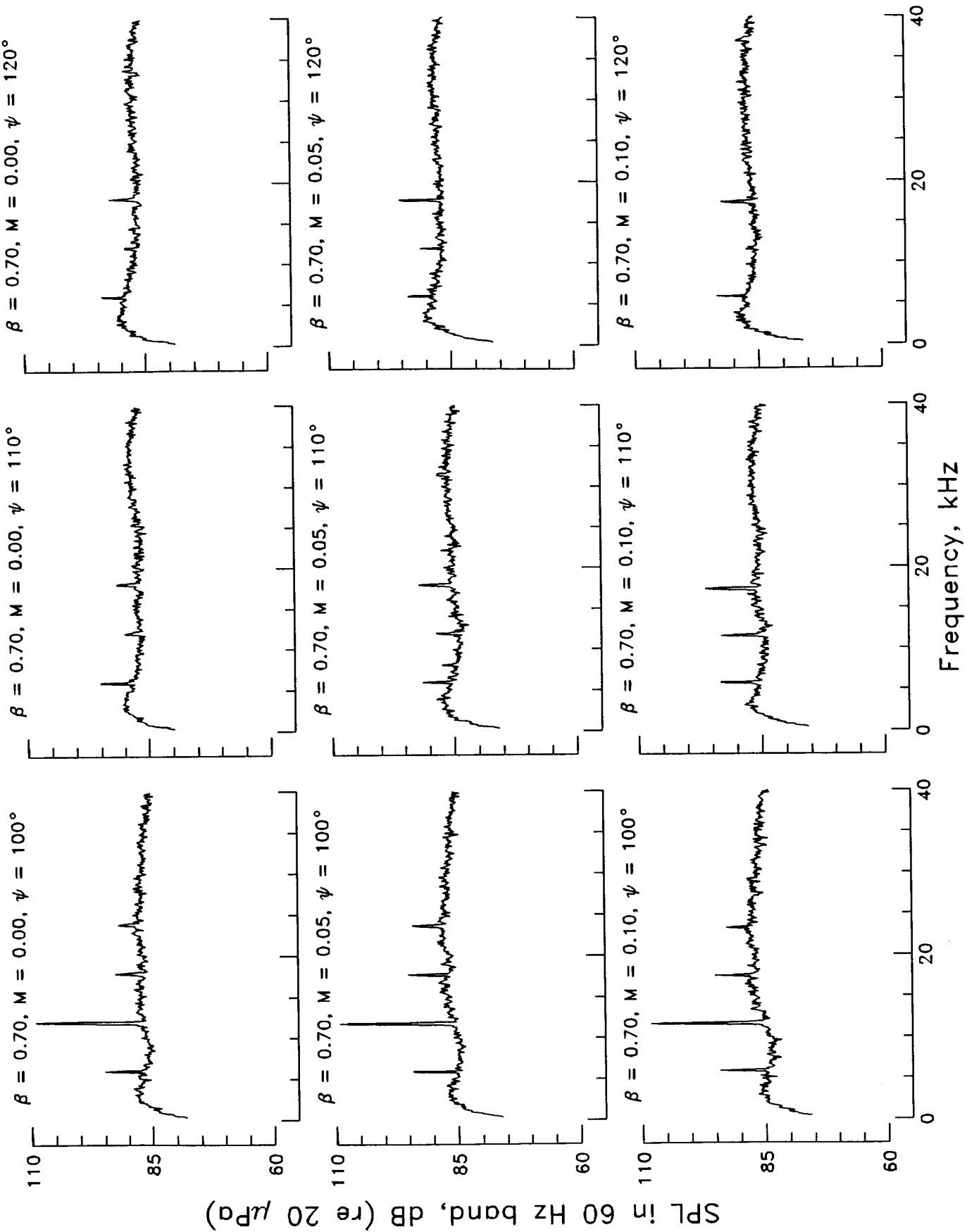




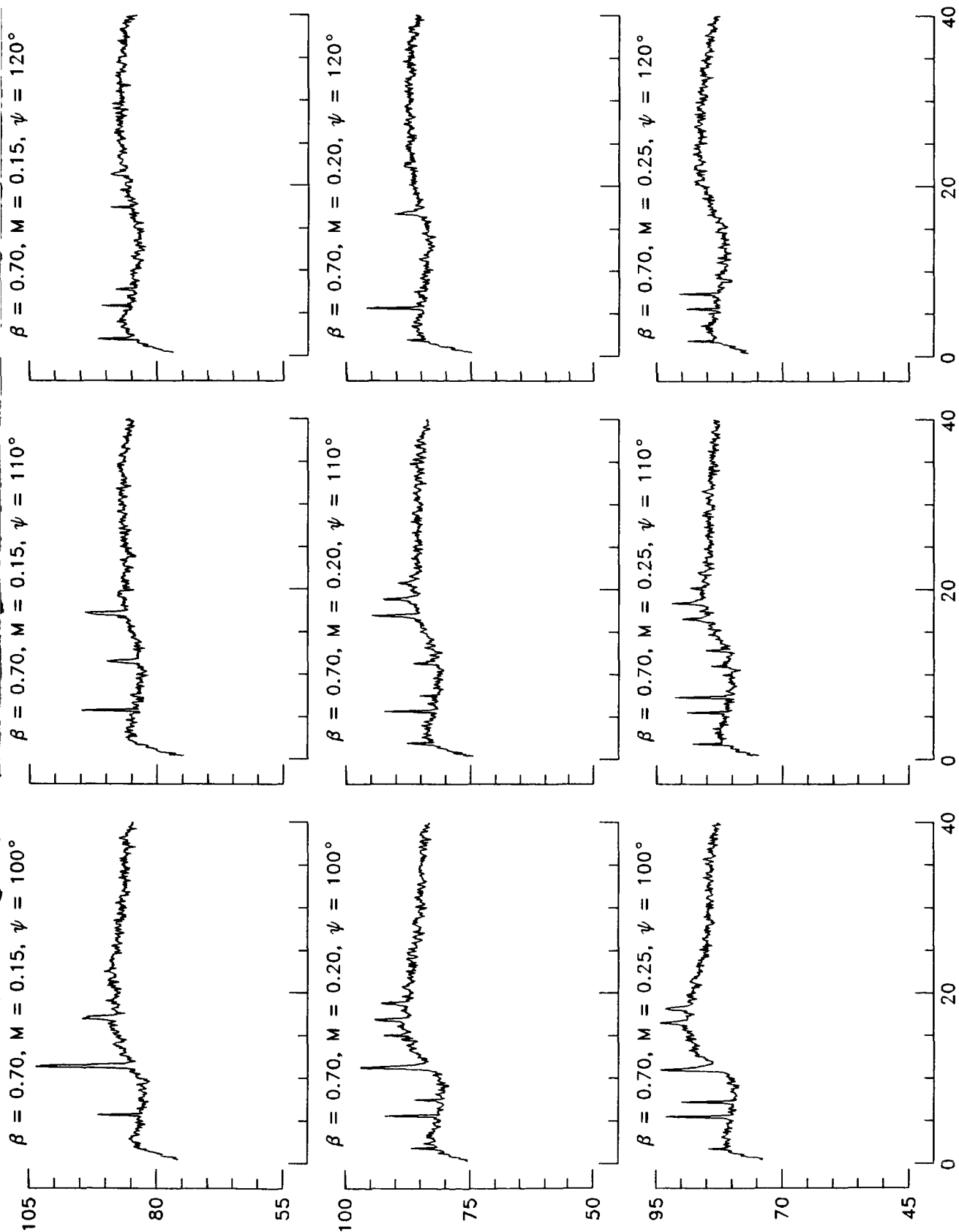






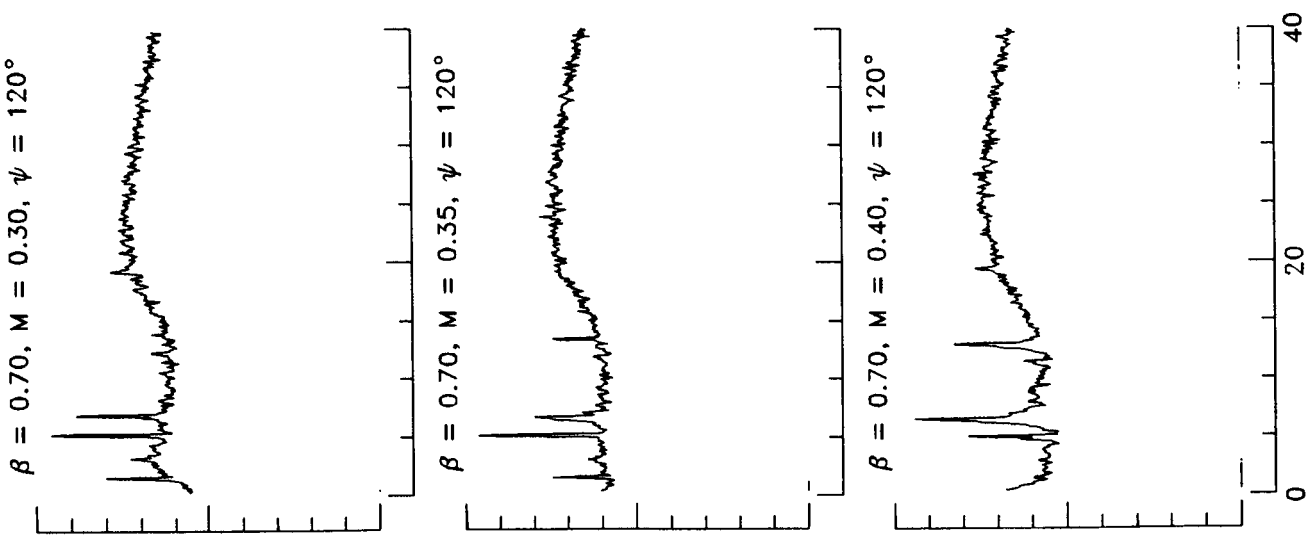
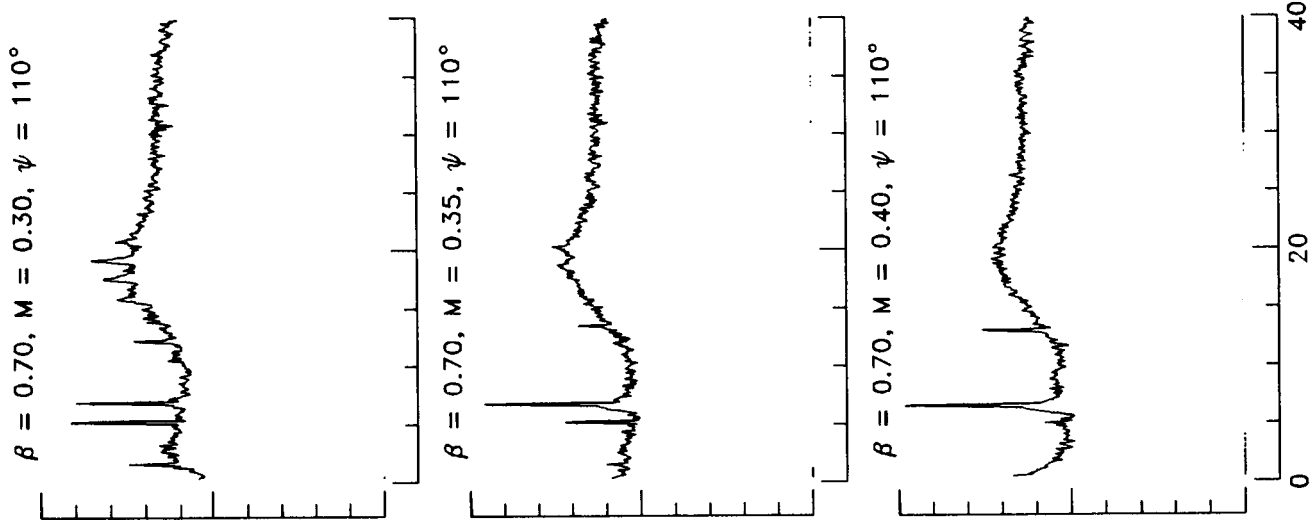
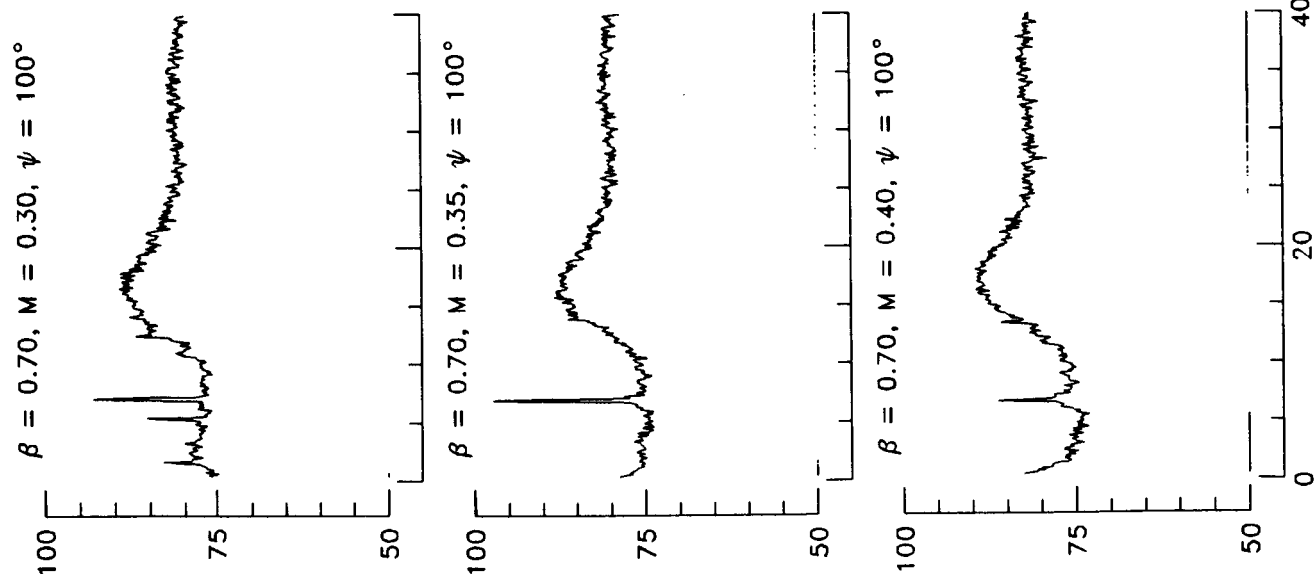


SPL in 60 Hz band, dB (re 20 μ Fa)

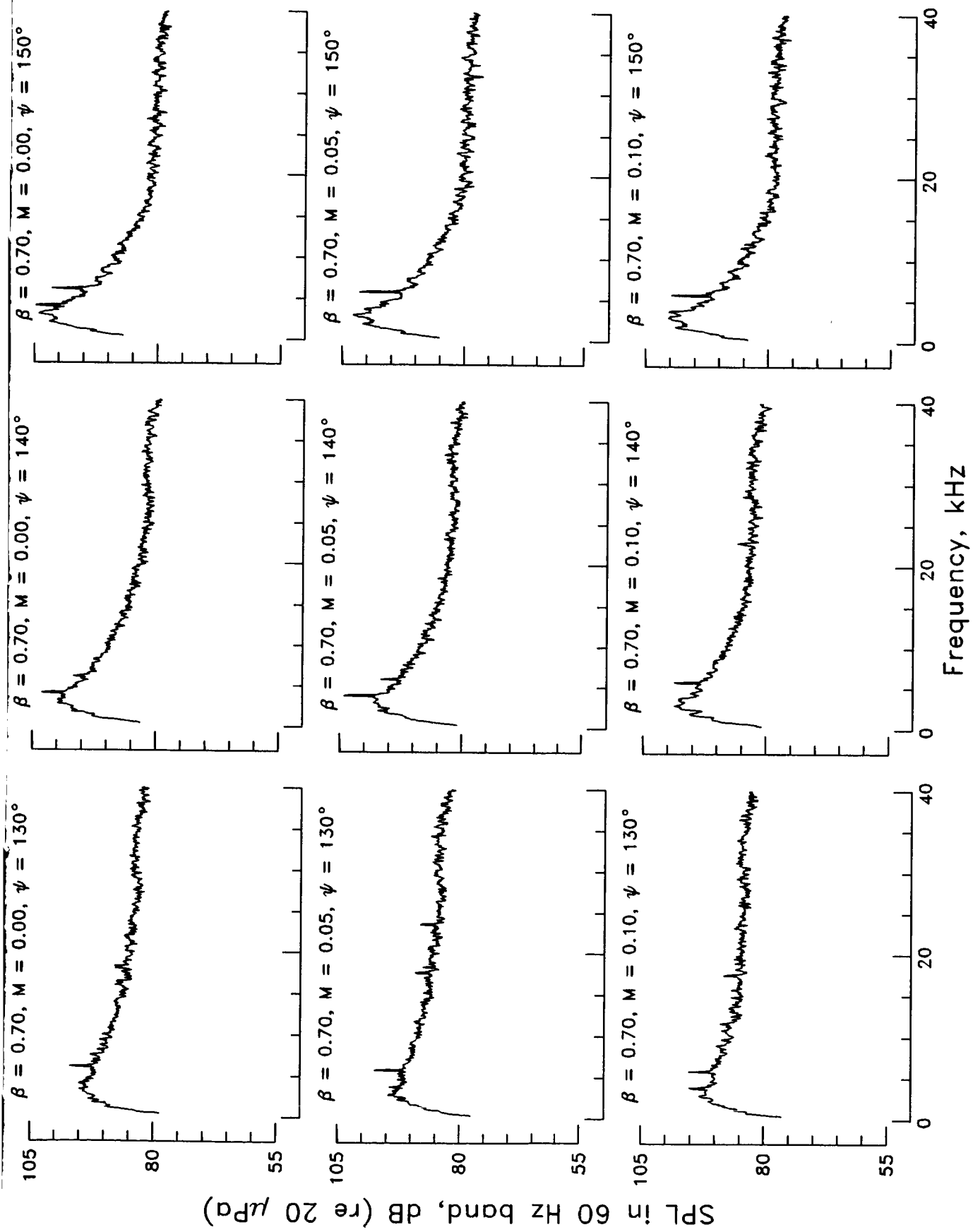


Frequency, kHz

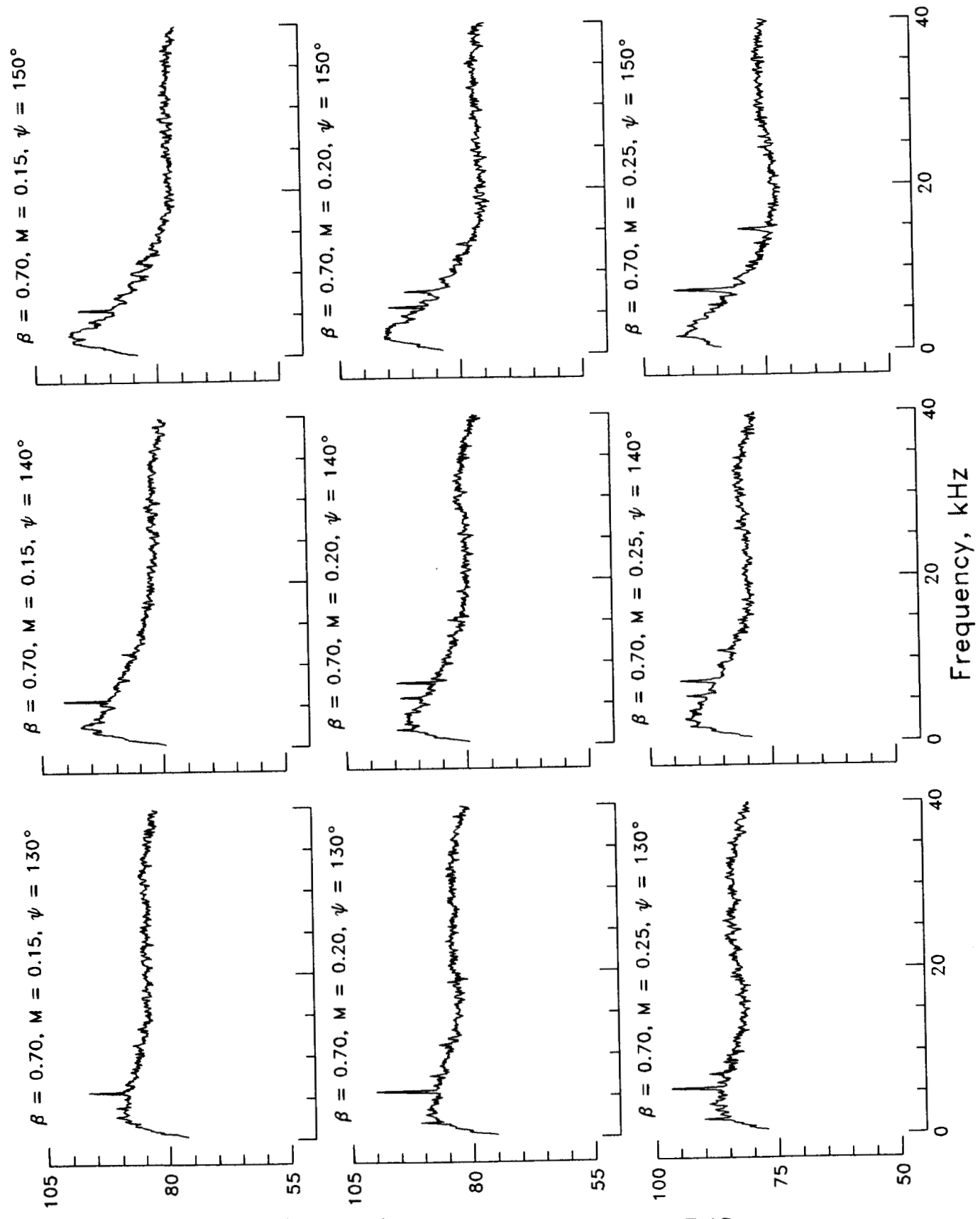
SPL in 60 Hz band, dB (re 20 μ Pd)

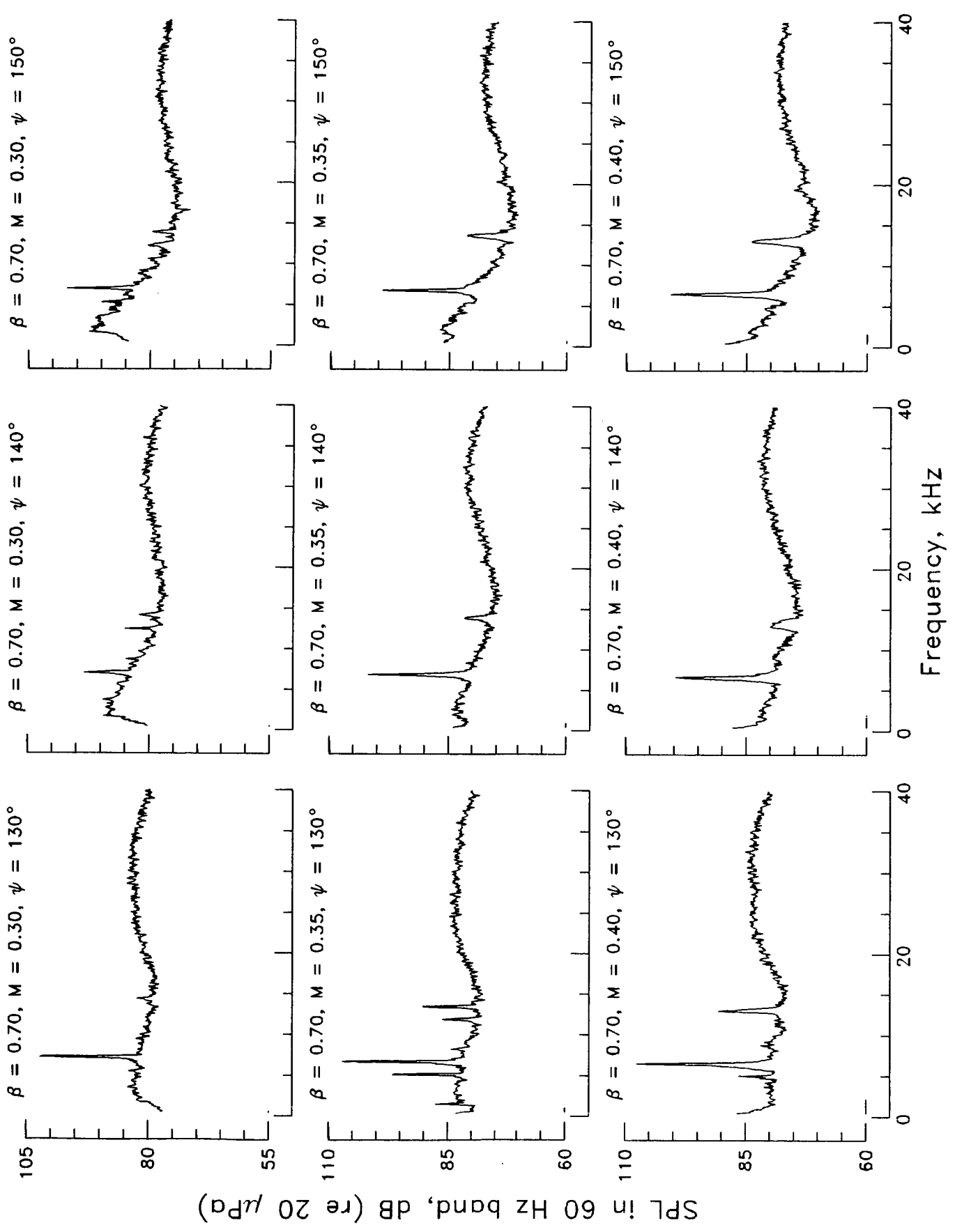


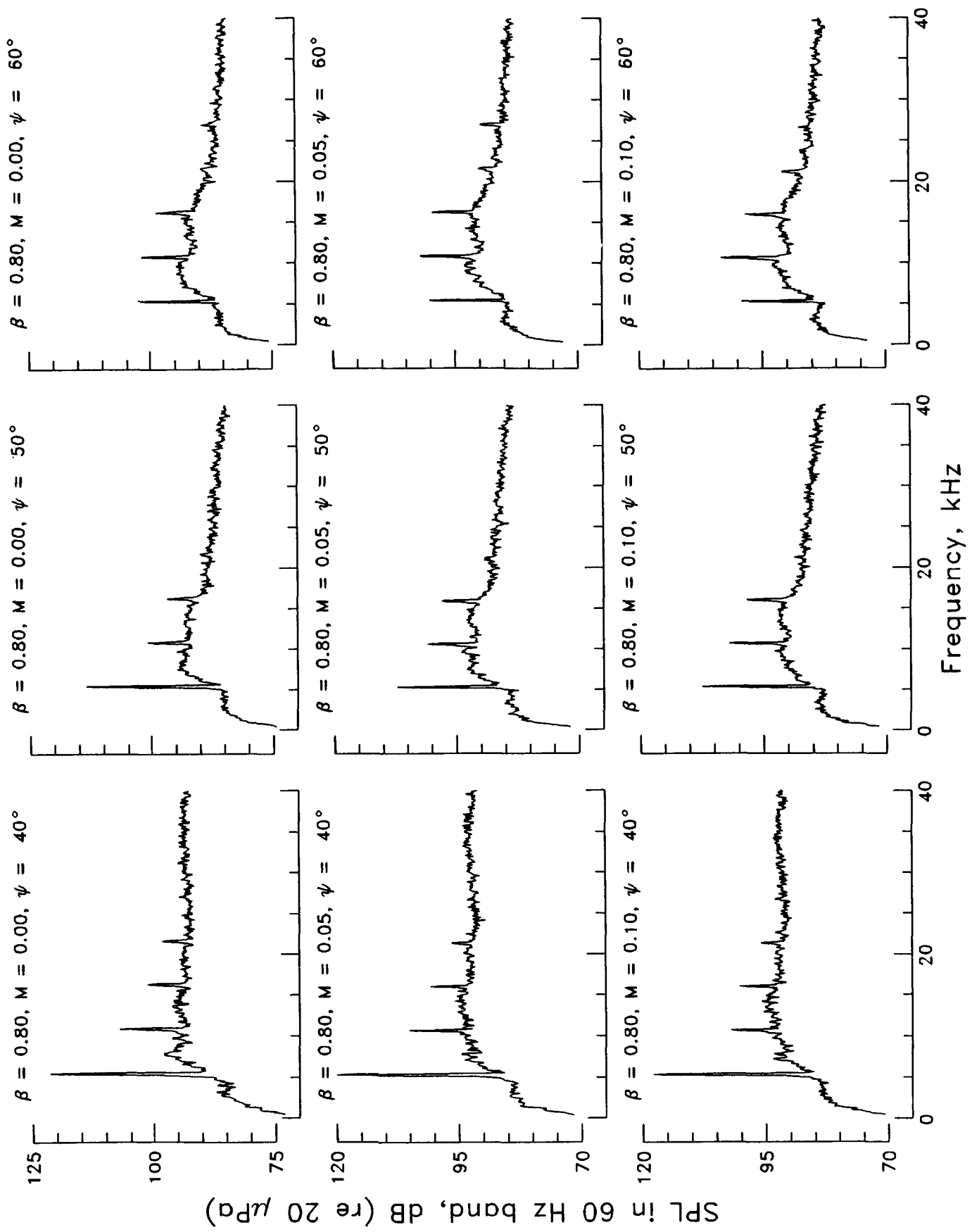
Frequency, kHz



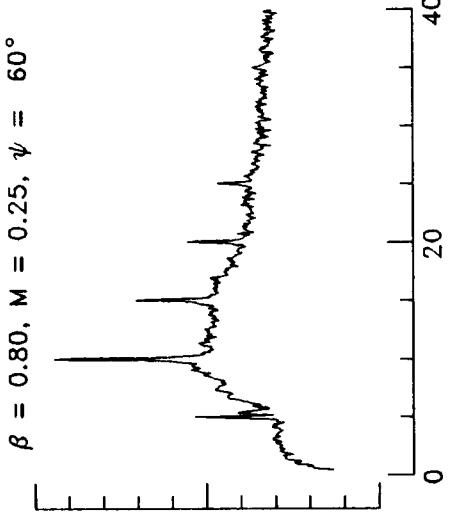
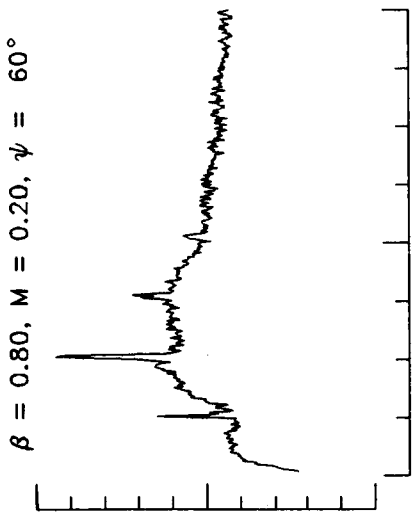
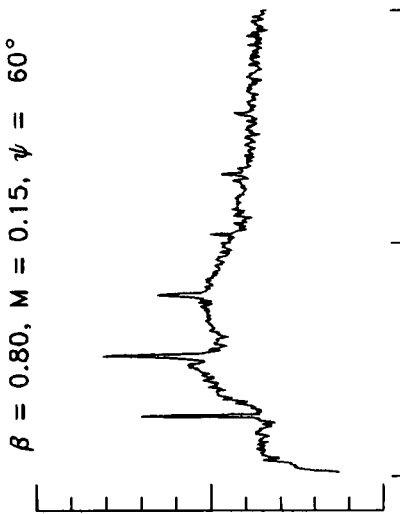
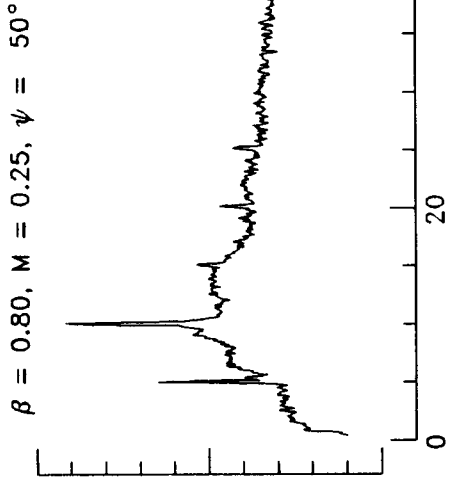
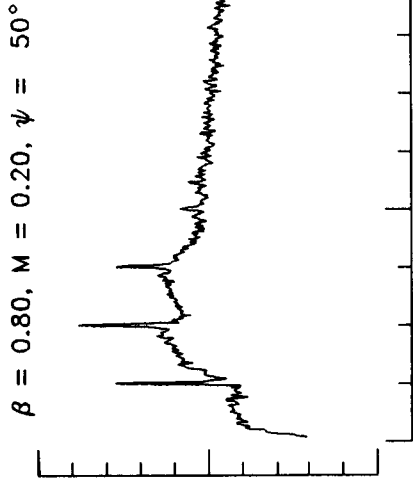
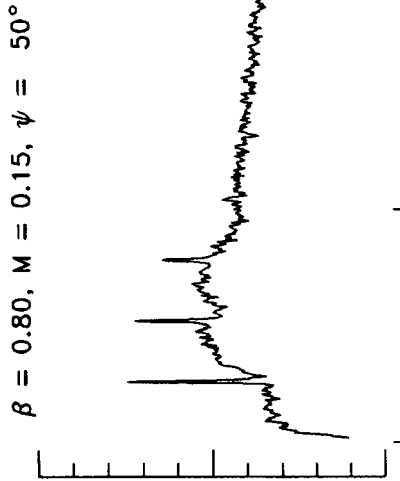
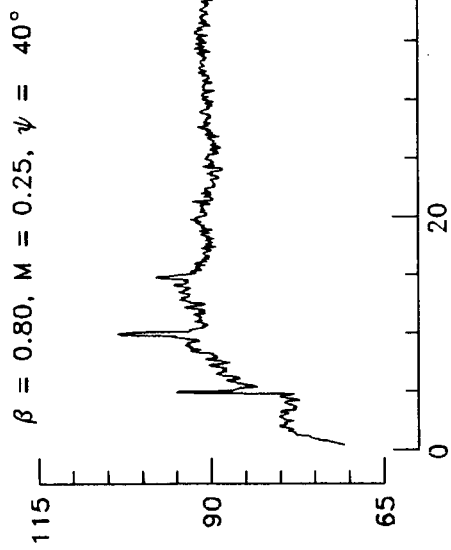
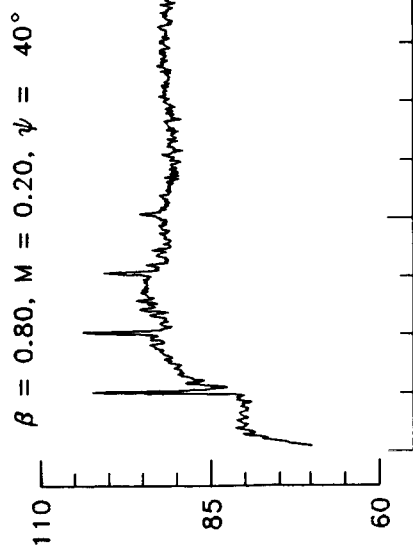
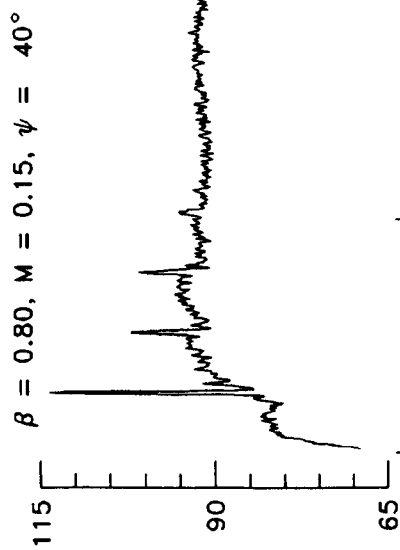
SPL in 60 Hz band, dB (re 20 μ Pa)



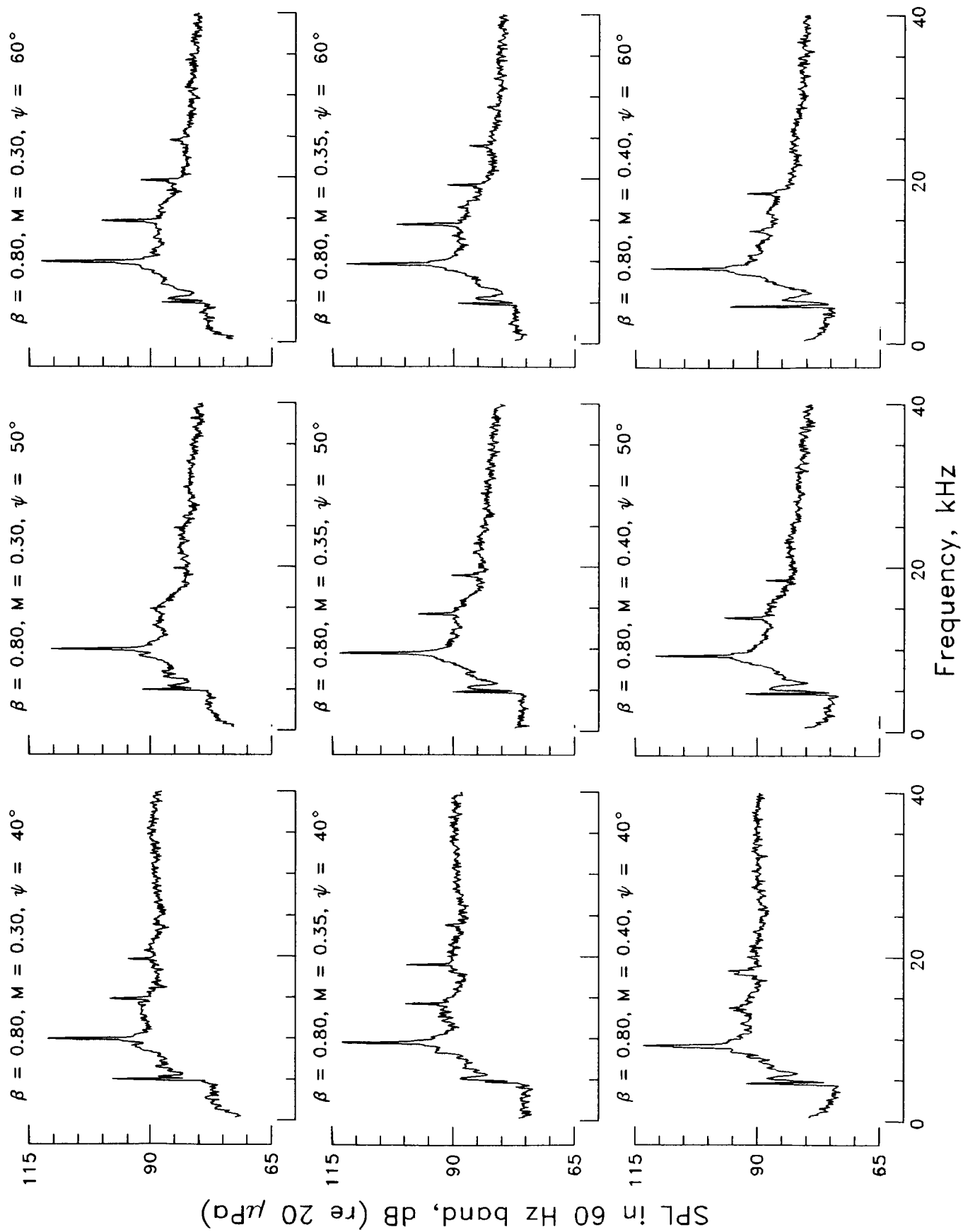


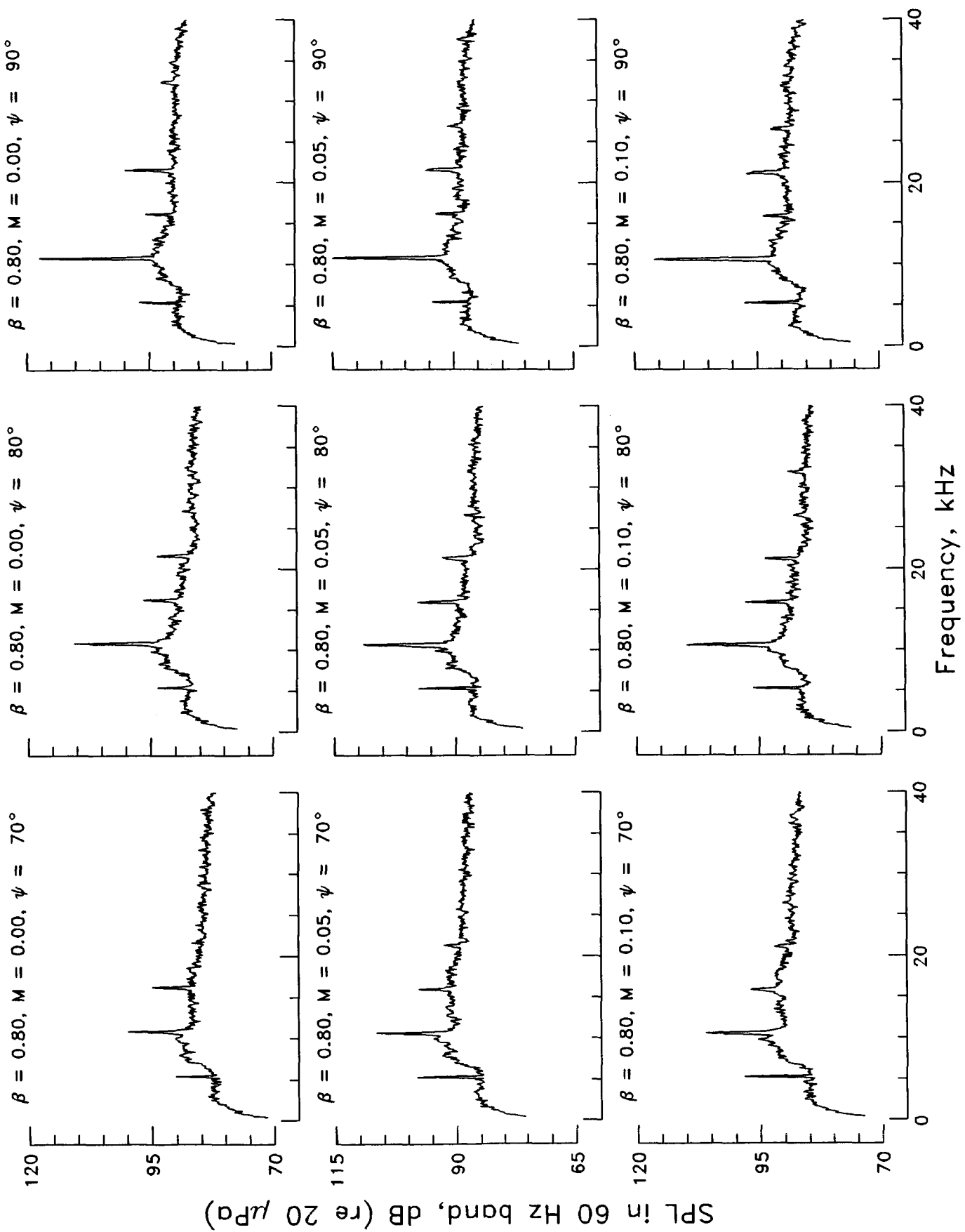


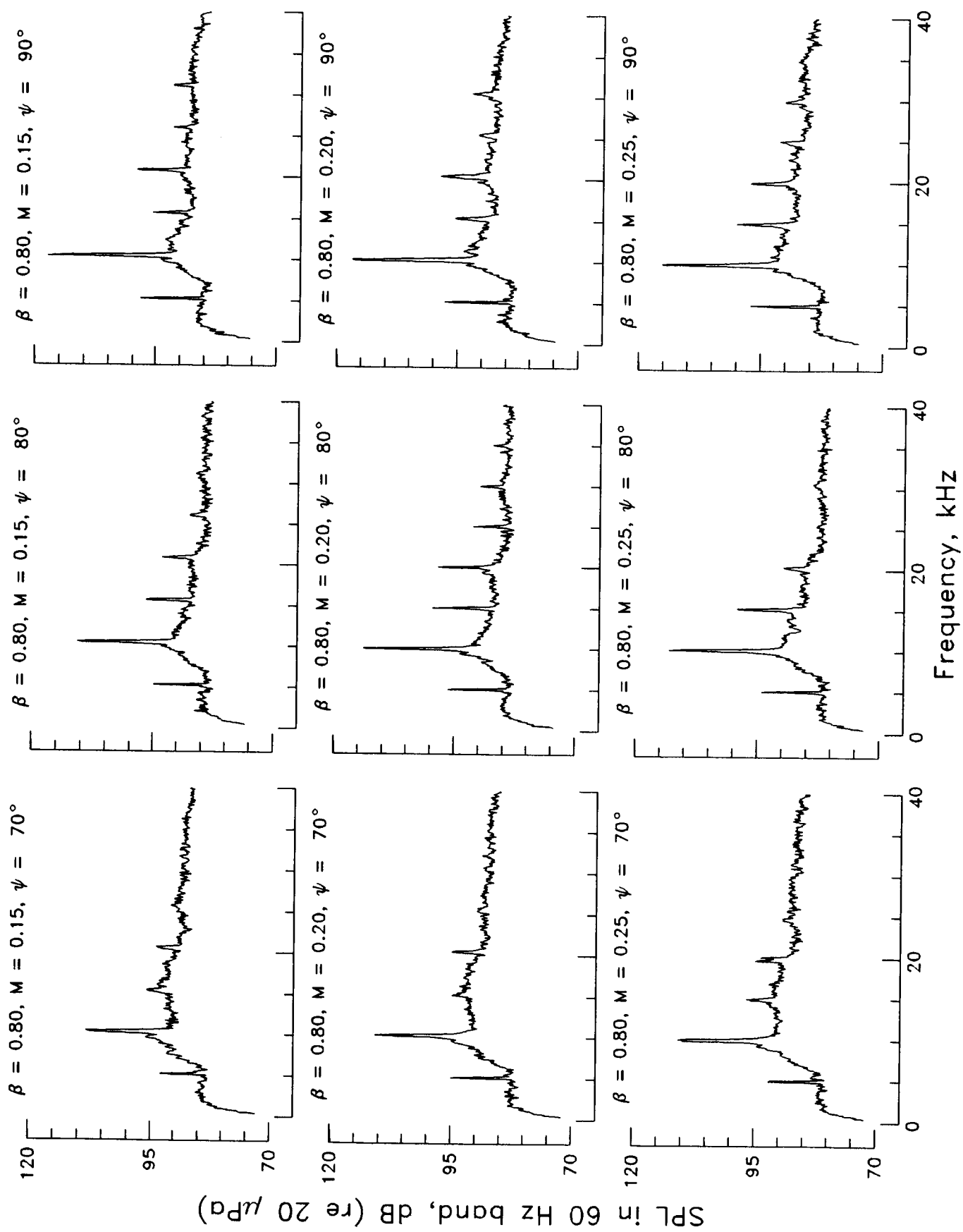
SPL in 60 Hz band, dB (re 20 μ Pd)



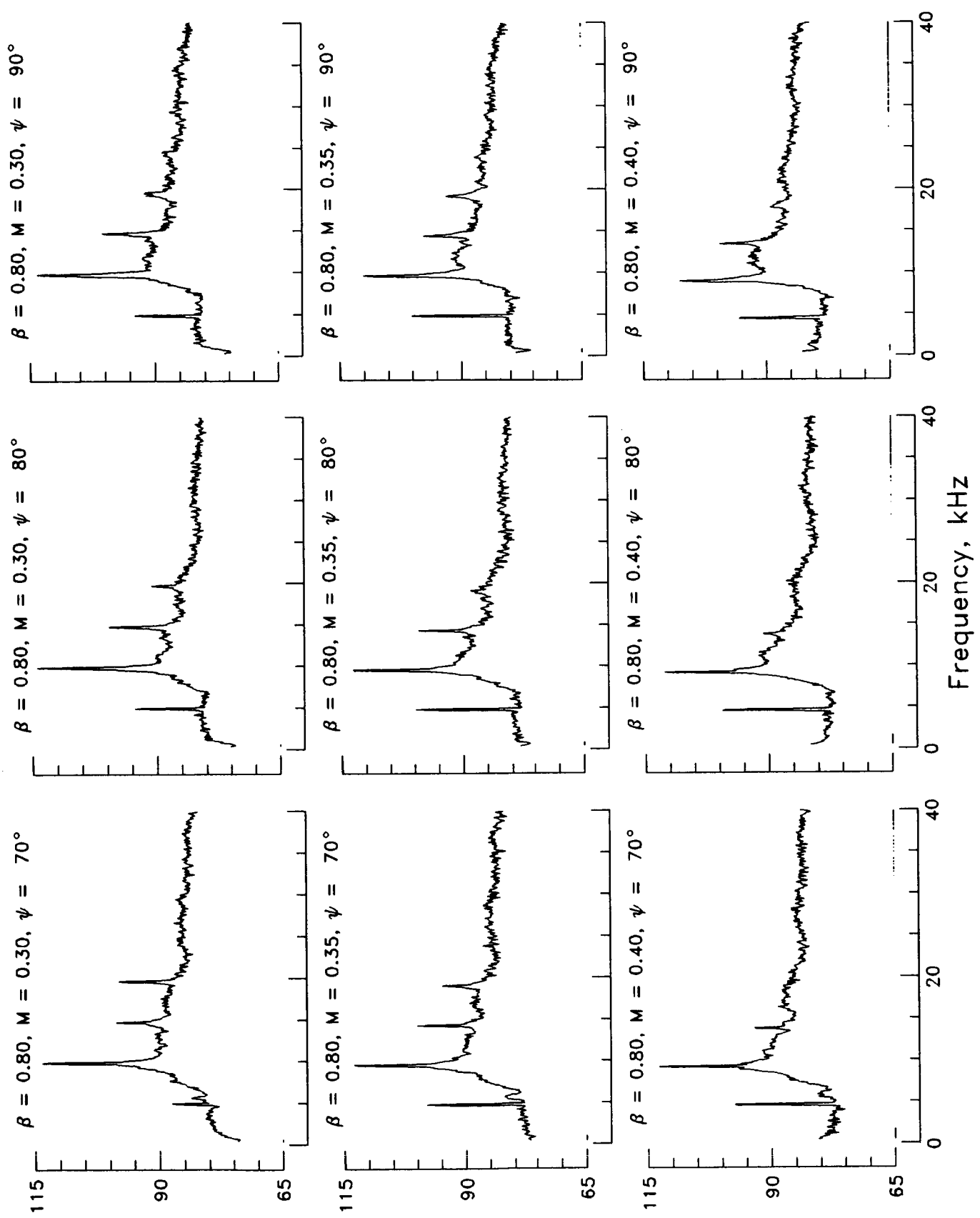
Frequency, kHz

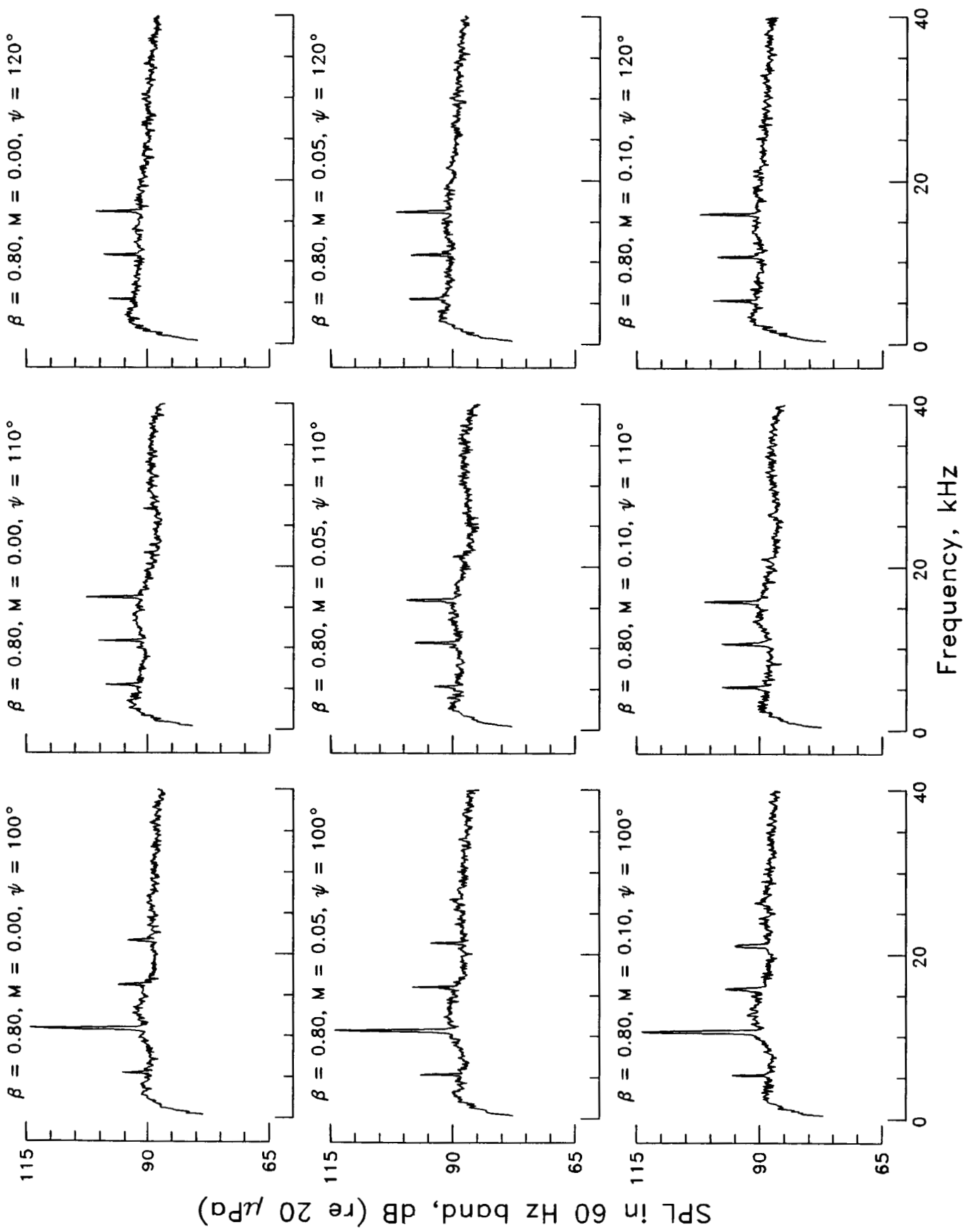


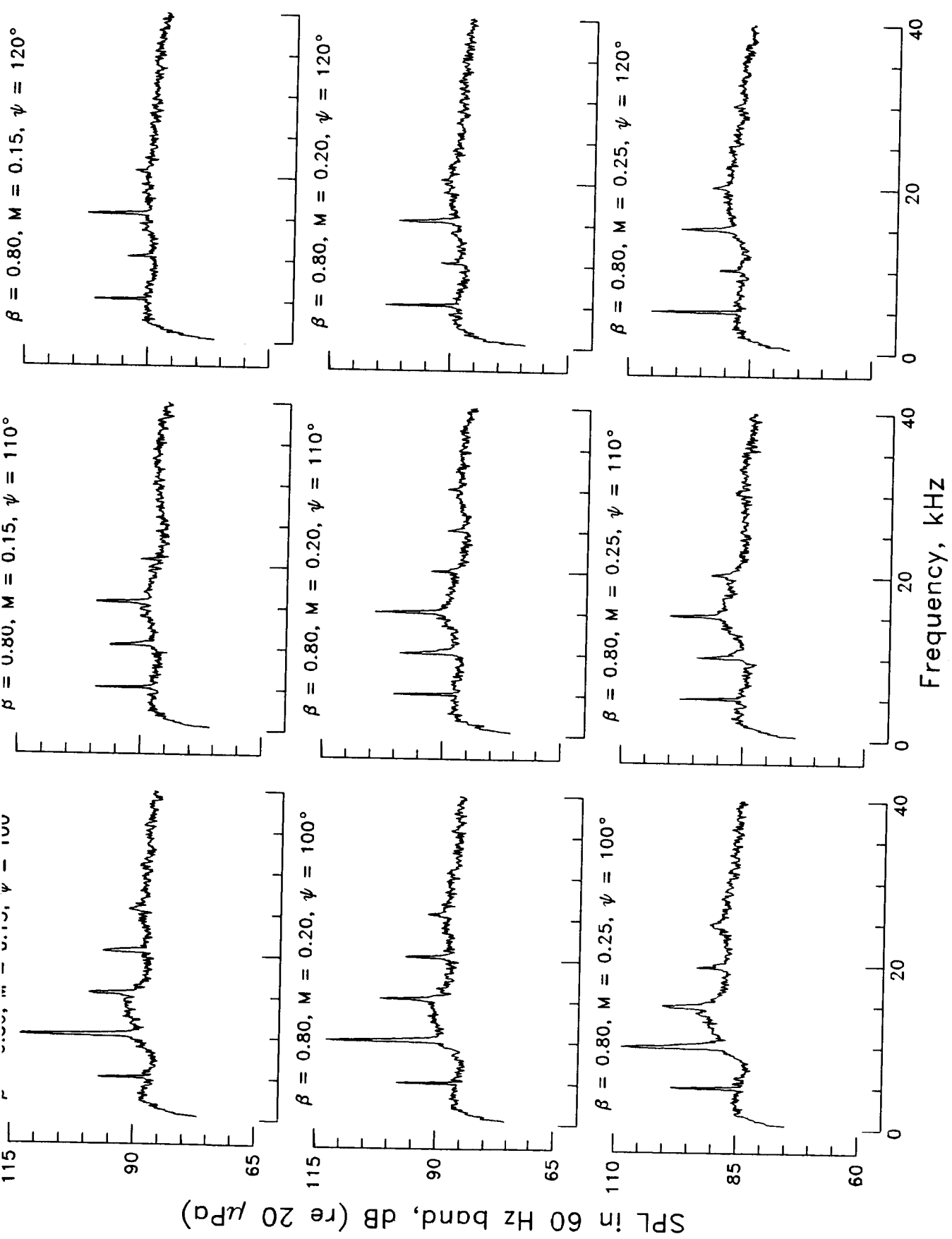


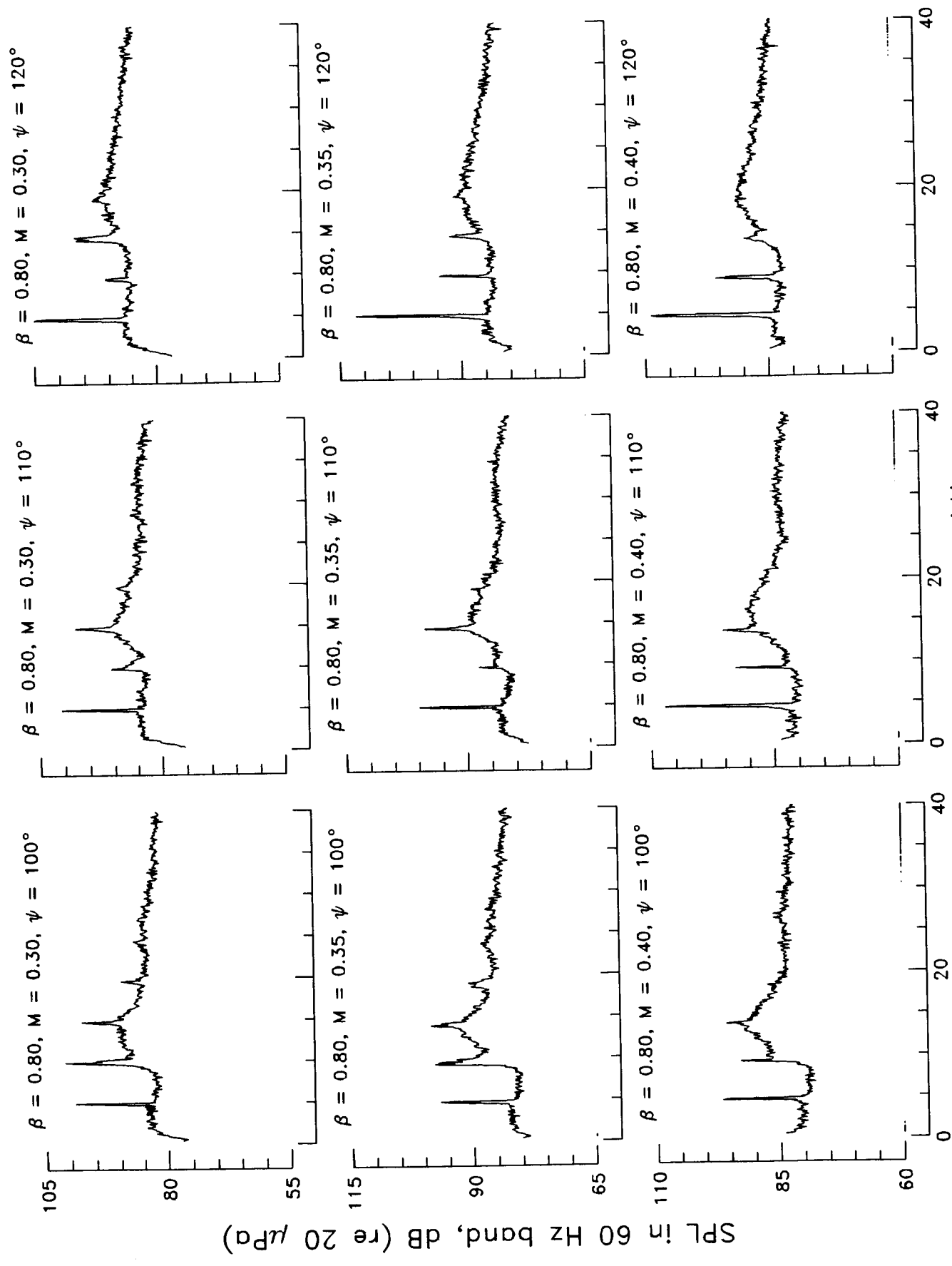


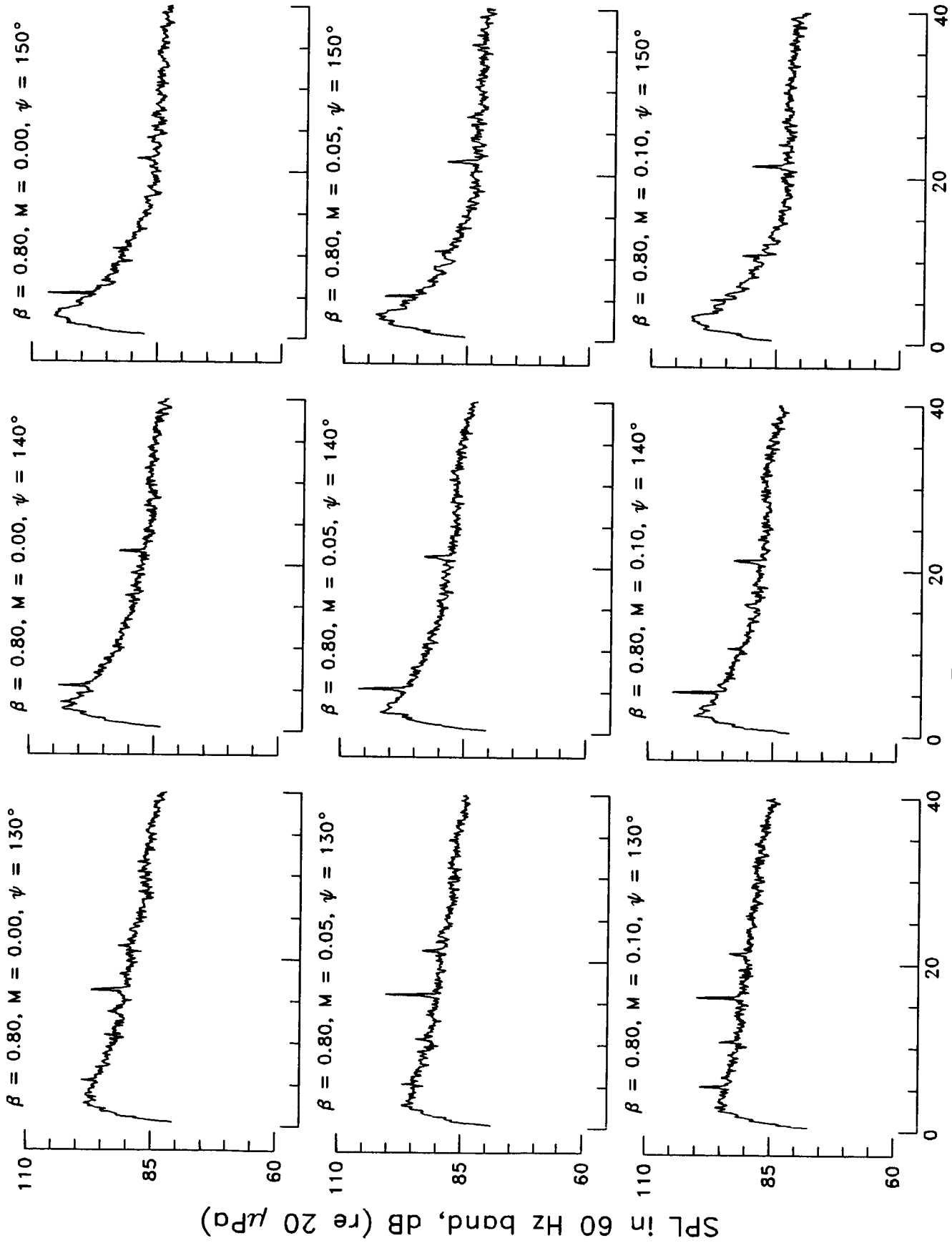
SPL in 60 Hz band, dB (re 20 μ Pa)

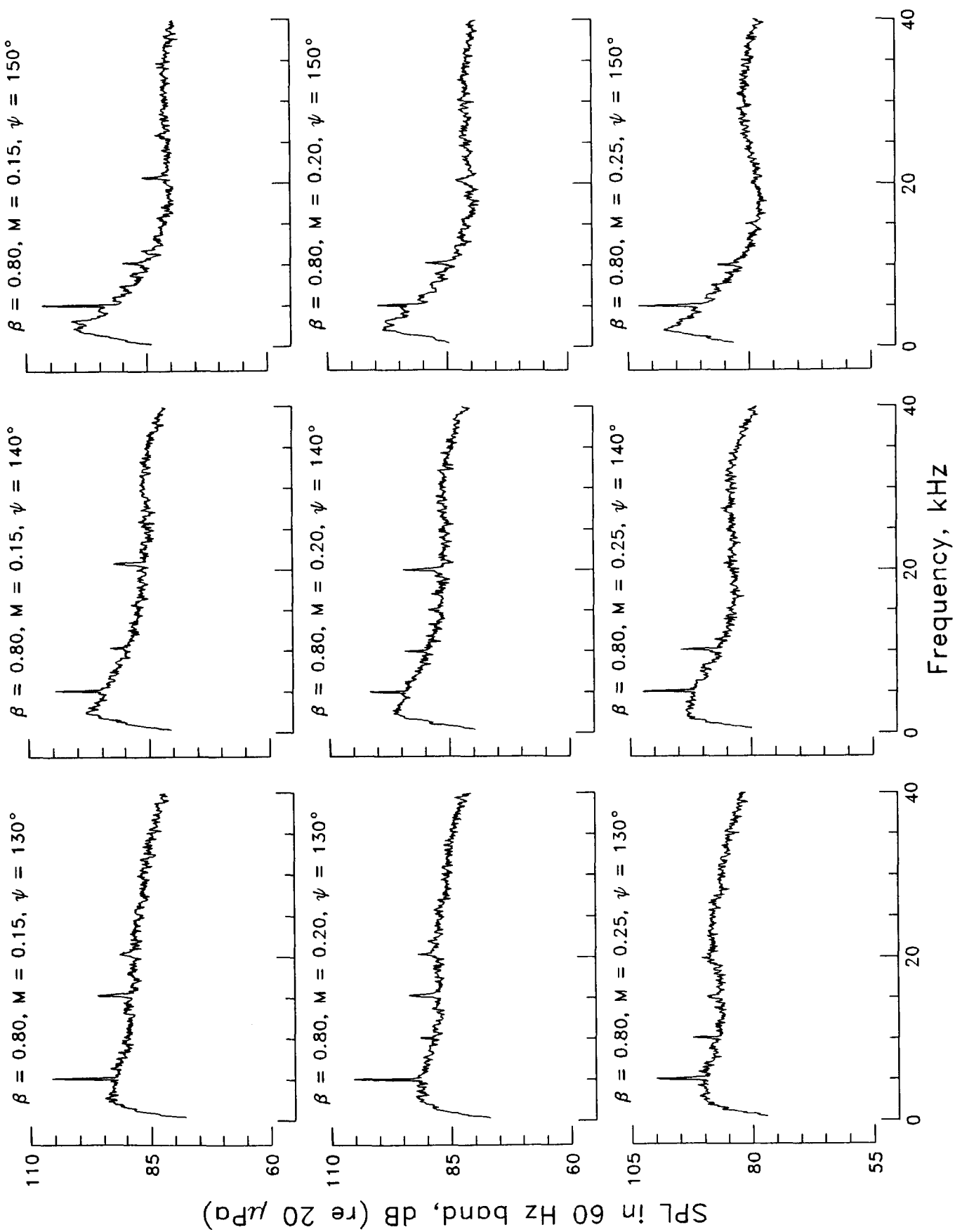






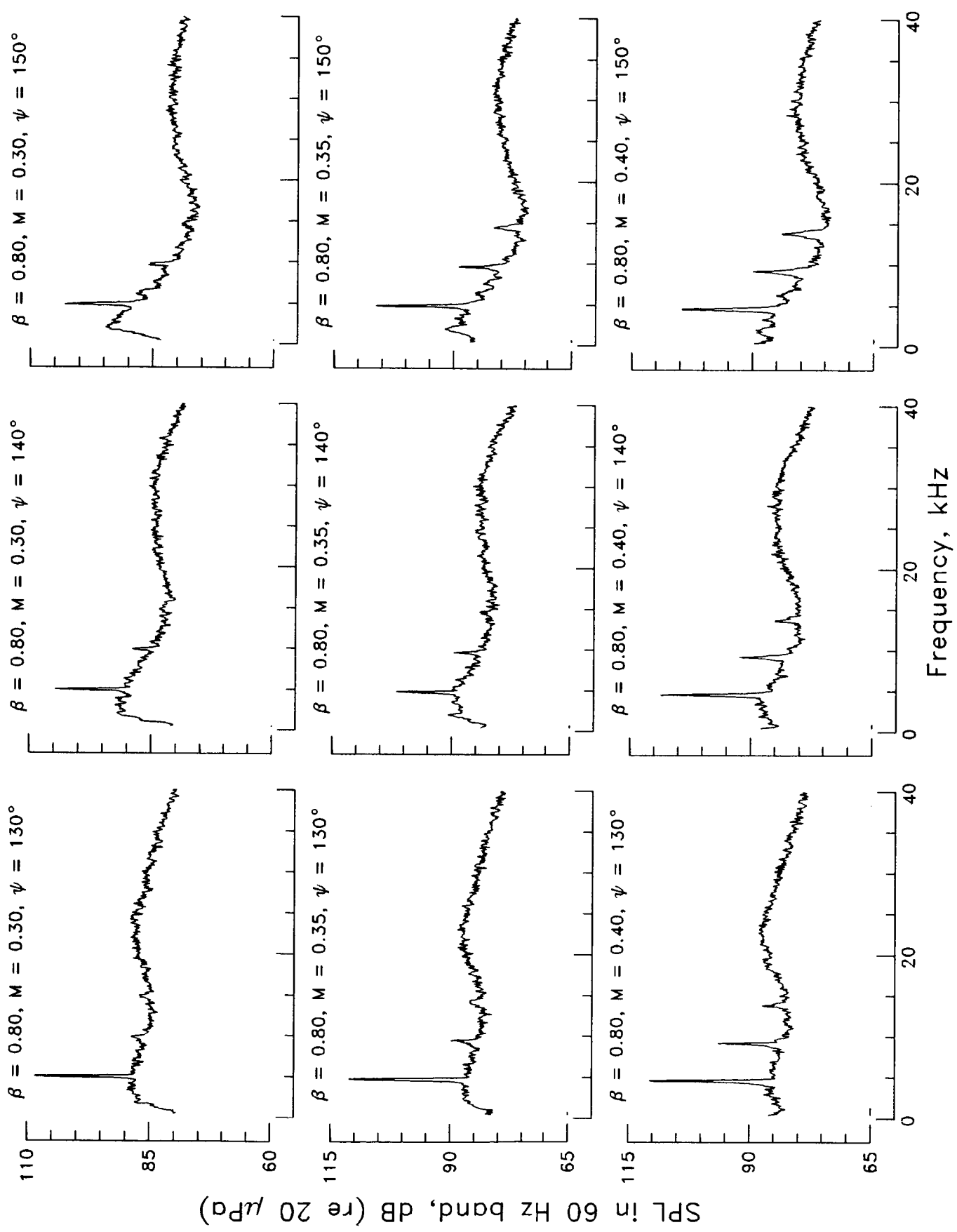


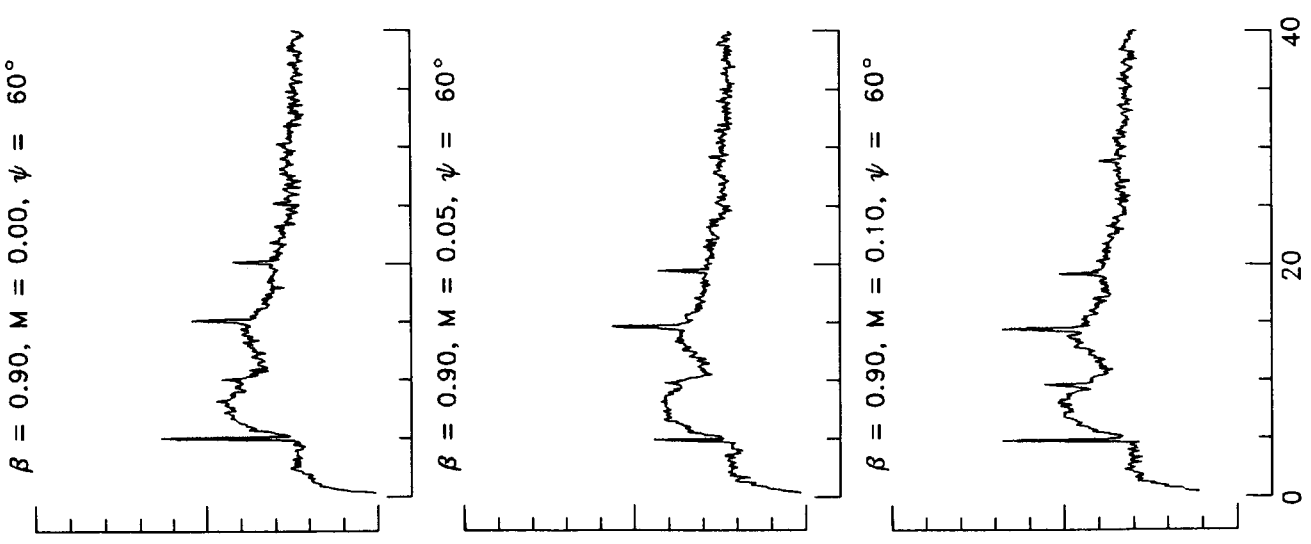
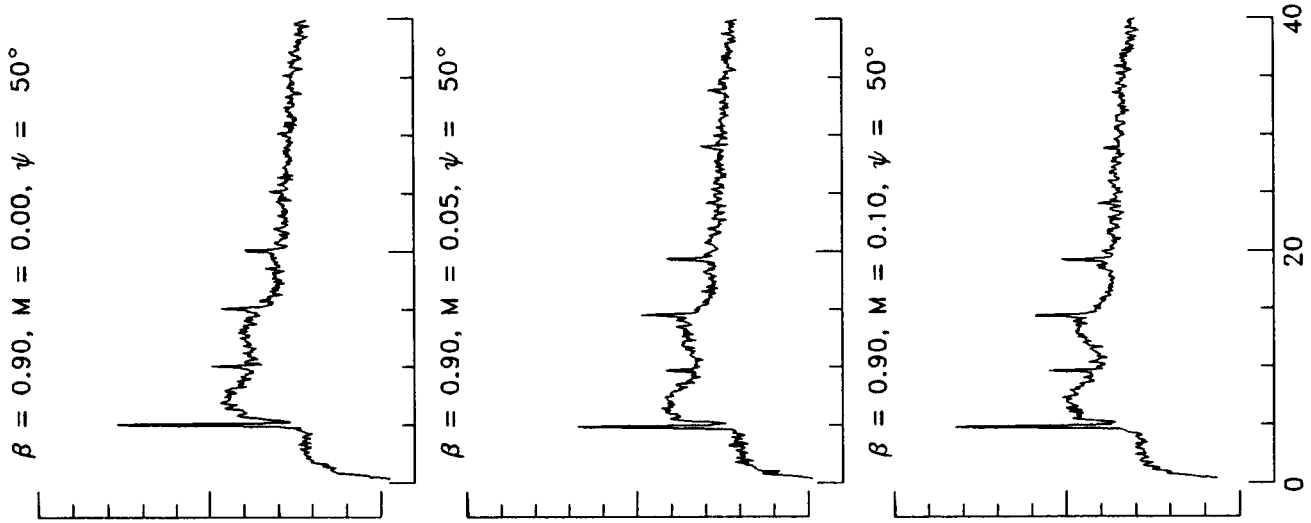
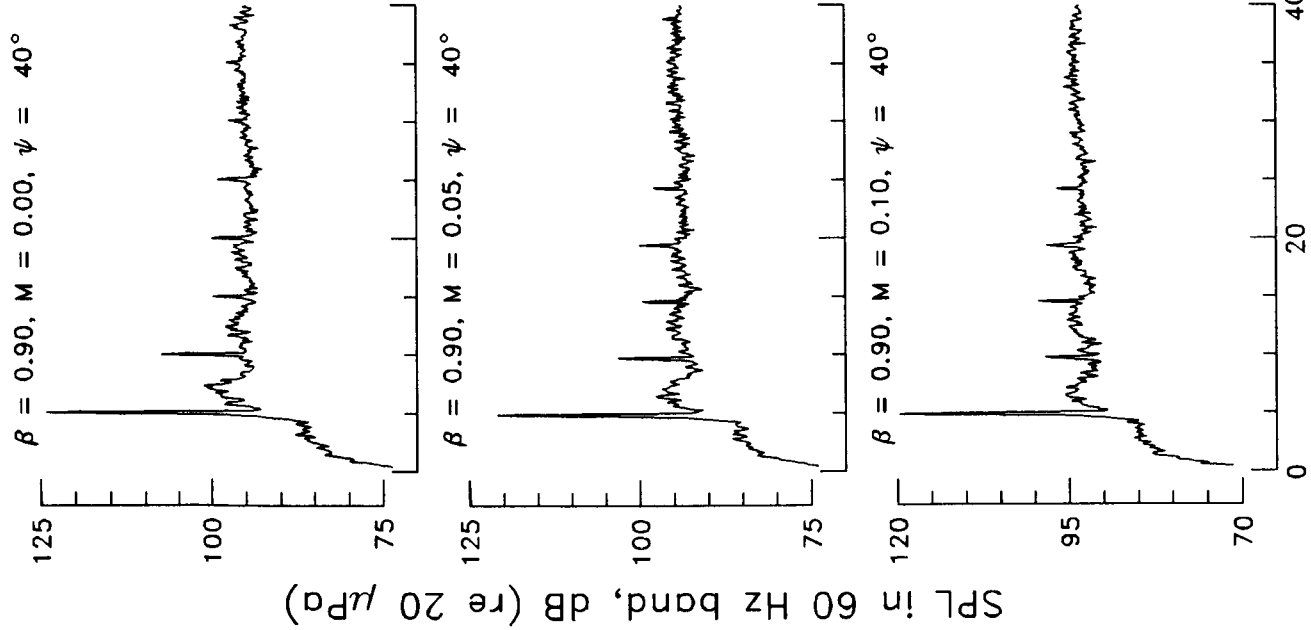




SPL in 60 Hz band, dB (re 20 μ Pa)

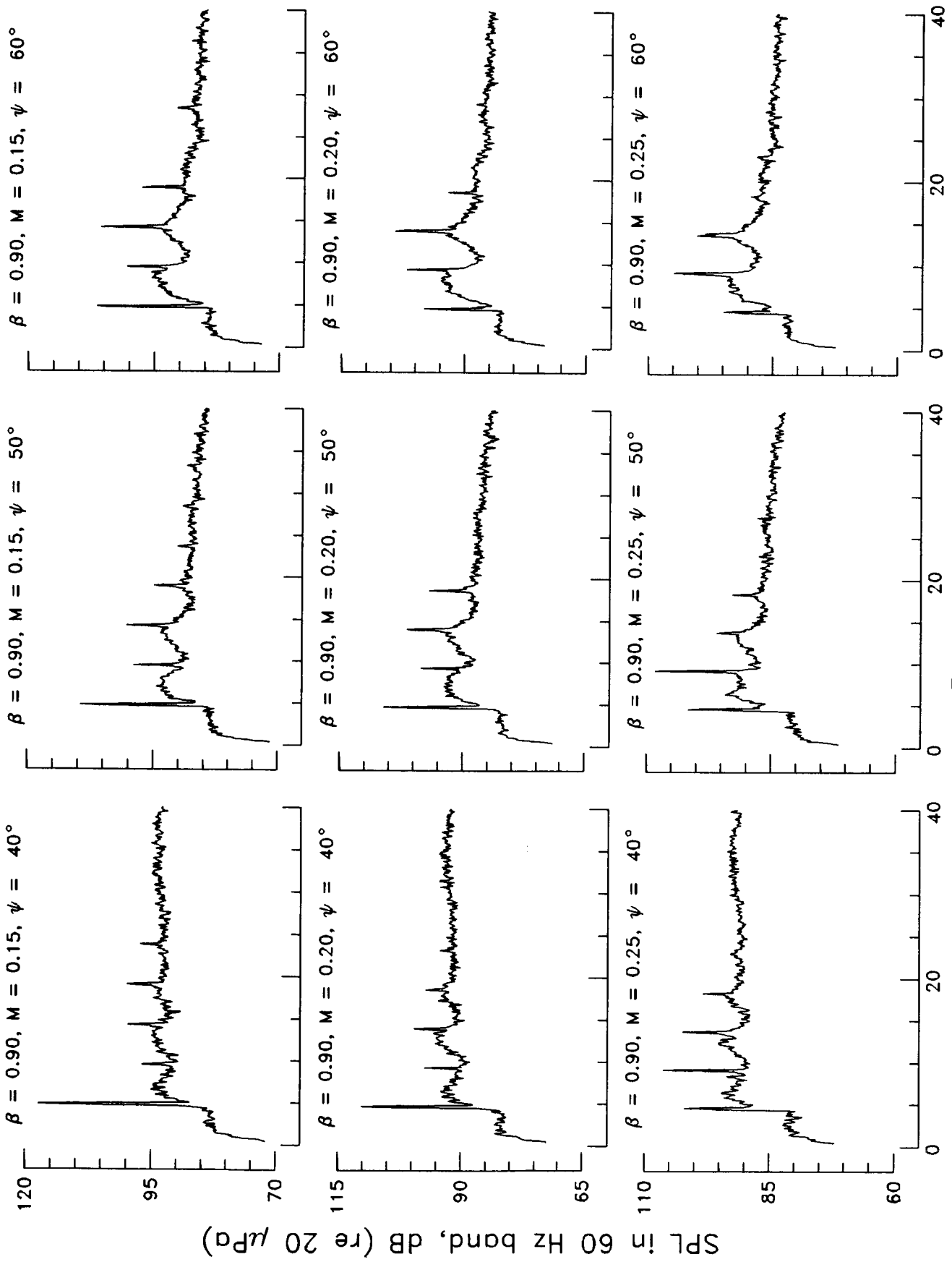
Frequency, kHz

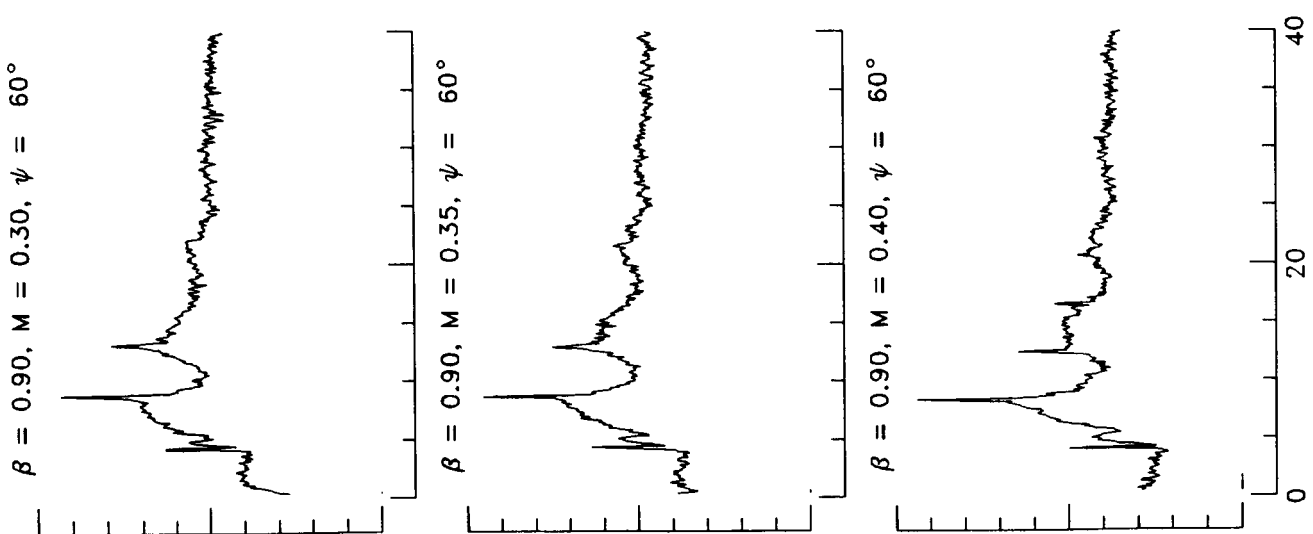
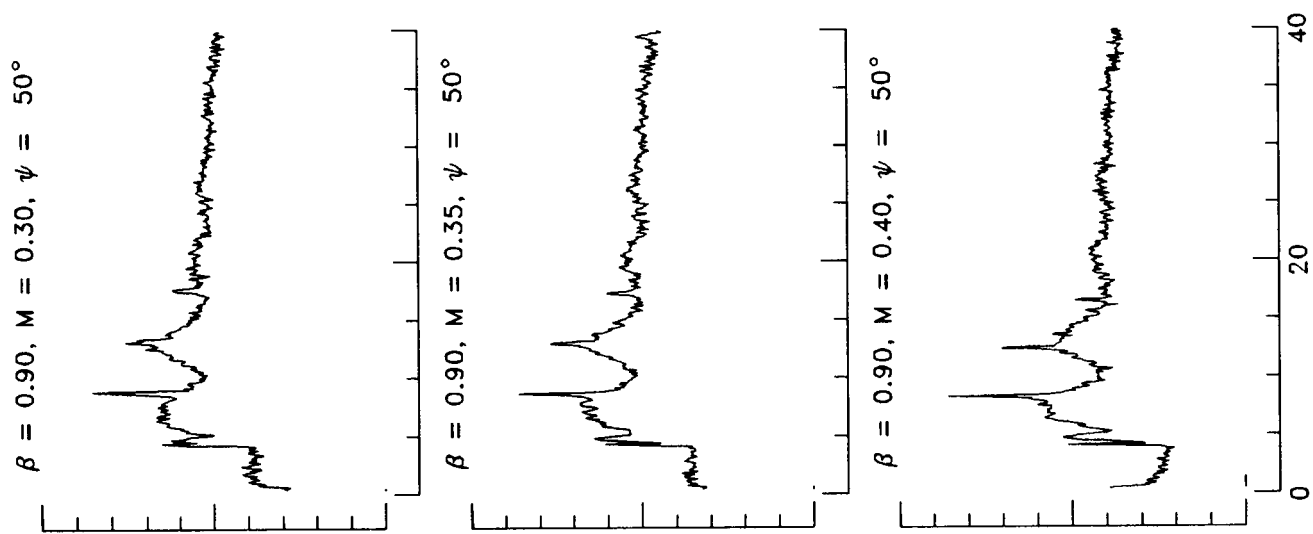
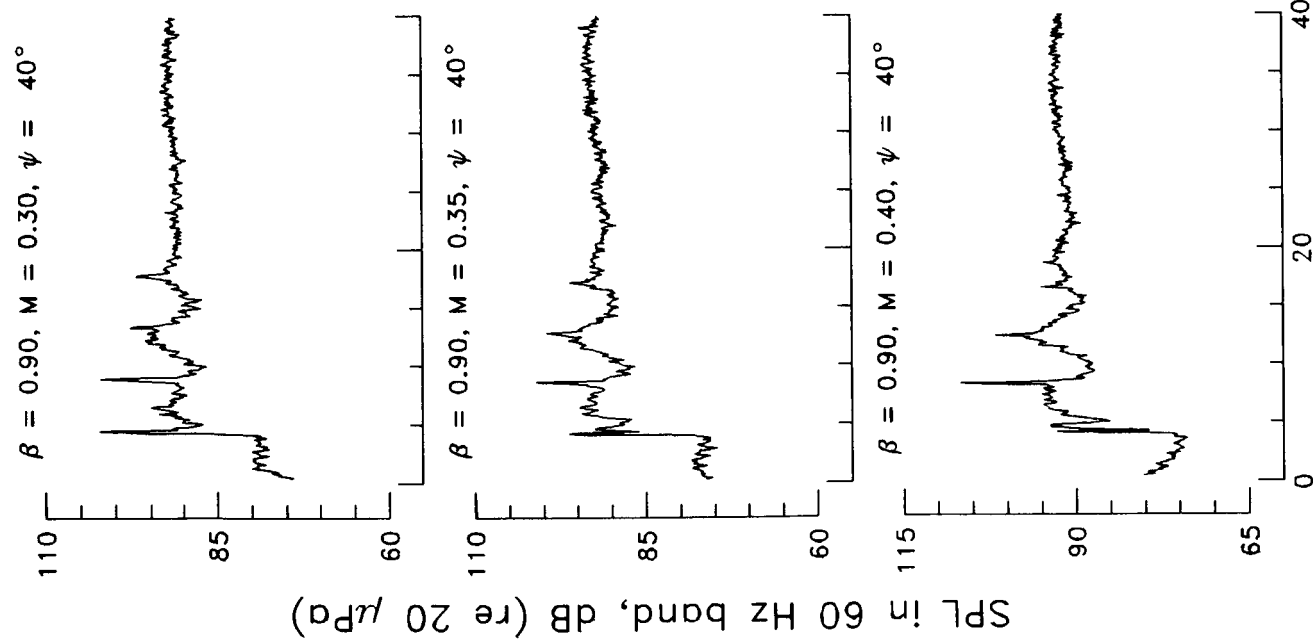




SPL in 60 Hz band, dB (re 20 μ Pa)

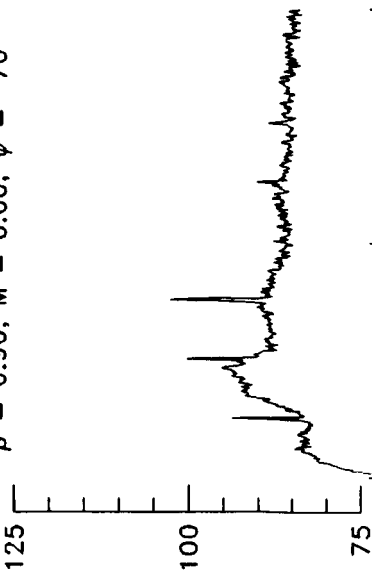
Frequency, kHz



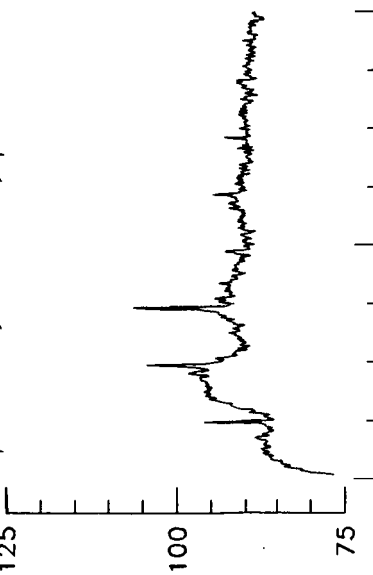


SPL in 60 Hz band, dB (re 20 μ Pa)

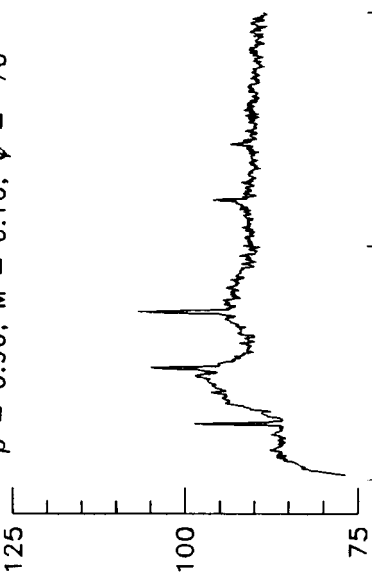
$\beta = 0.90, M = 0.00, \psi = 70^\circ$



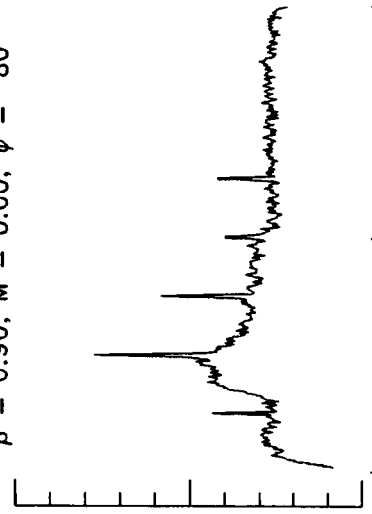
$\beta = 0.90, M = 0.05, \psi = 70^\circ$



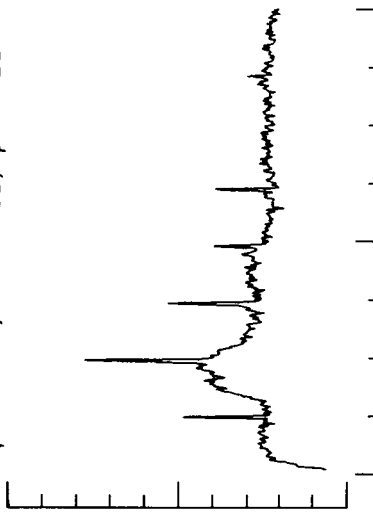
$\beta = 0.90, M = 0.10, \psi = 70^\circ$



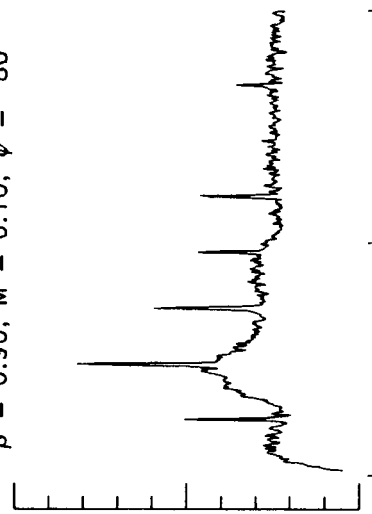
$\beta = 0.90, M = 0.00, \psi = 80^\circ$



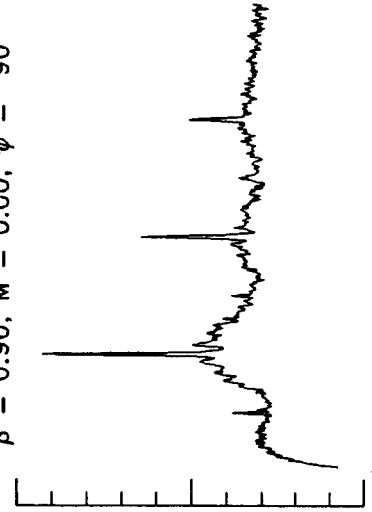
$\beta = 0.90, M = 0.05, \psi = 80^\circ$



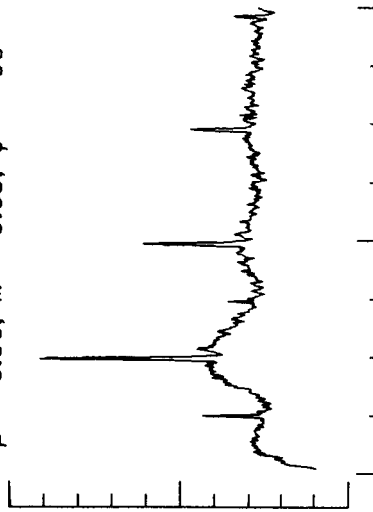
$\beta = 0.90, M = 0.10, \psi = 80^\circ$



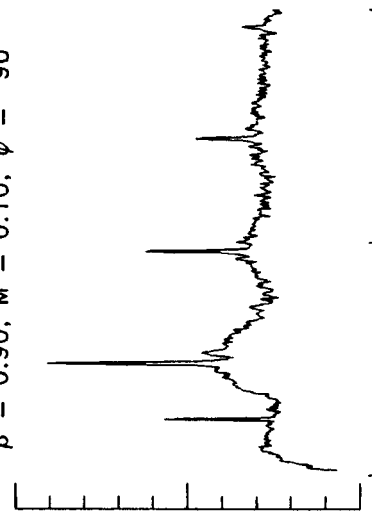
$\beta = 0.90, M = 0.00, \psi = 90^\circ$



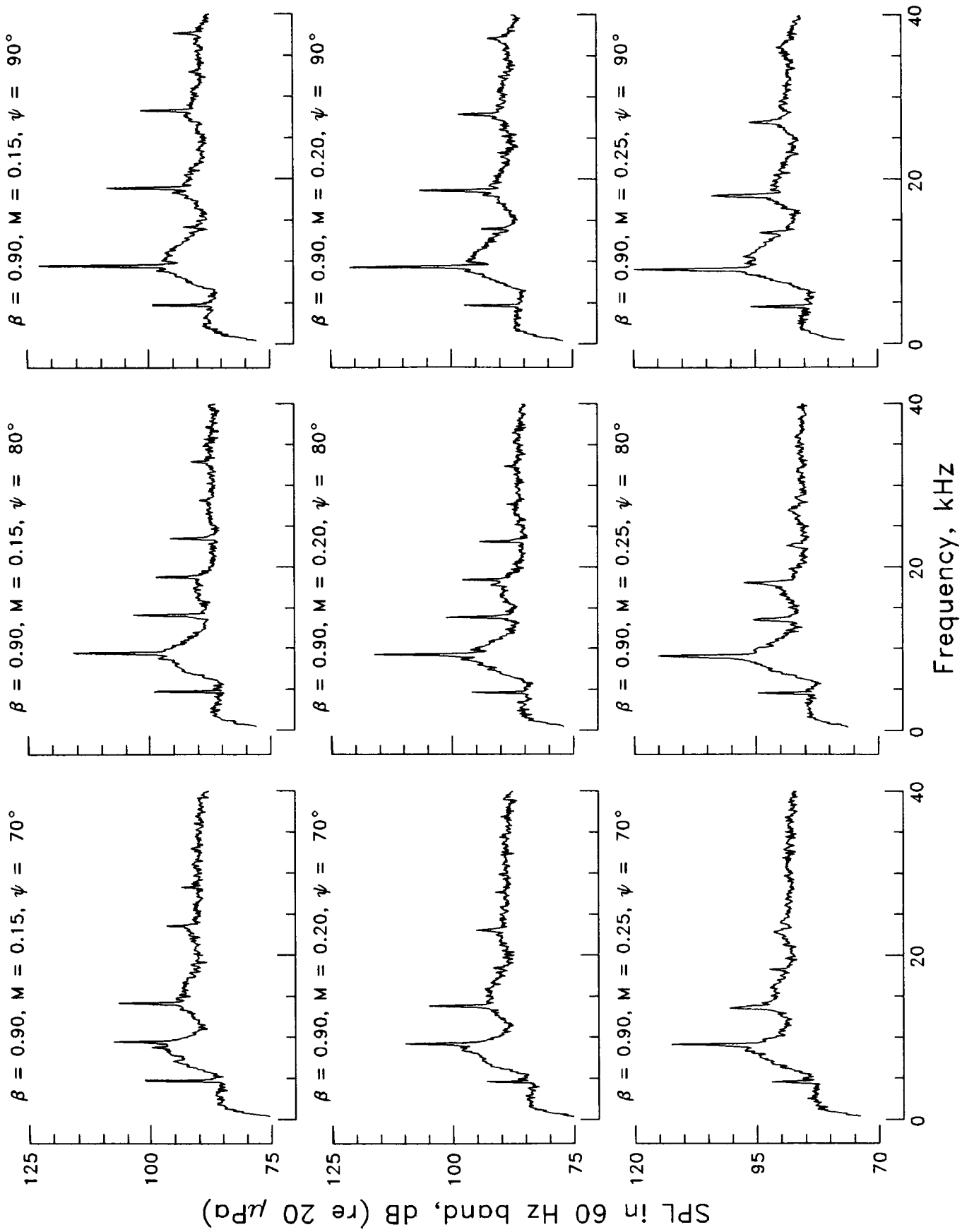
$\beta = 0.90, M = 0.05, \psi = 90^\circ$



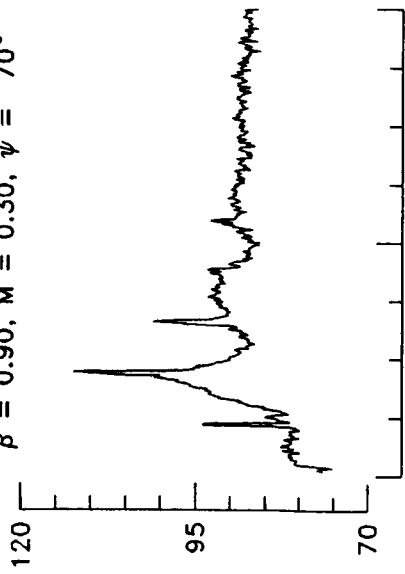
$\beta = 0.90, M = 0.10, \psi = 90^\circ$



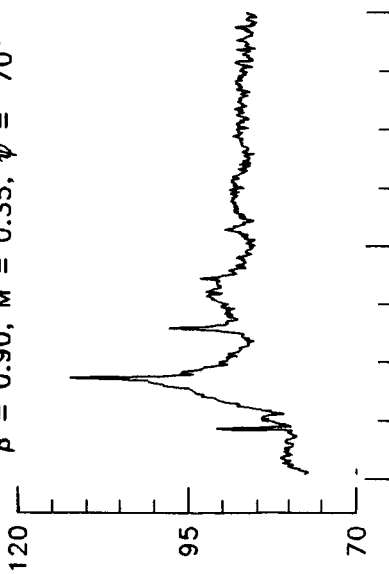
Frequency, kHz



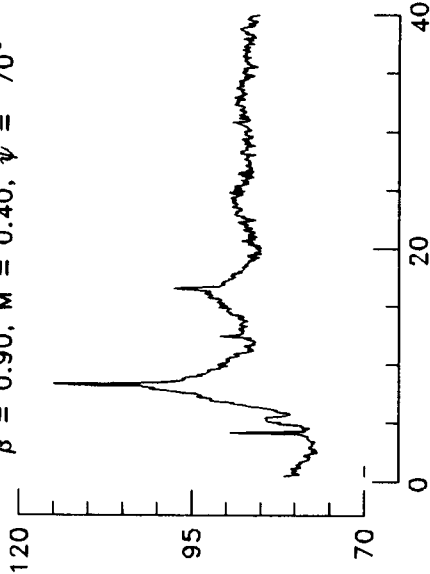
$\beta = 0.90, M = 0.30, \psi = 70^\circ$



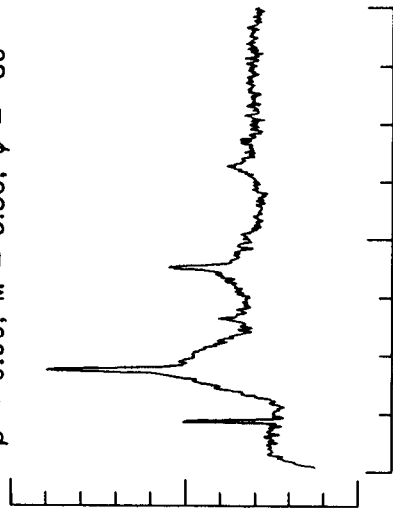
$\beta = 0.90, M = 0.35, \psi = 70^\circ$



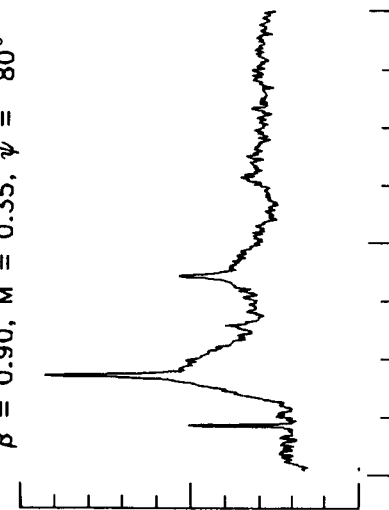
$\beta = 0.90, M = 0.40, \psi = 70^\circ$



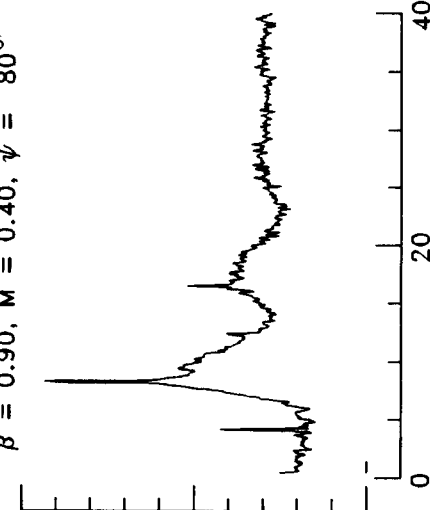
$\beta = 0.90, M = 0.30, \psi = 80^\circ$



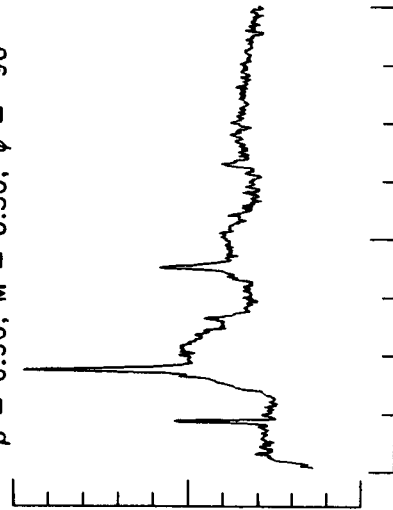
$\beta = 0.90, M = 0.35, \psi = 80^\circ$



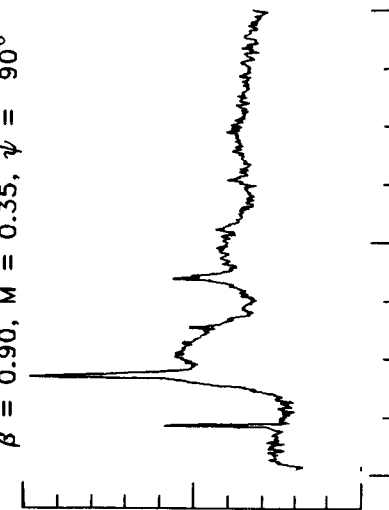
$\beta = 0.90, M = 0.40, \psi = 80^\circ$



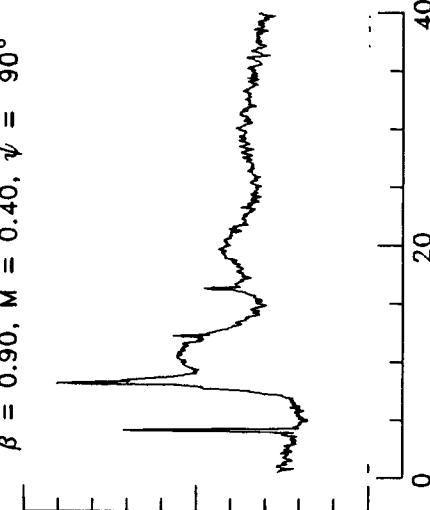
$\beta = 0.90, M = 0.30, \psi = 90^\circ$



$\beta = 0.90, M = 0.35, \psi = 90^\circ$

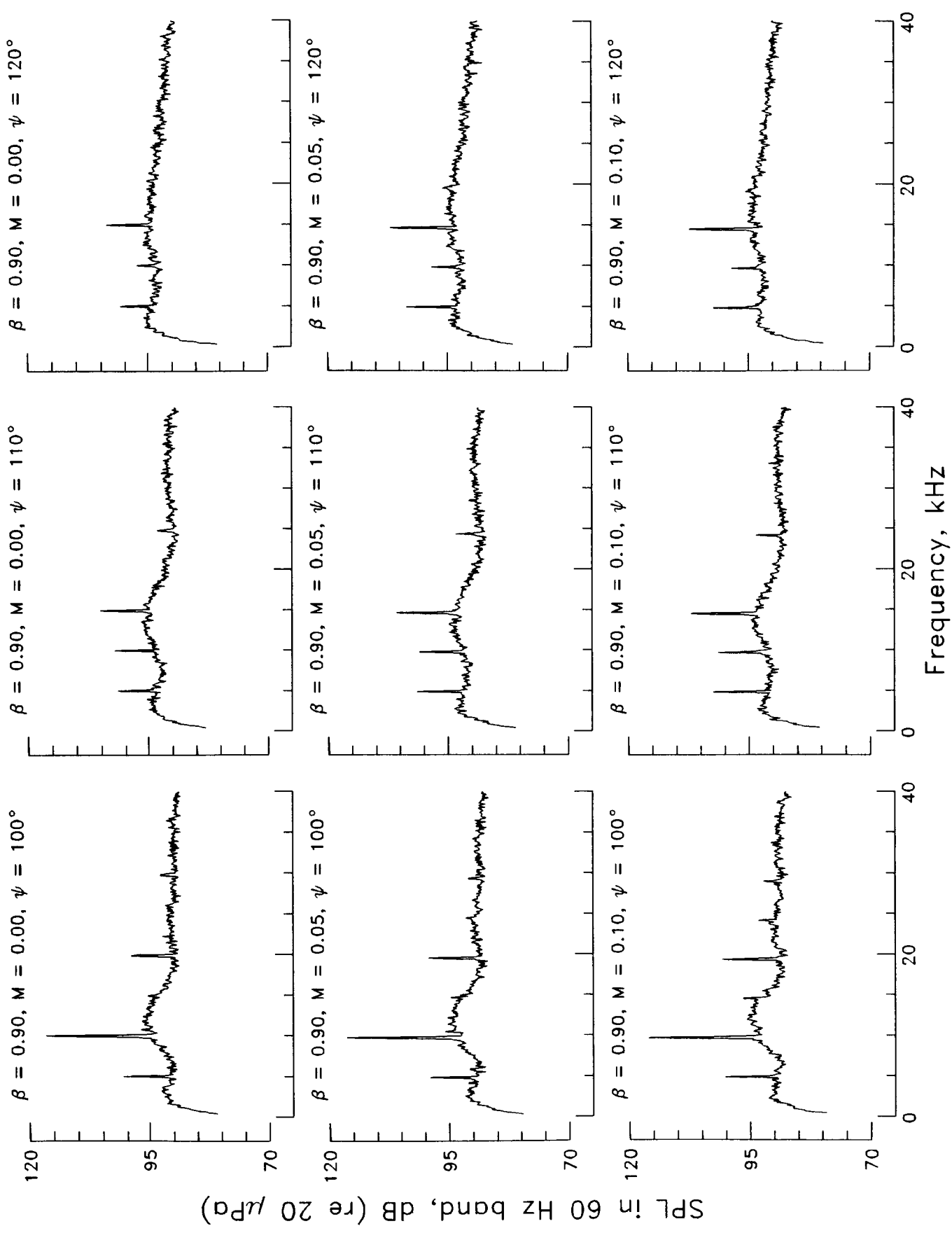


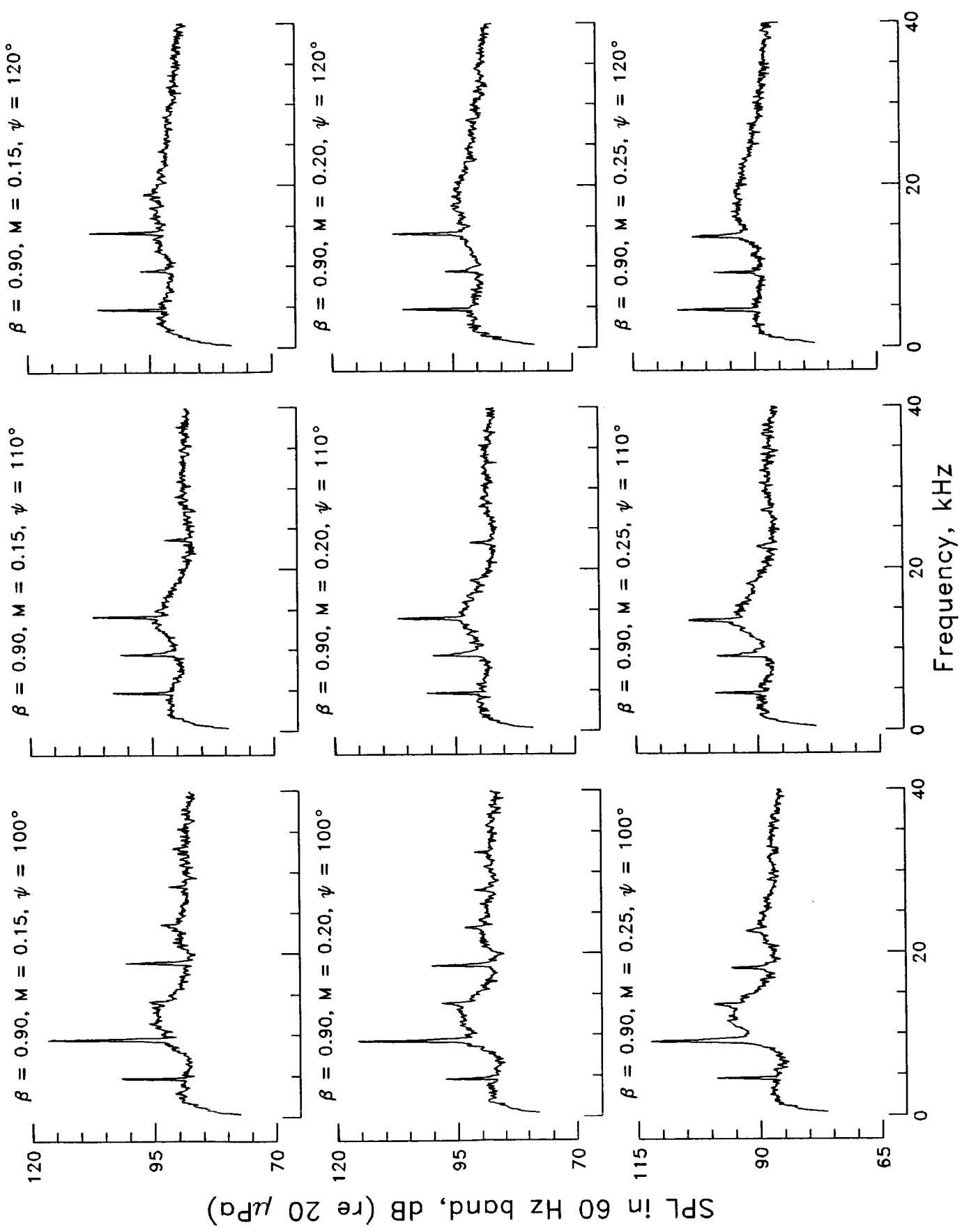
$\beta = 0.90, M = 0.40, \psi = 90^\circ$

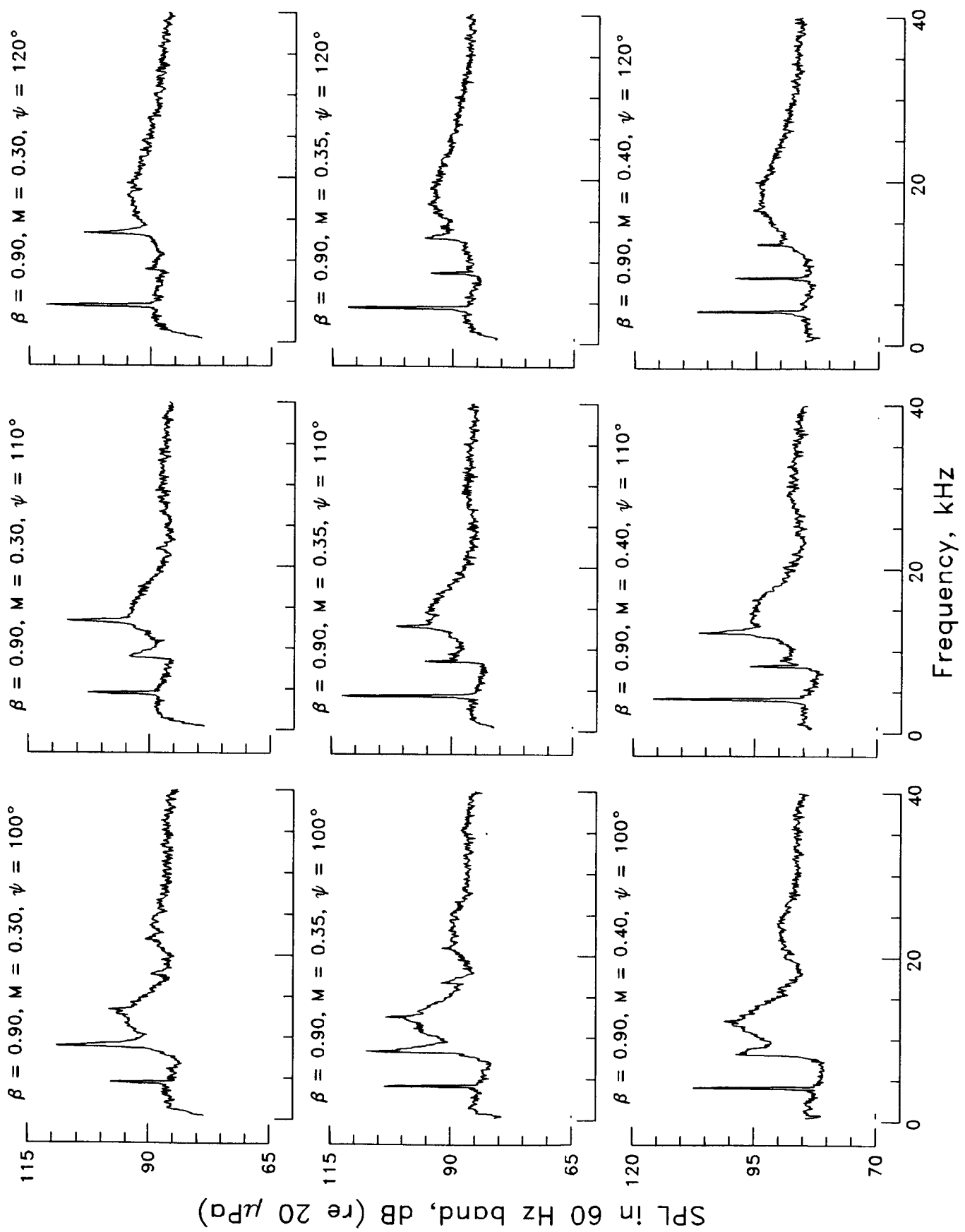


Frequency, kHz

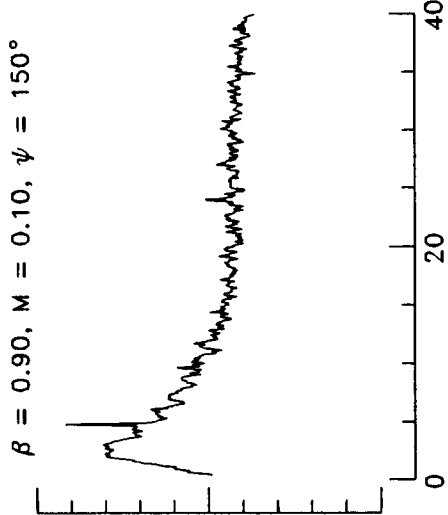
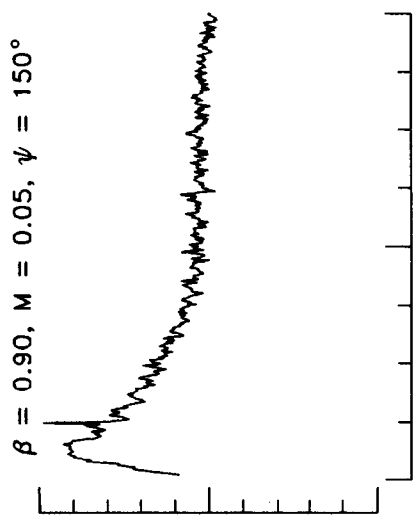
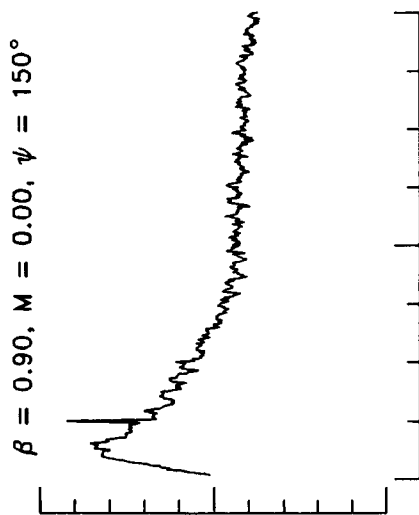
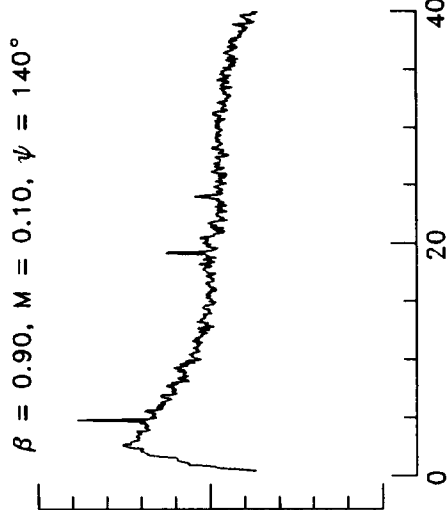
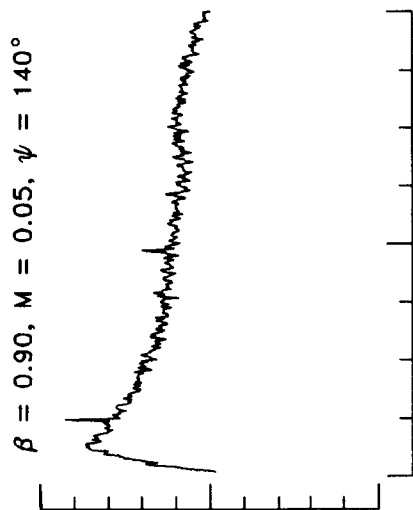
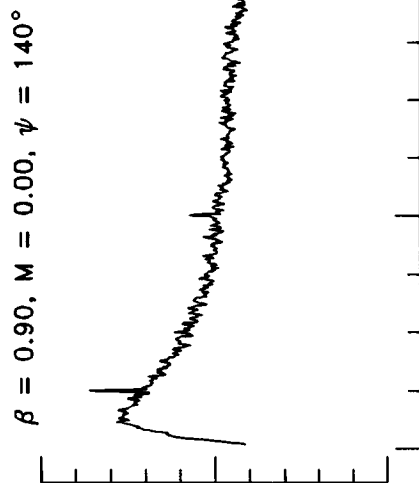
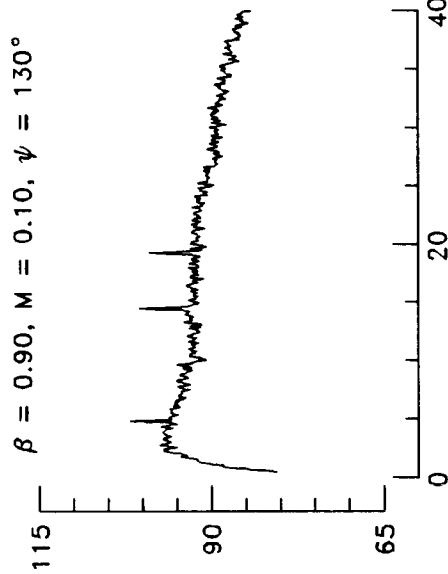
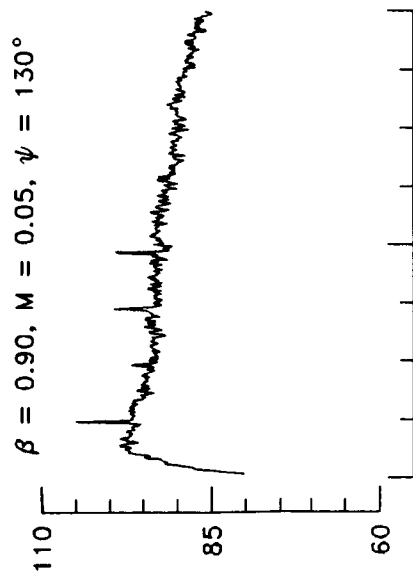
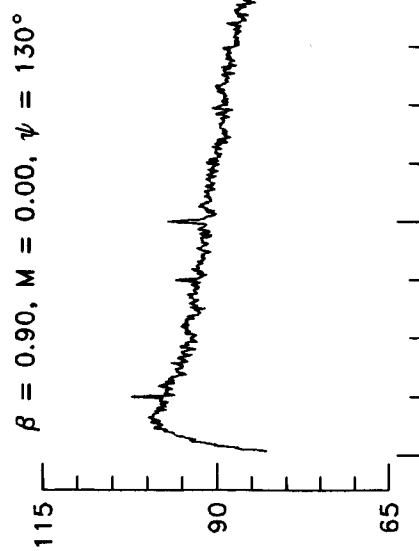
SPL in 60 Hz band, dB (re 20 μPa)



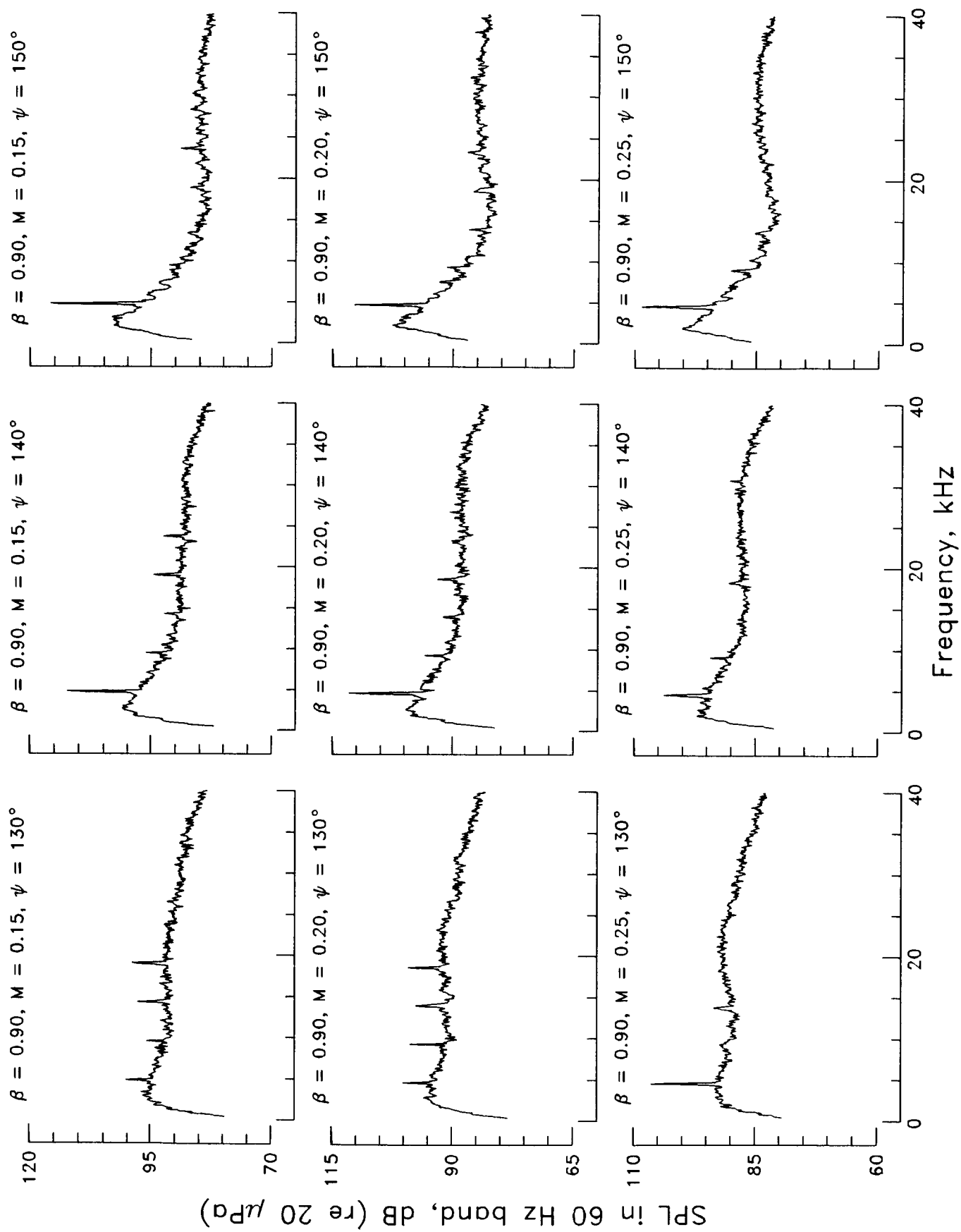


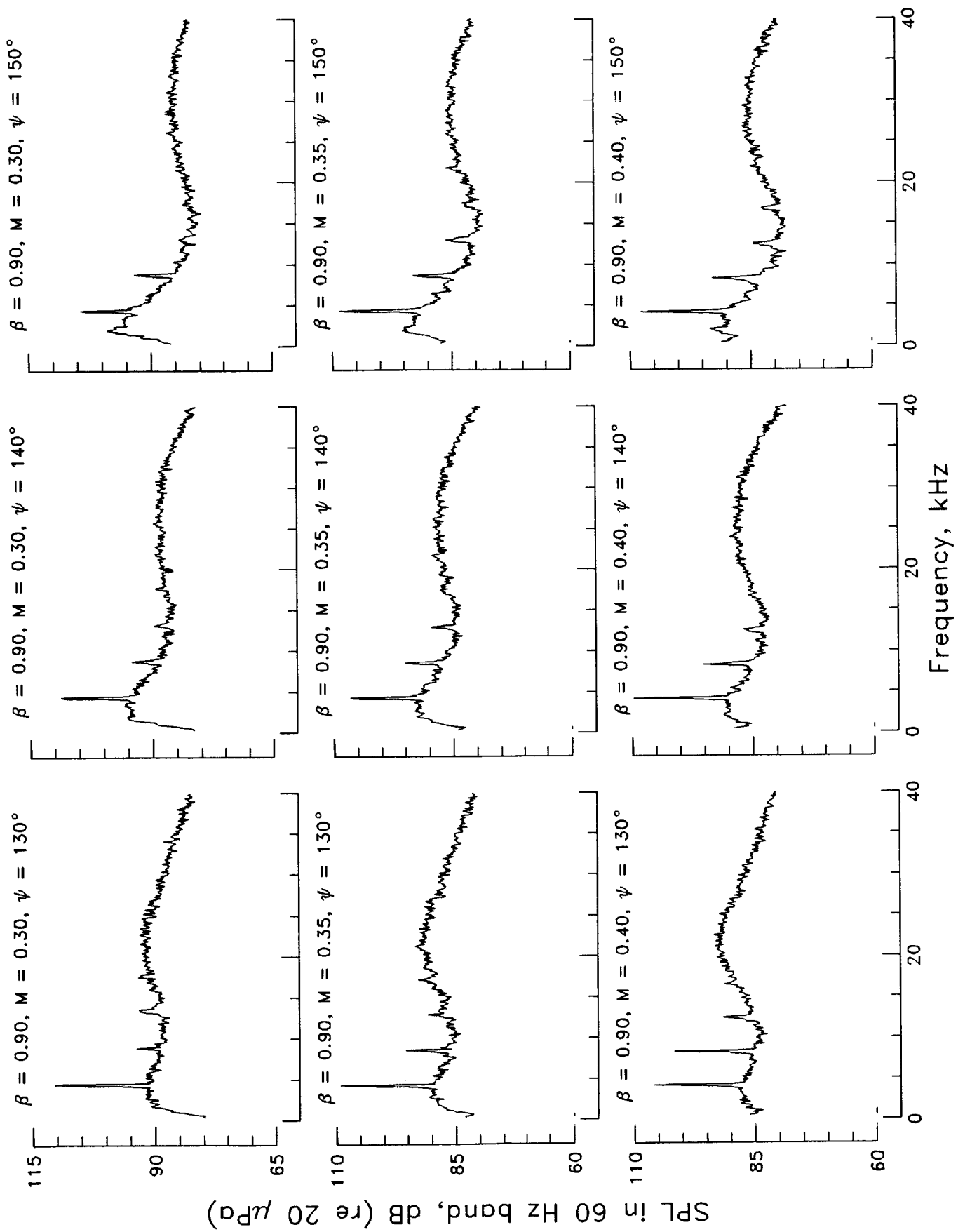


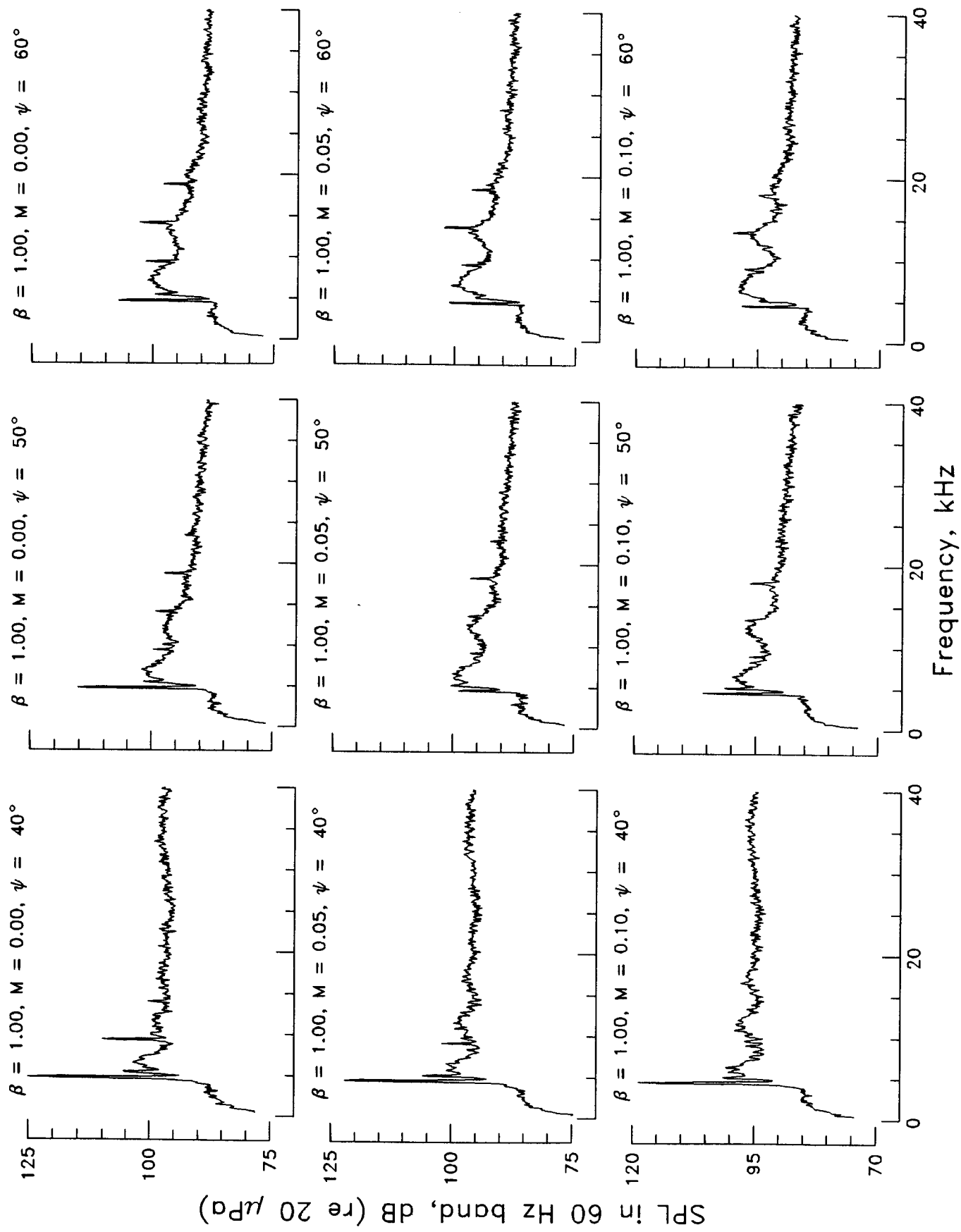
SPL in 60 Hz band, dB (re 20 μ Pa)

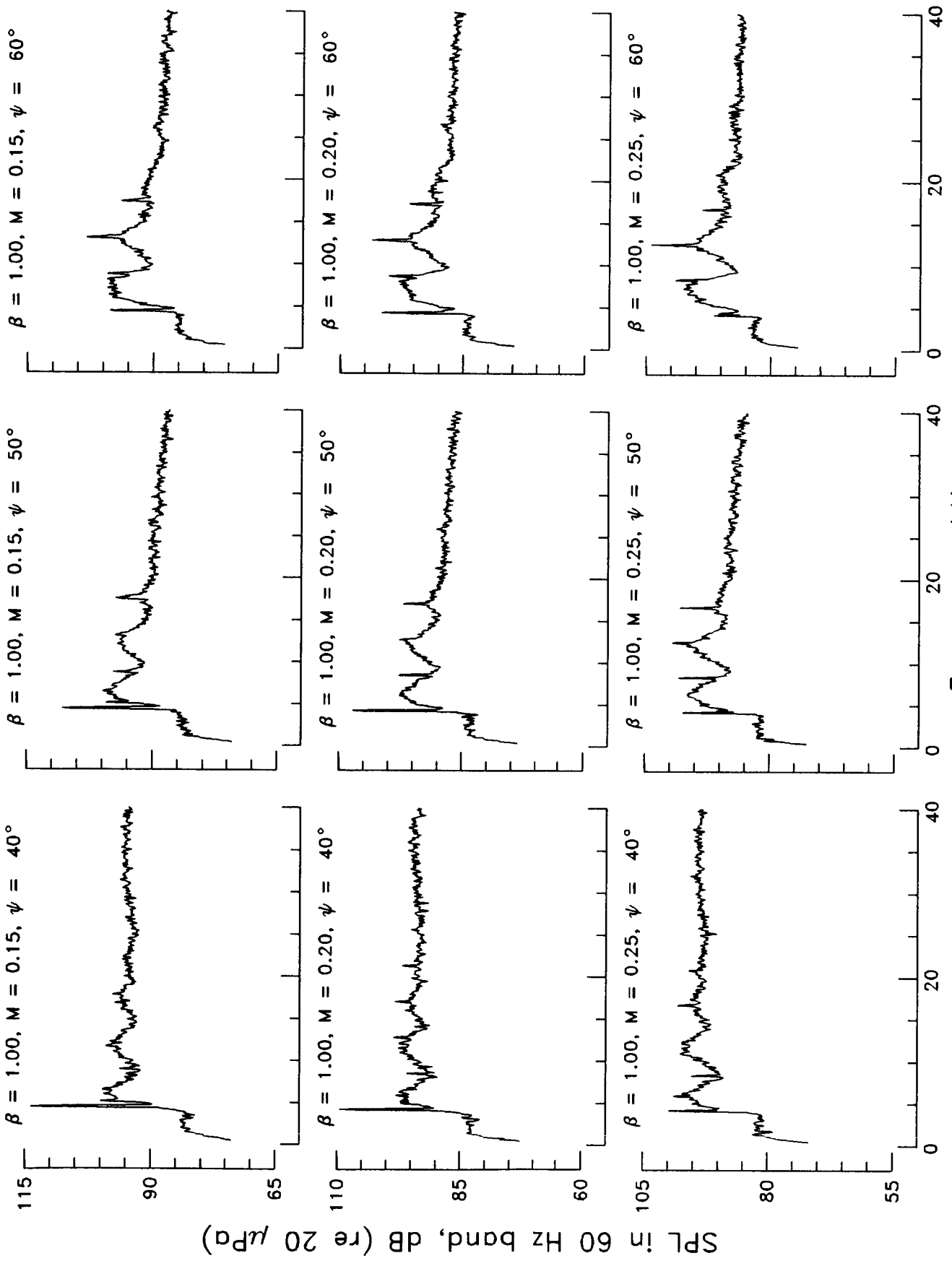


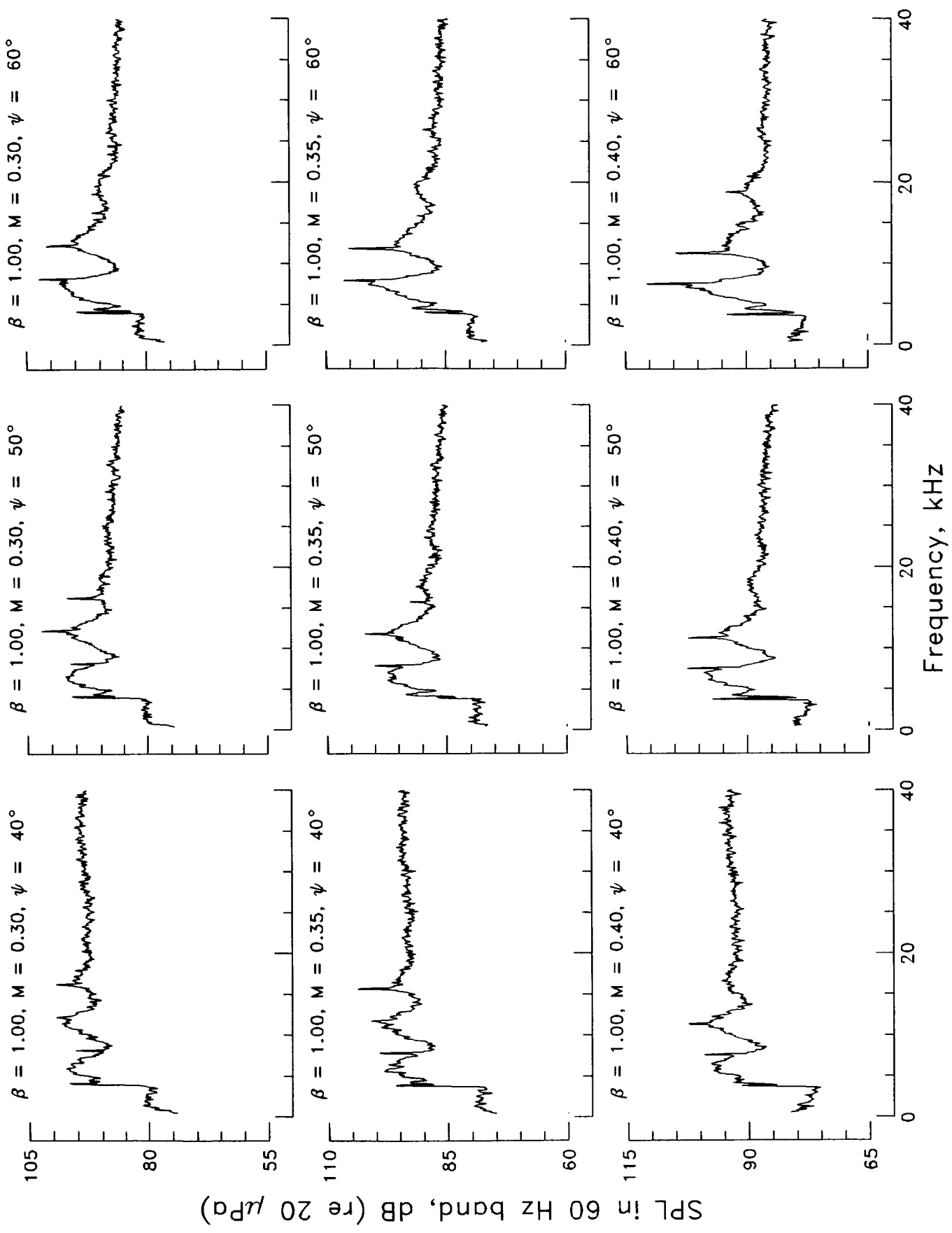
Frequency, kHz

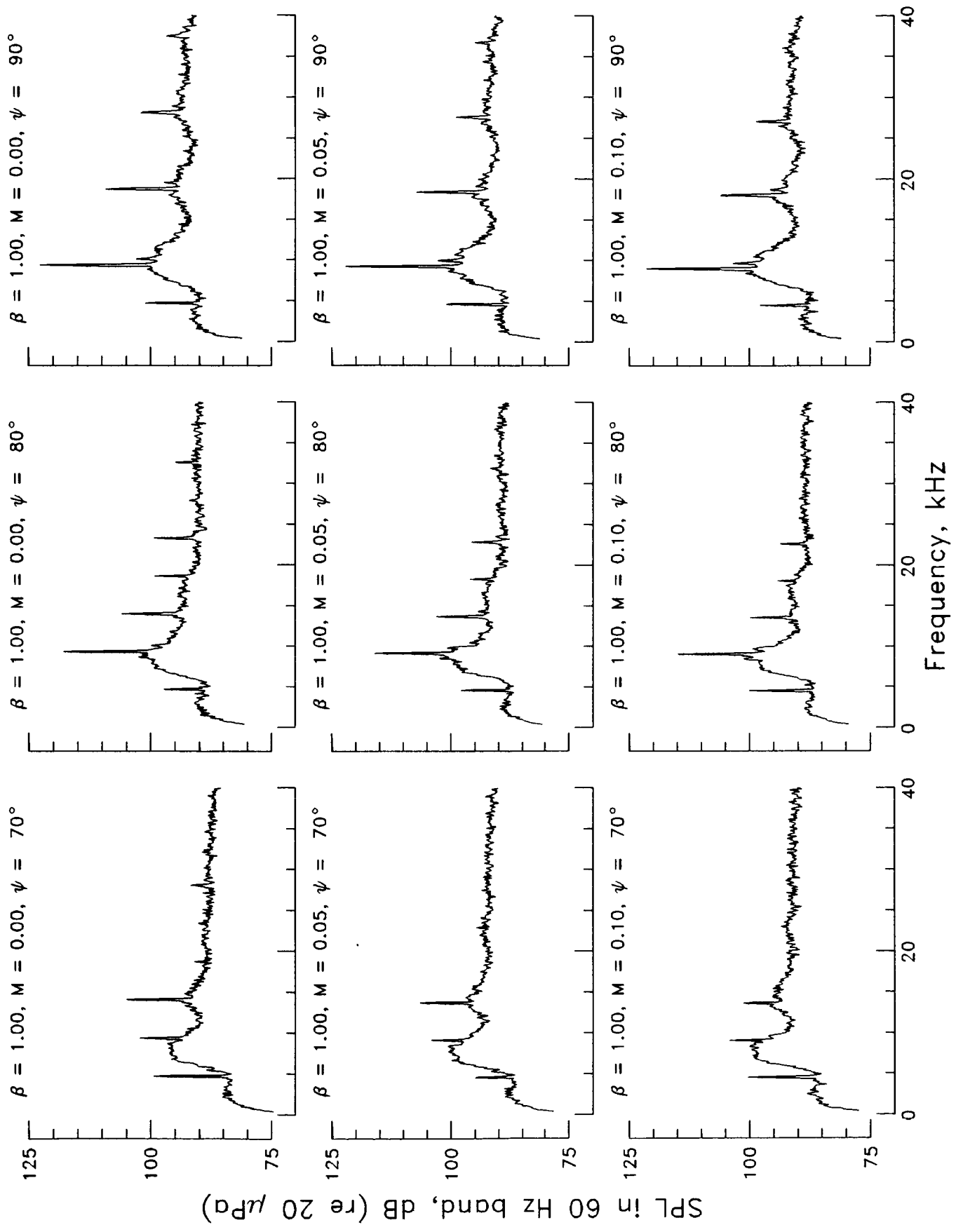


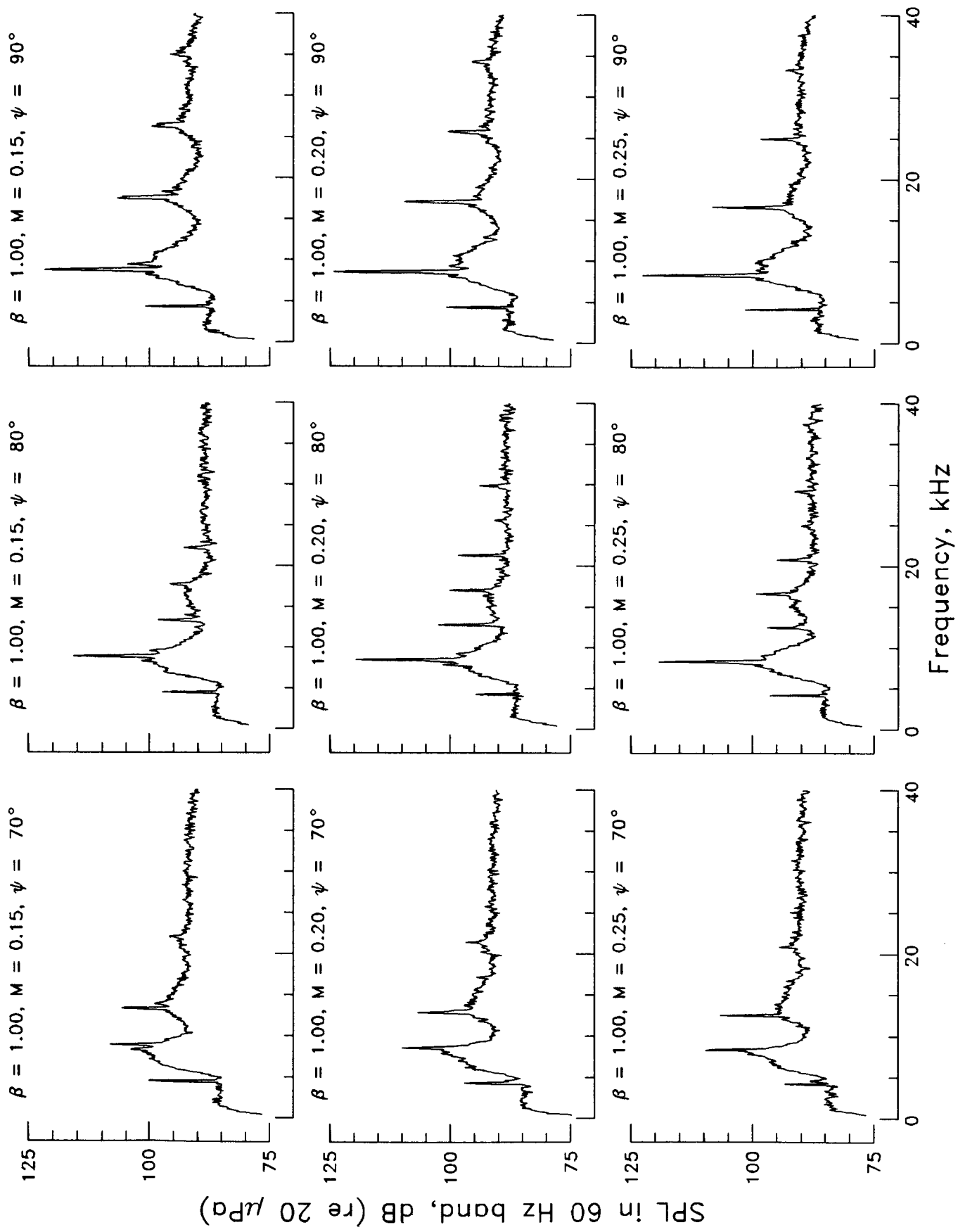


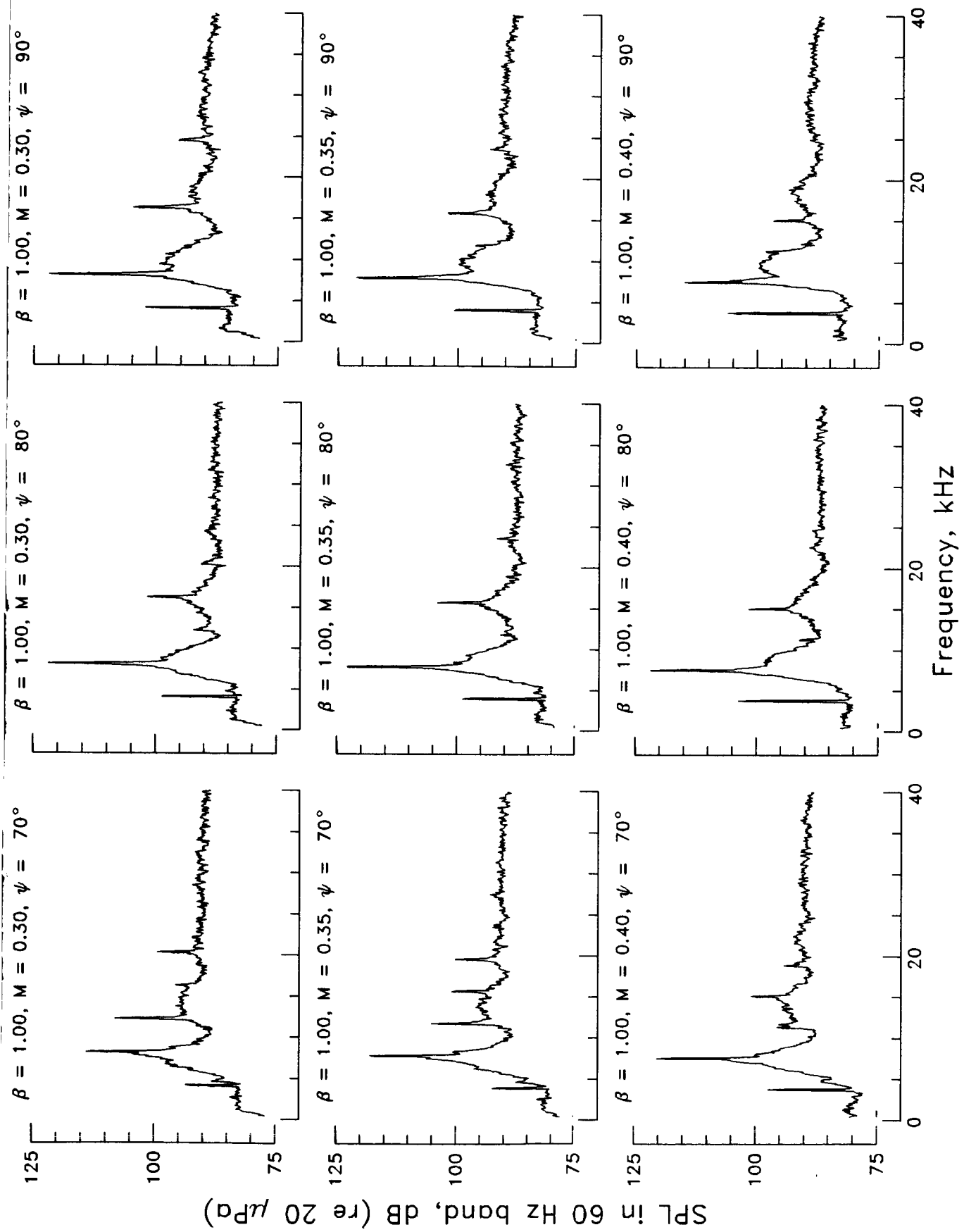


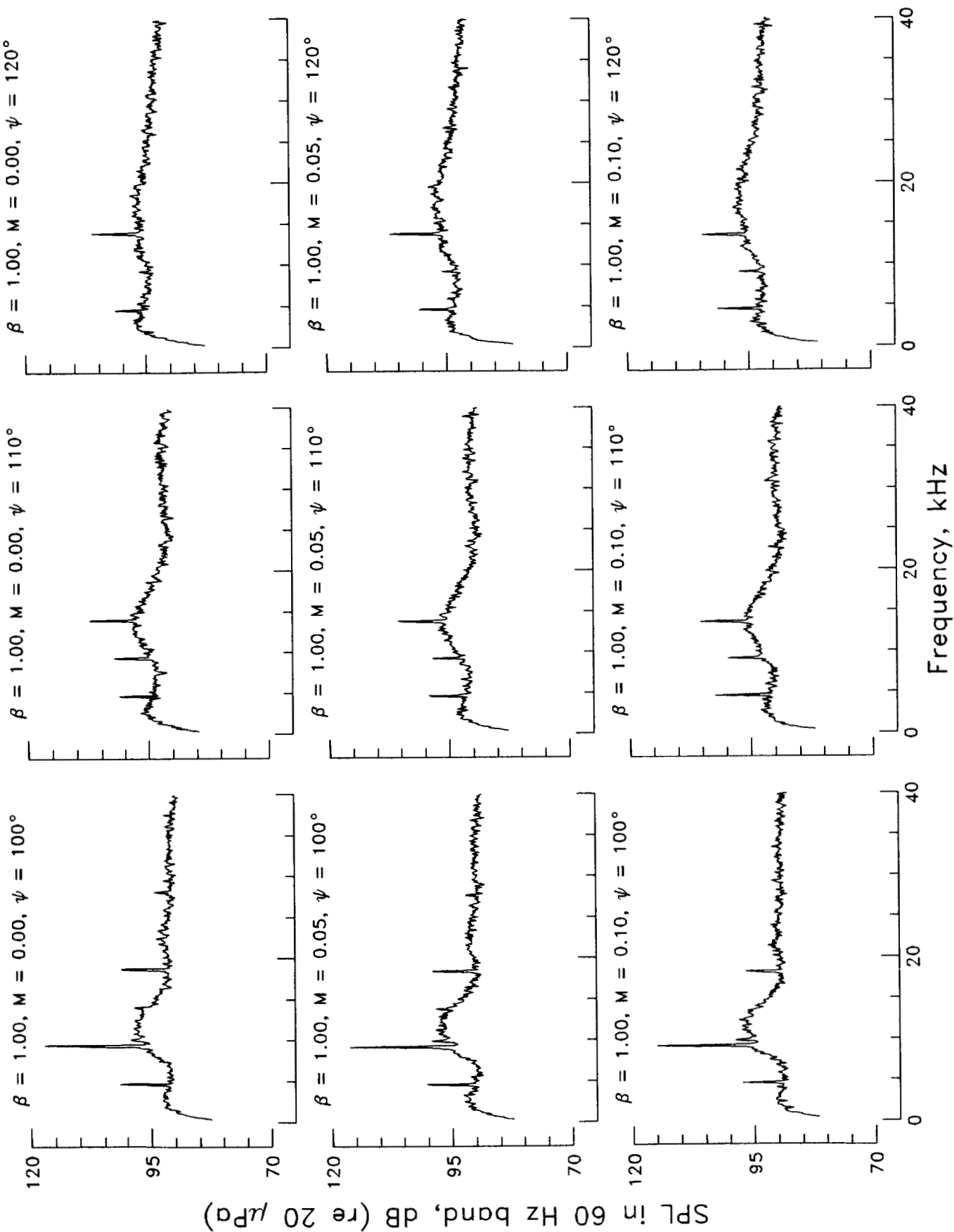


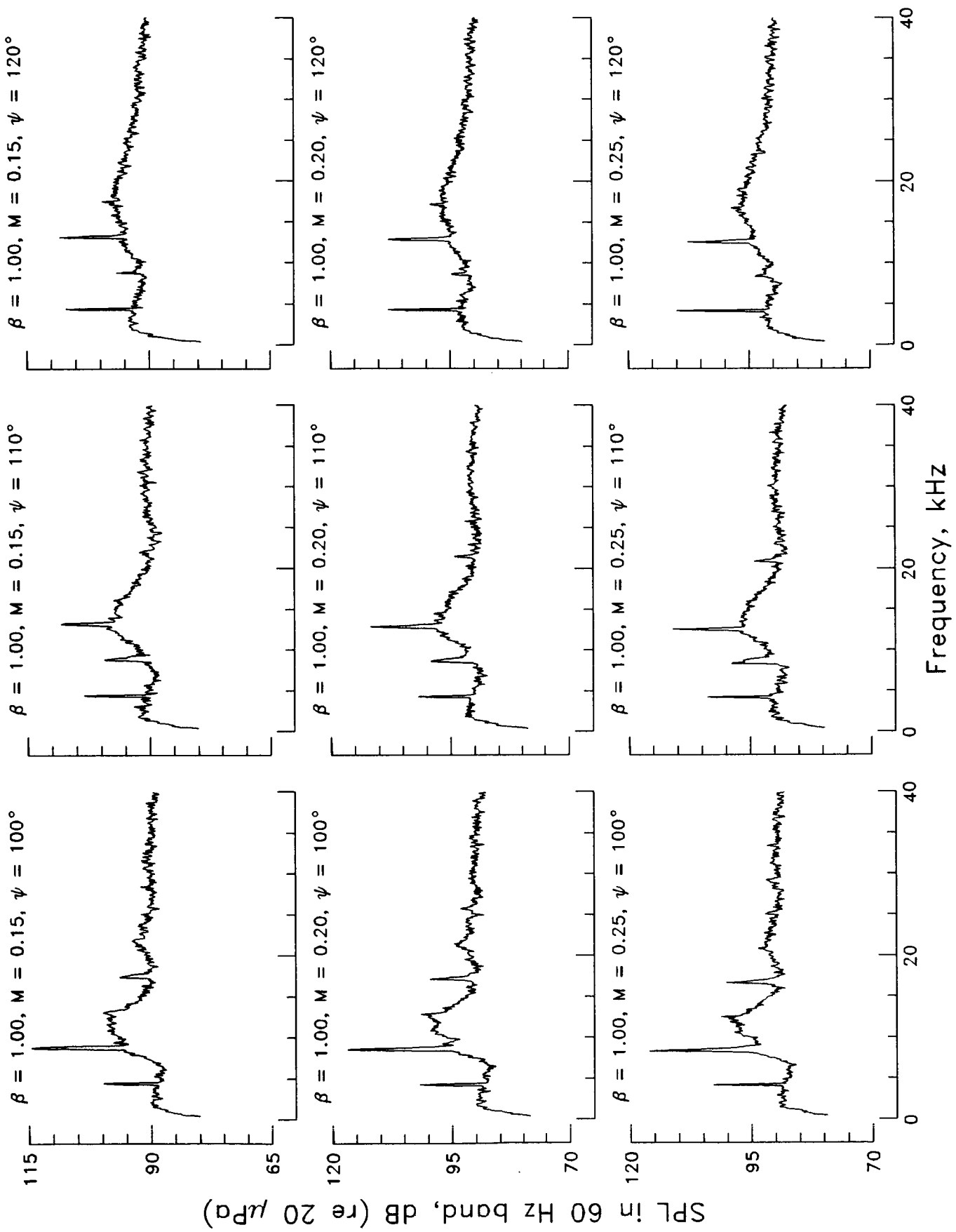




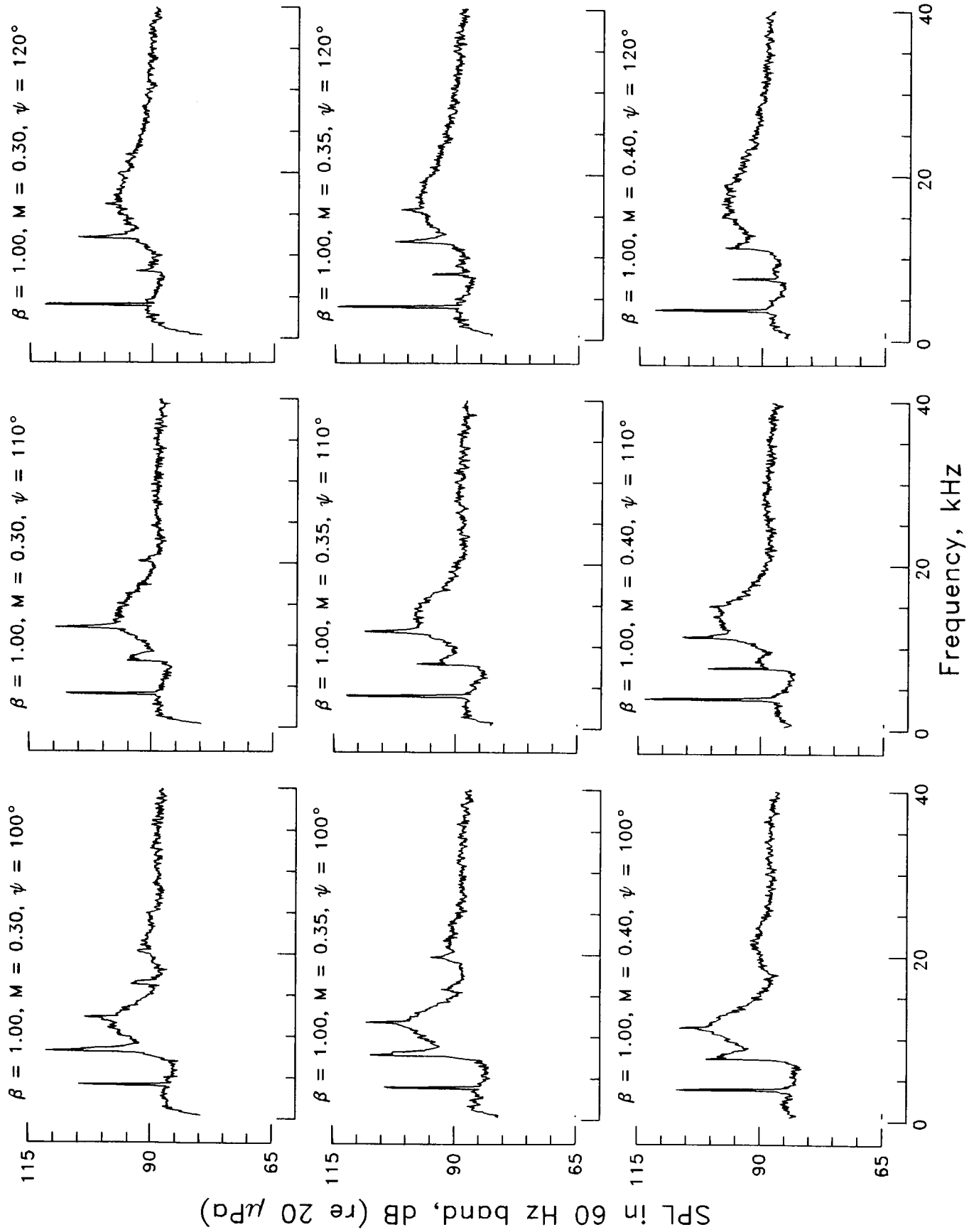


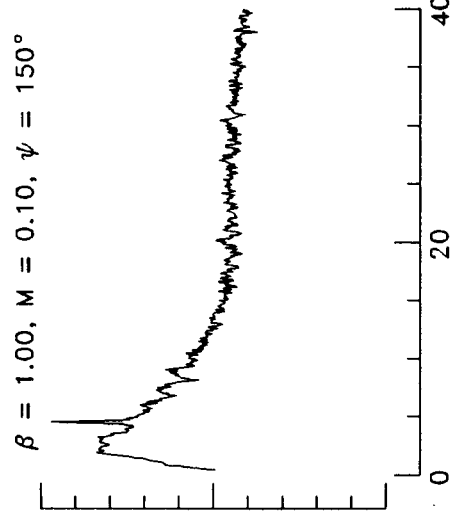
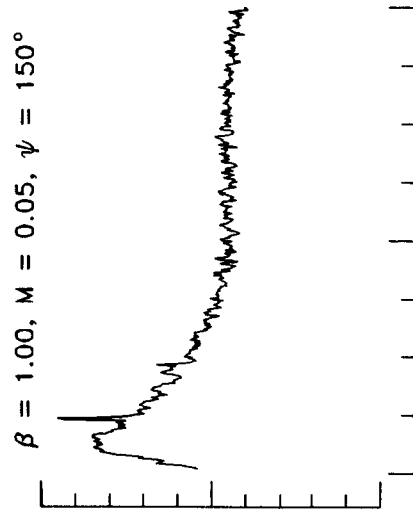
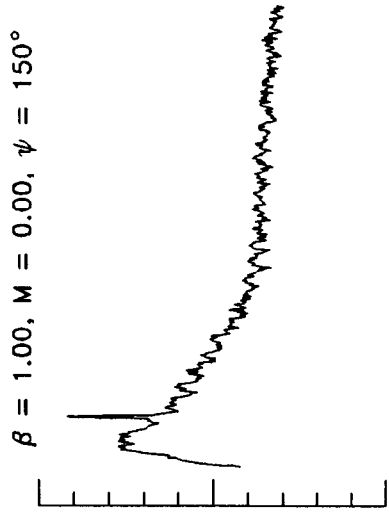
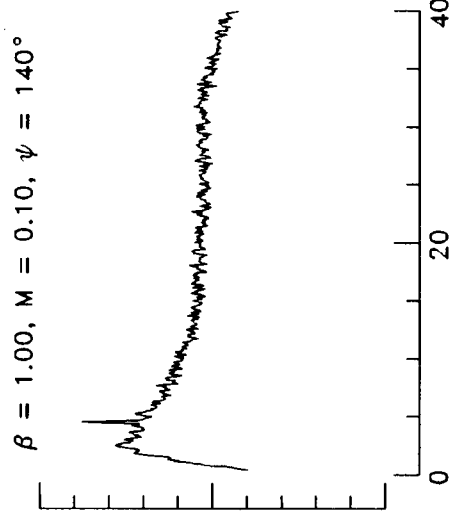
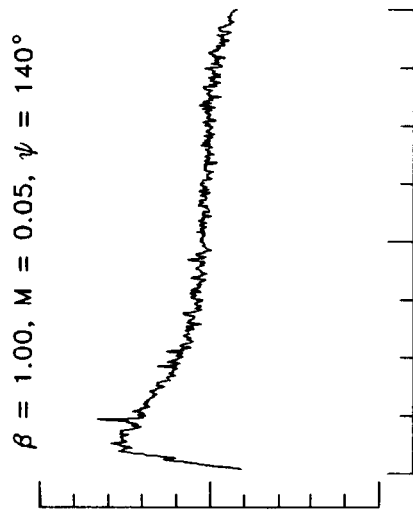
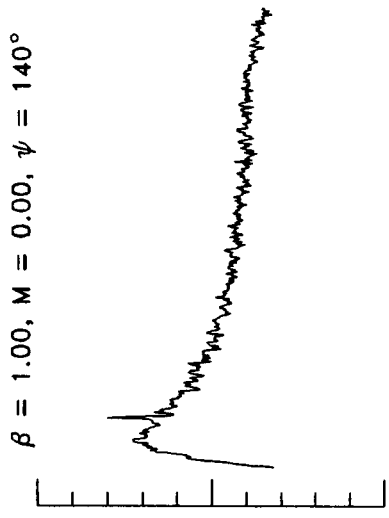
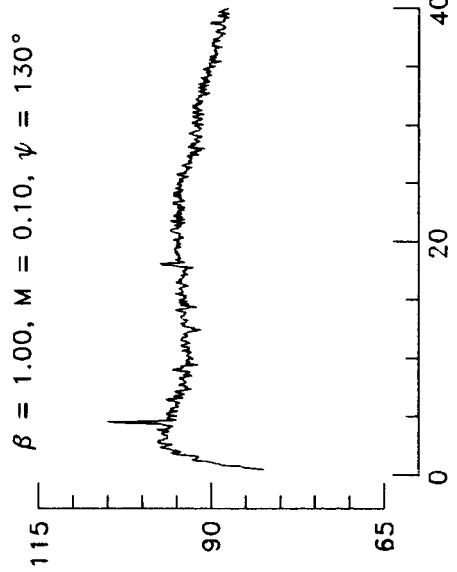
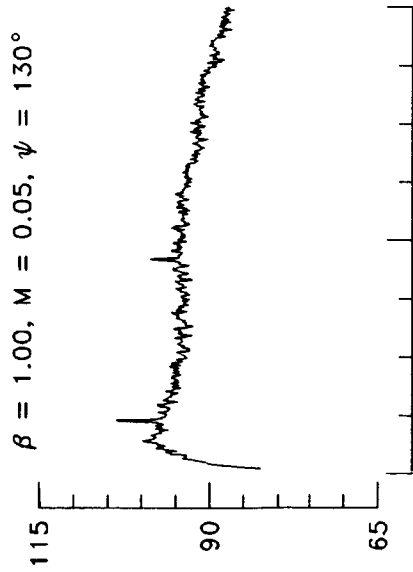
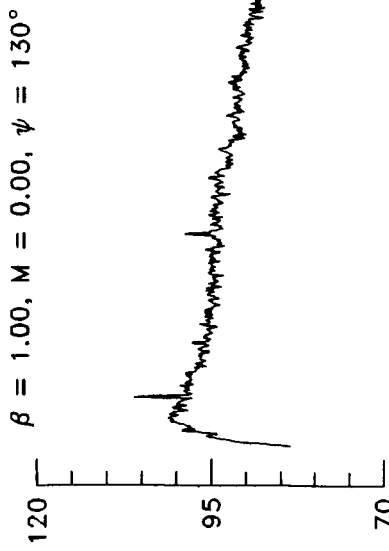






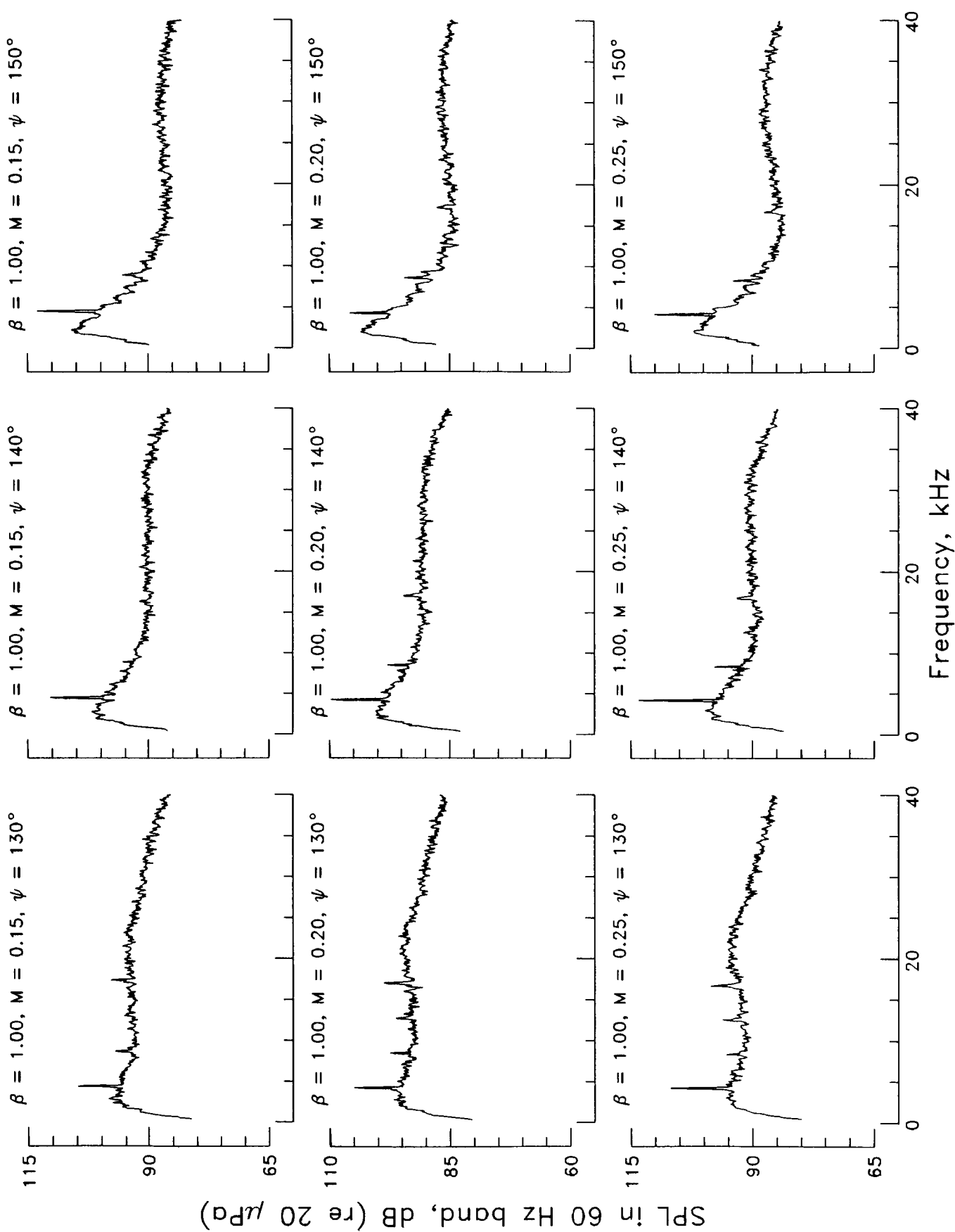
C-2

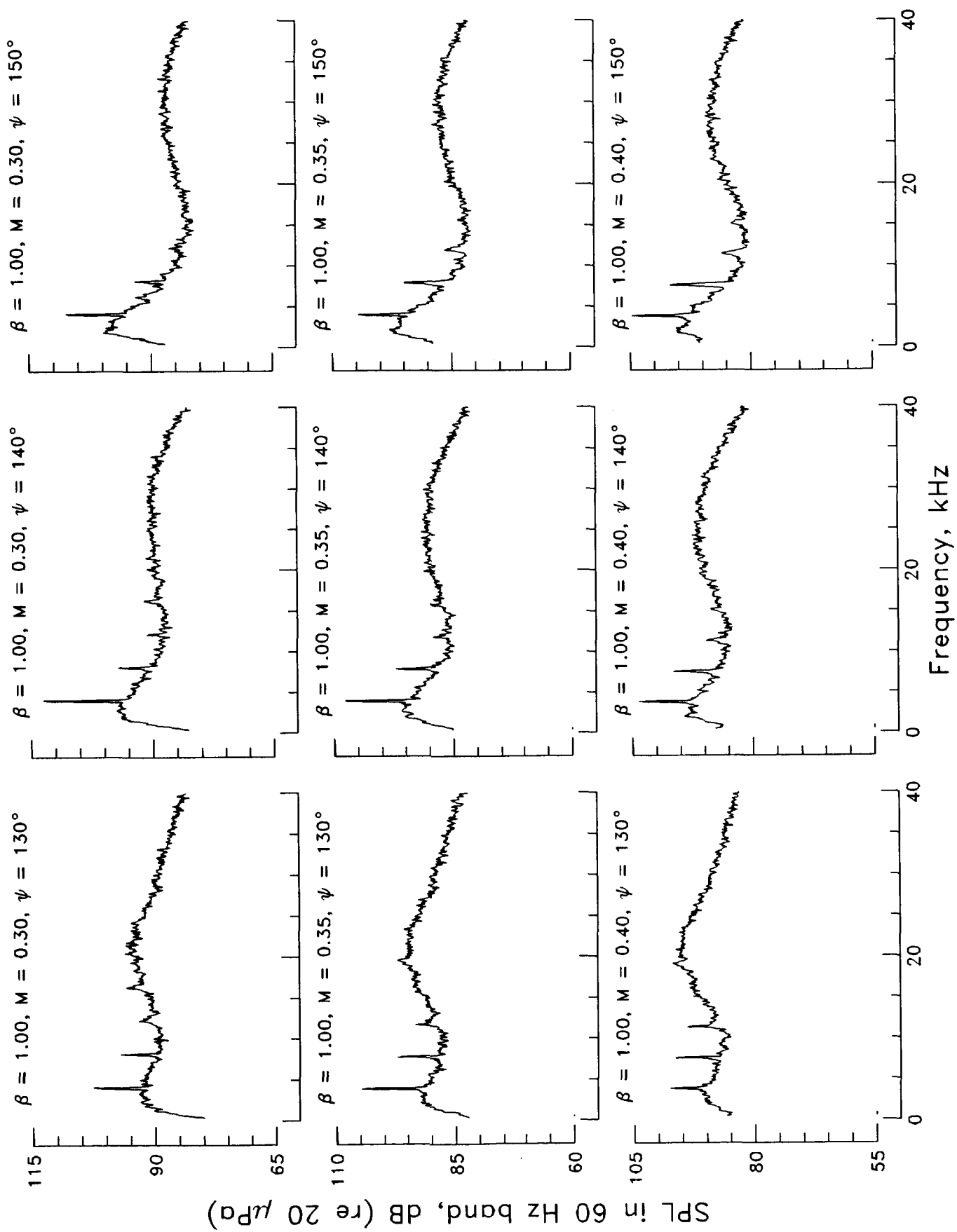


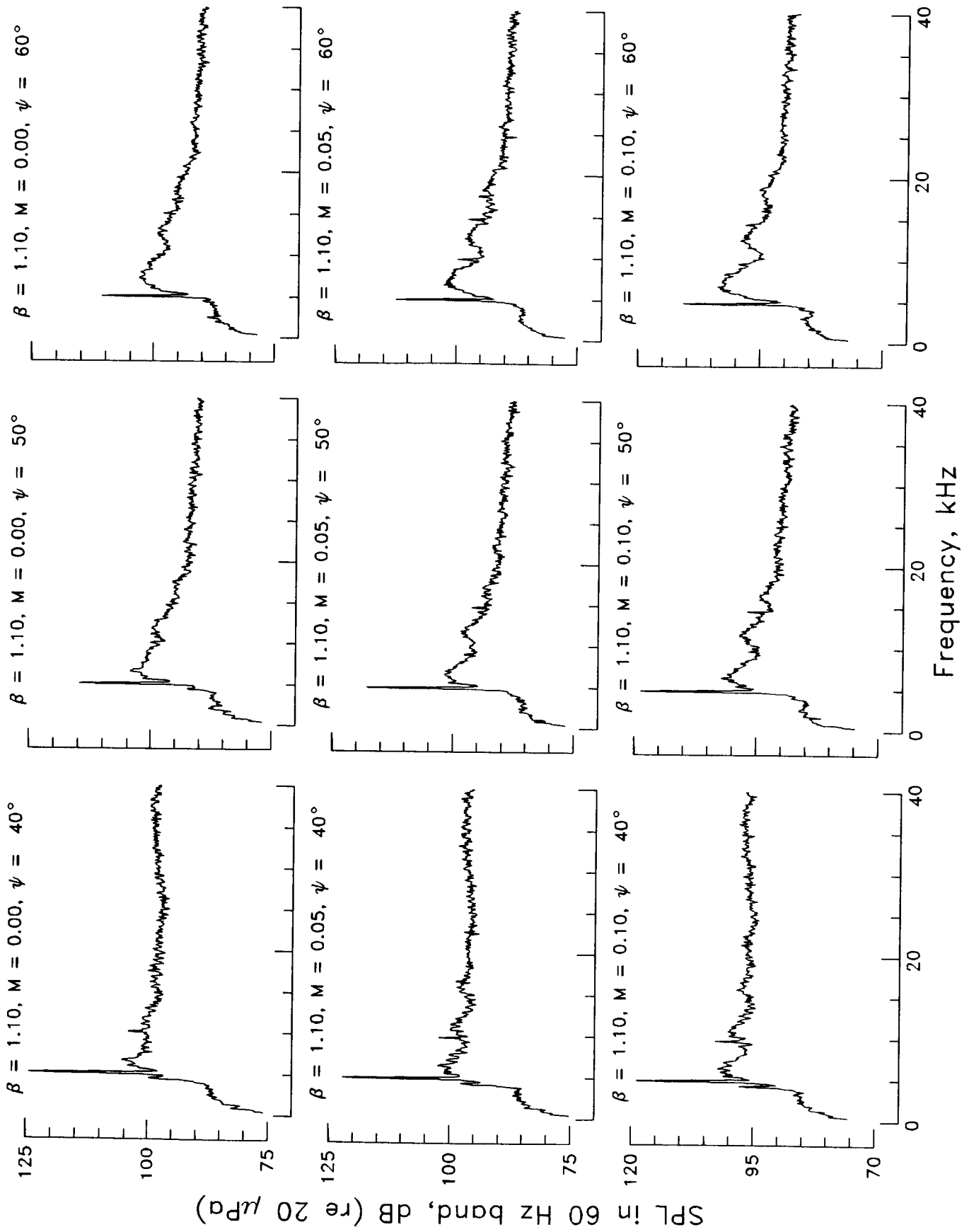


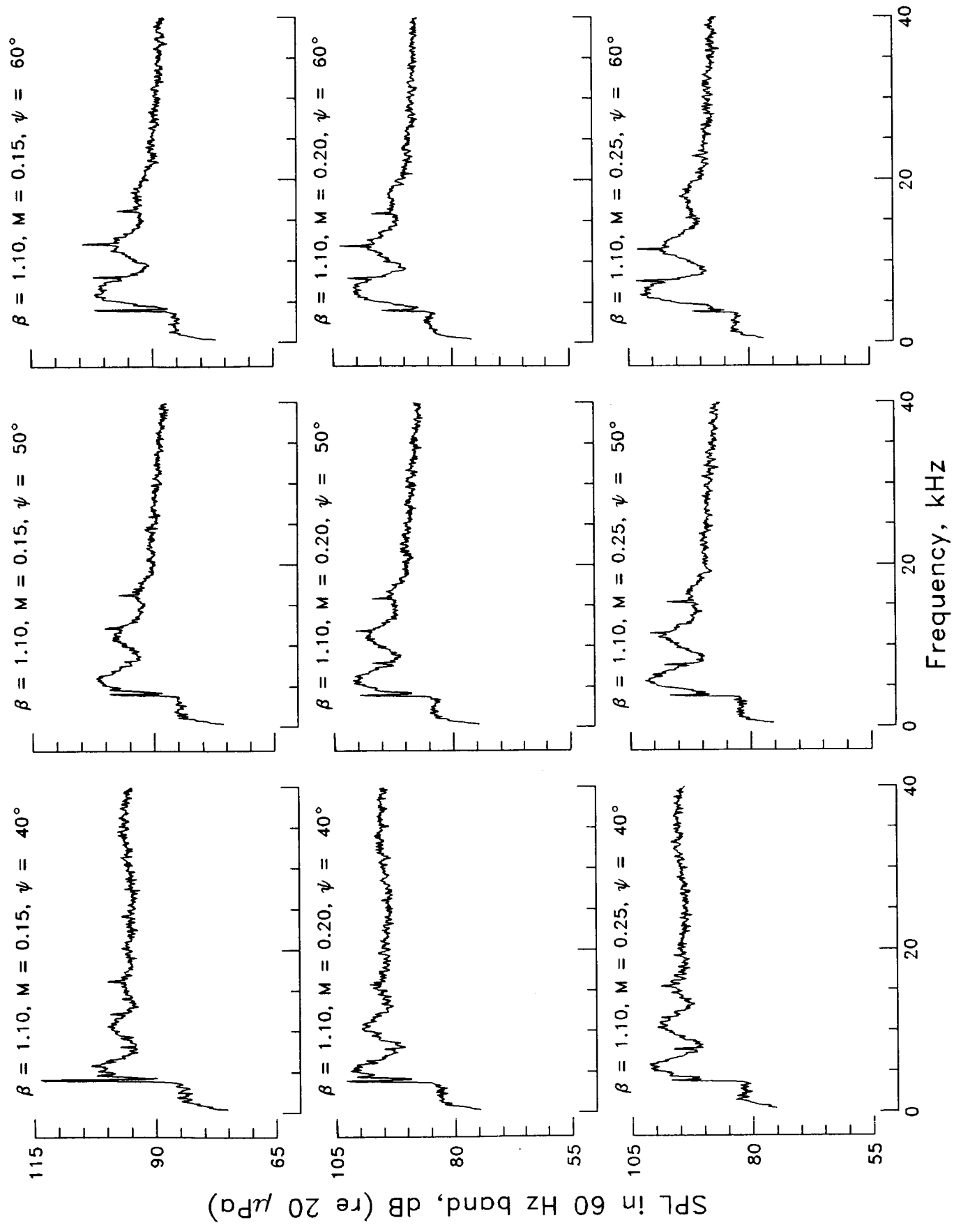
SPL in 60 Hz band, dB (re 20 μ Pa)

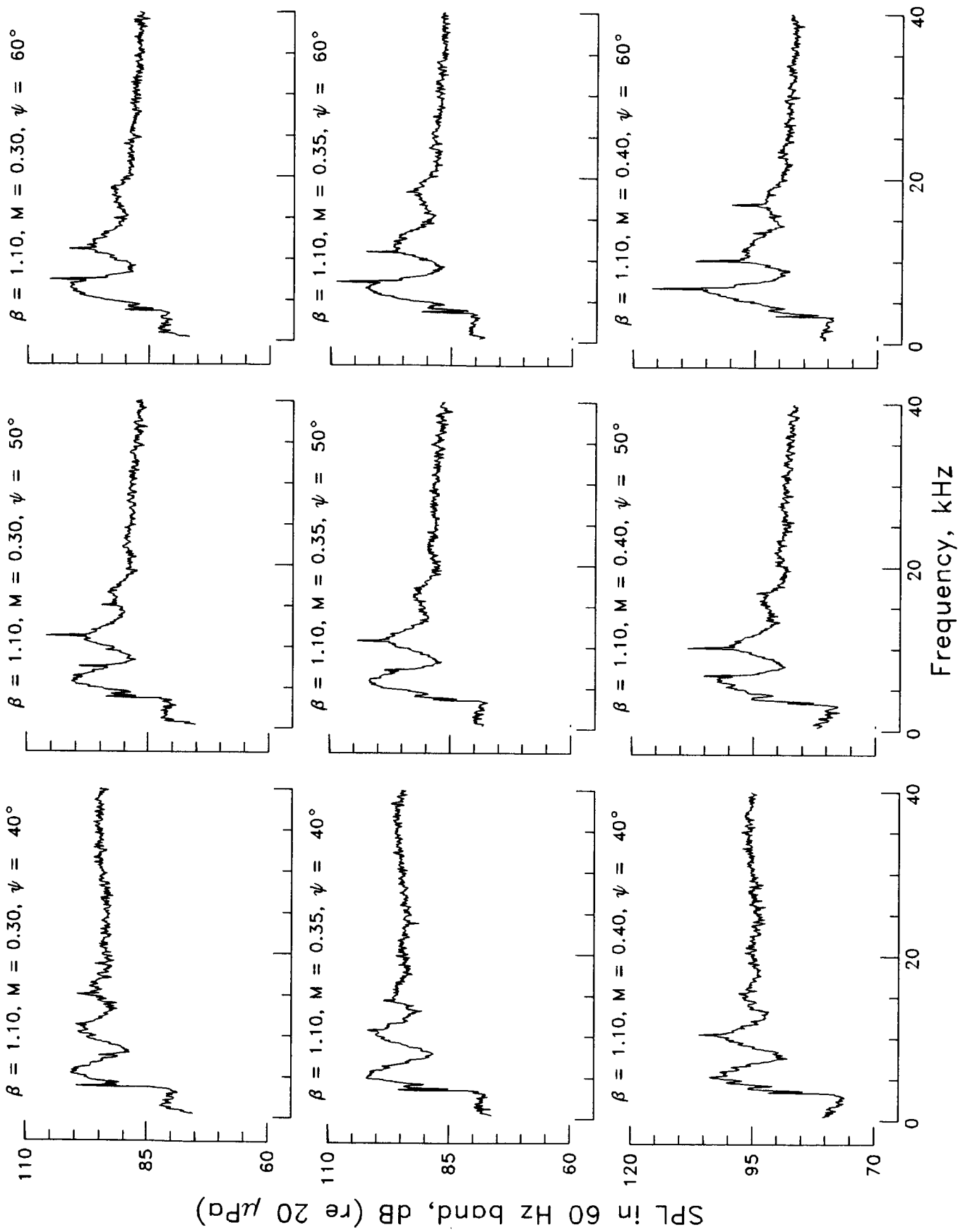
Frequency, kHz

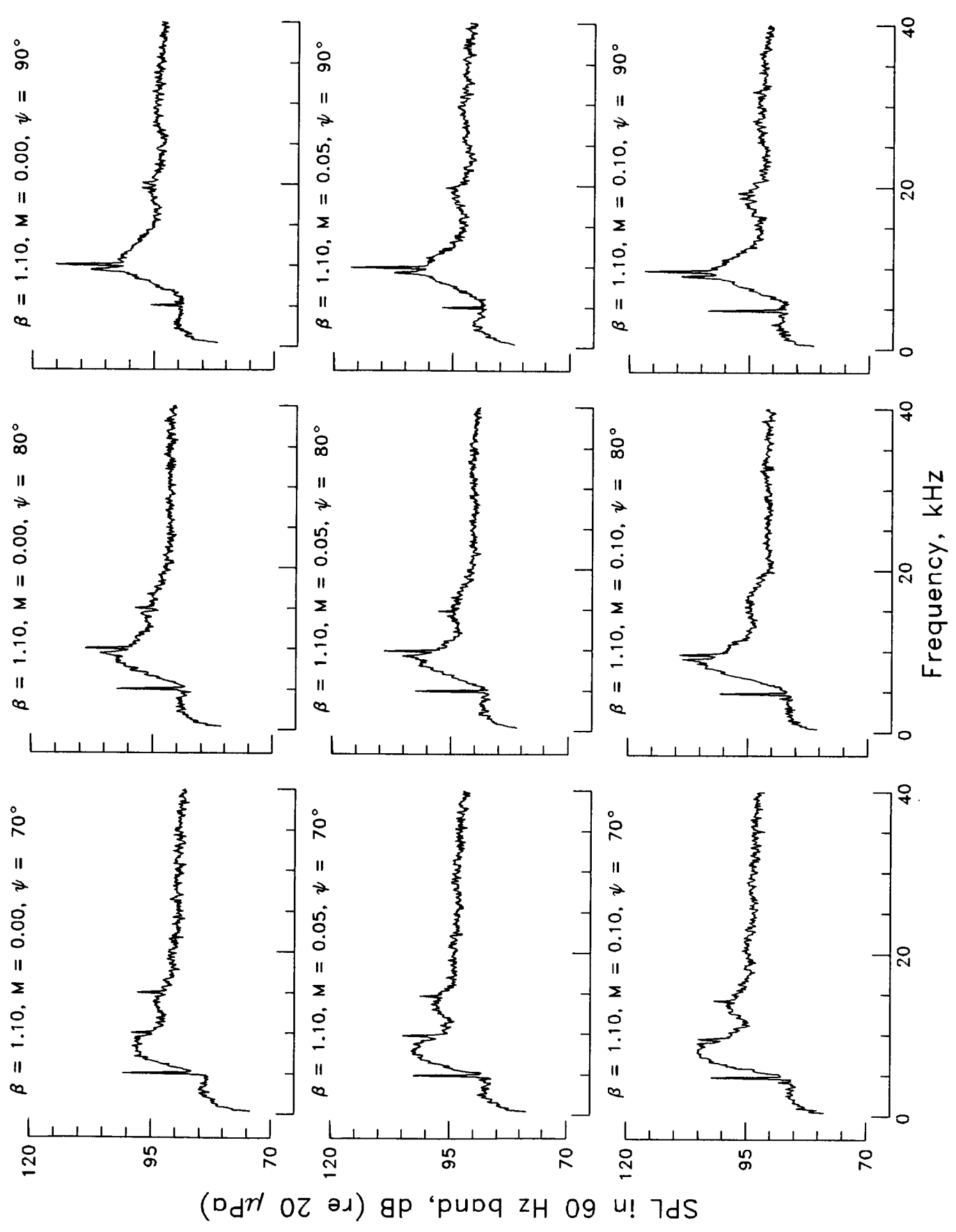


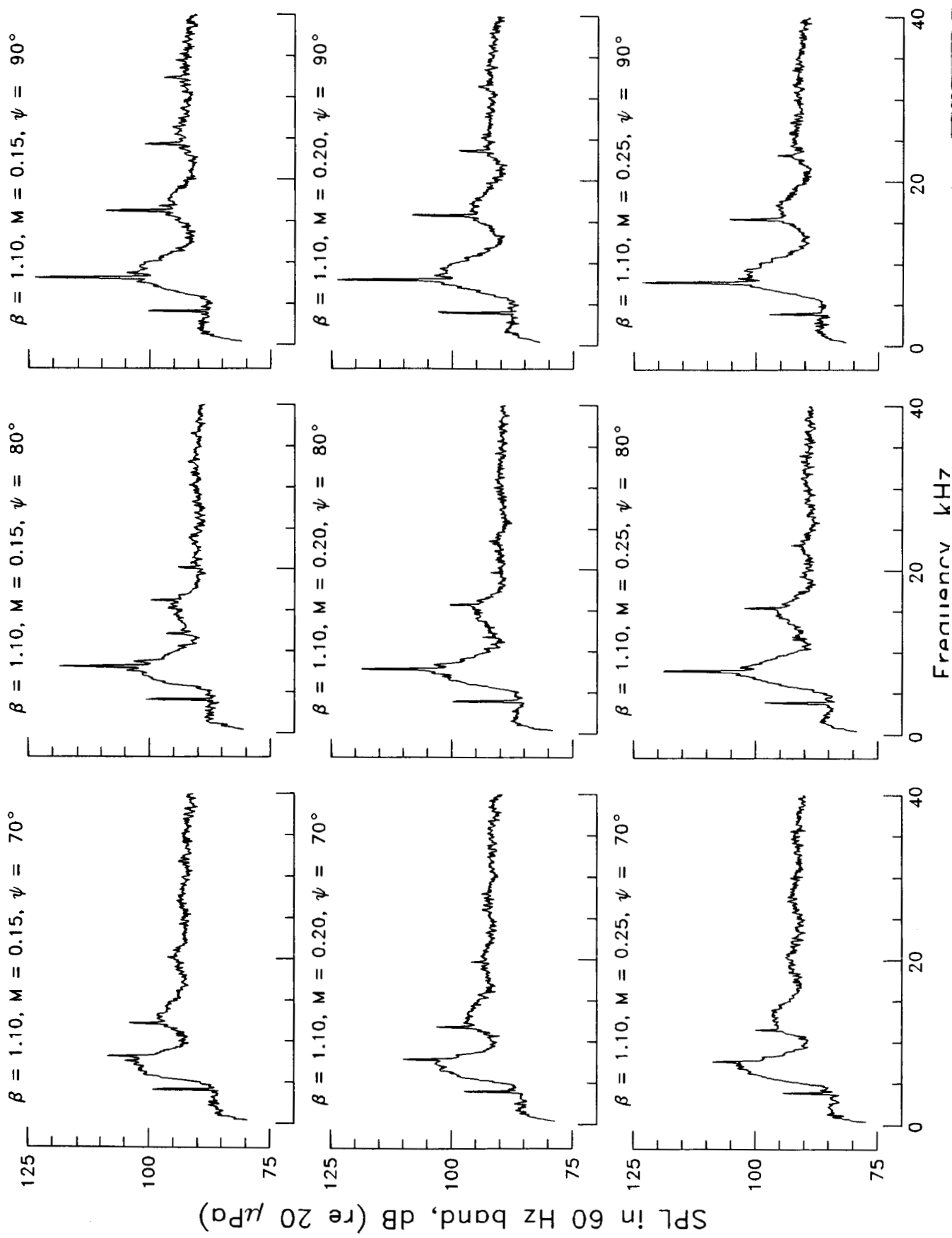


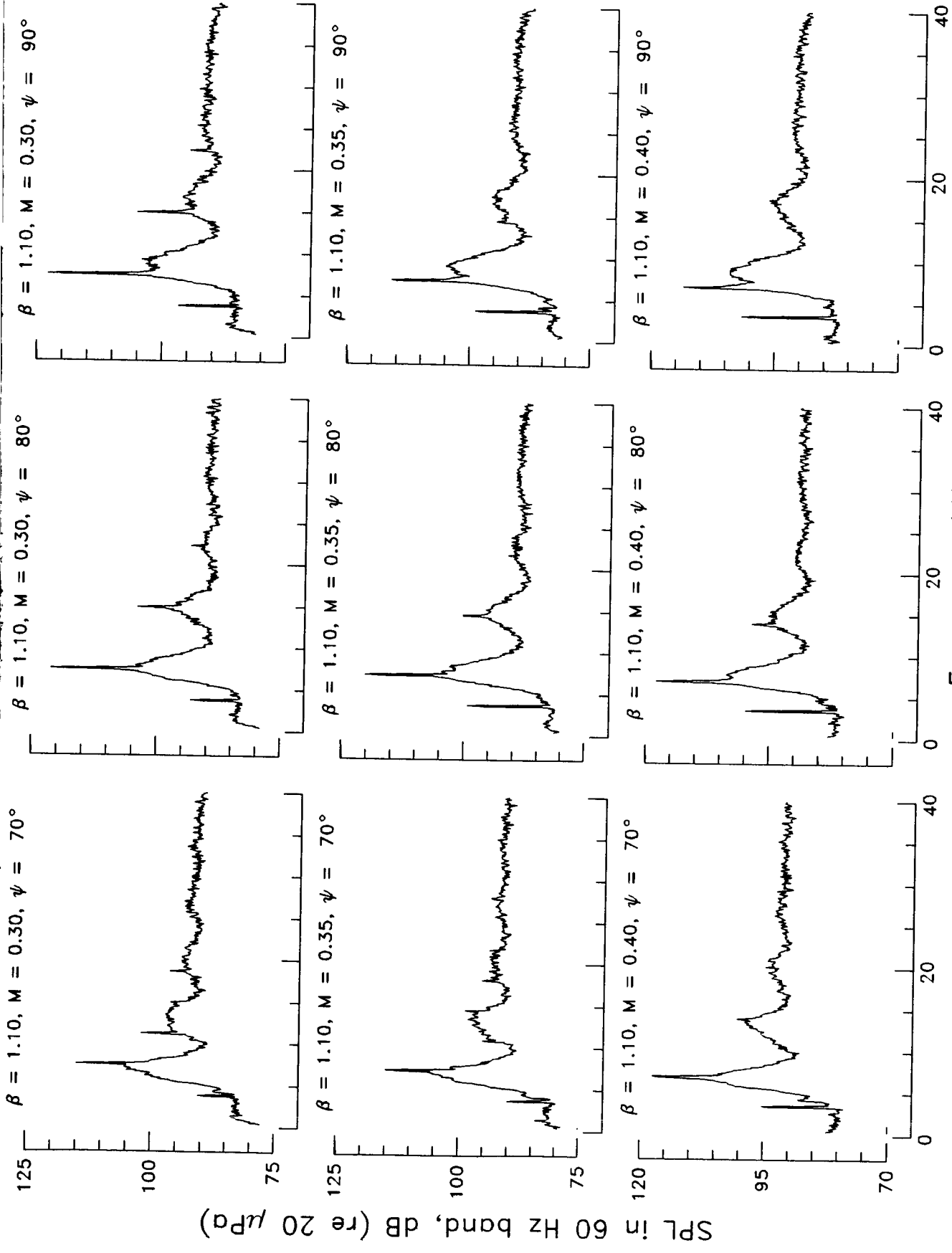


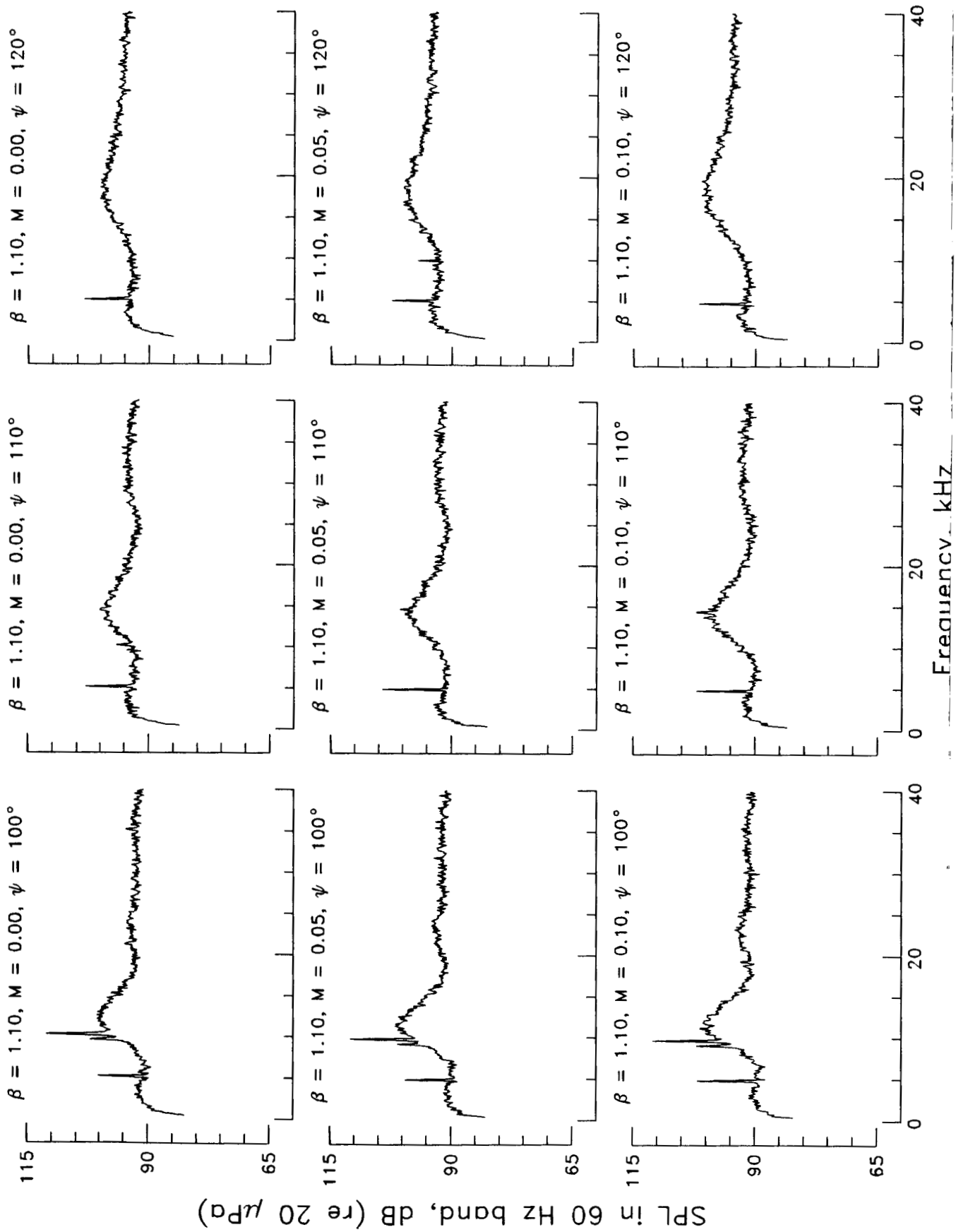


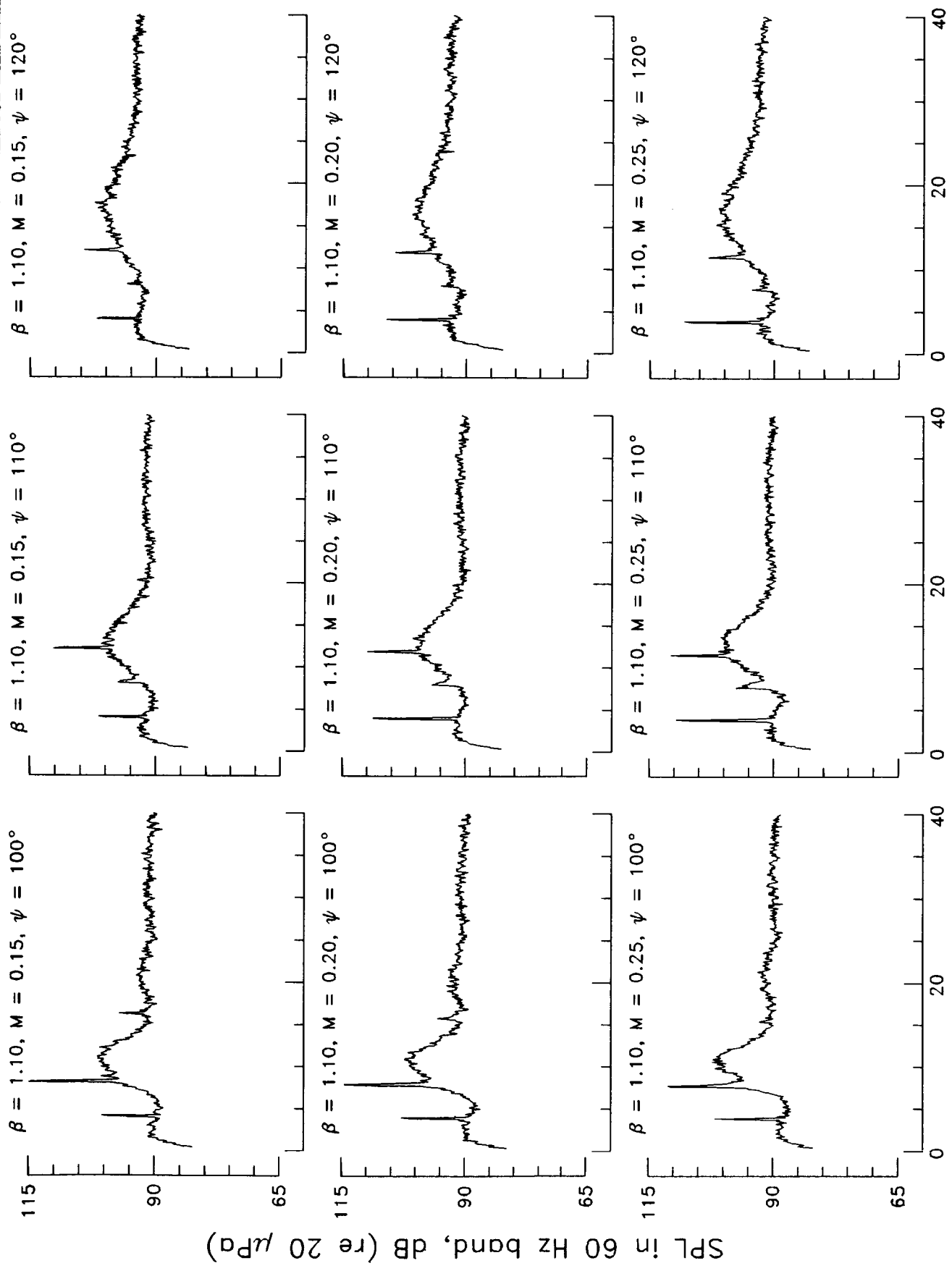




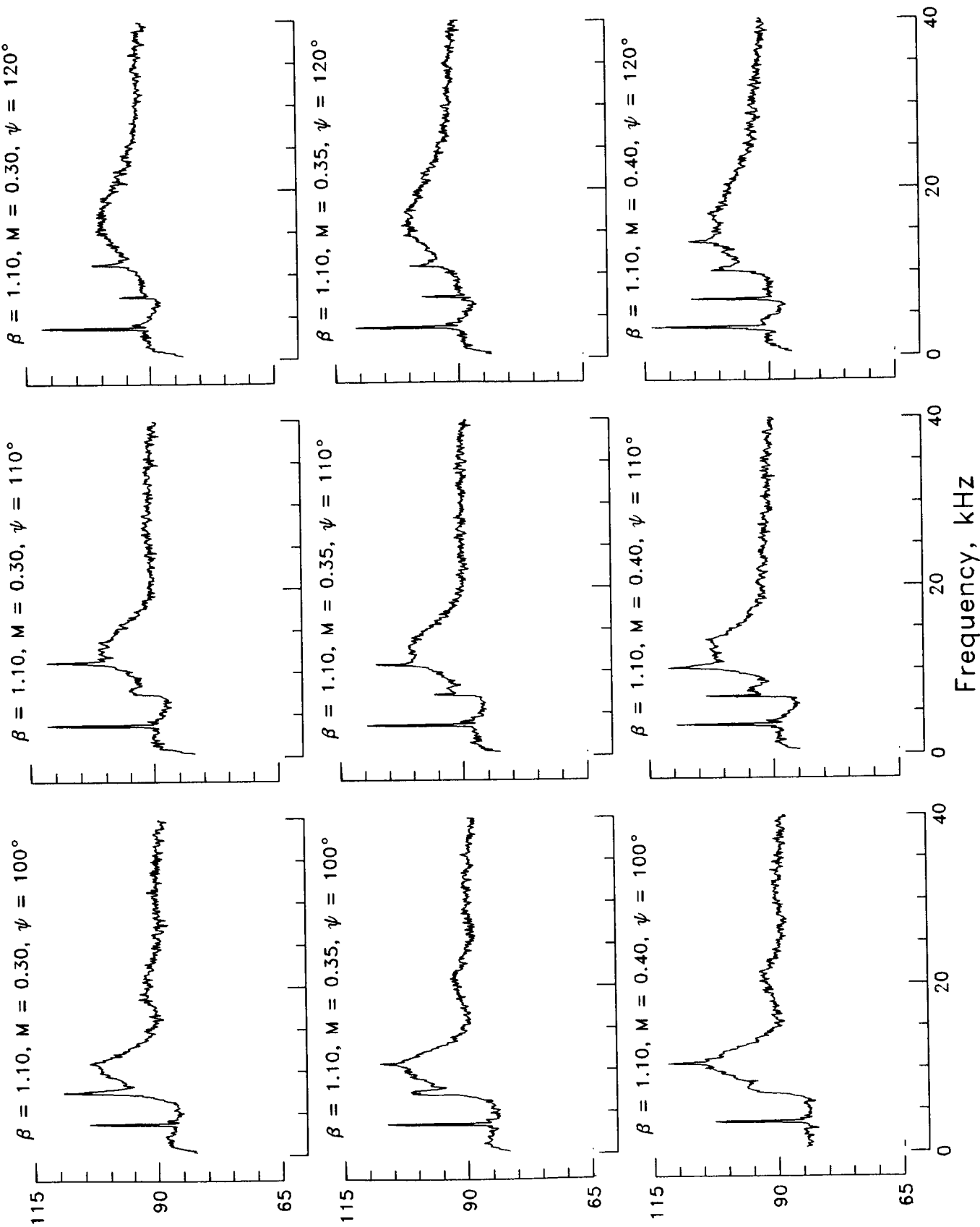




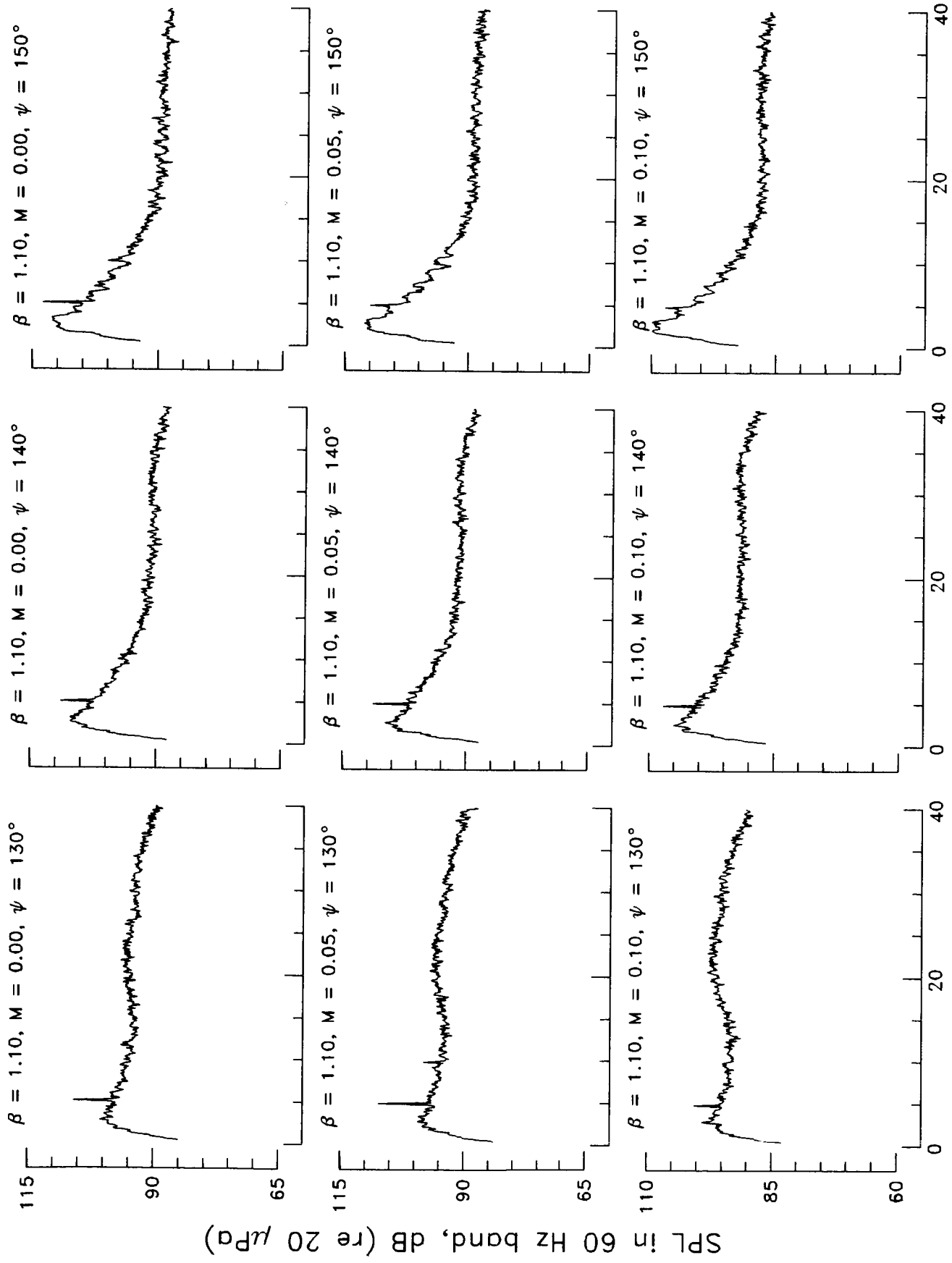


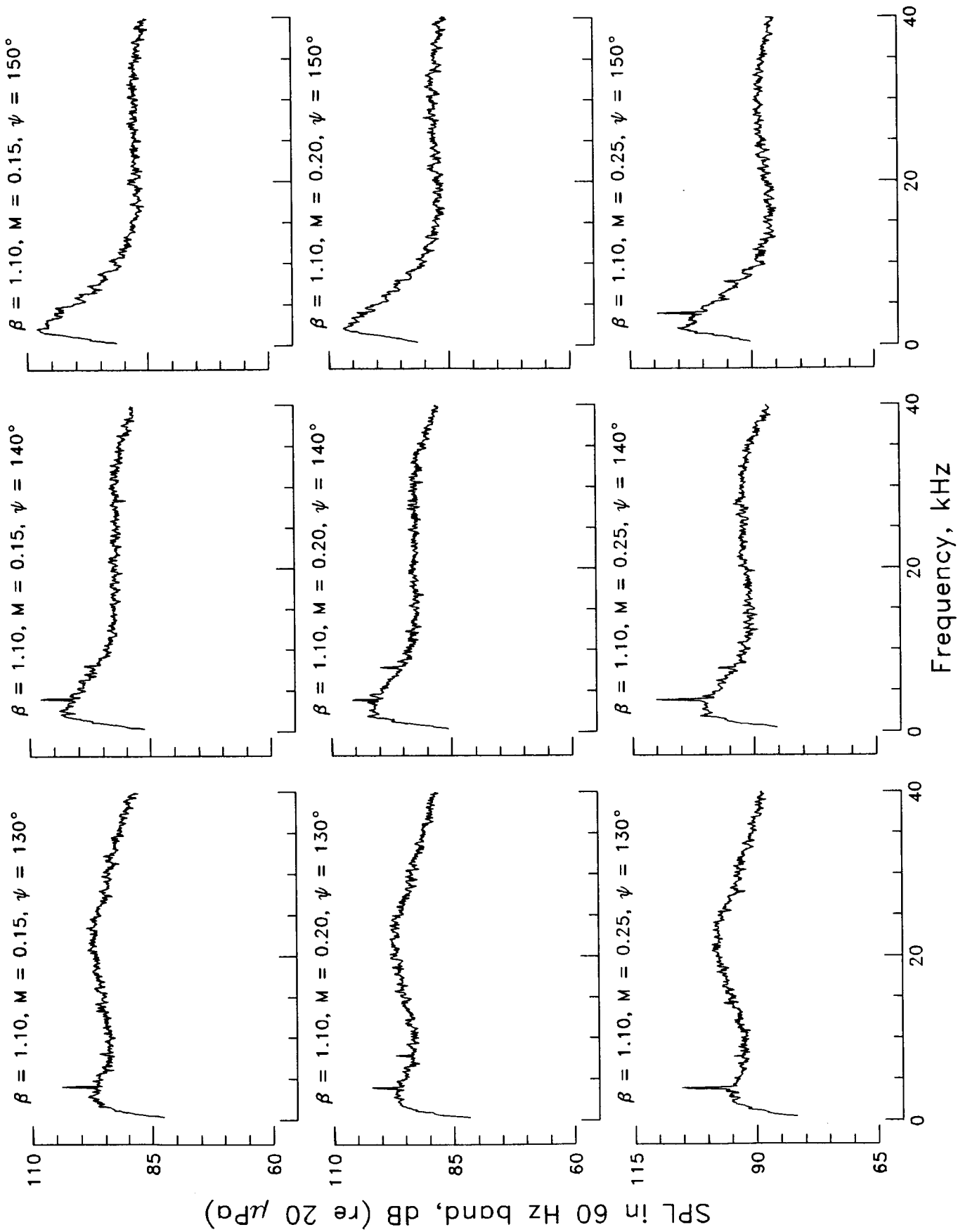


SPL in 60 Hz band, dB (re 20 μ Pa)

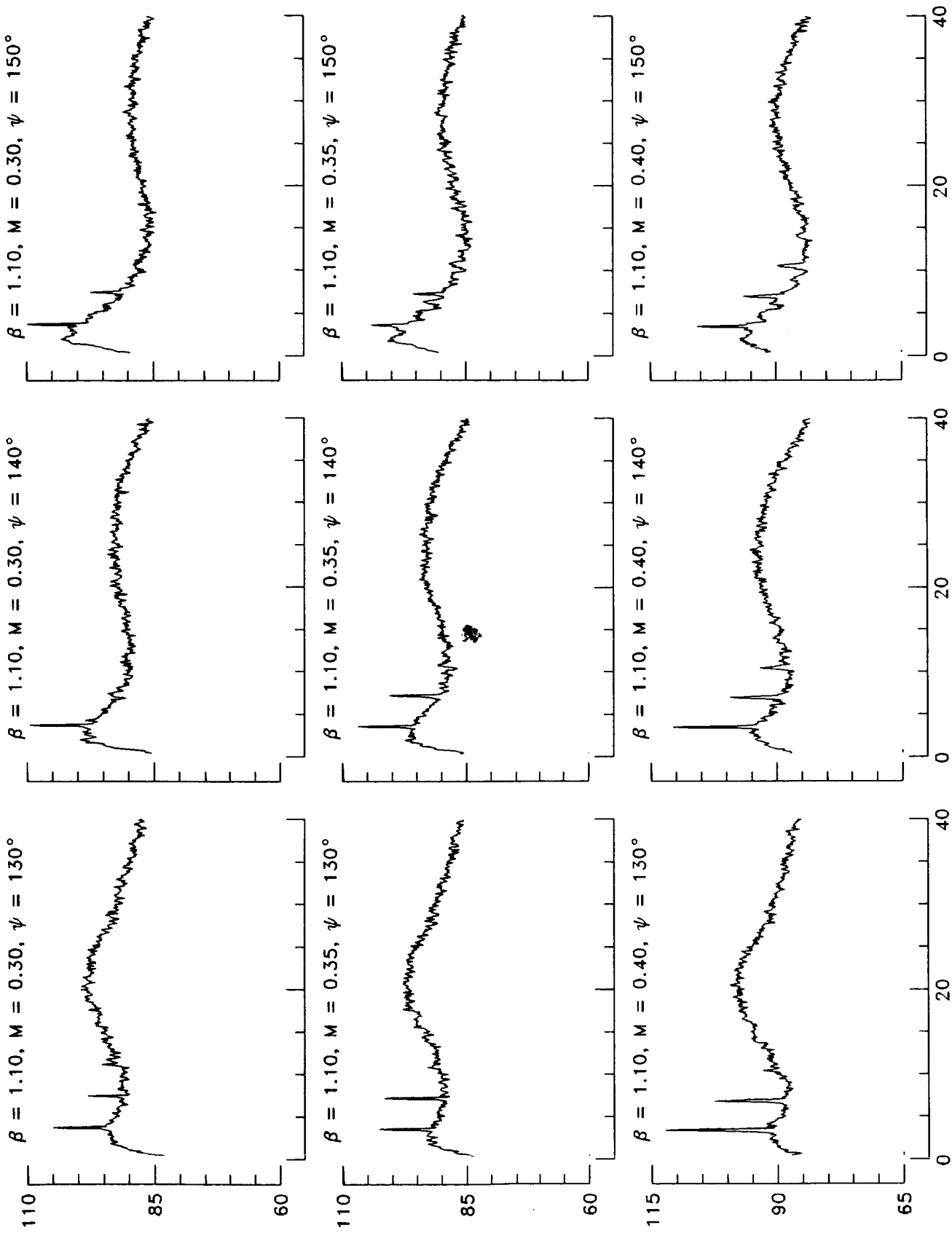


Frequency, kHz

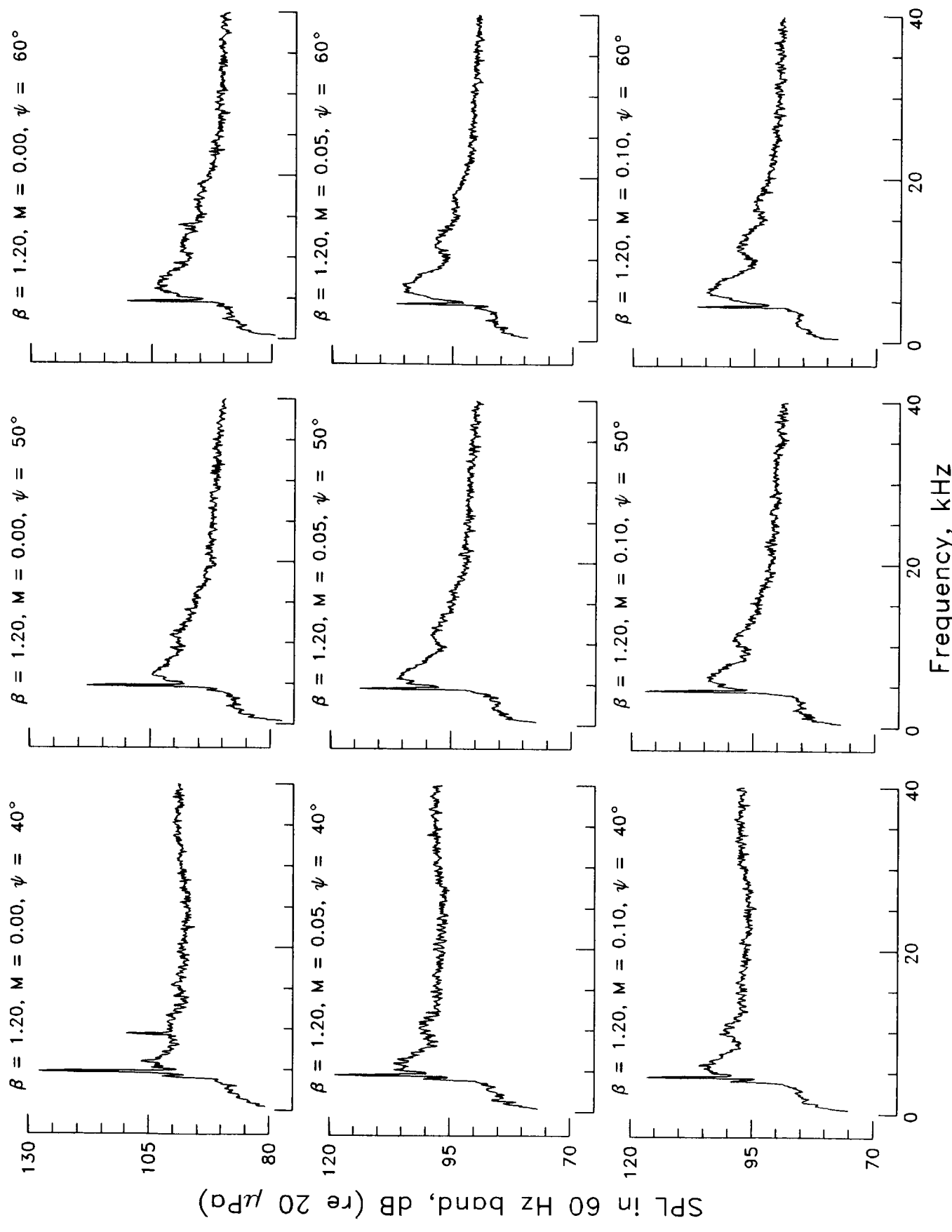


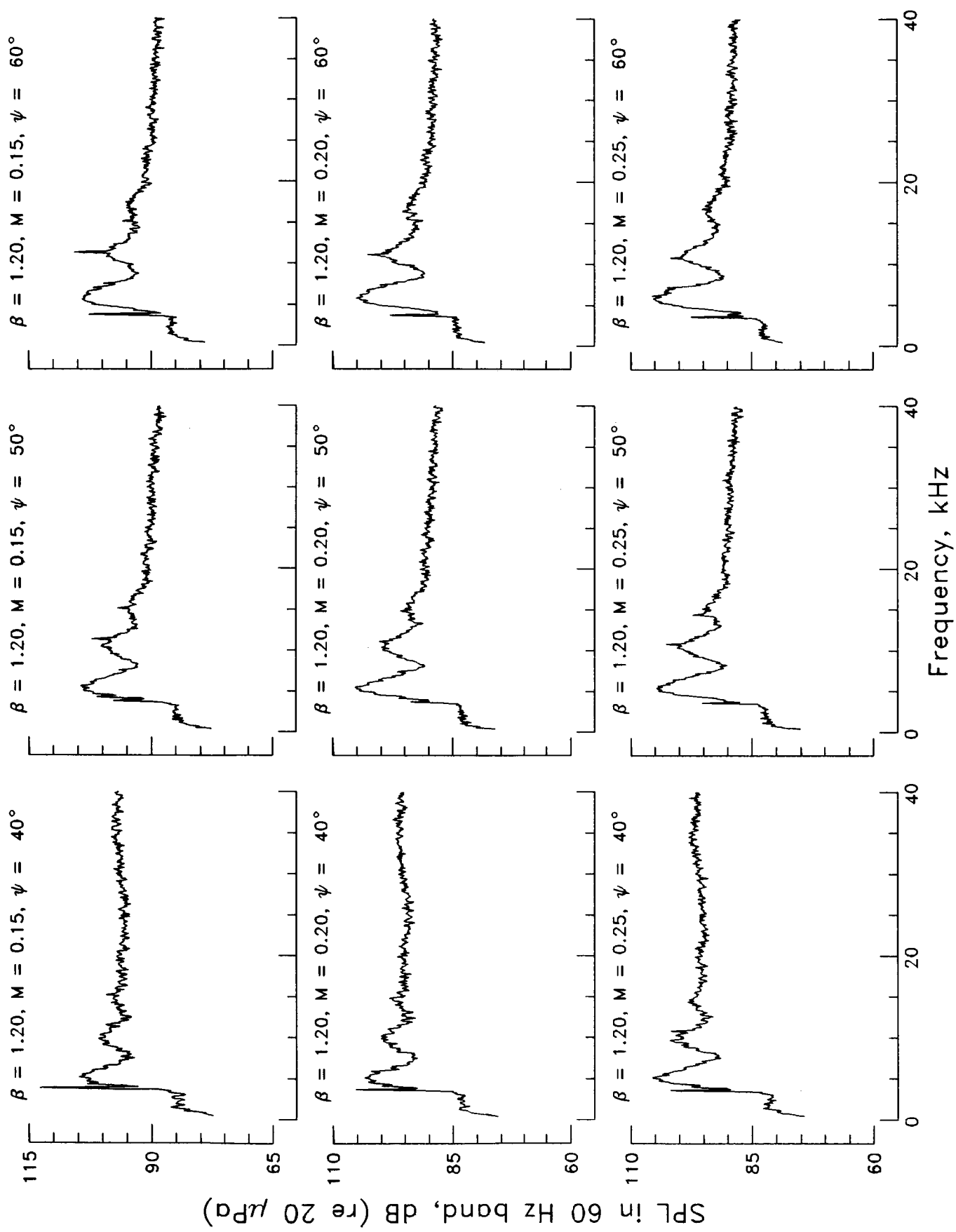


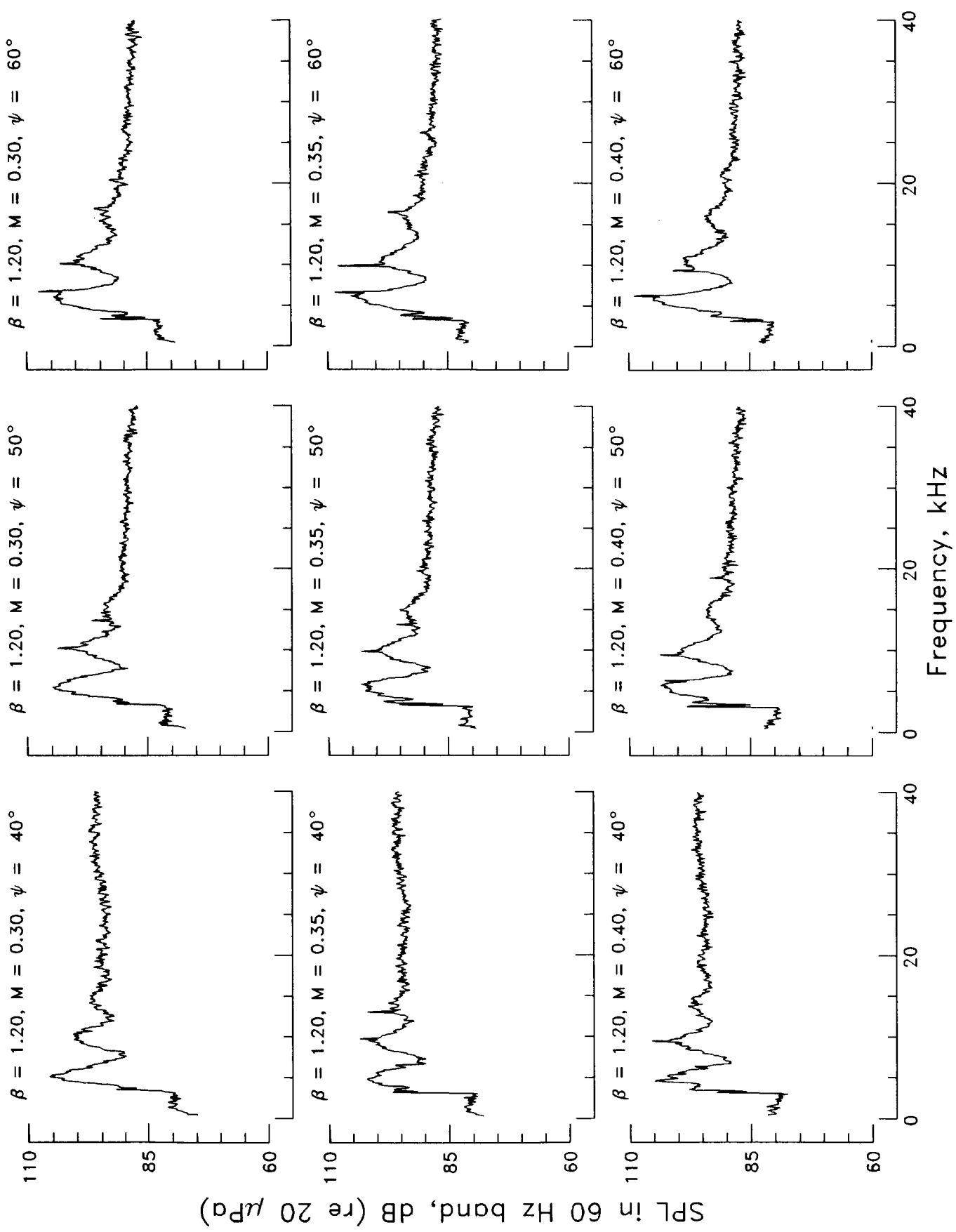
SPL in 60 Hz band, dB (re 20 μ Pa)

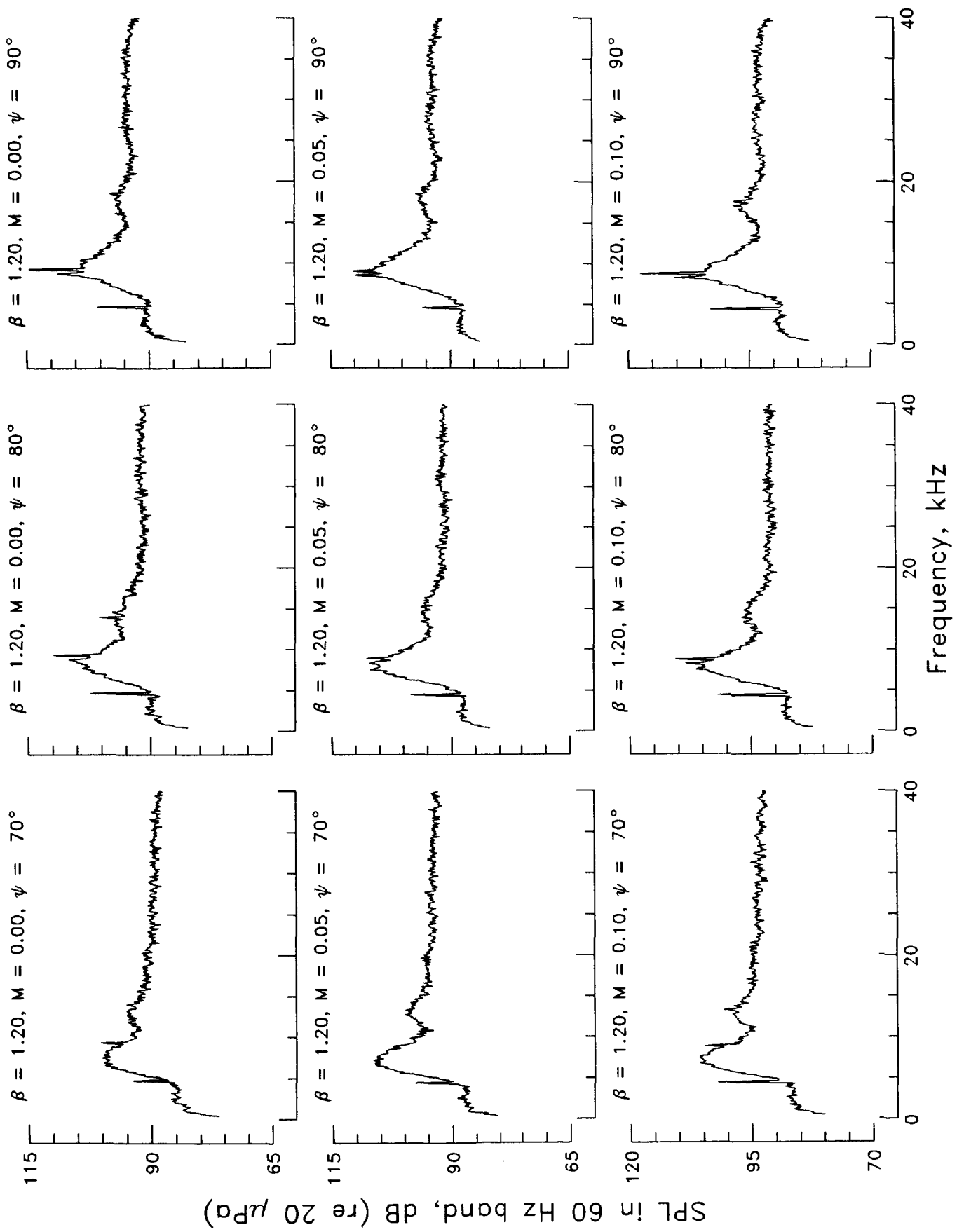


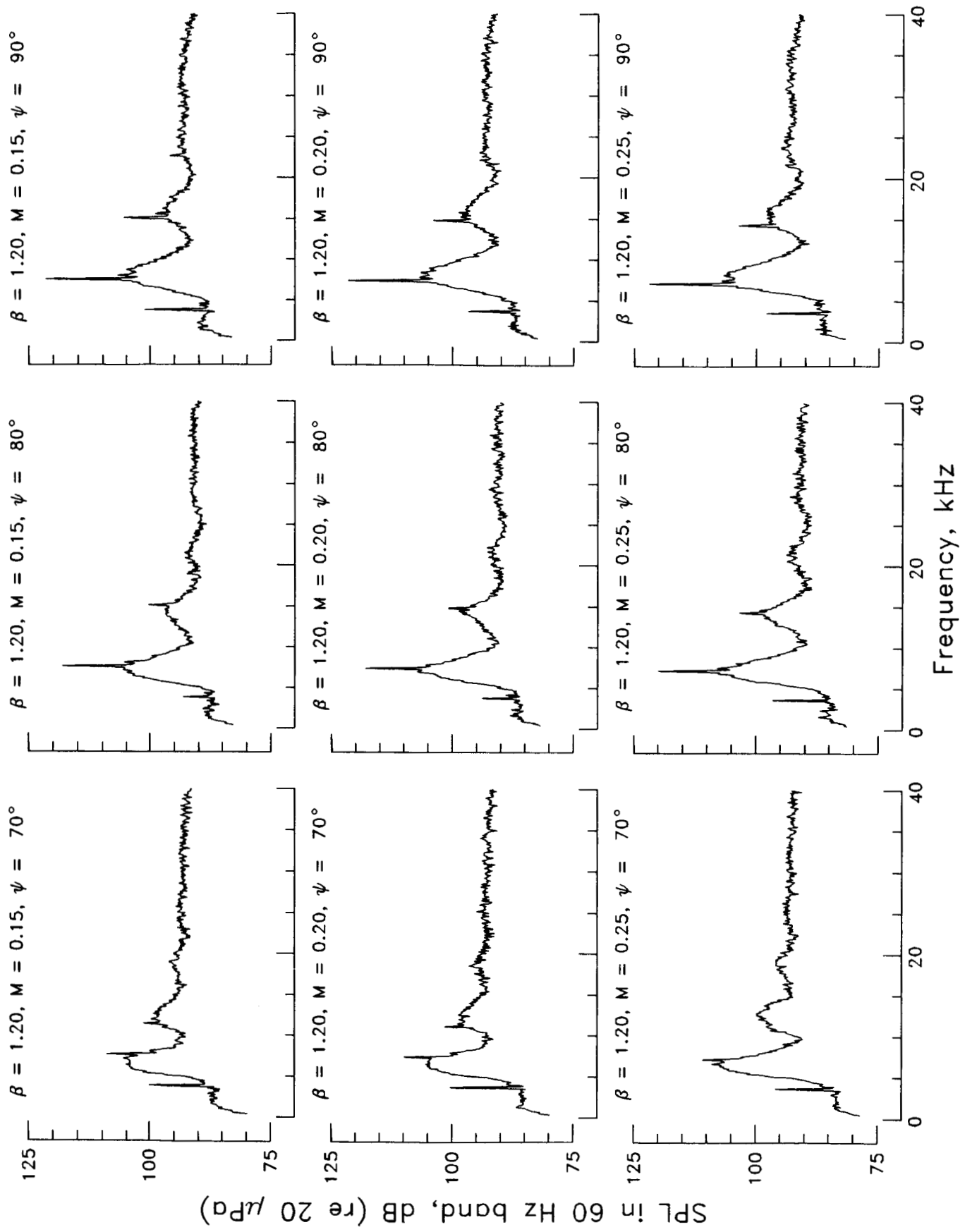
Frequency, kHz

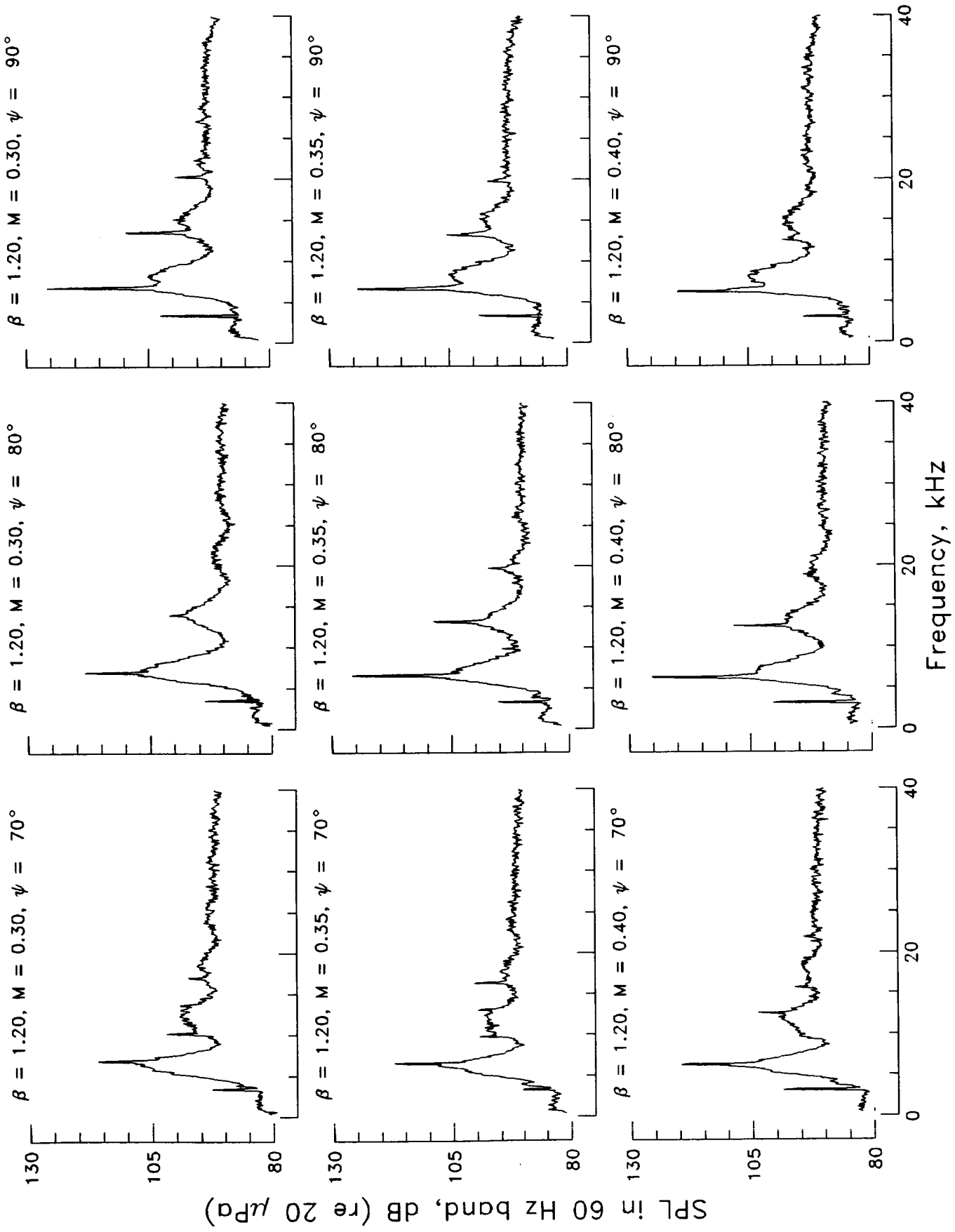


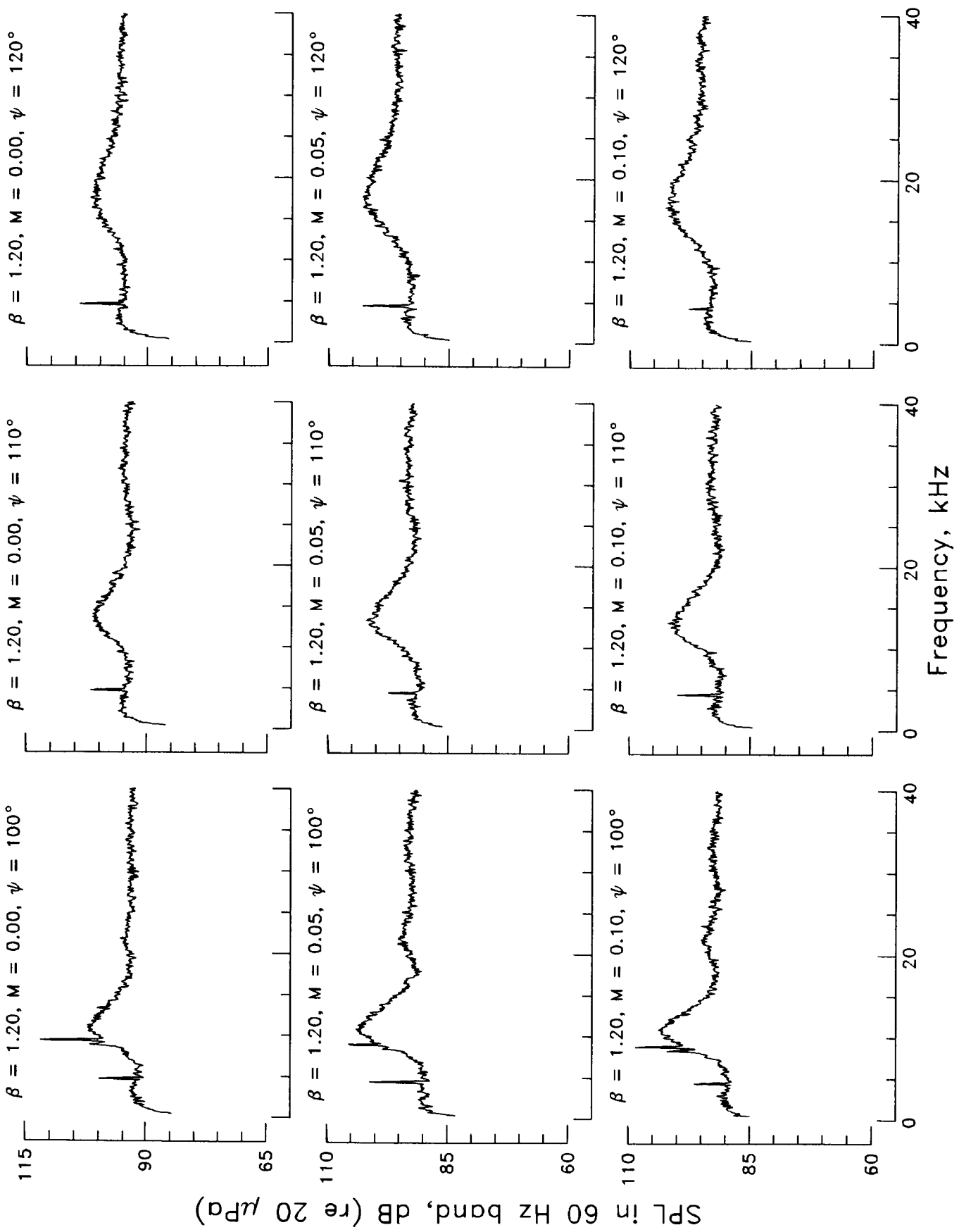


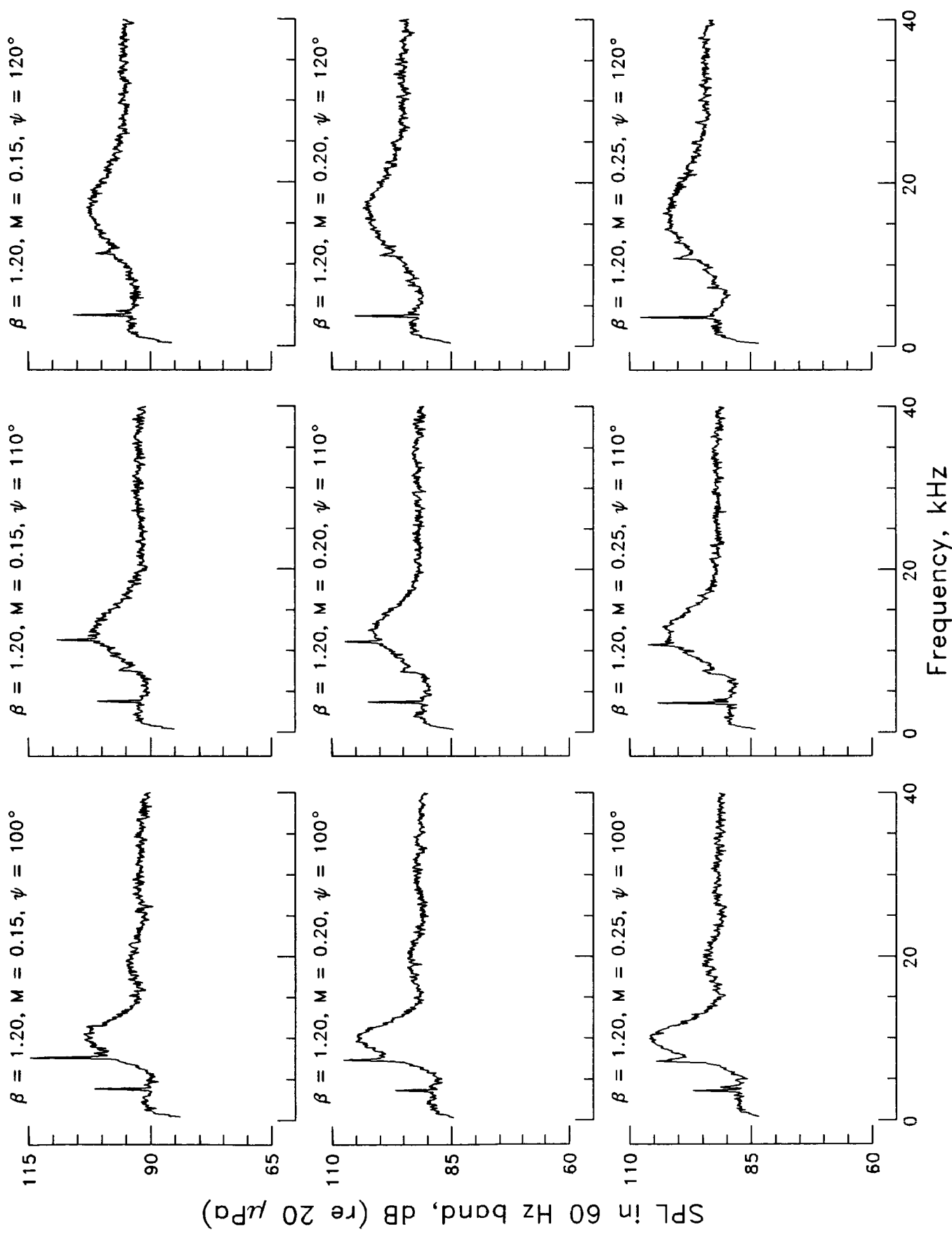


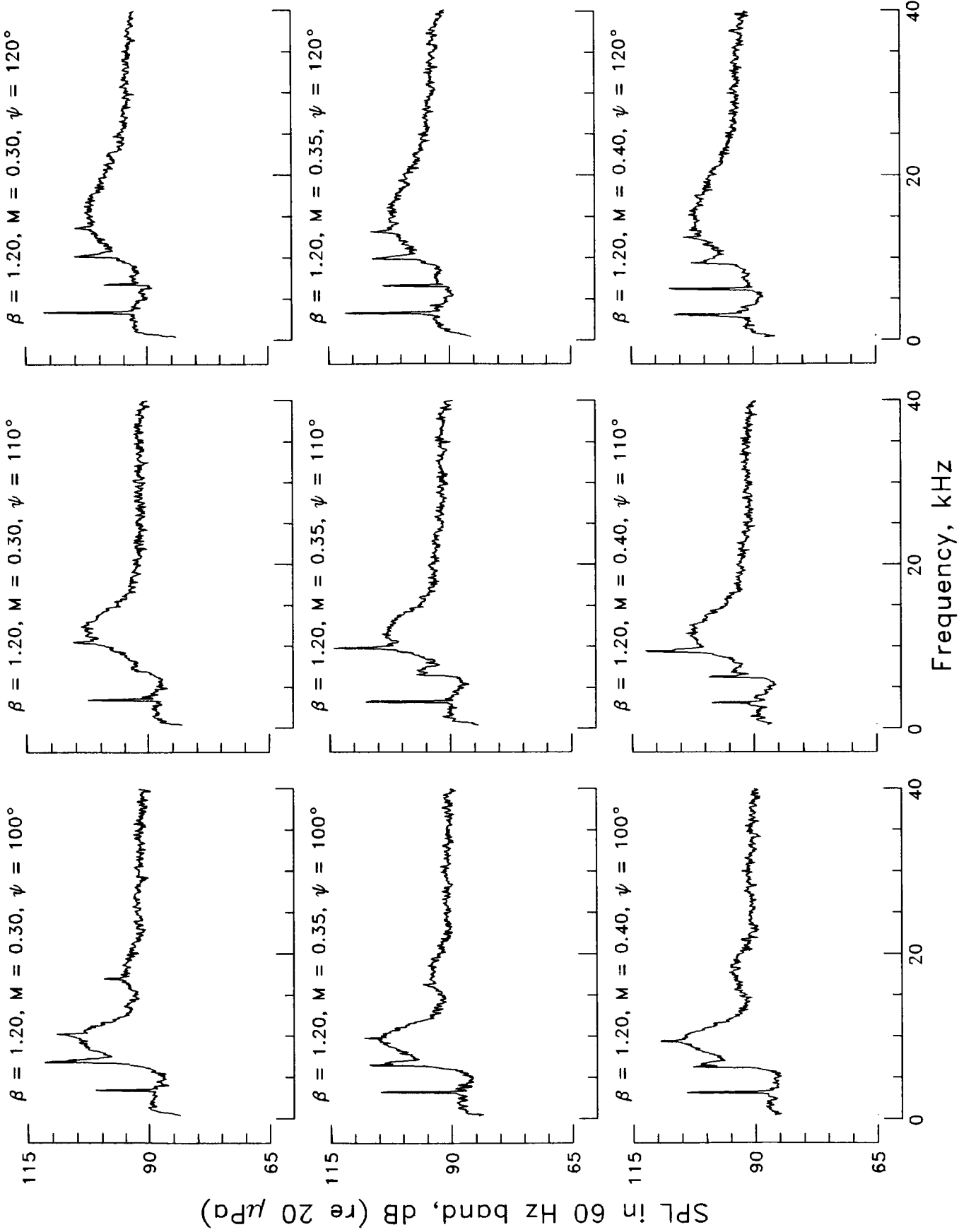


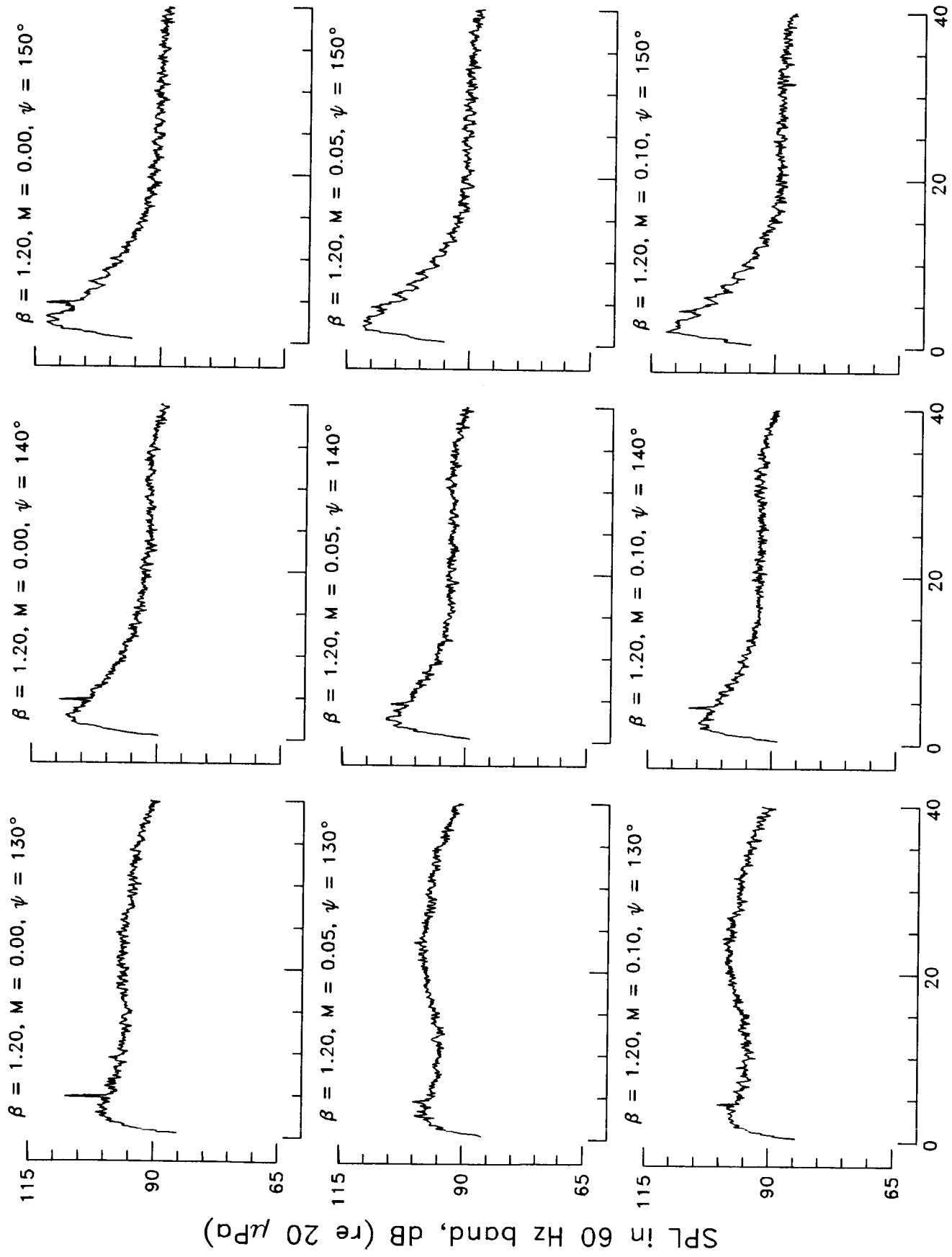


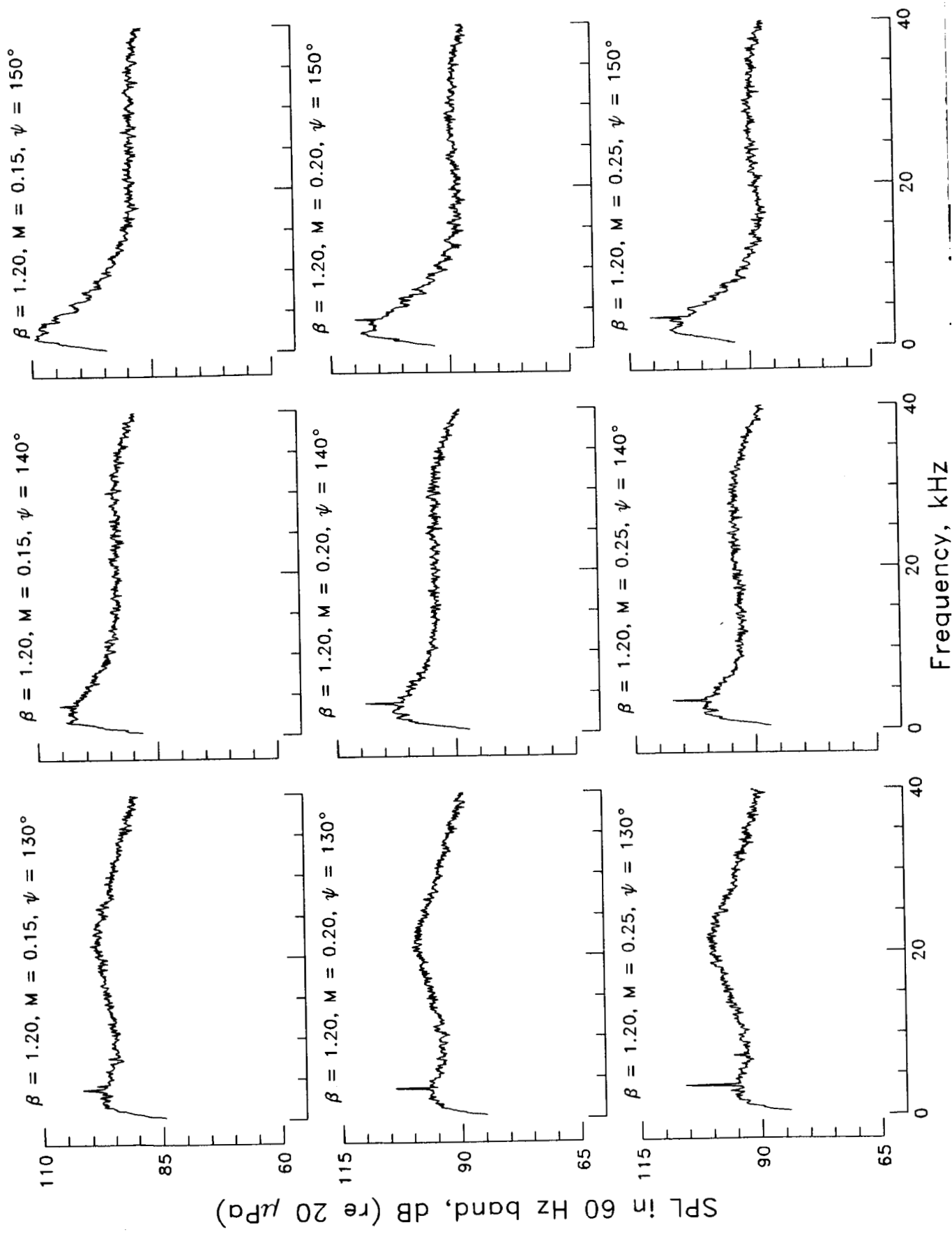


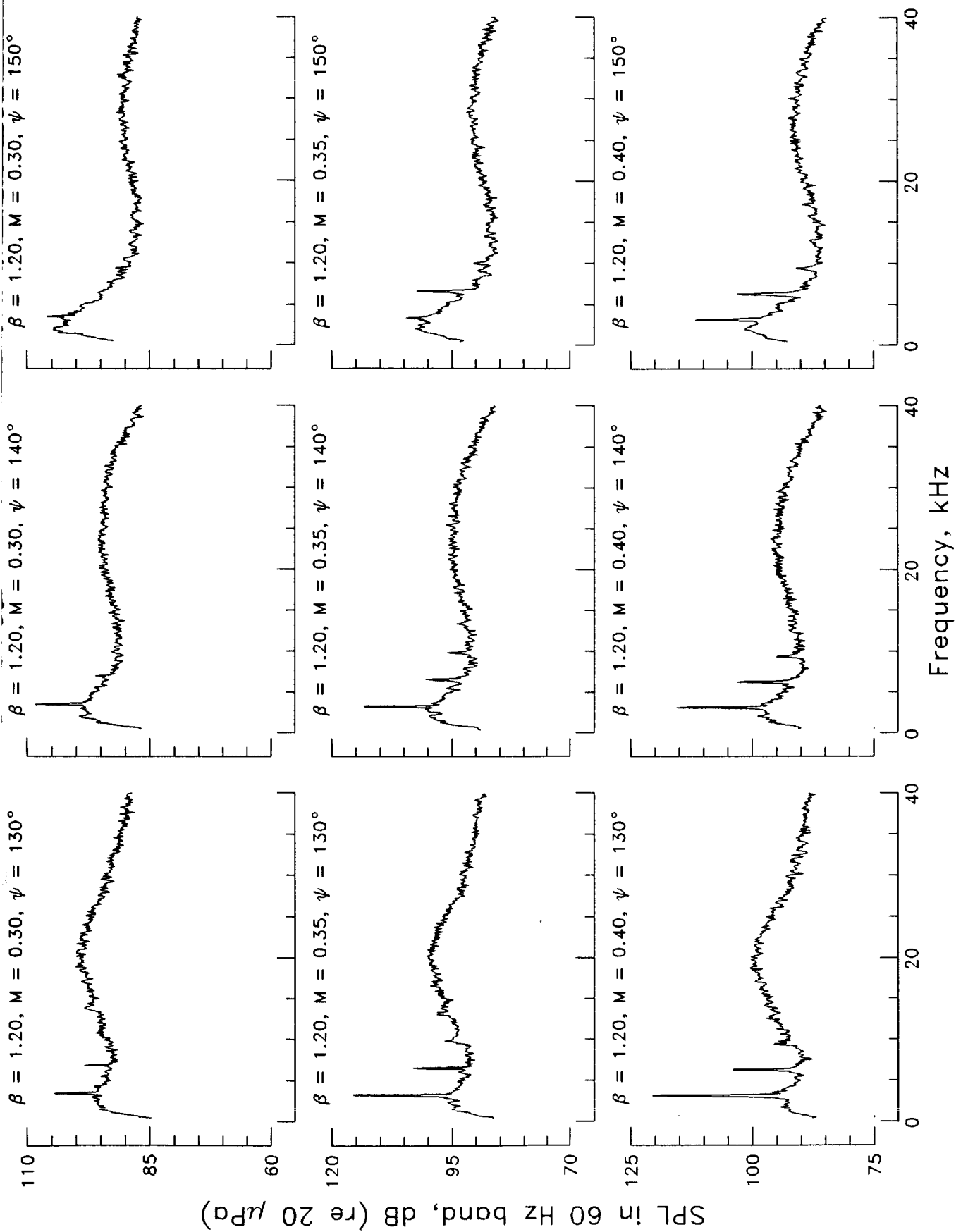


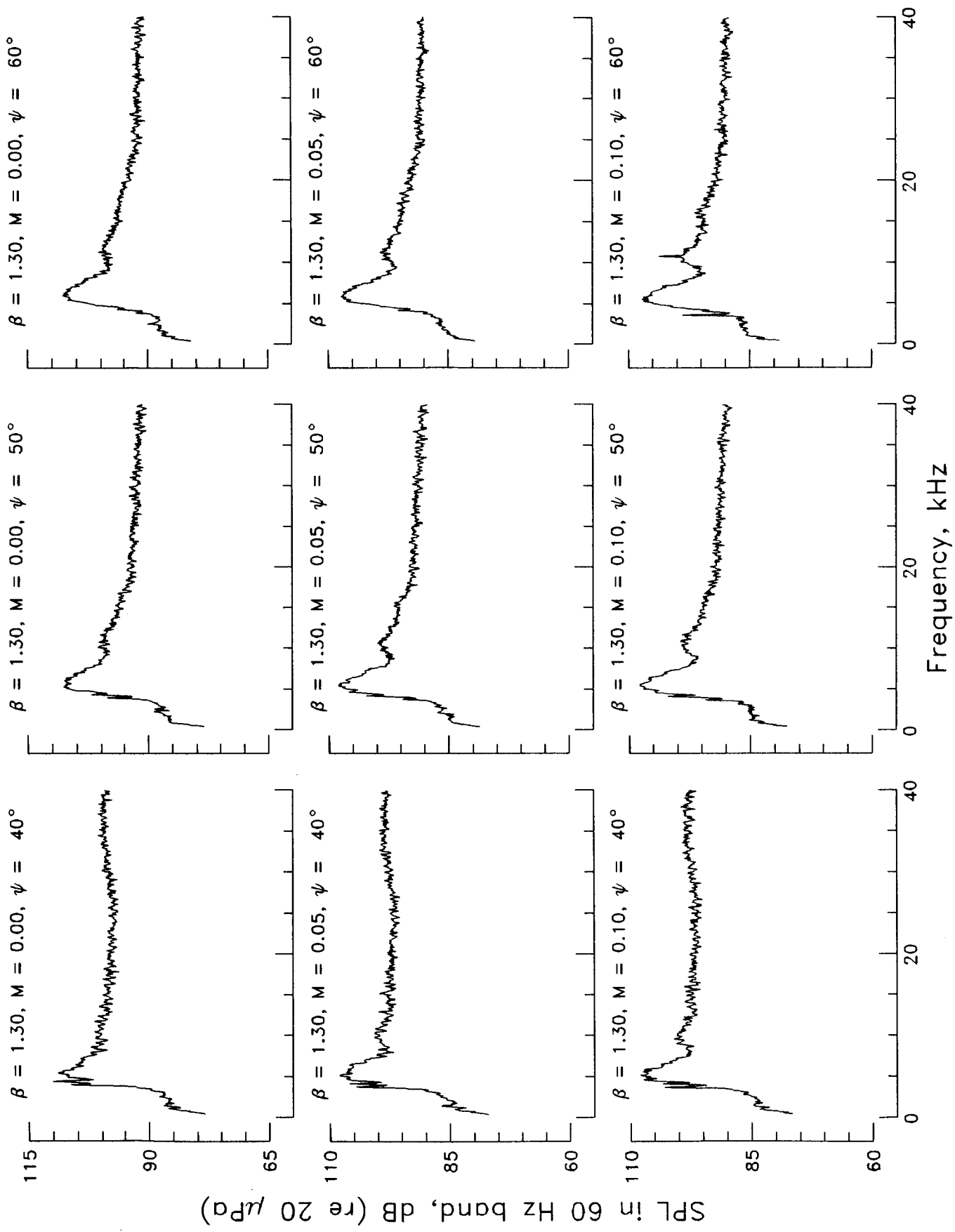


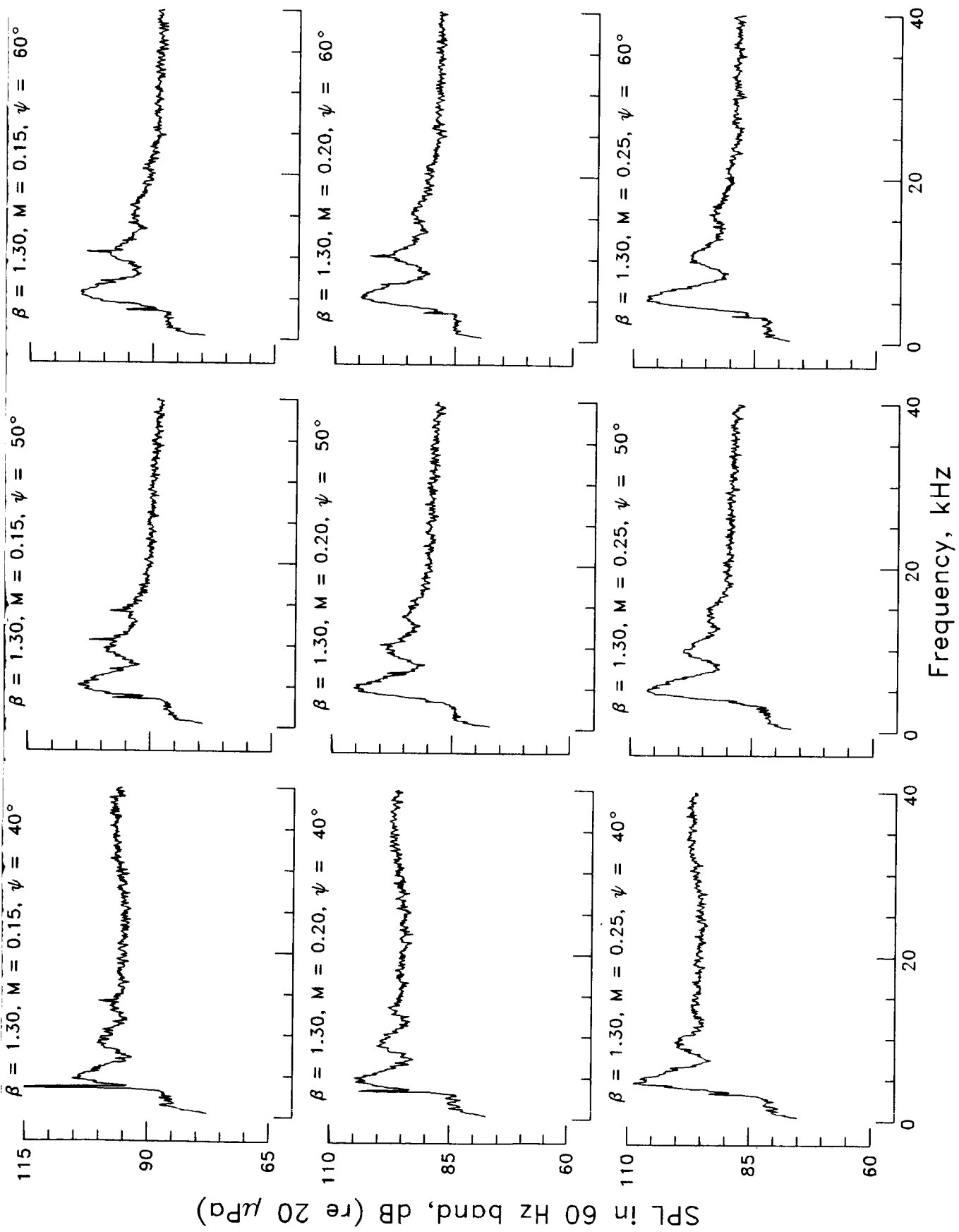


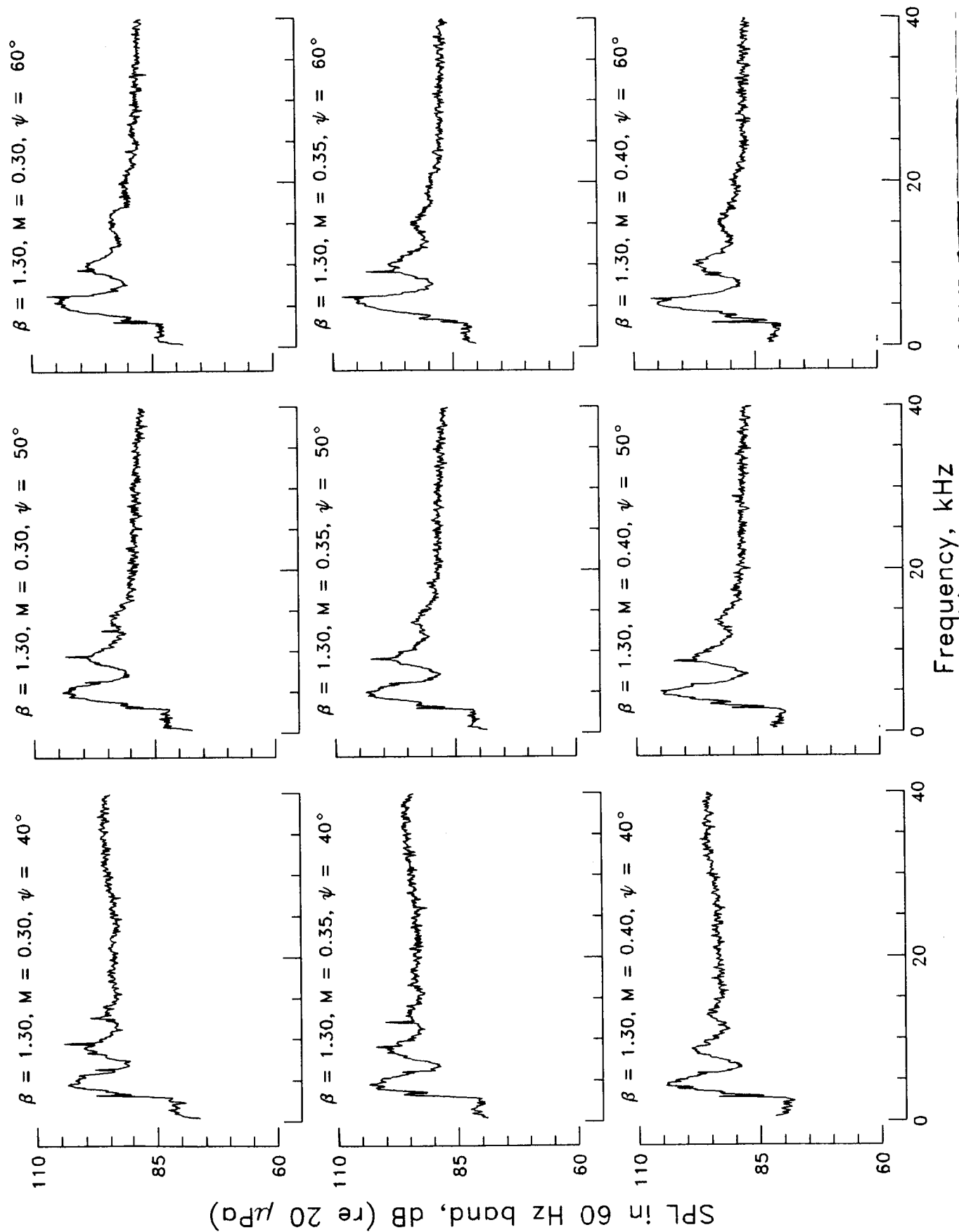


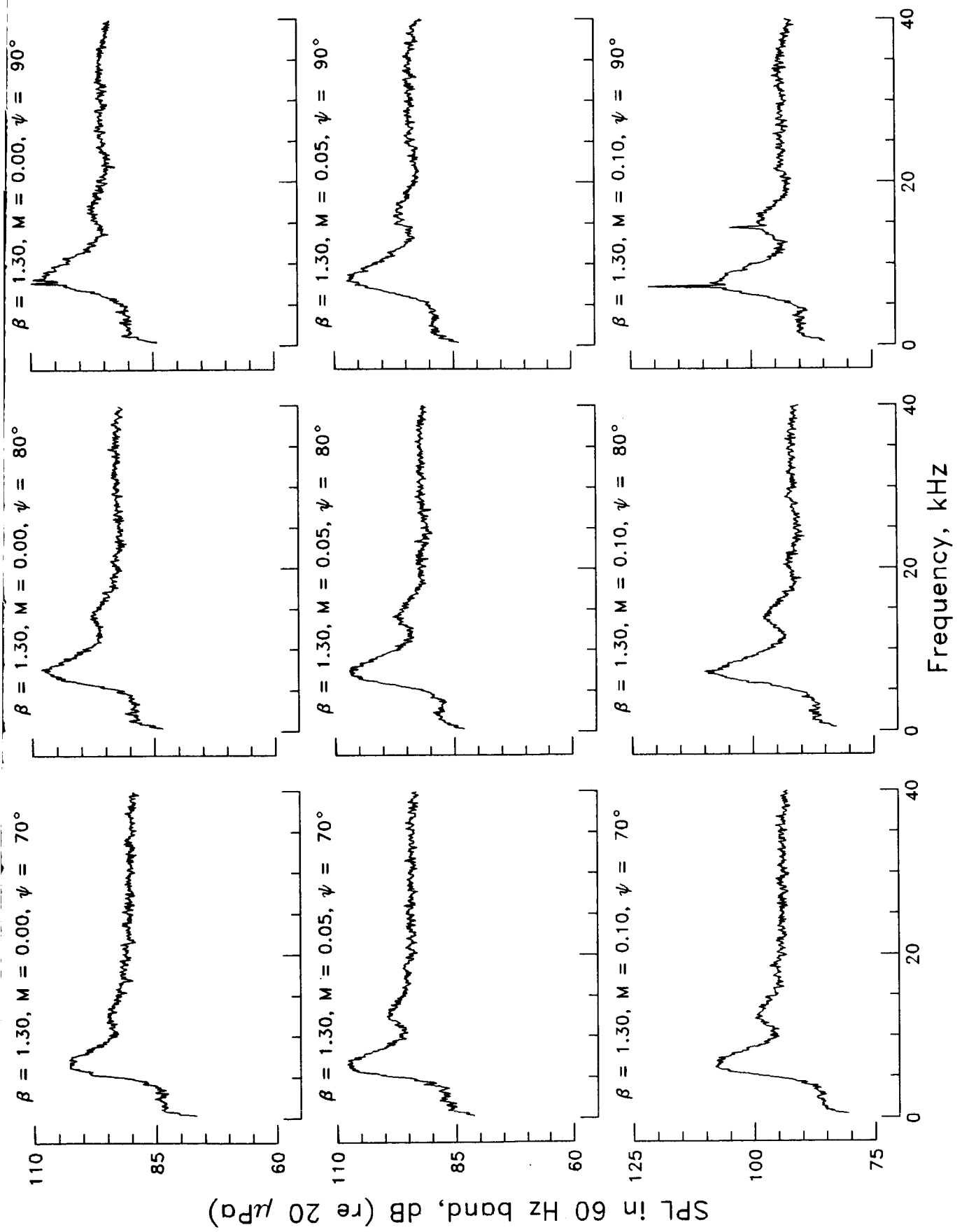


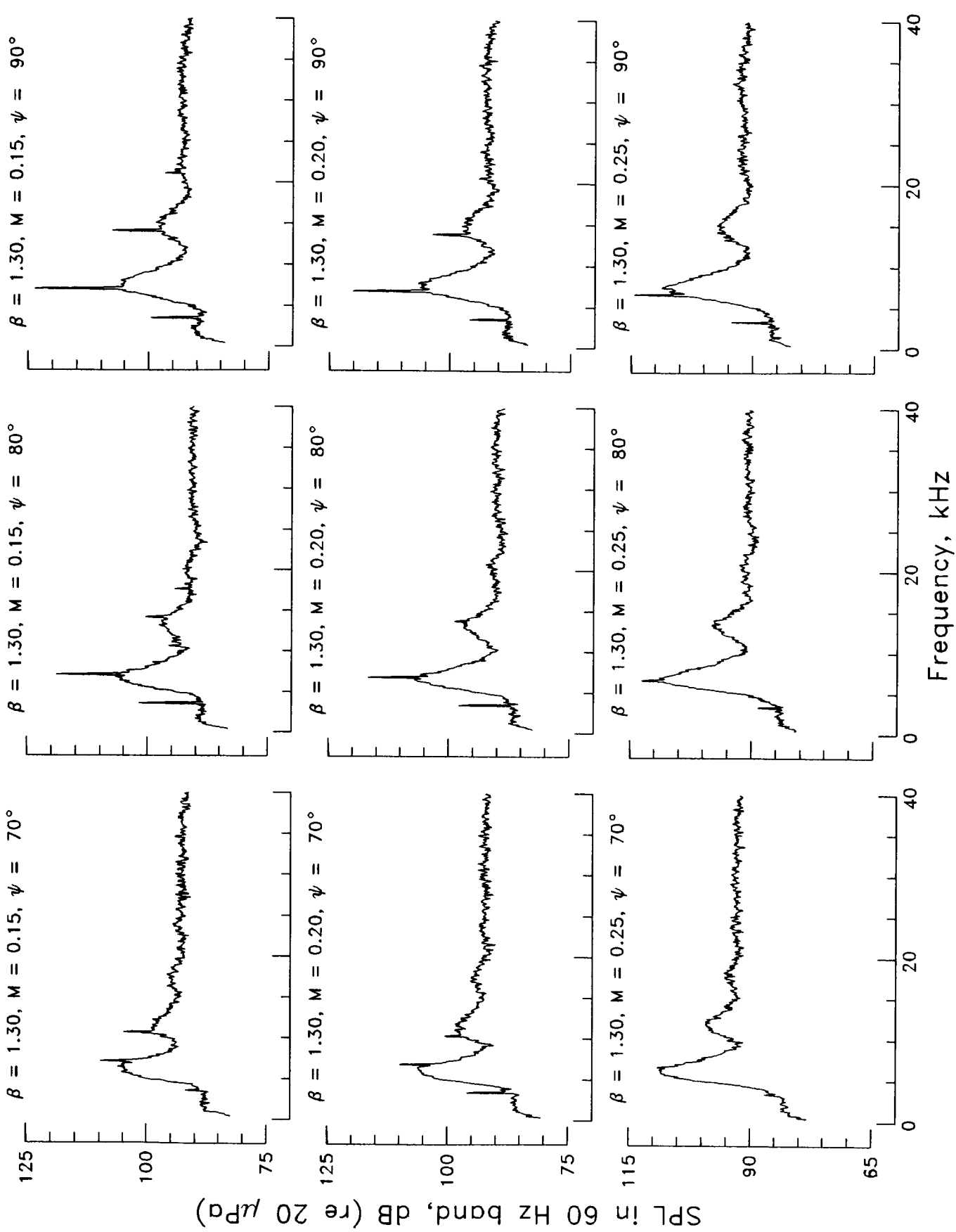




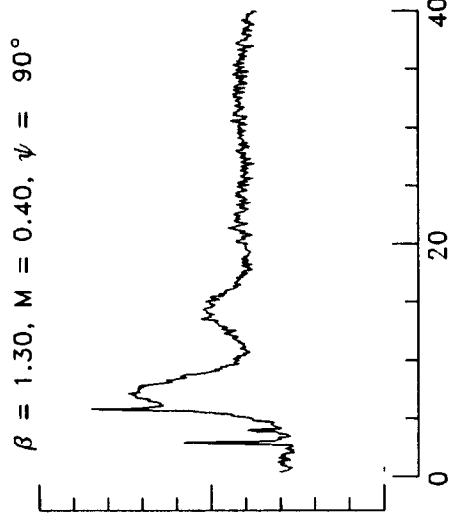
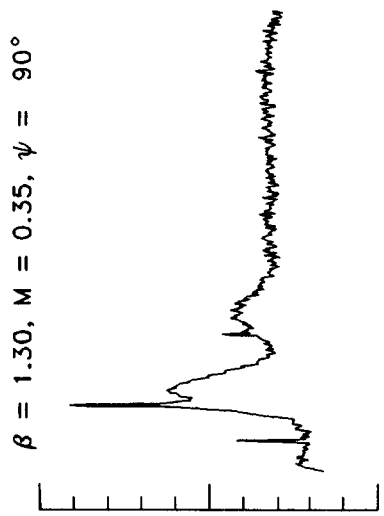
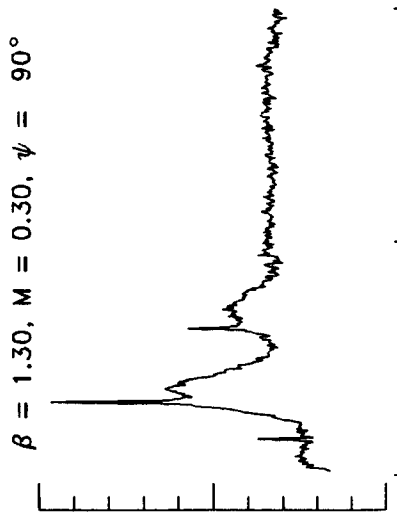
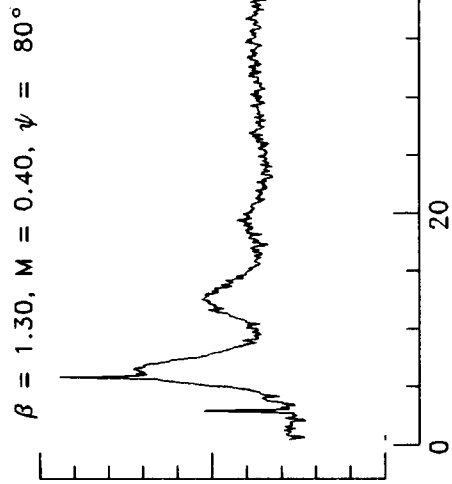
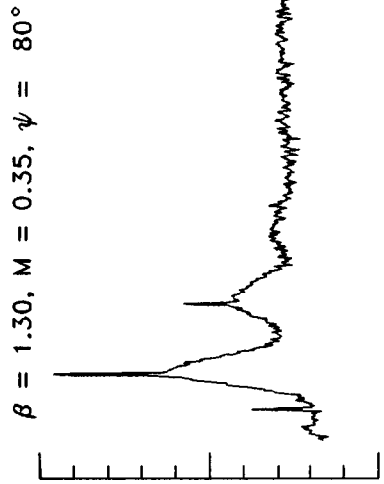
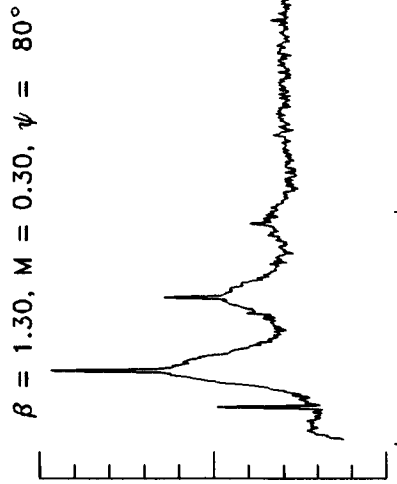
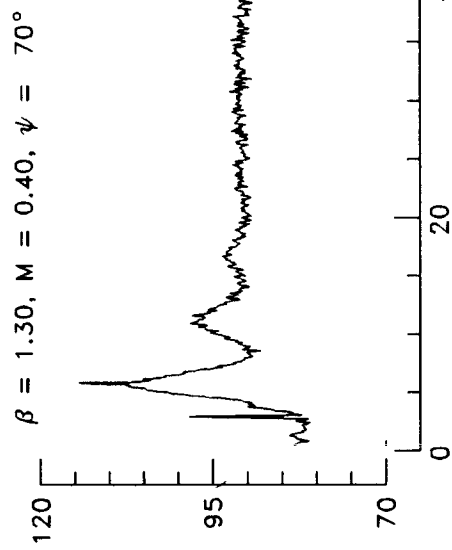
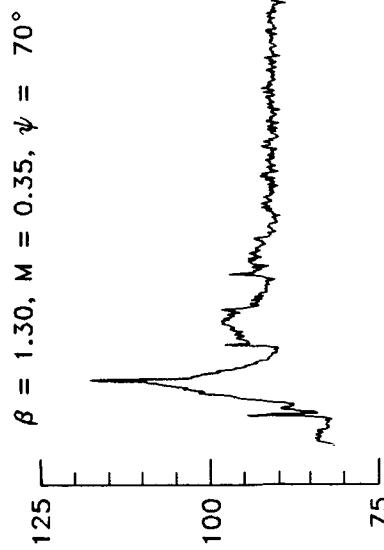
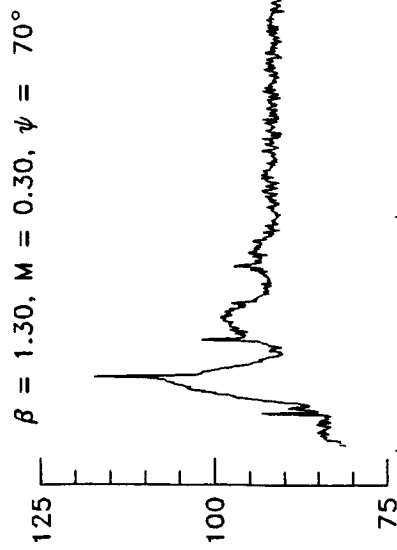




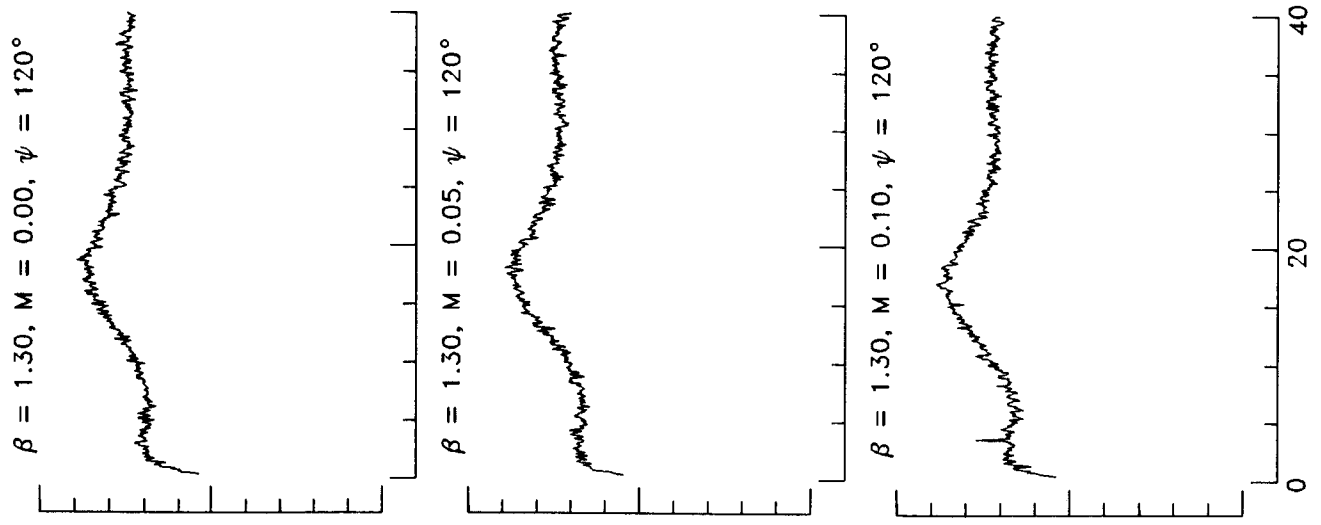
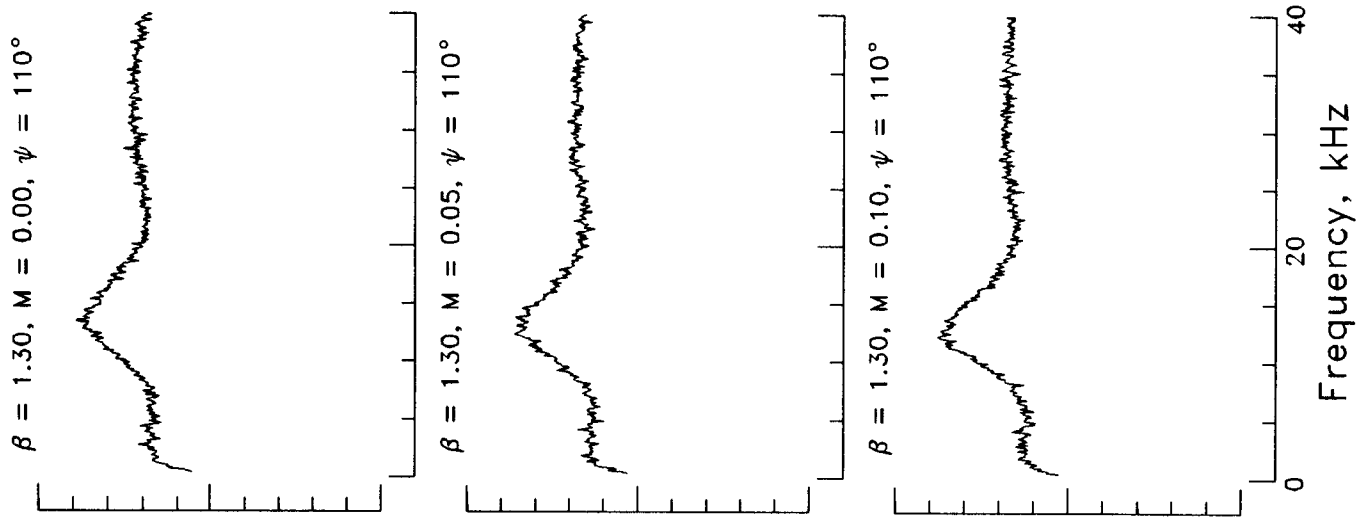
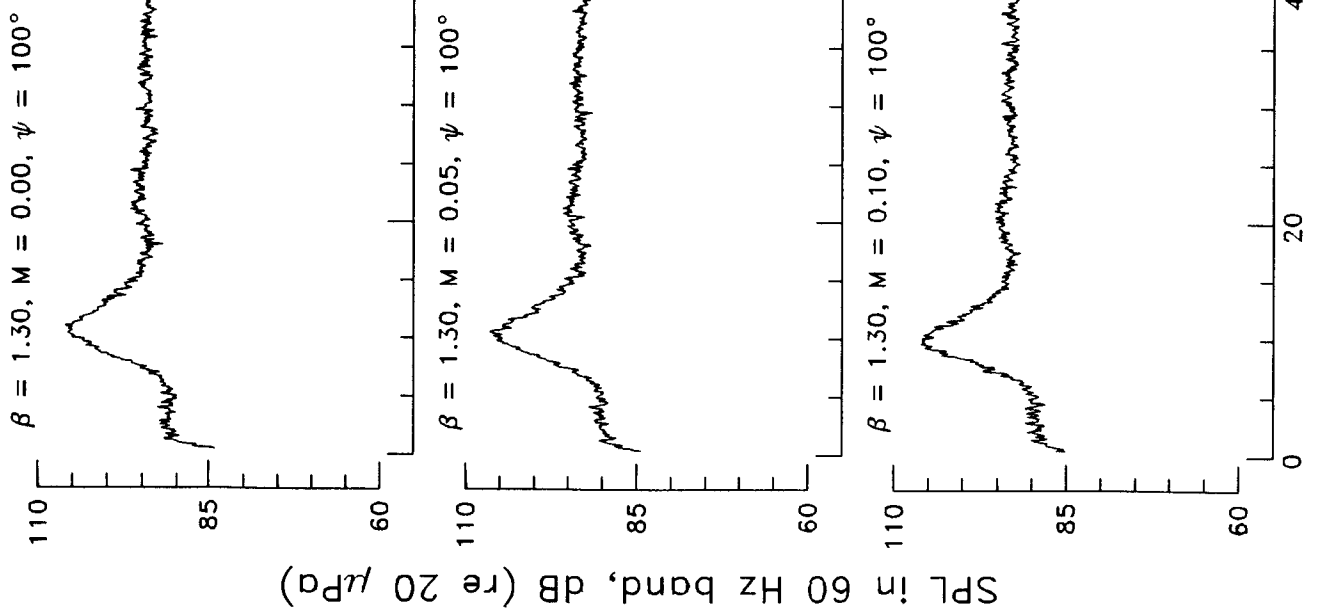


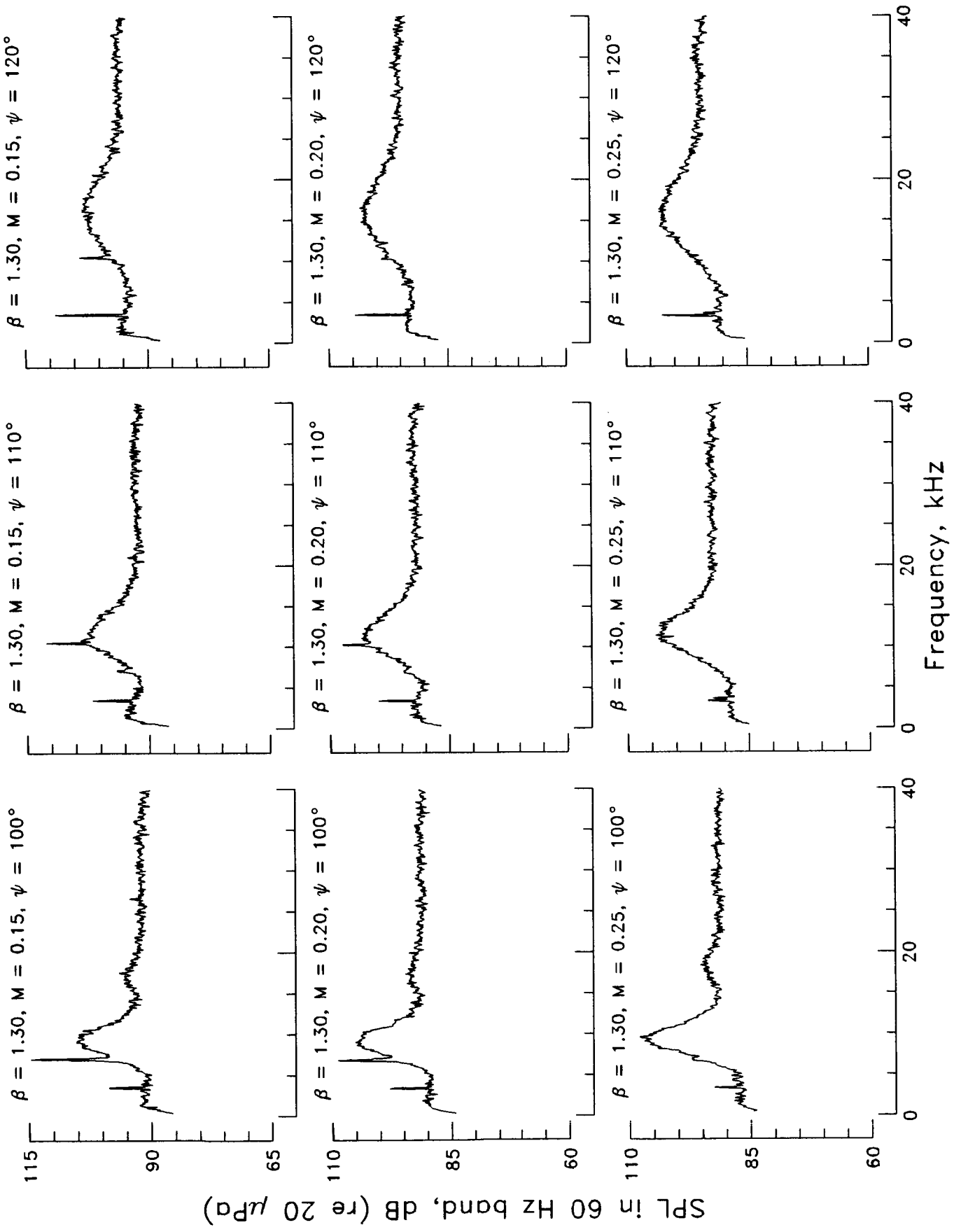


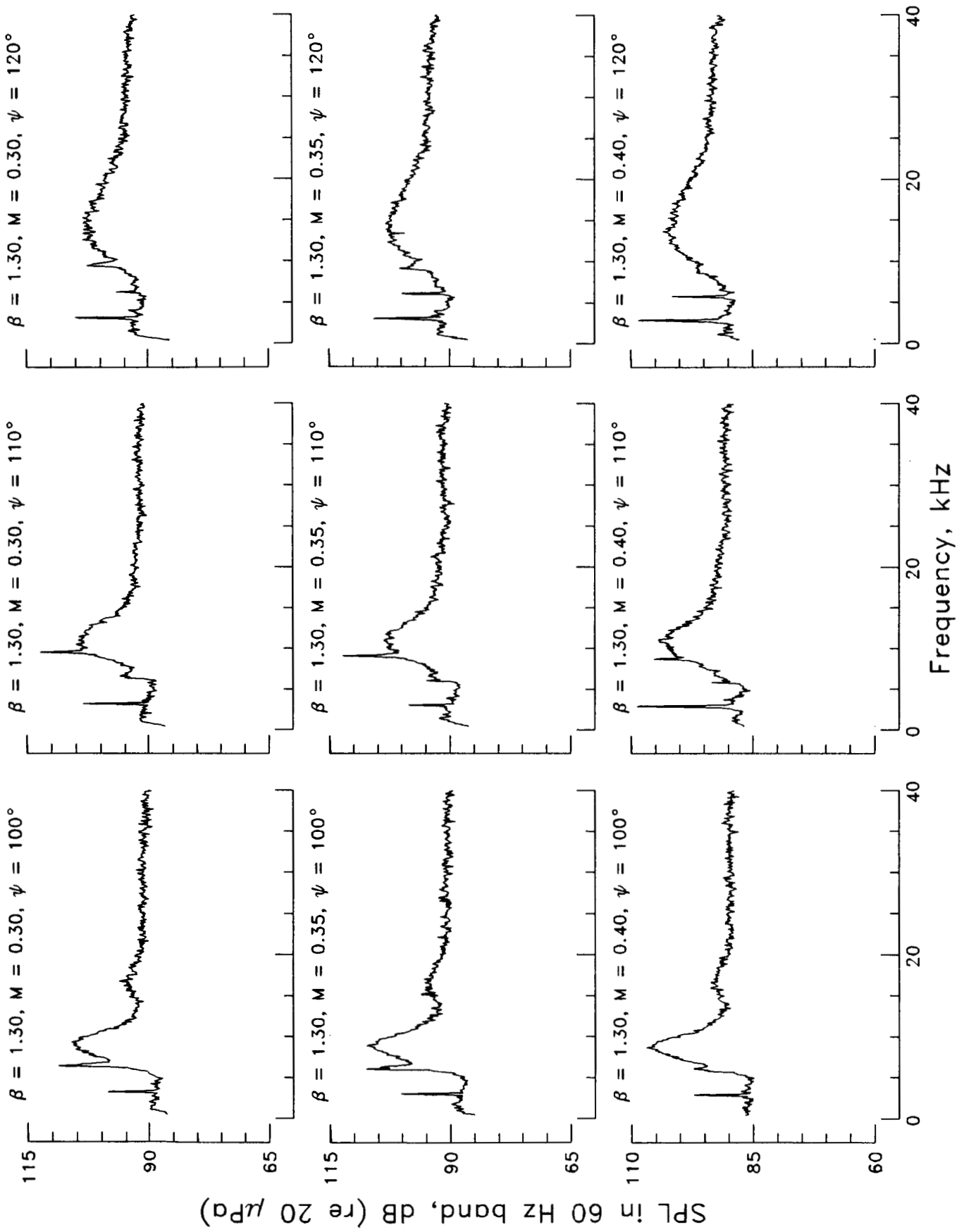
SPL in 60 Hz band, dB (re 20 μ Pd)

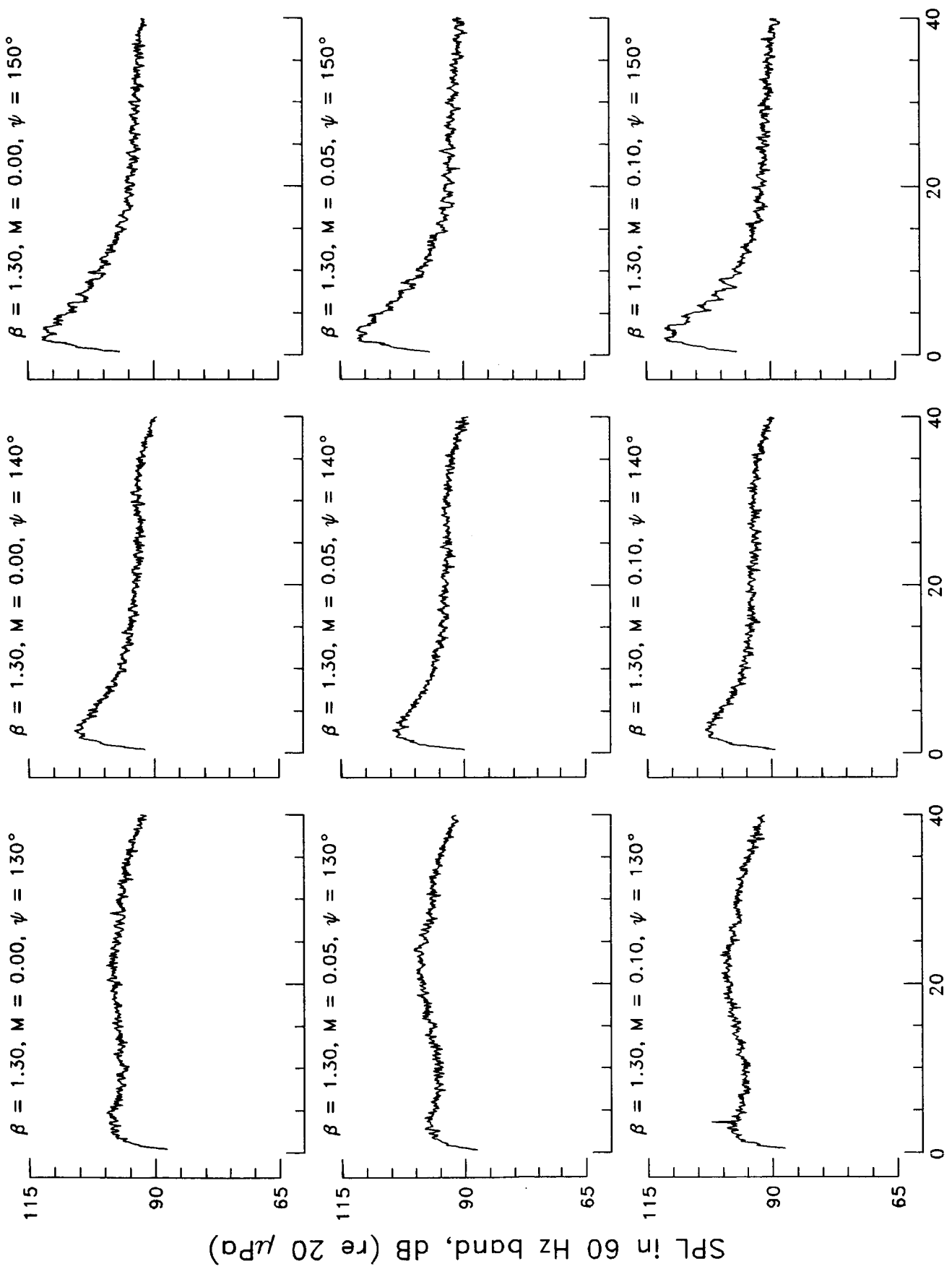


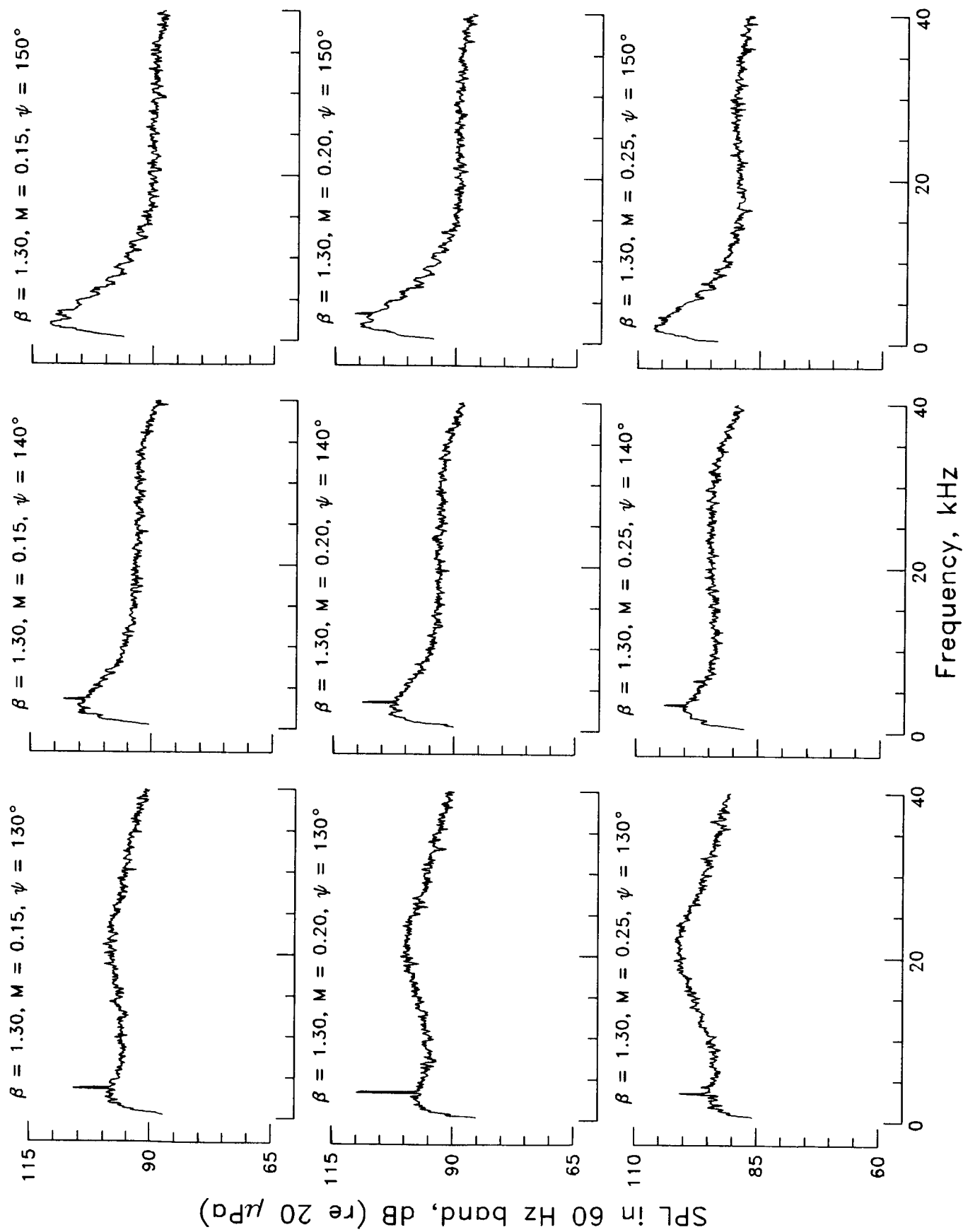
Frequency, kHz

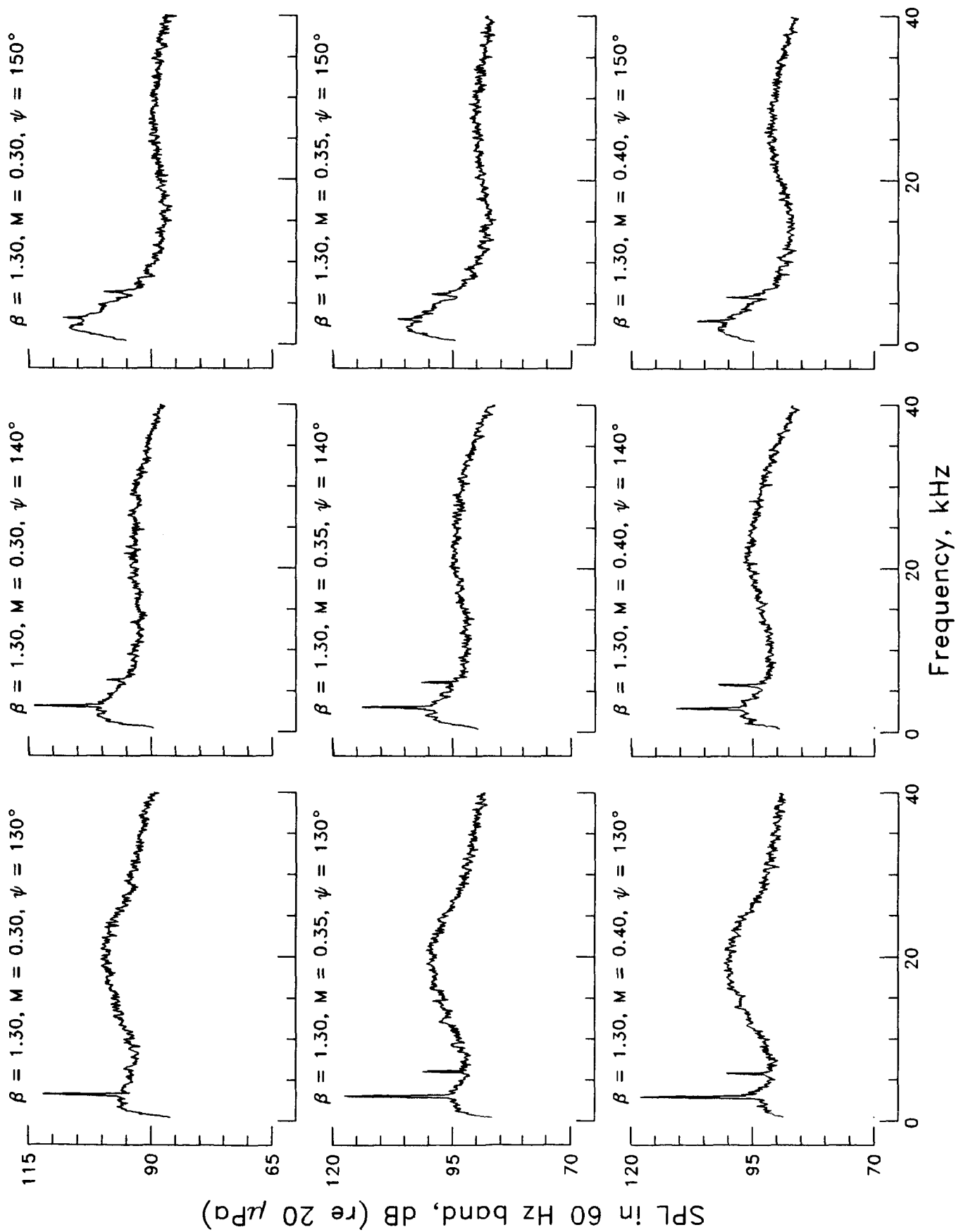


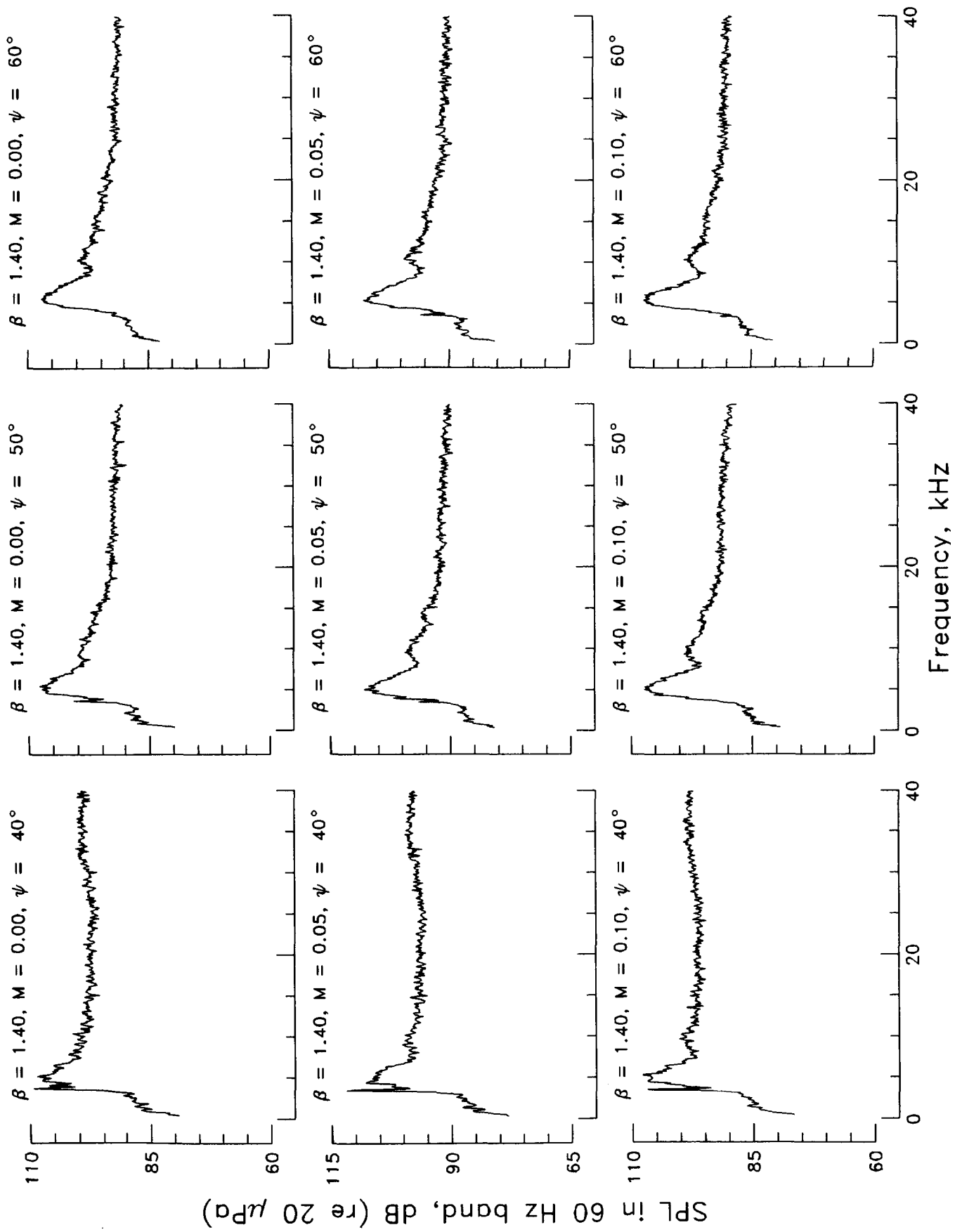




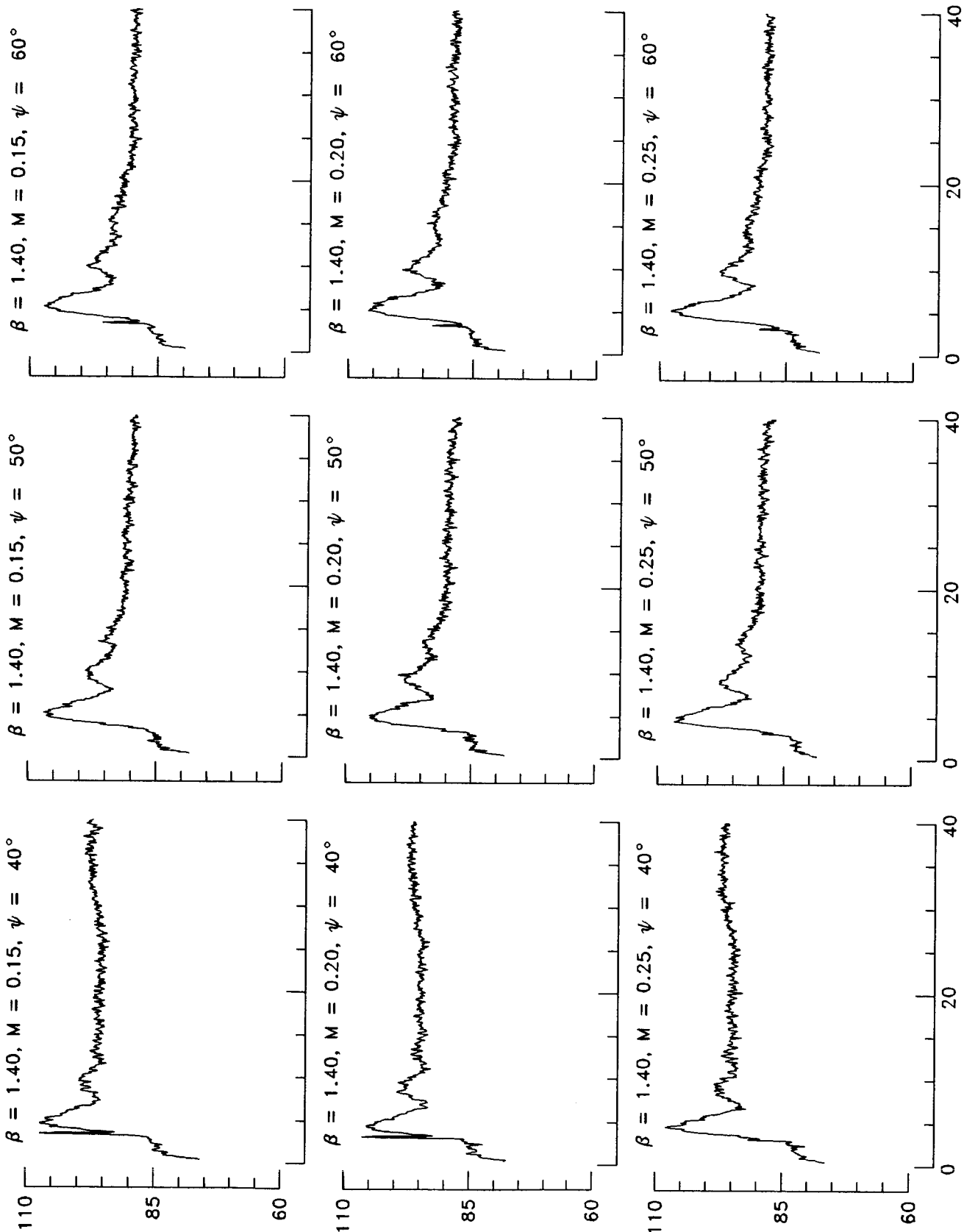




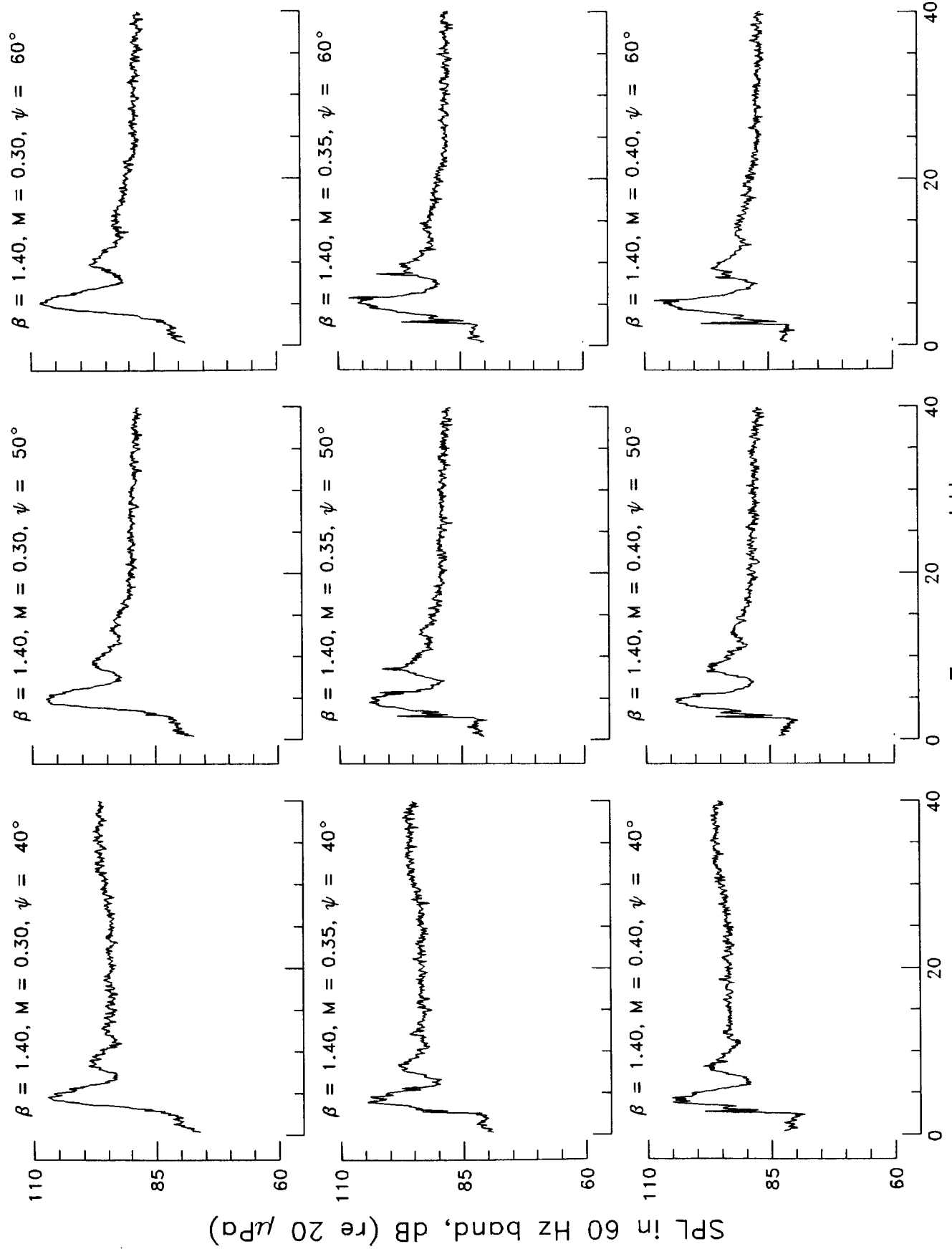




SPL in 60 Hz band, dB (re 20 μ Pa)

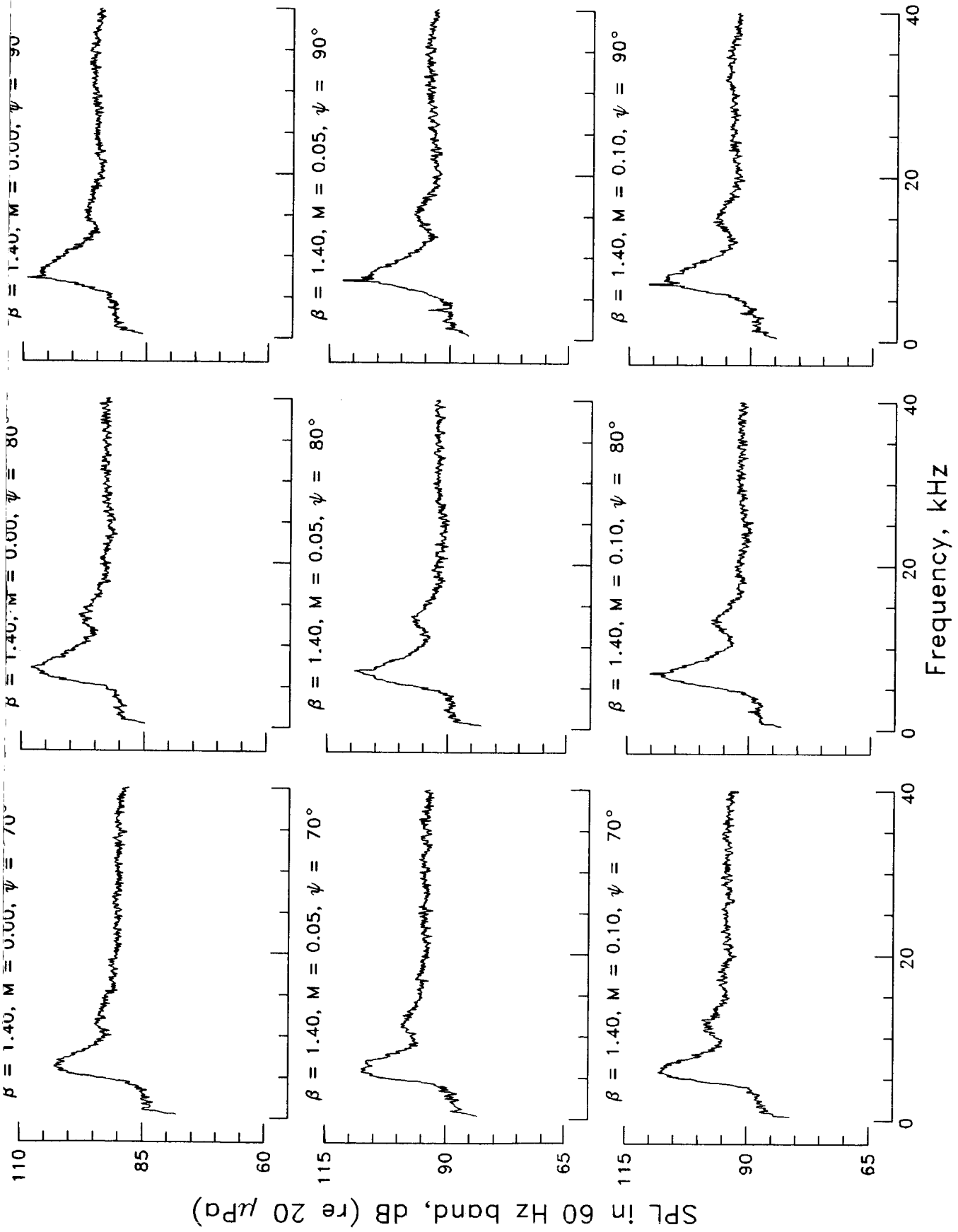


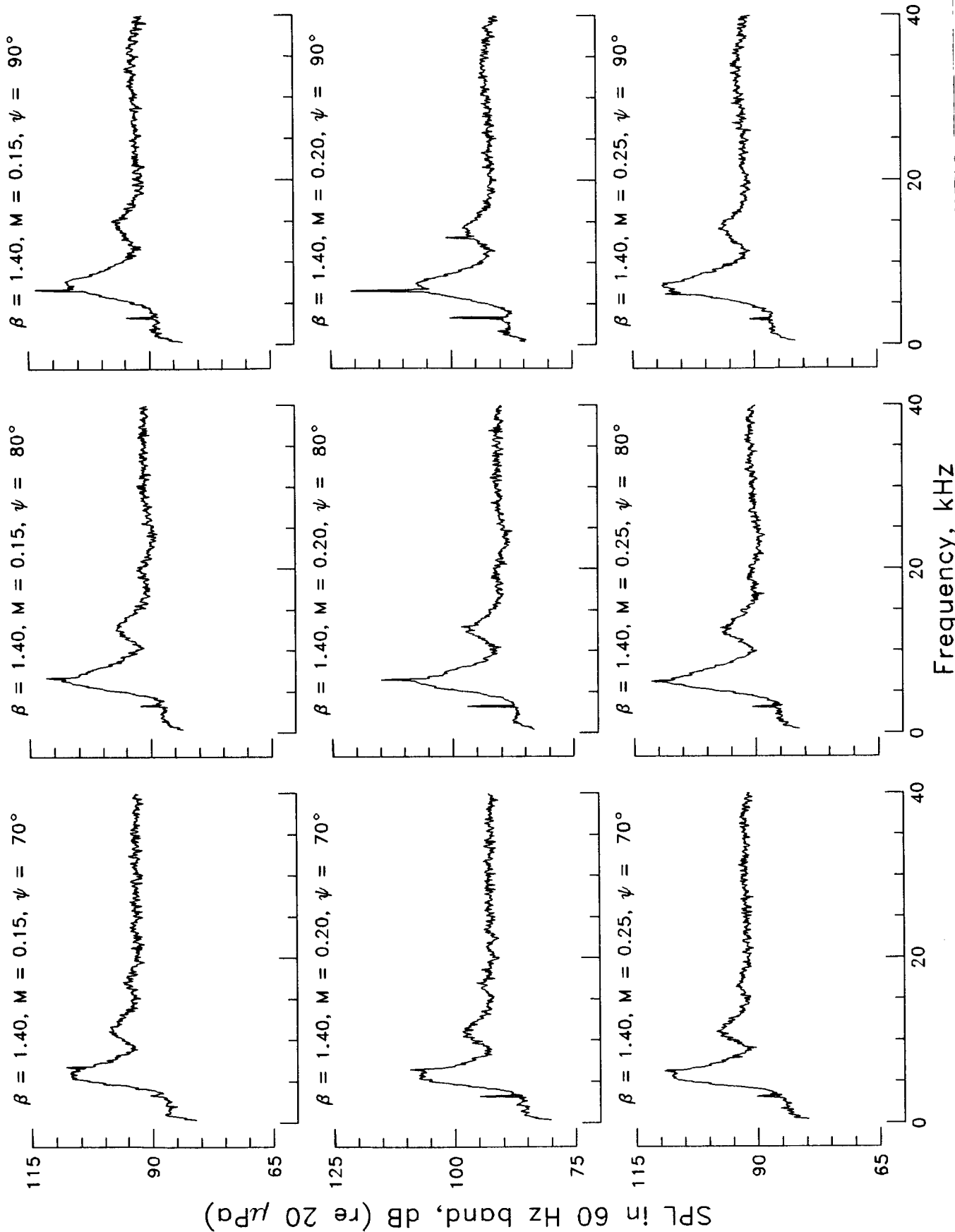
Frequency, kHz

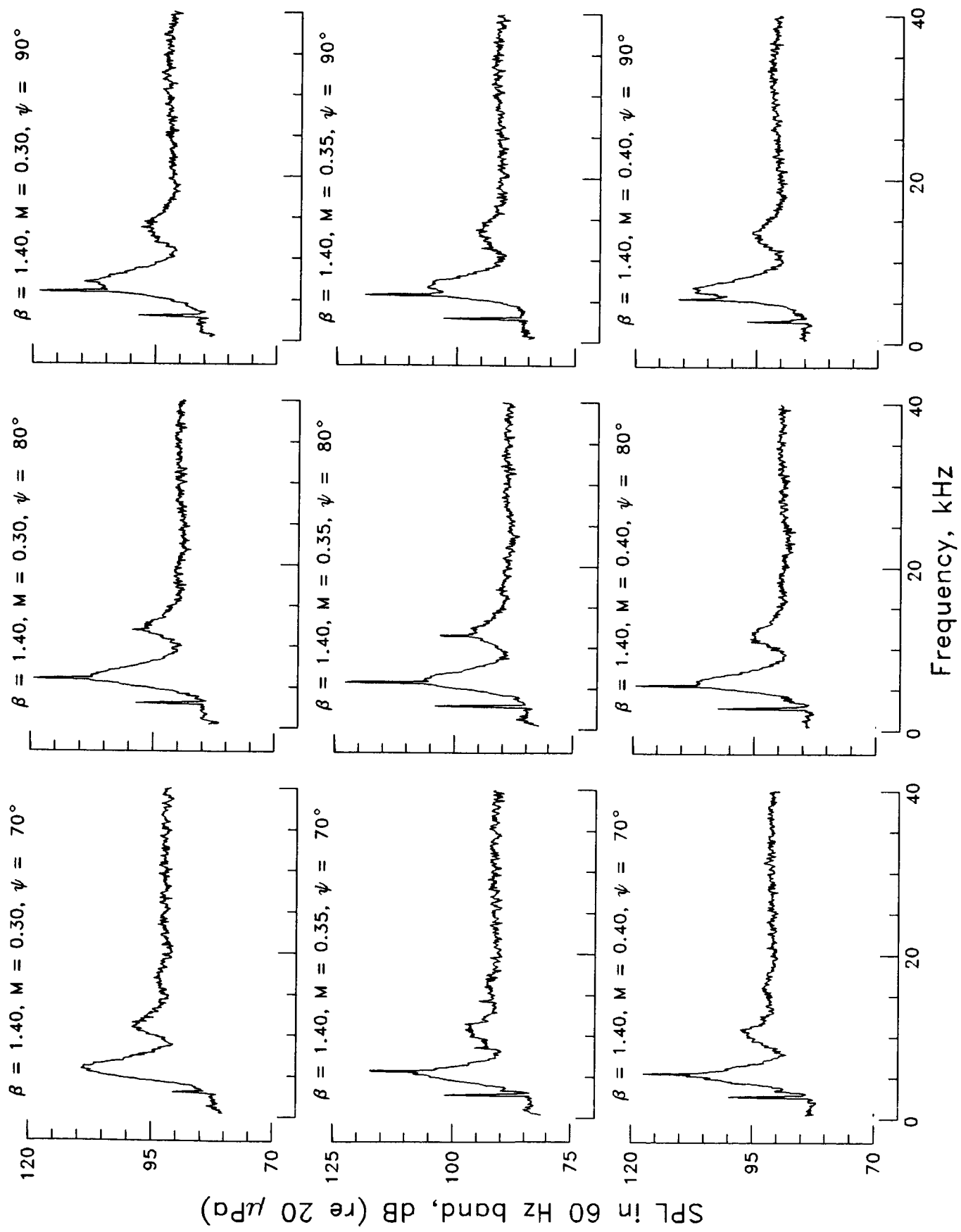


SPL in 60 Hz band, dB (re 20 μ Pa)

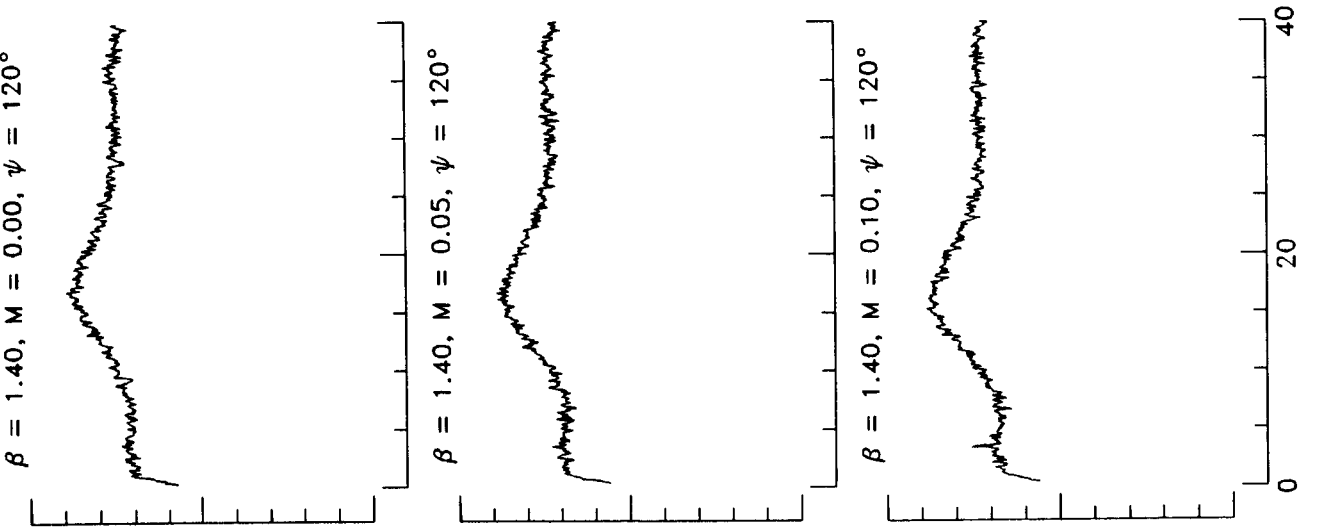
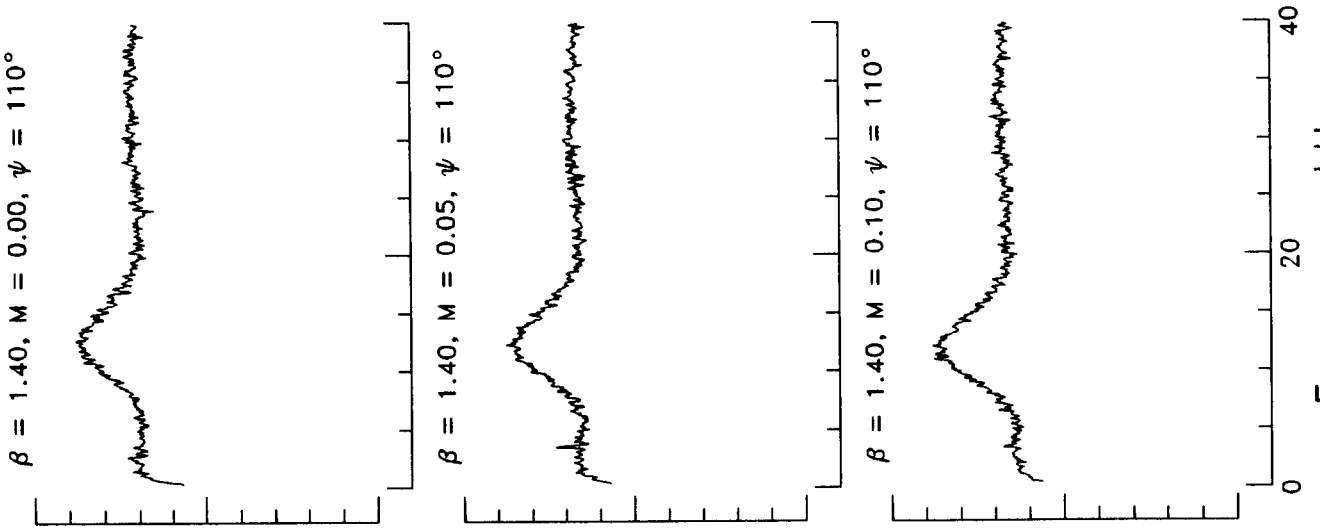
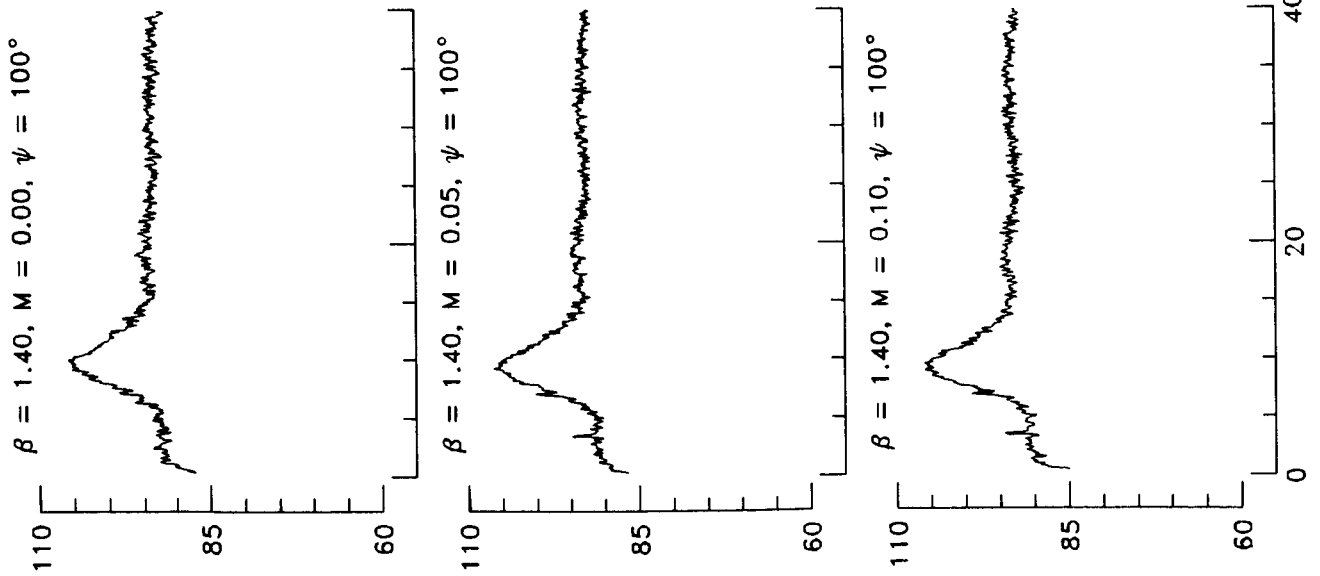
Frequency, kHz





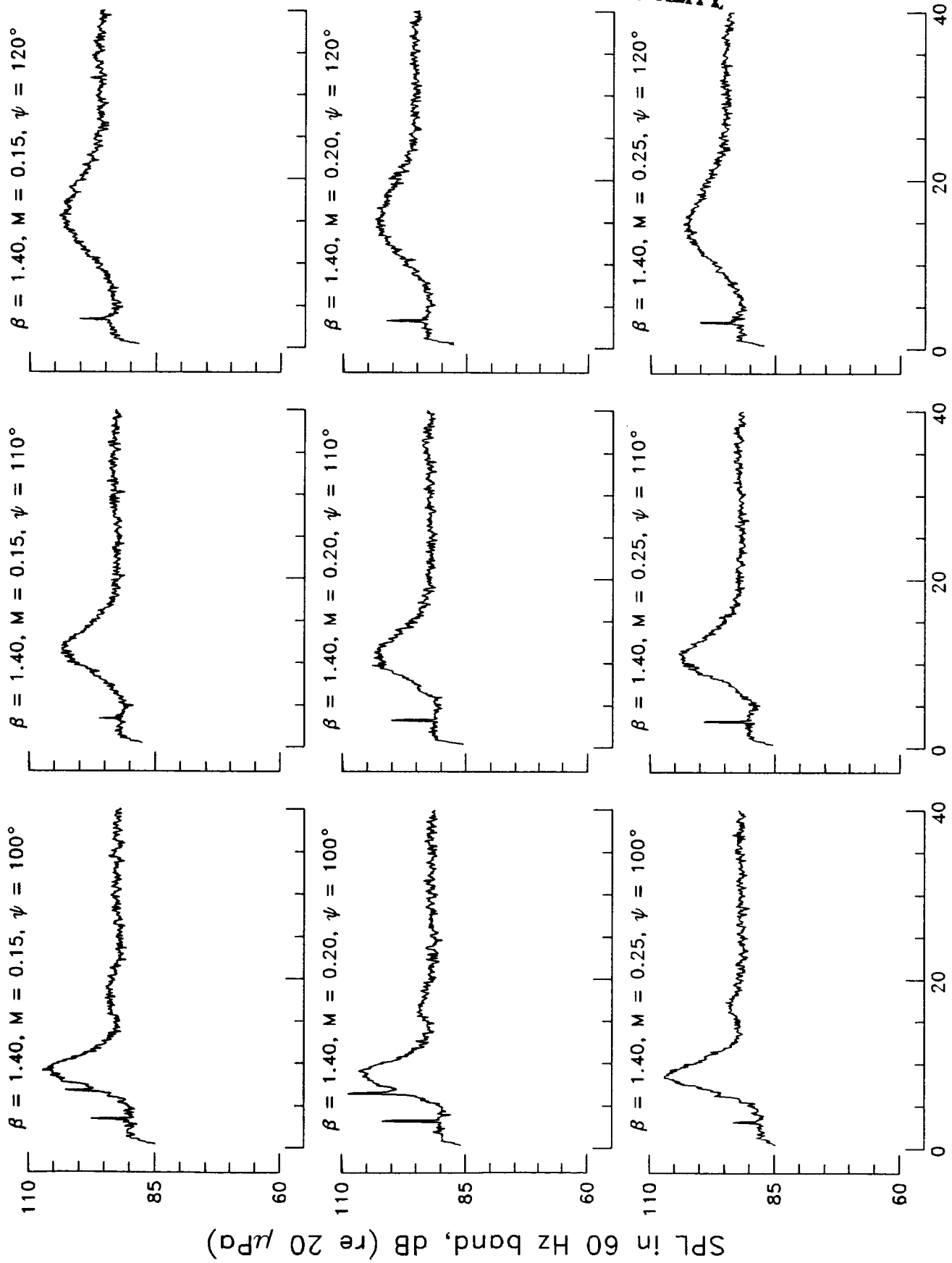


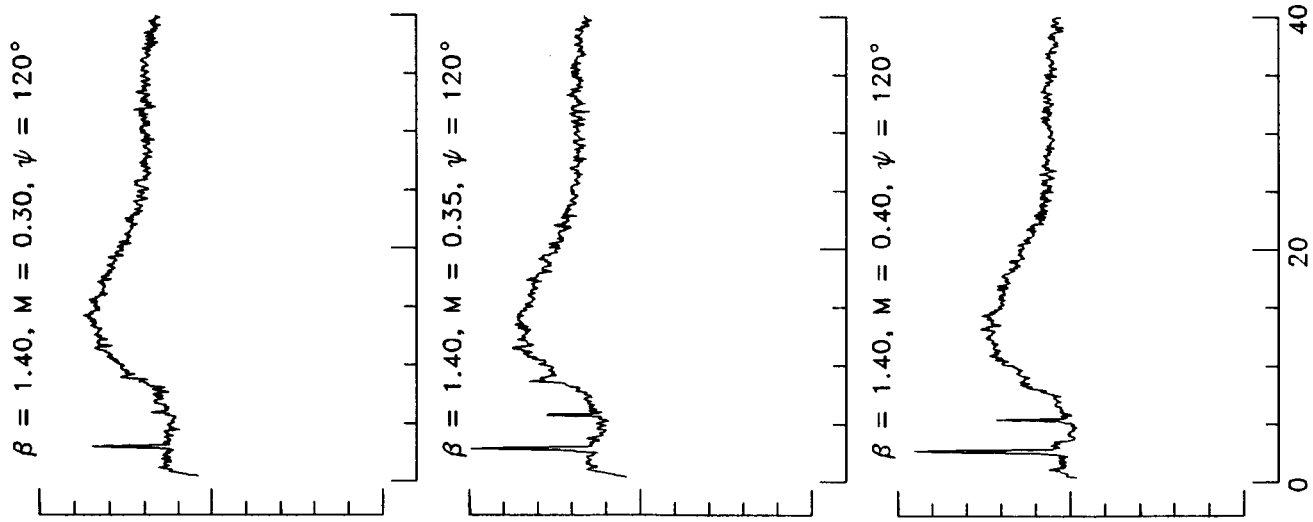
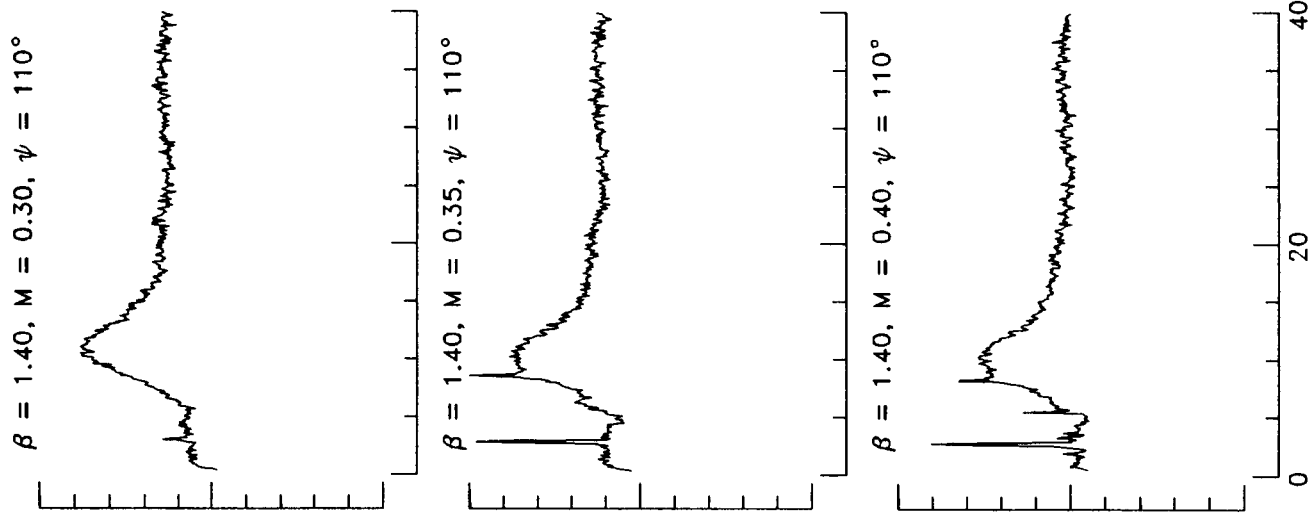
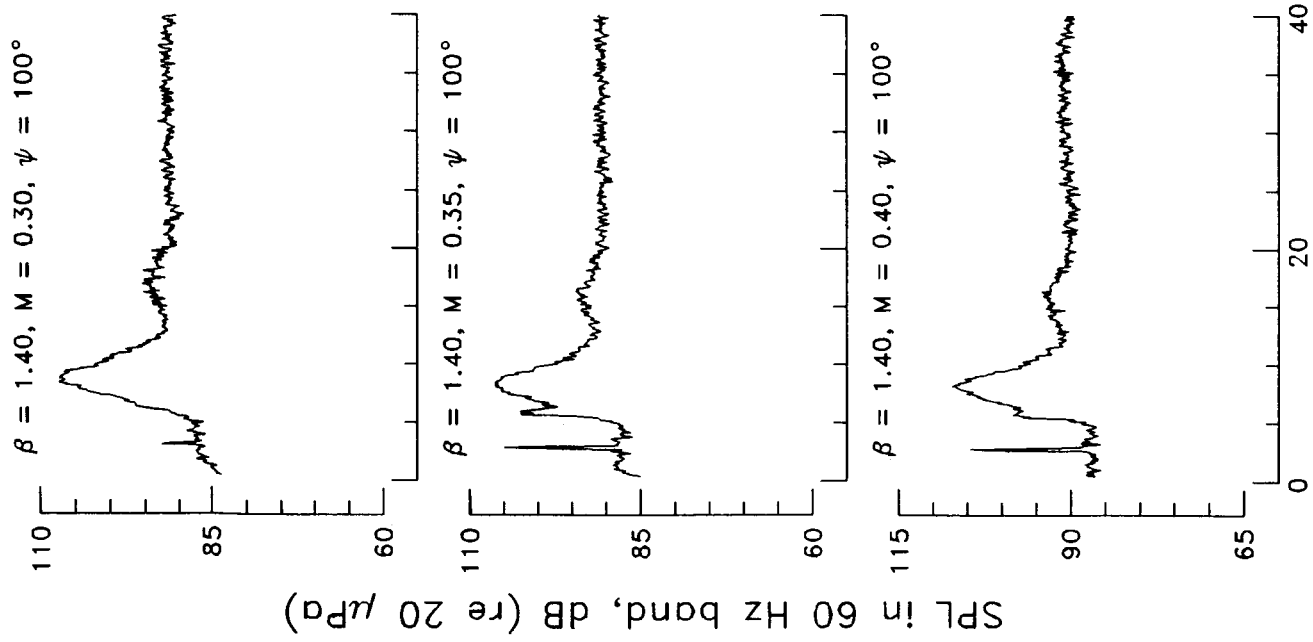
SPL in 60 Hz band, dB (re 20 μ Pa)



Frequency, kHz

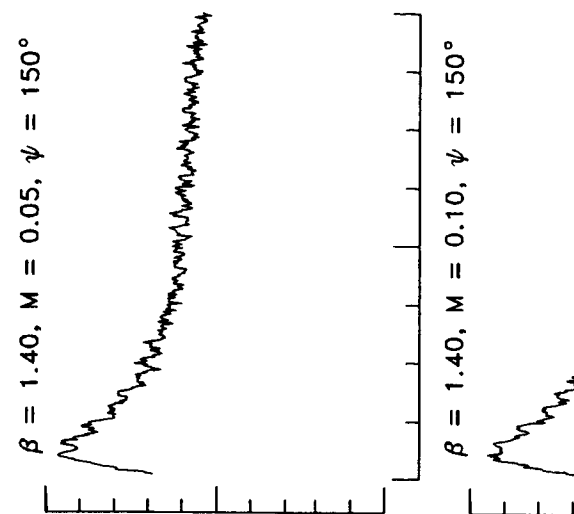
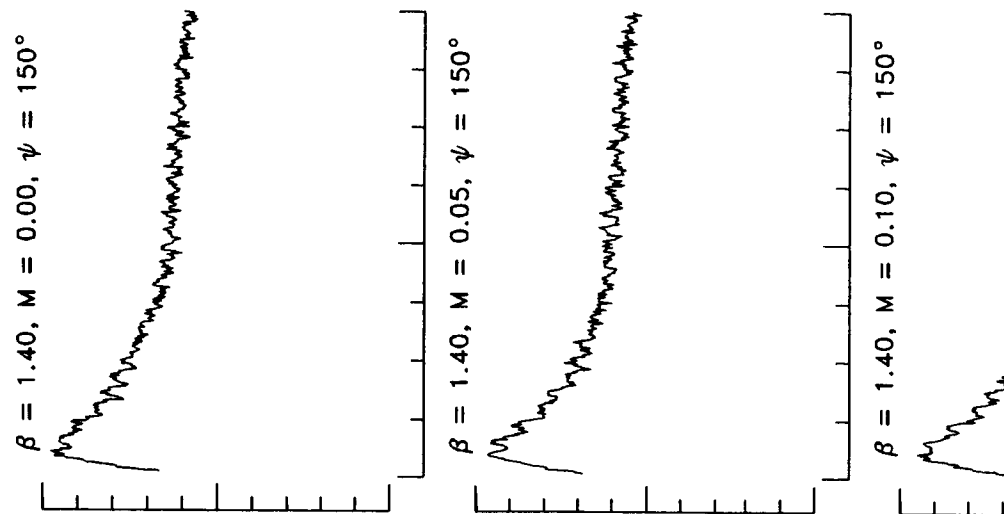
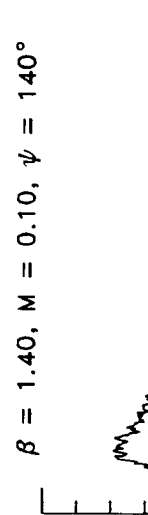
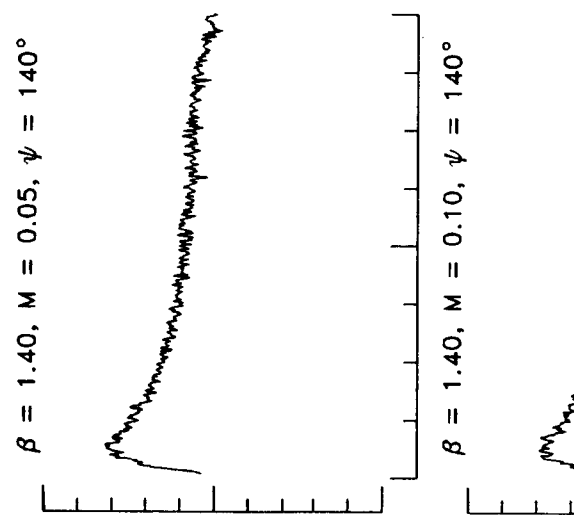
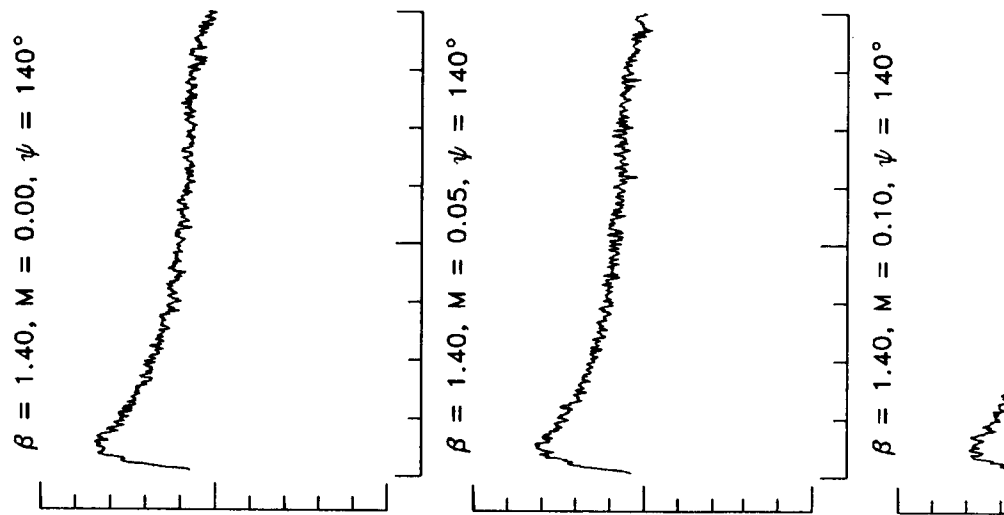
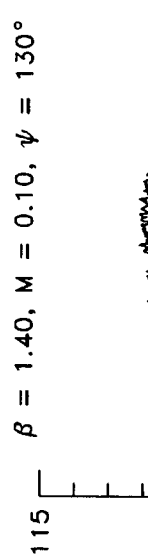
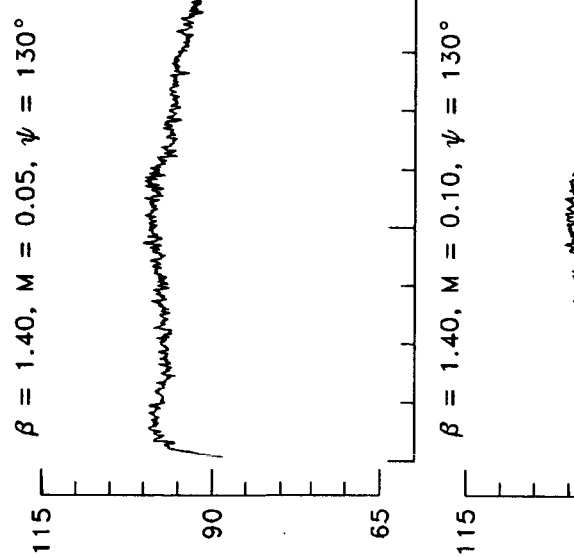
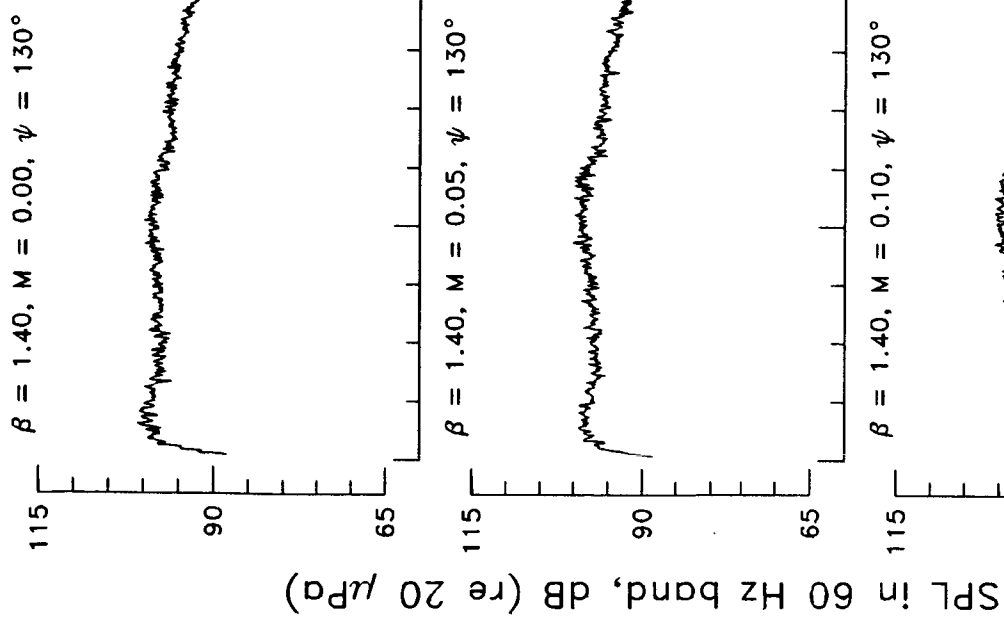
ORIGINAL PAGE IS
OF POOR QUALITY



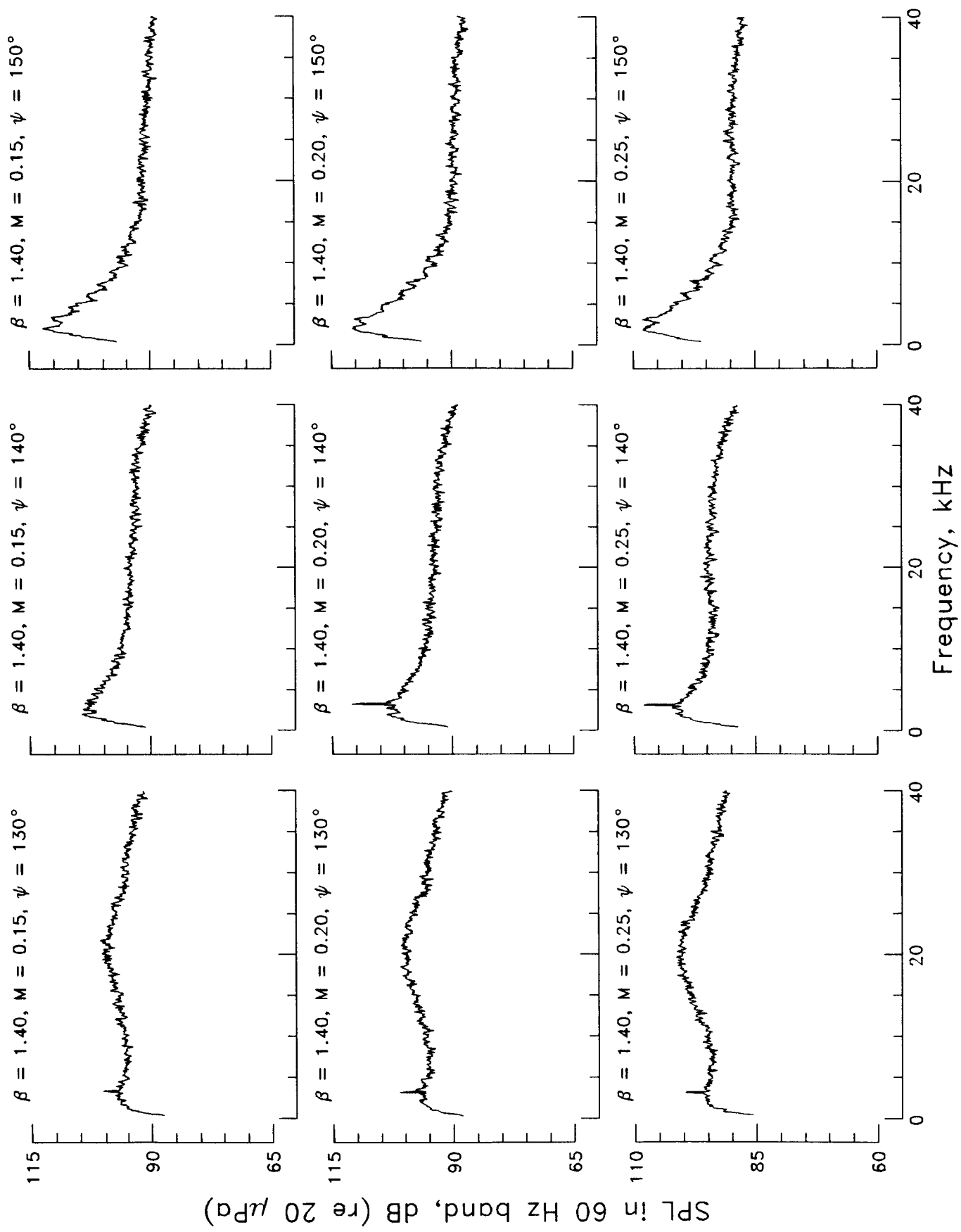


SPL in 60 Hz band, dB (re 20 μ Pa)

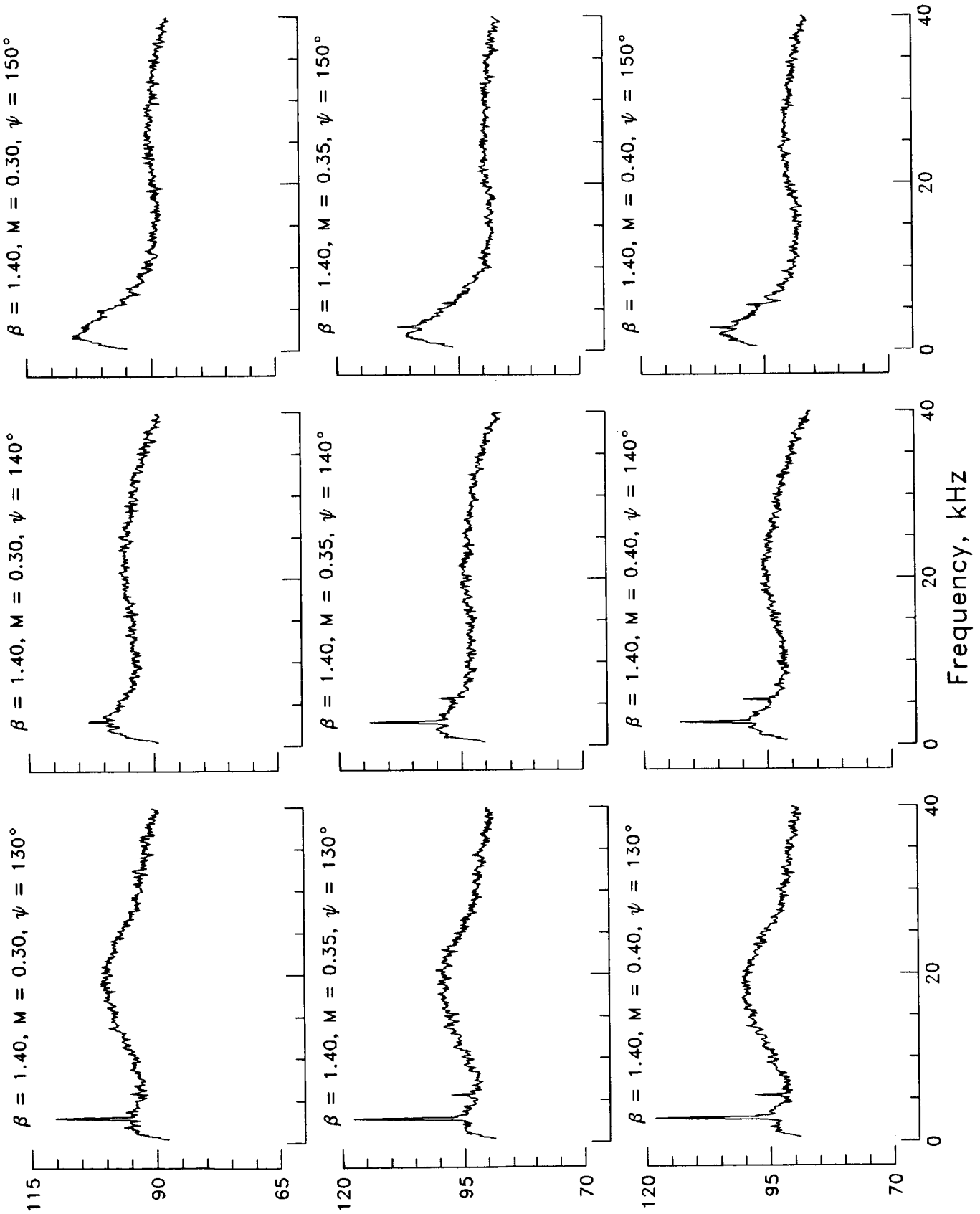
Frequency, kHz

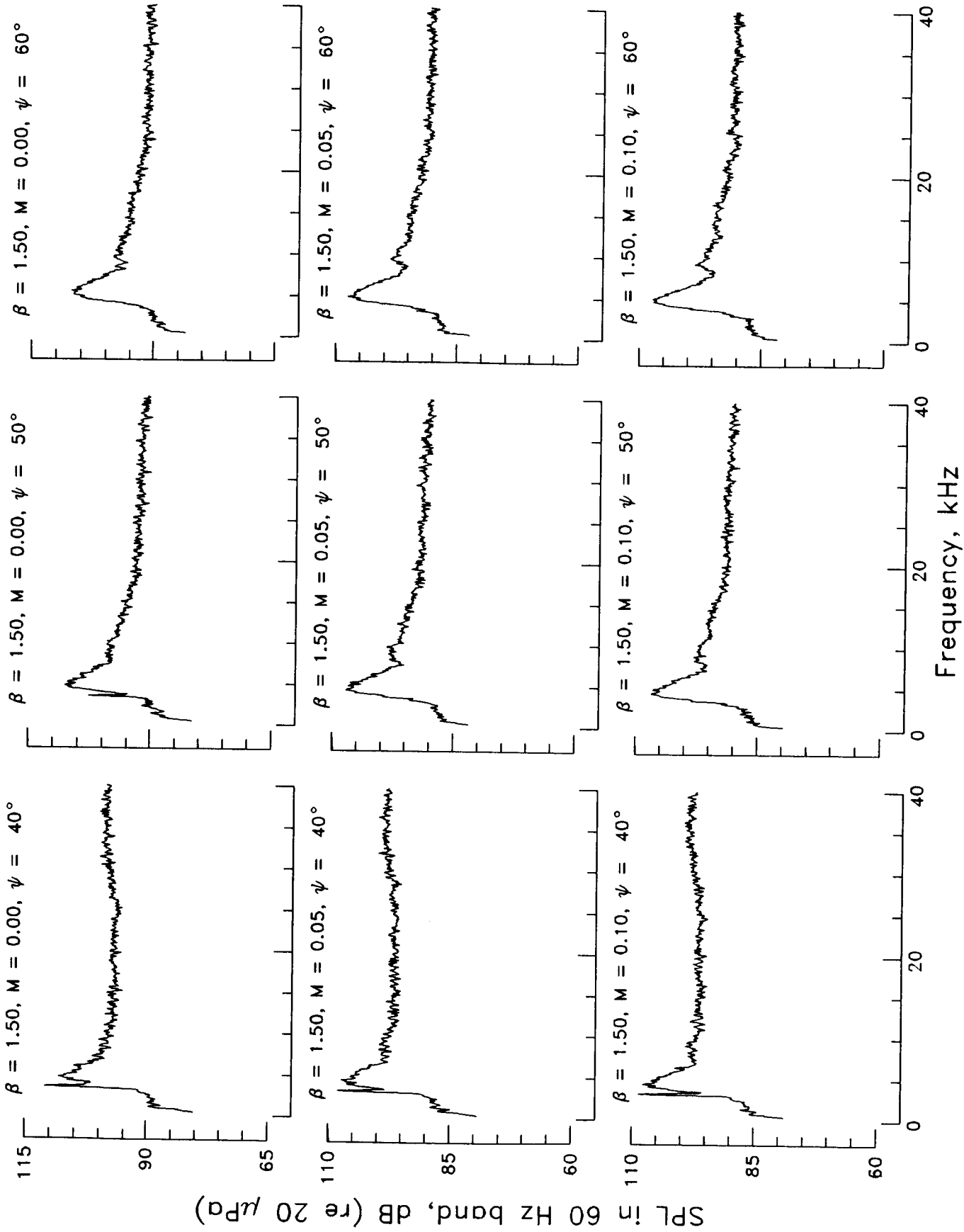


Frequency, kHz



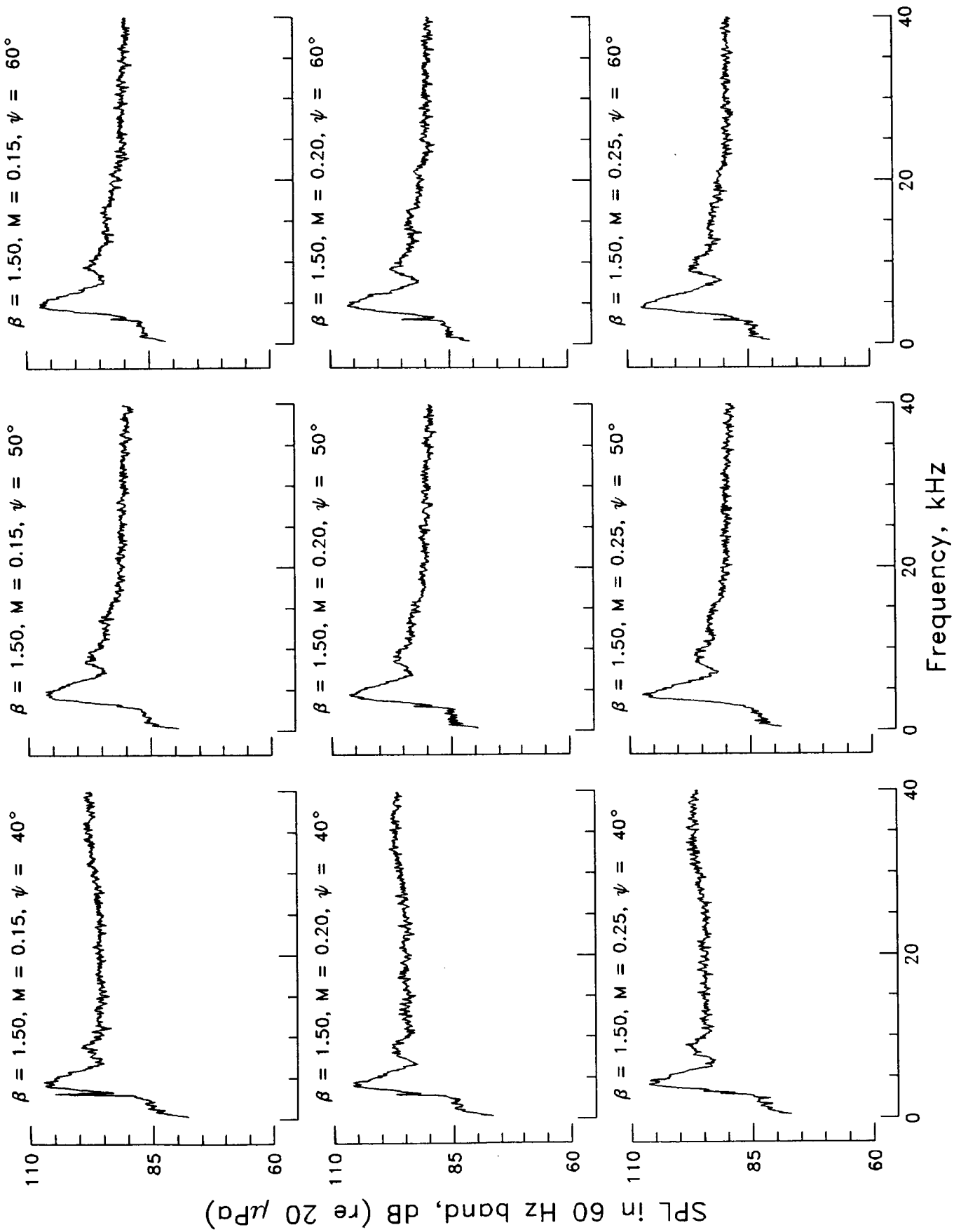
SPL in 60 Hz band, dB (re 20 μ Fa)

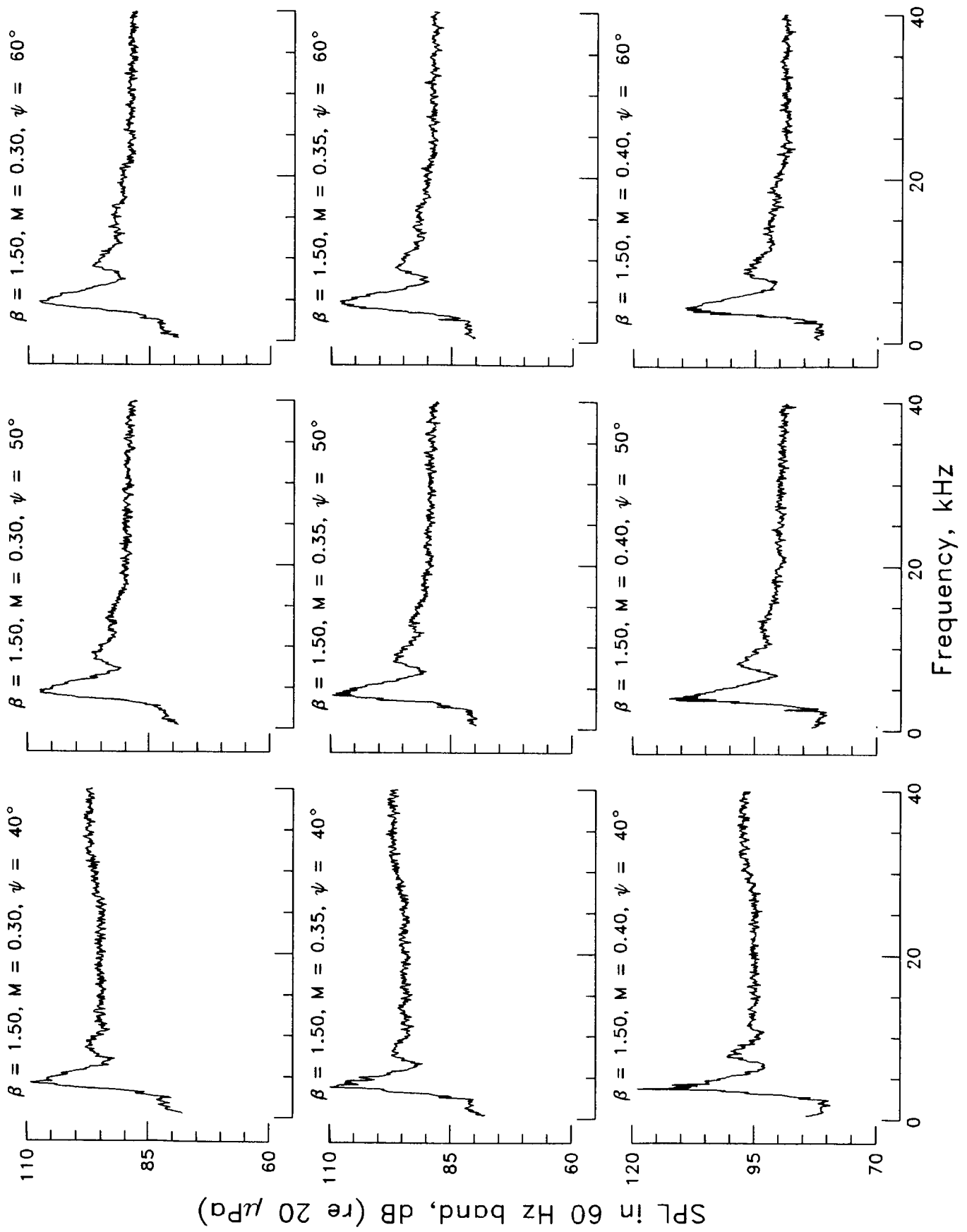


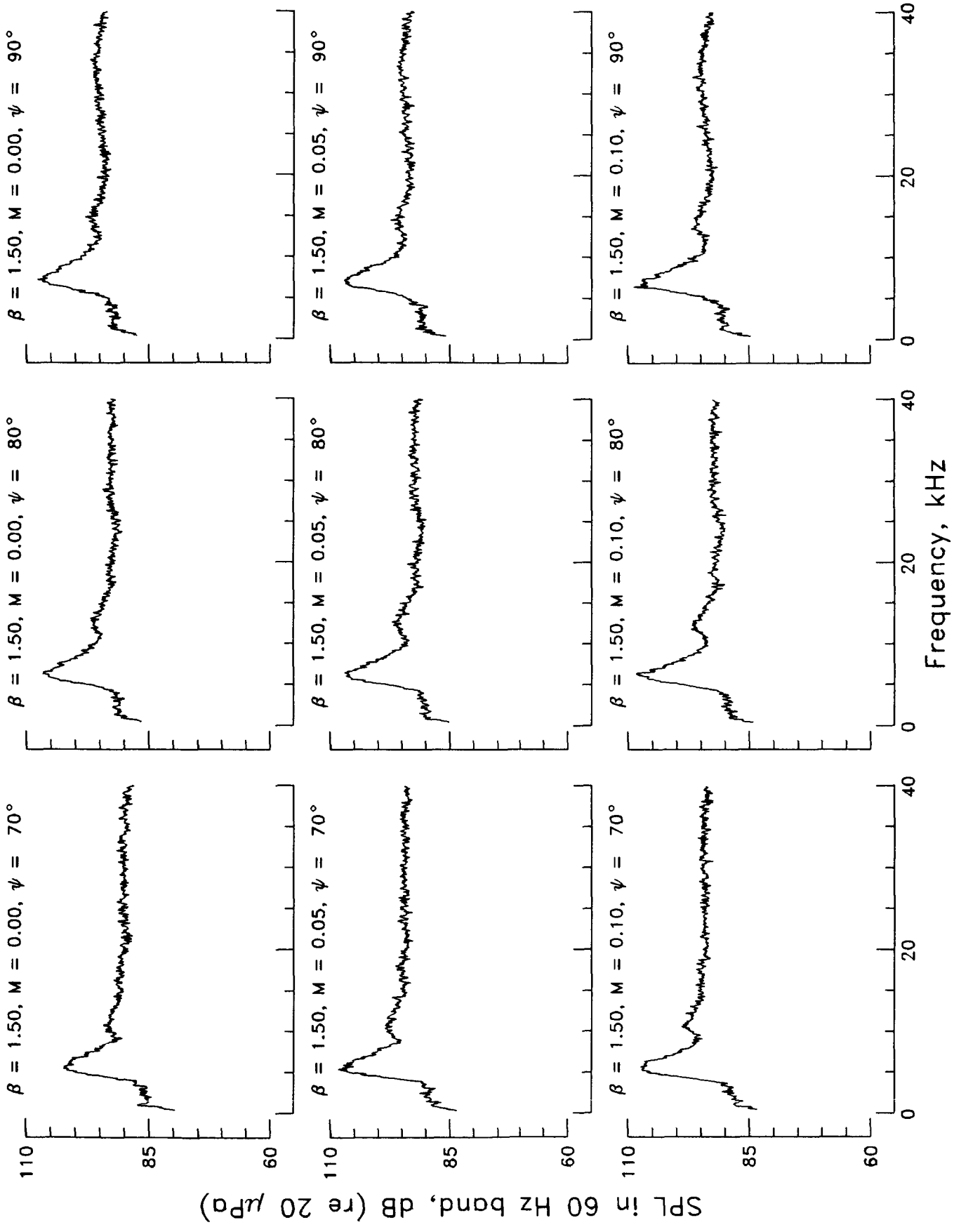


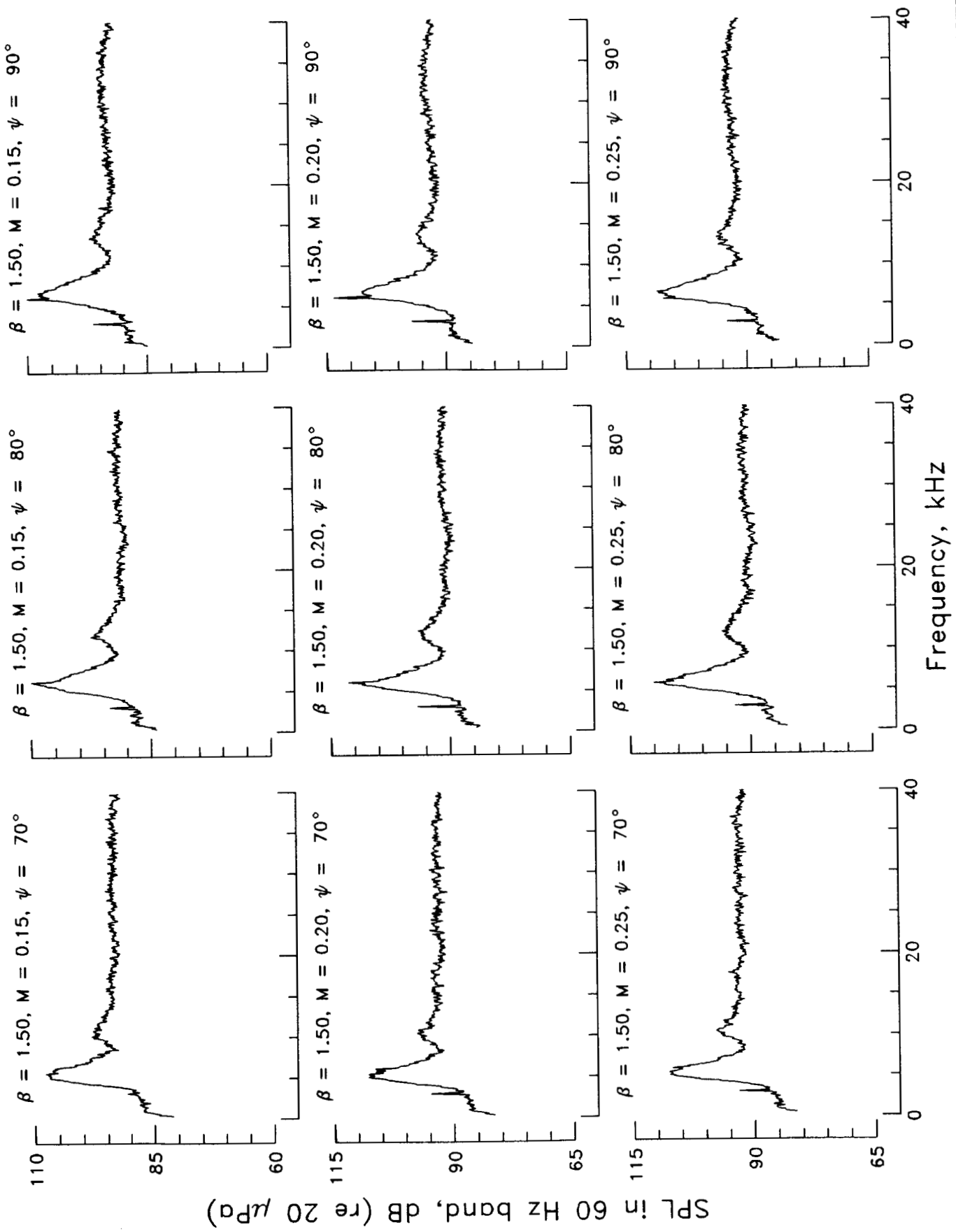
SPL in 60 Hz band, dB (re 20 μ Pa)

Frequency, kHz

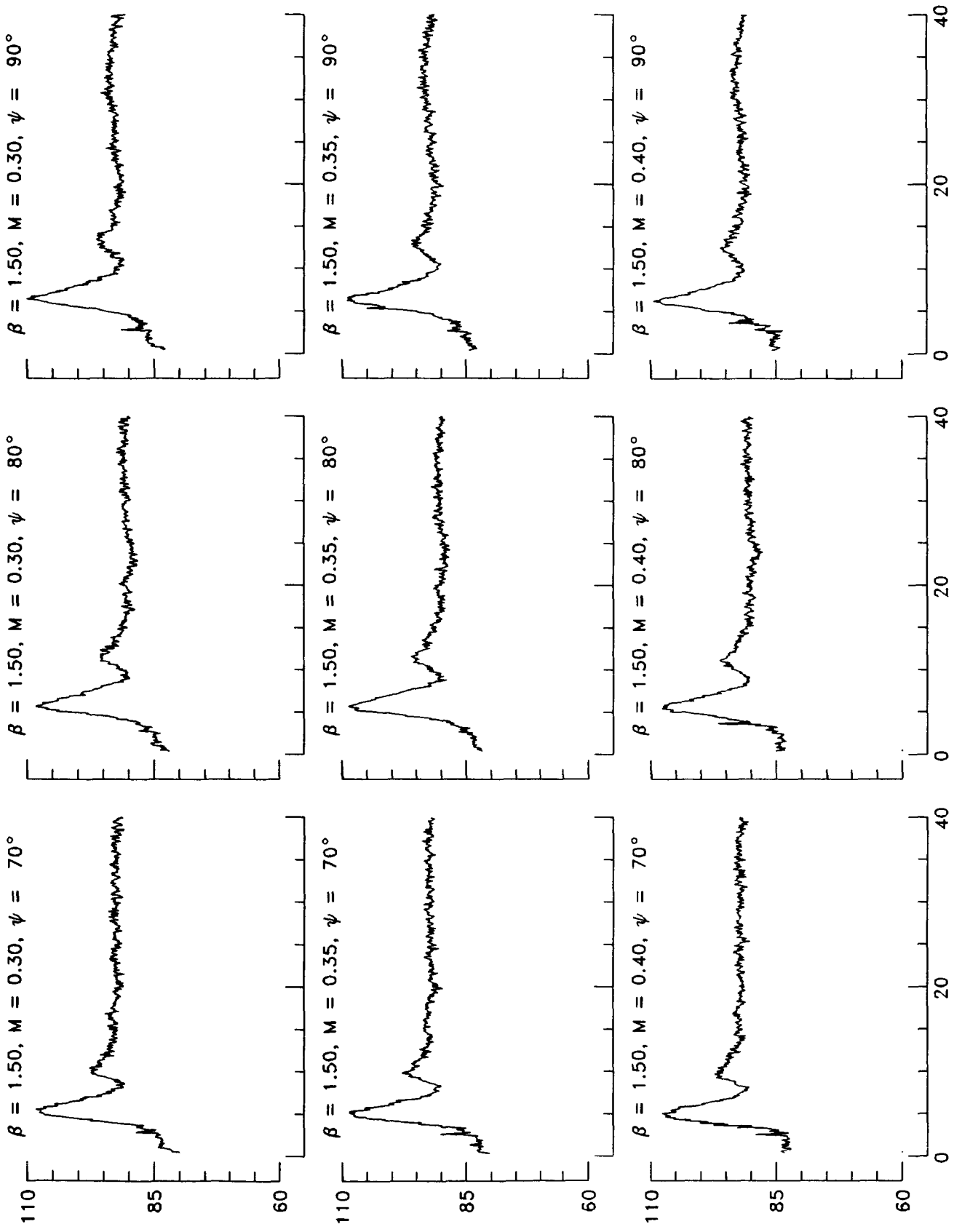




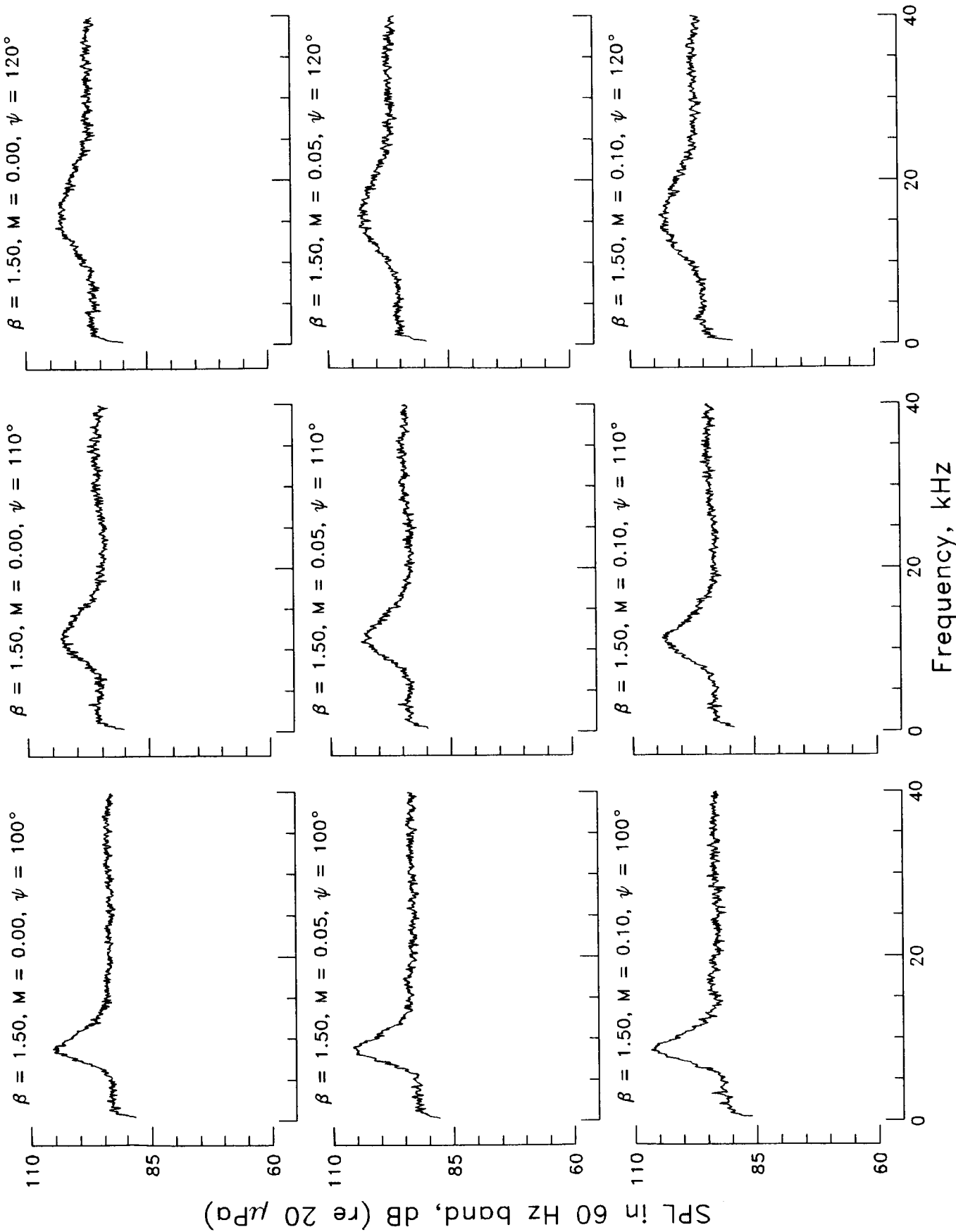


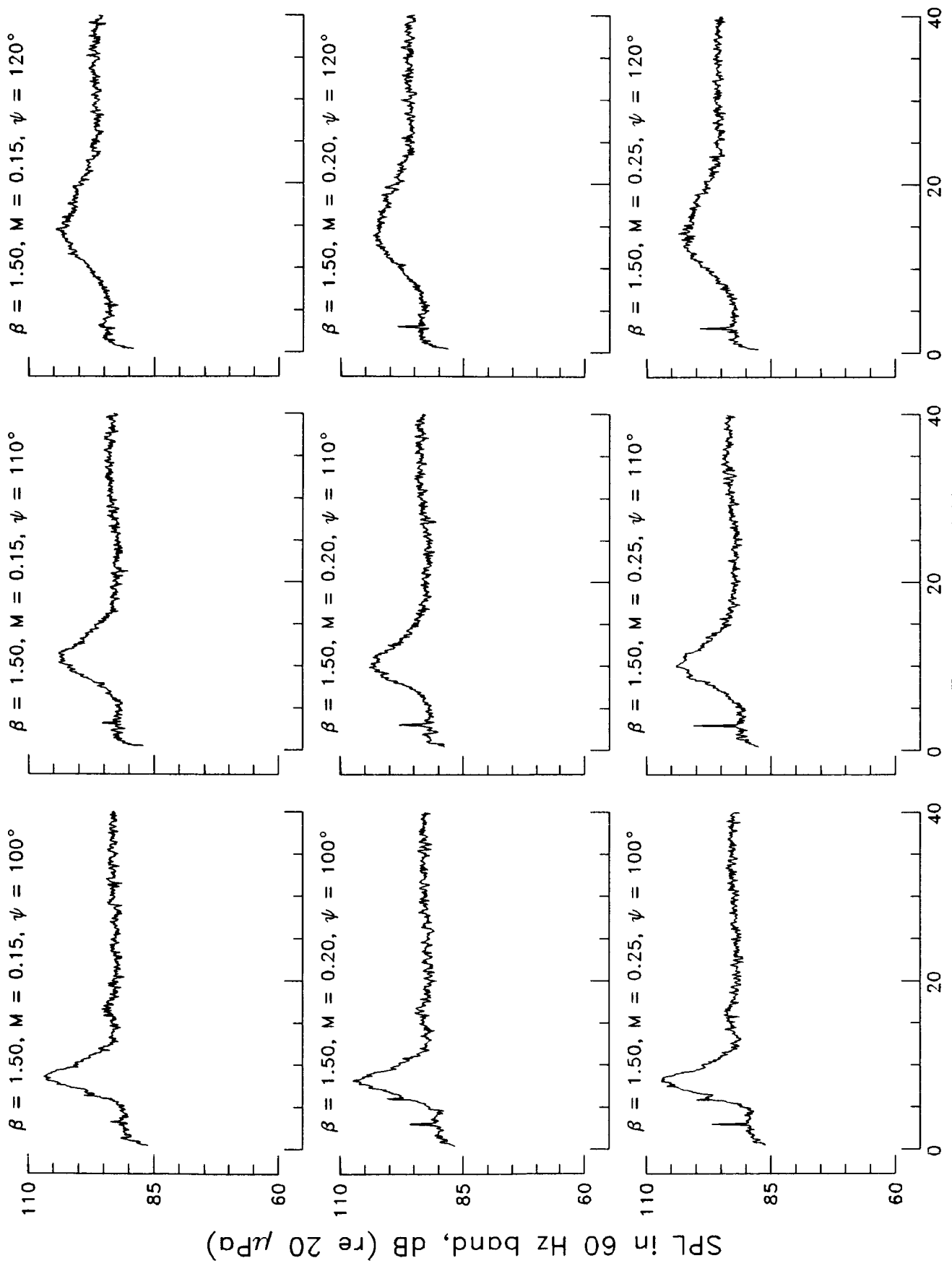


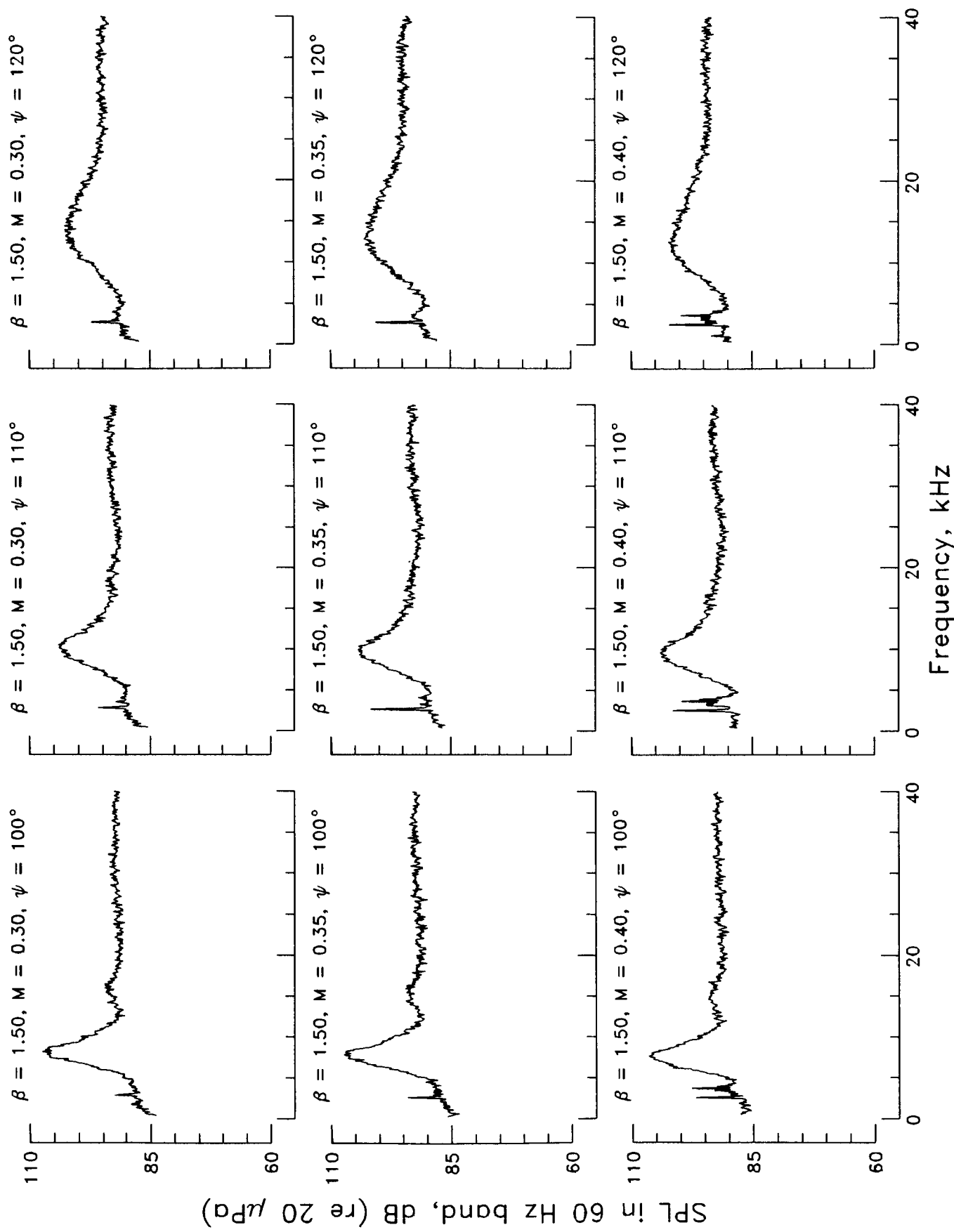
SPL in 60 Hz band, dB (re 20 μ Pa)



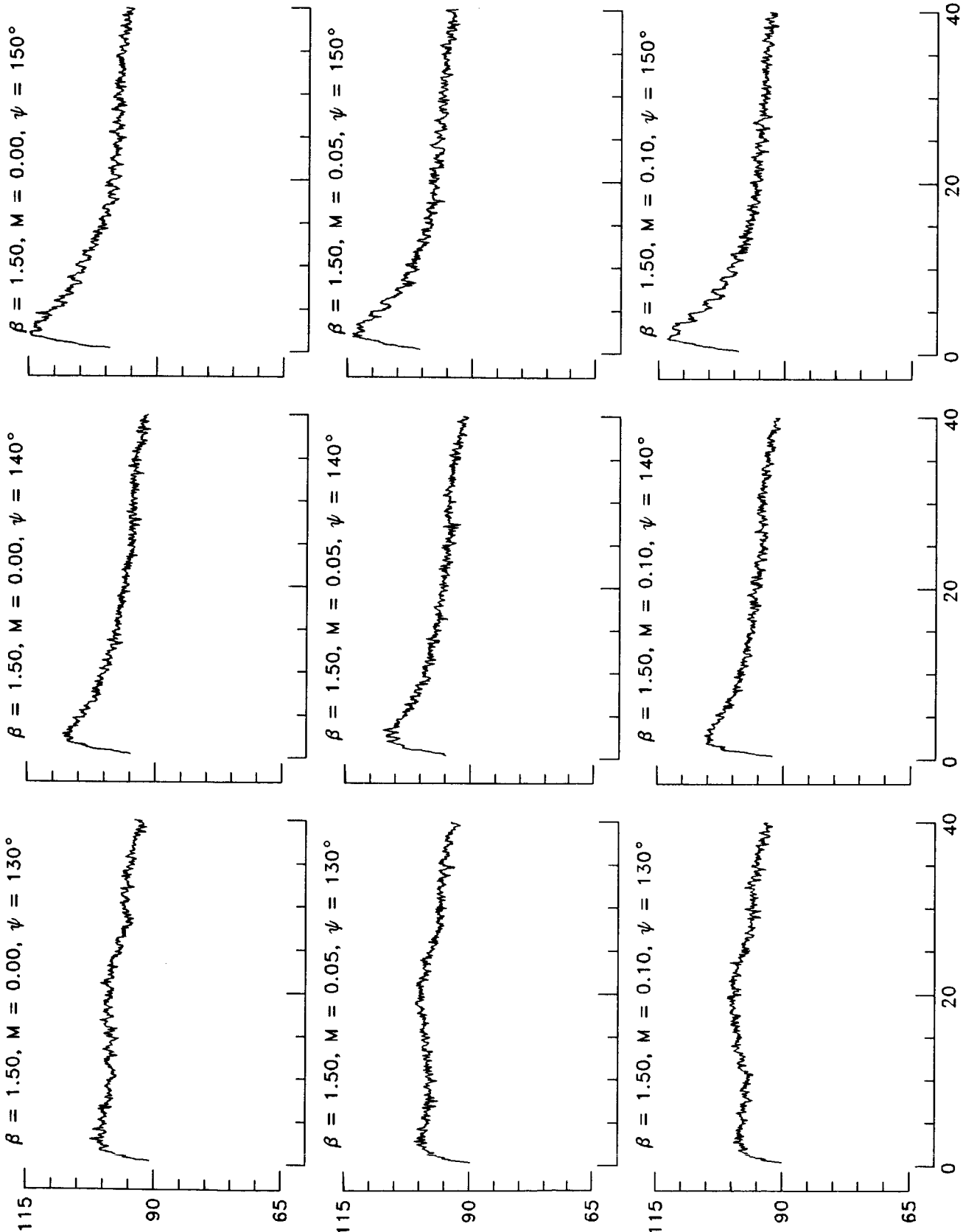
Frequency, kHz

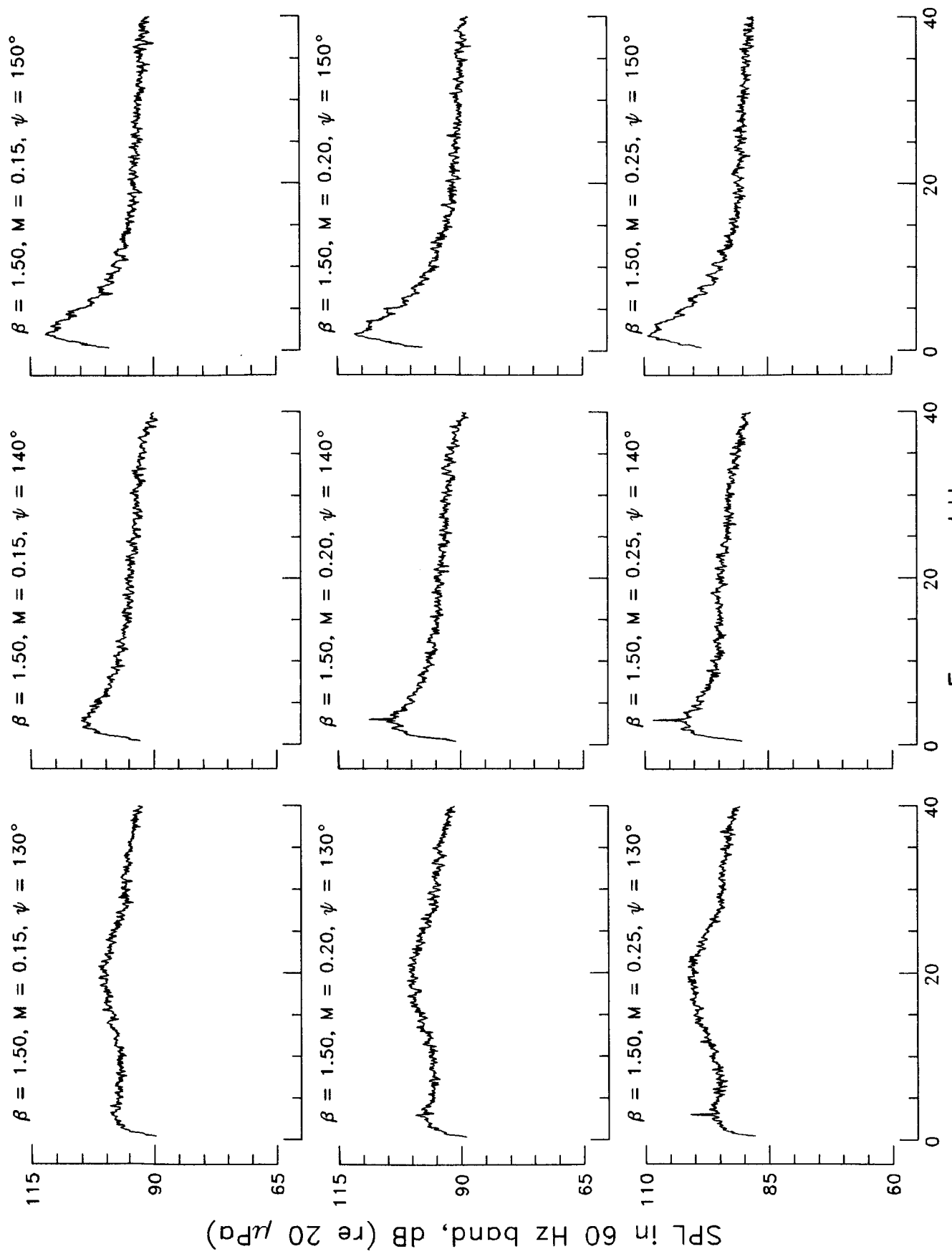






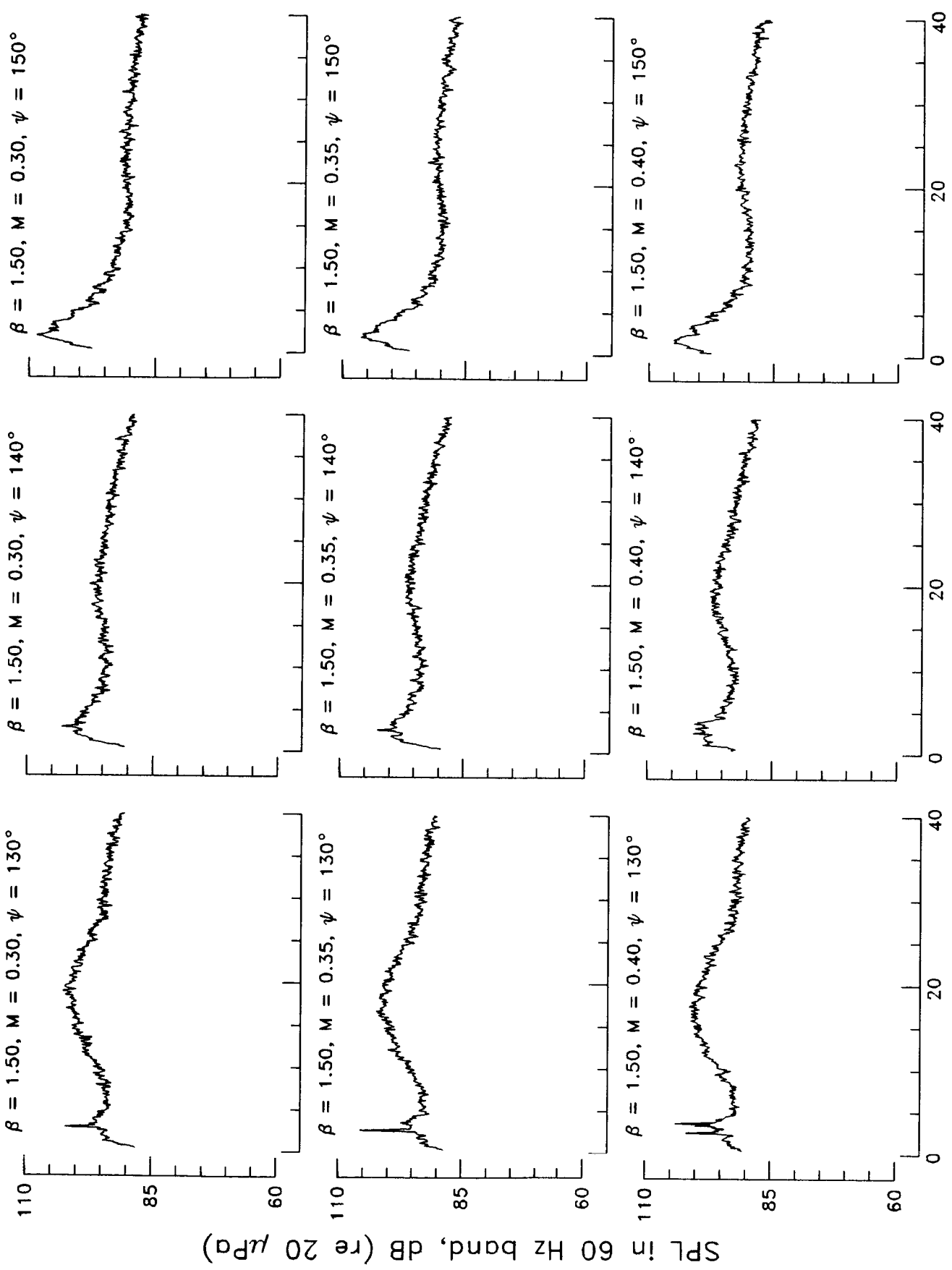
SPL in 60 Hz band, dB (re 20 μ Pd)





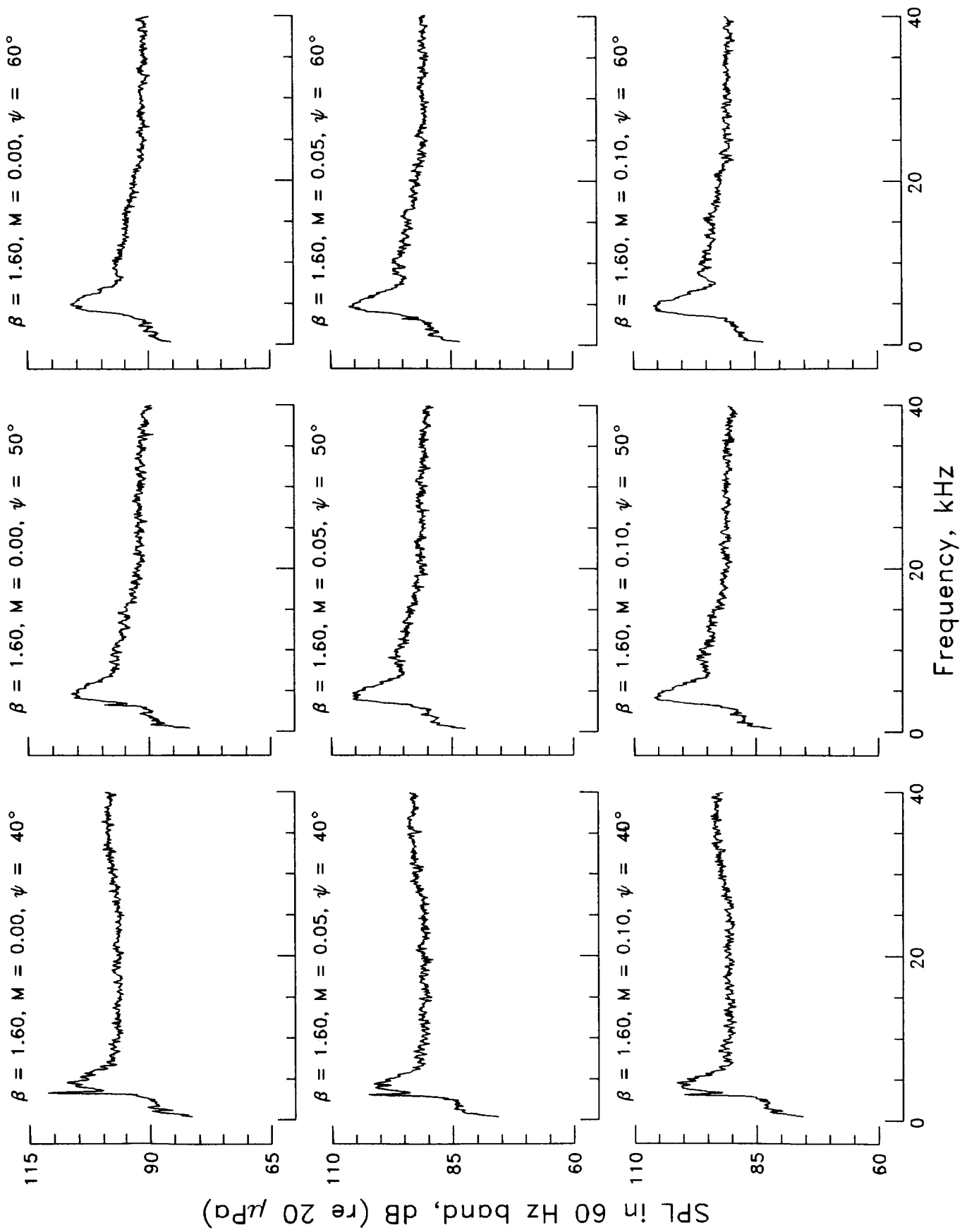
SPL in 60 Hz band, dB (re 20 μ Pa)

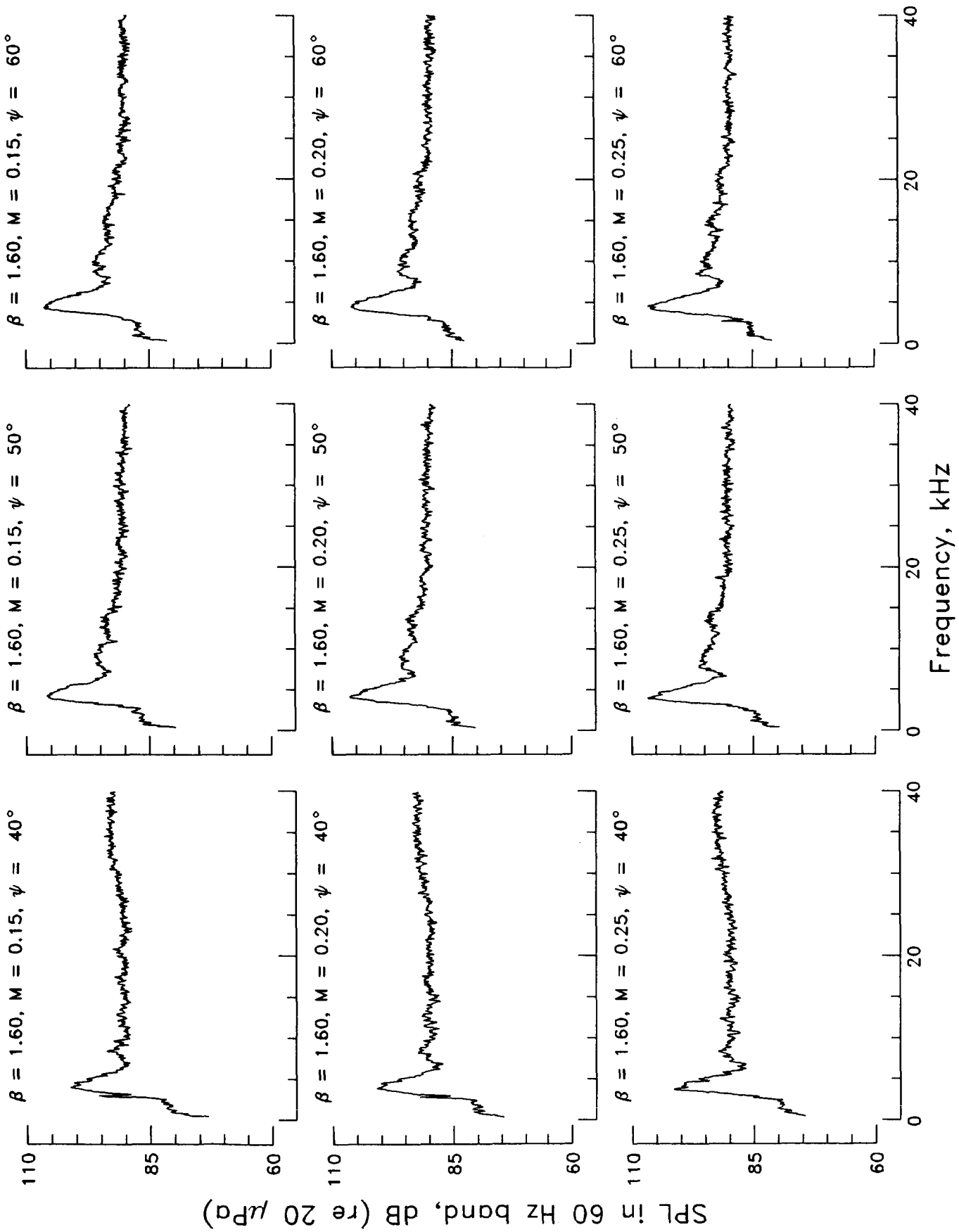
Frequency, kHz

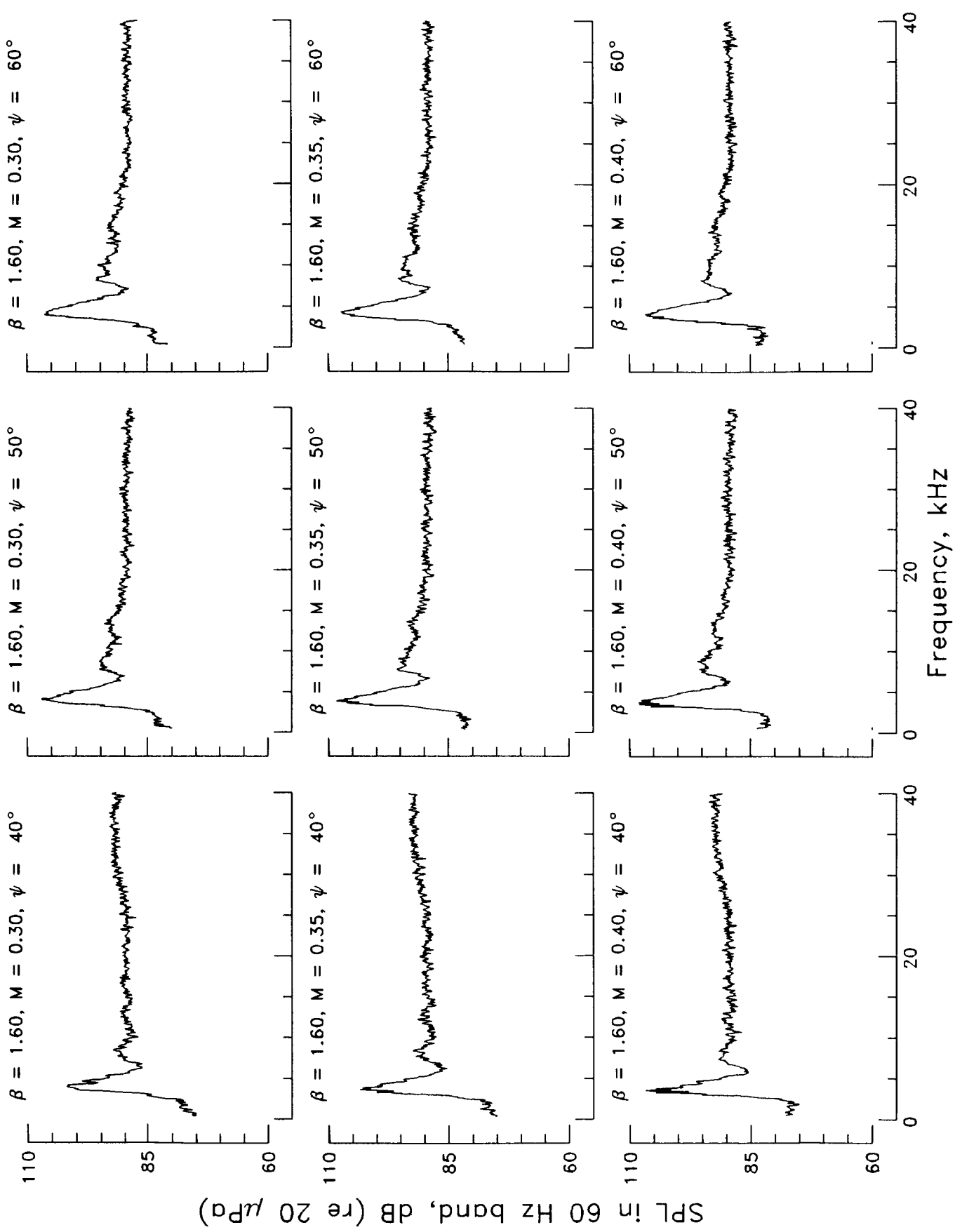


Frequency, kHz

SPL in 60 Hz band, dB (re 20 μ Pa)

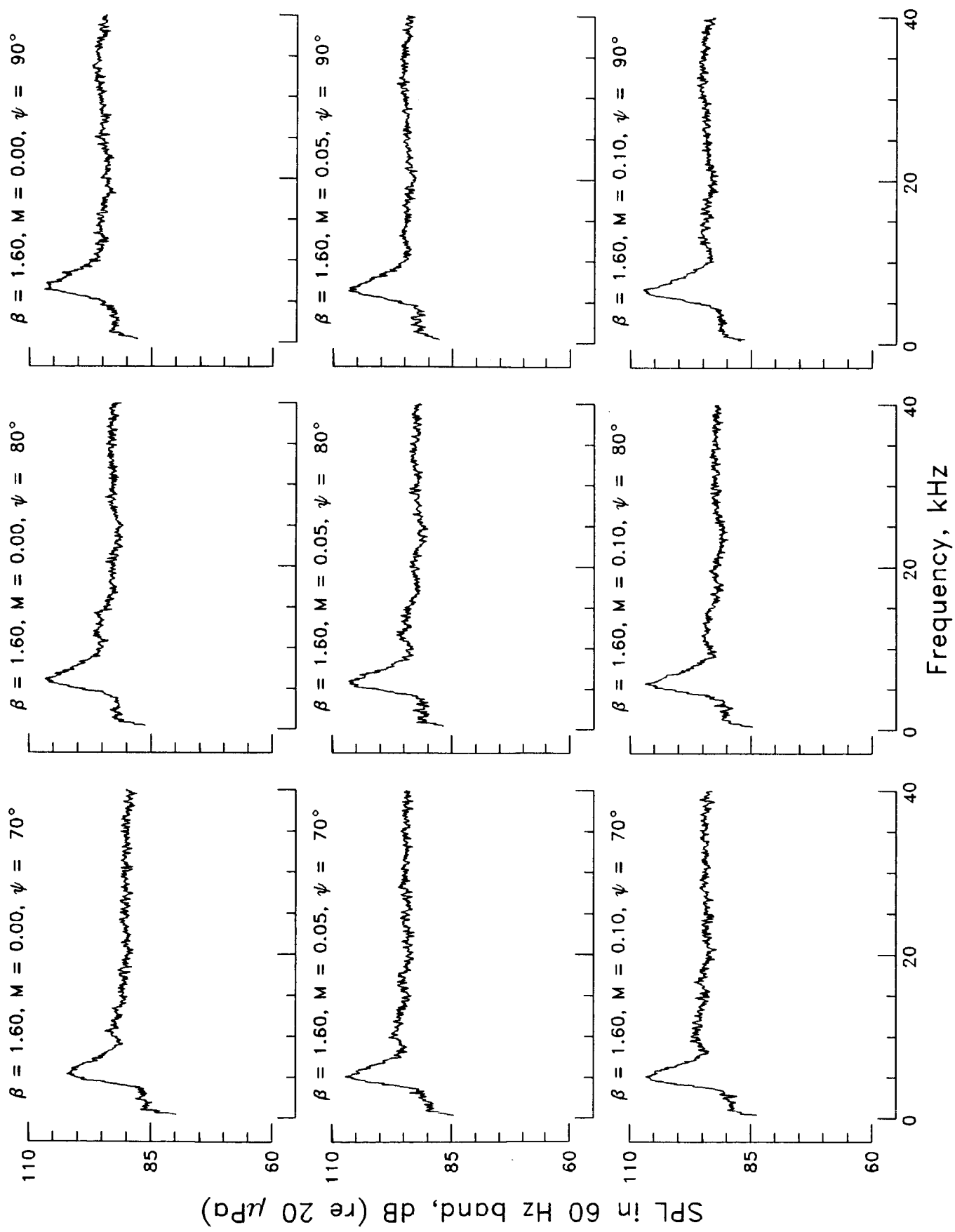


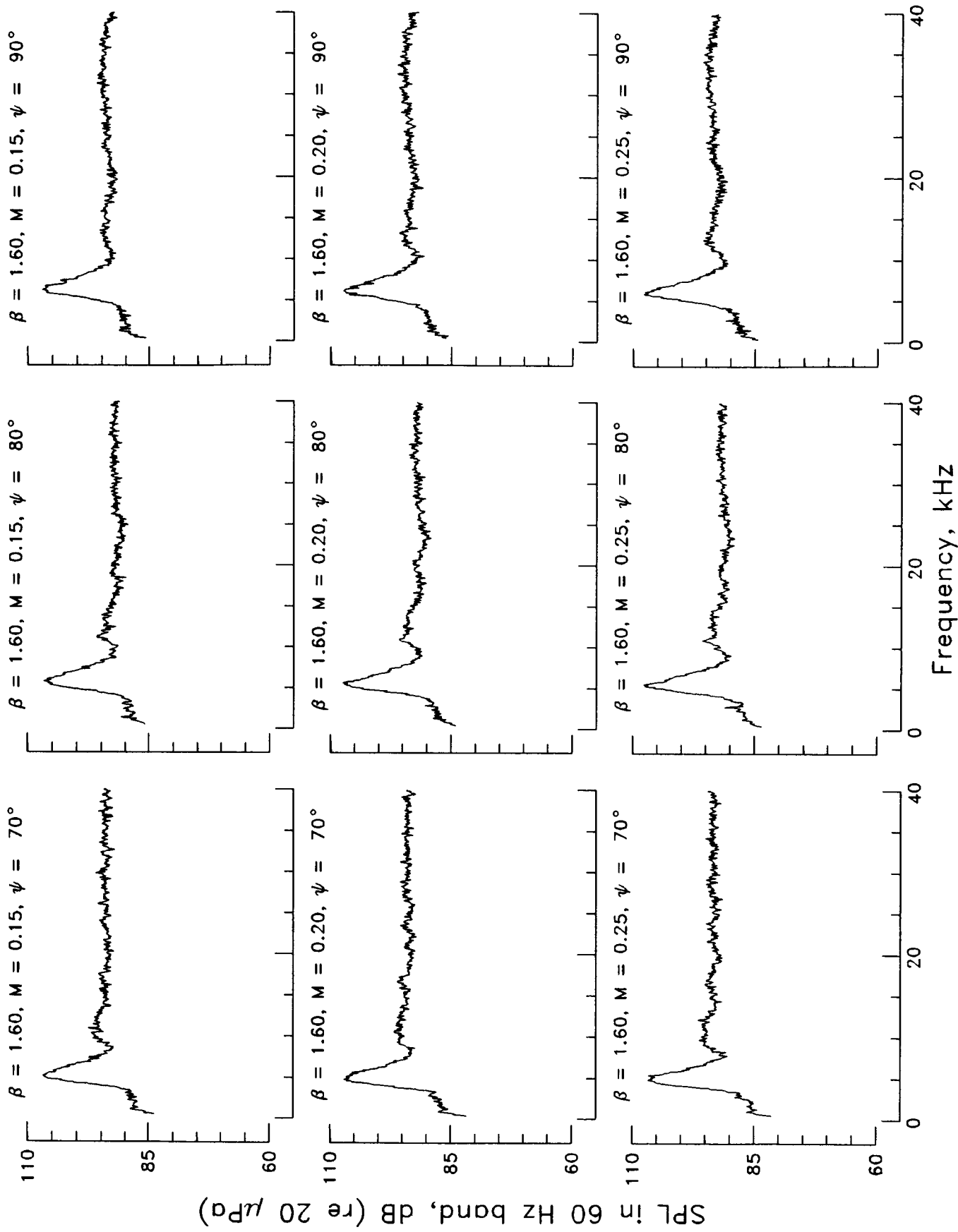




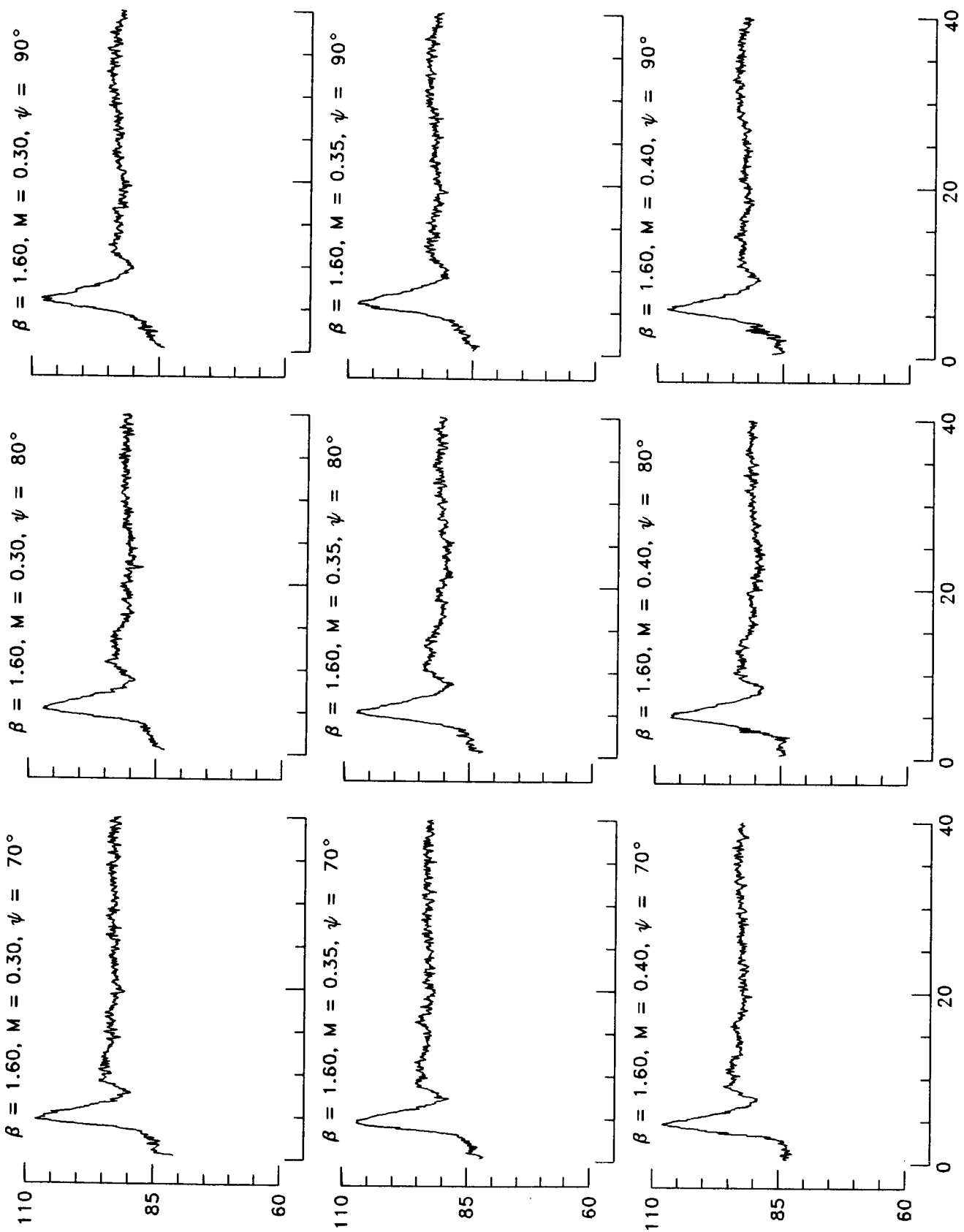
SPL in 60 Hz band, dB (re 20 μ Pa)

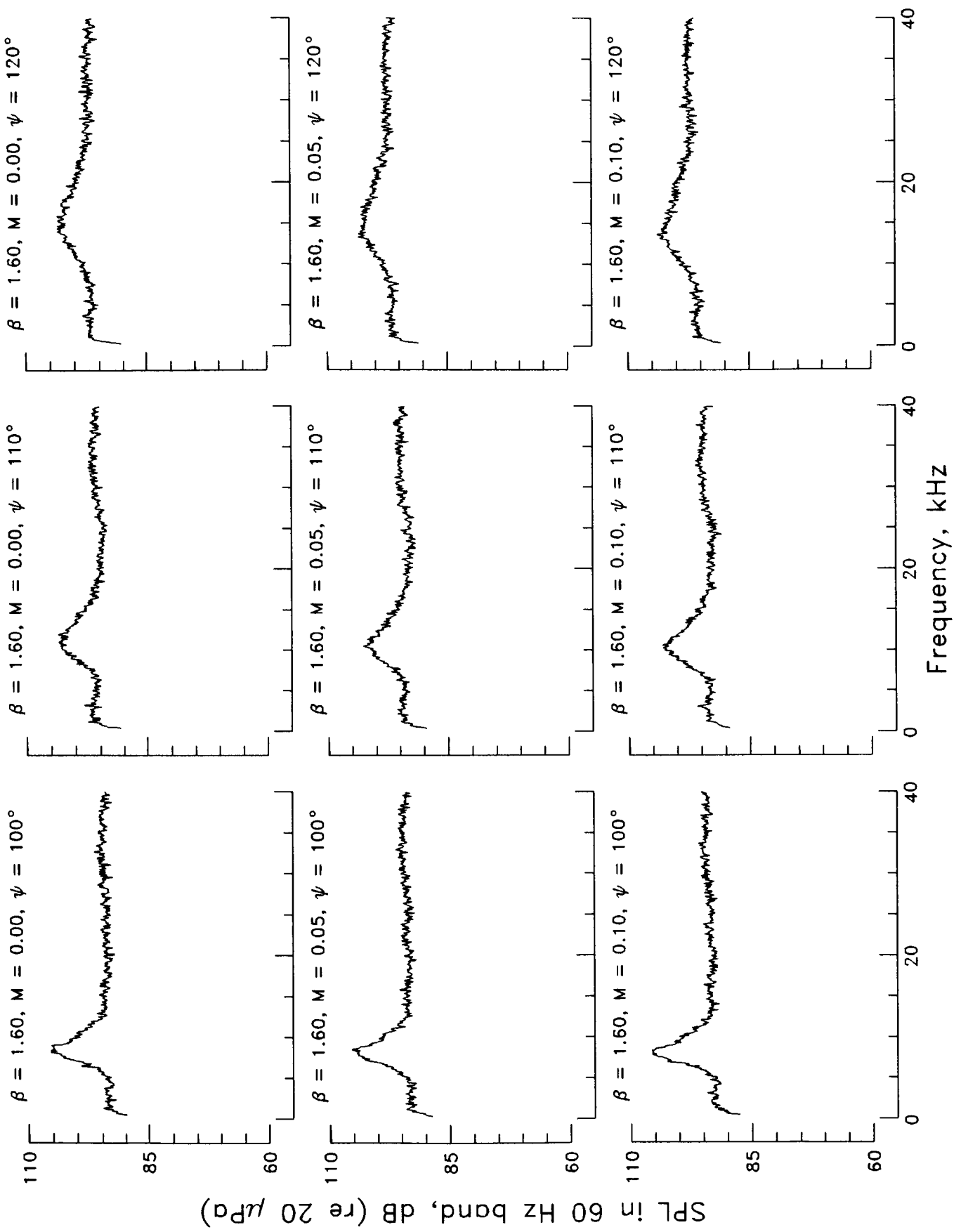
Frequency, kHz

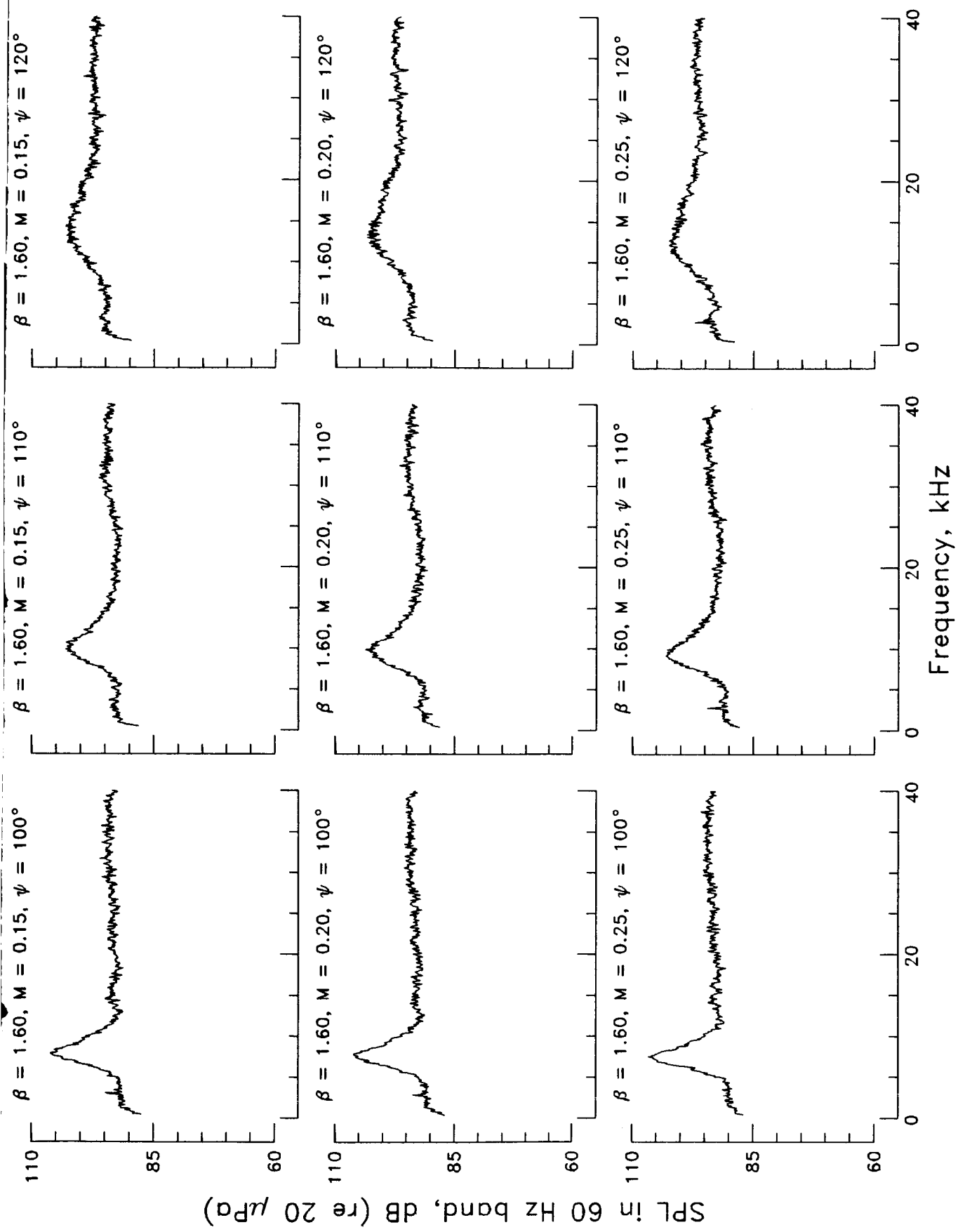


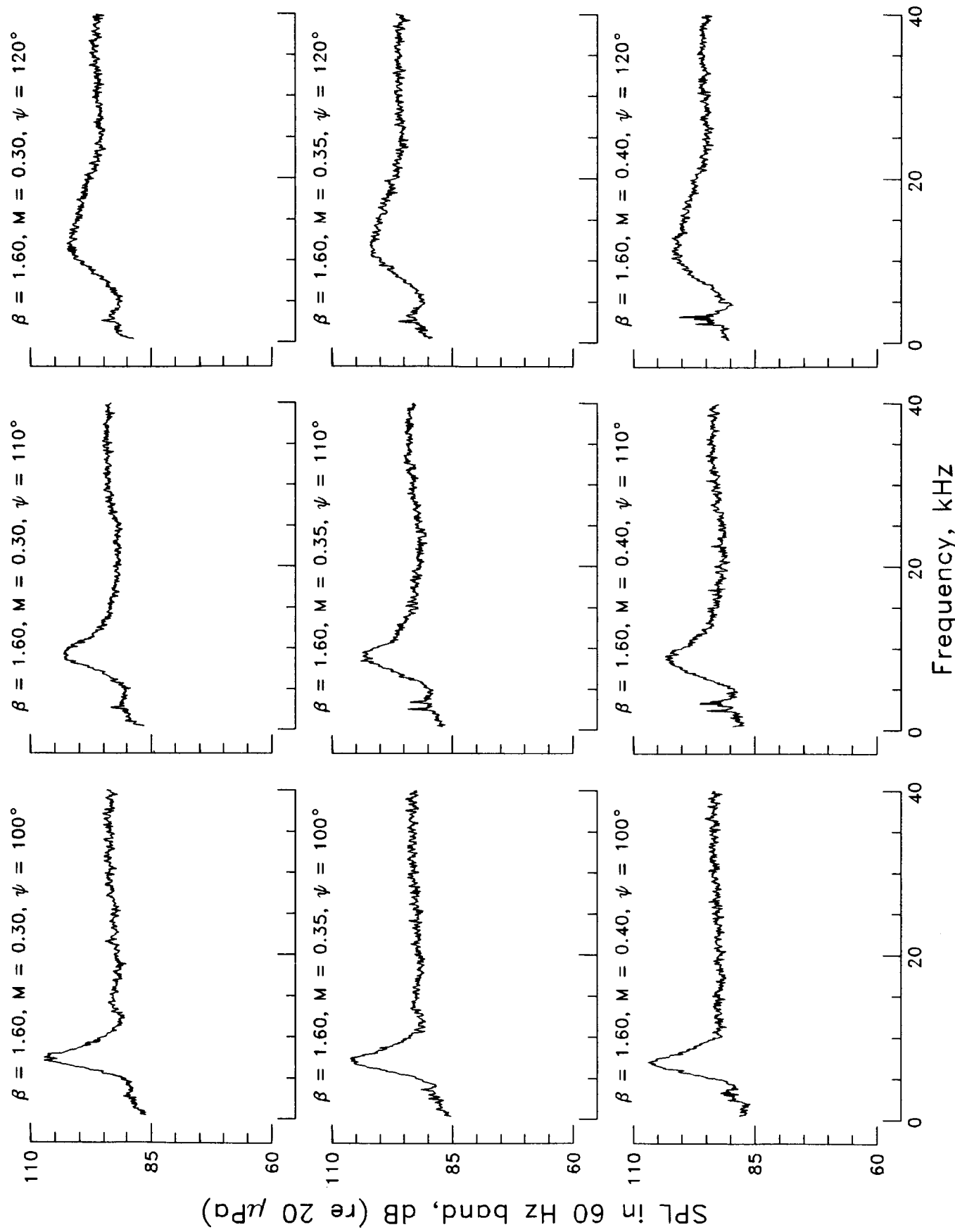


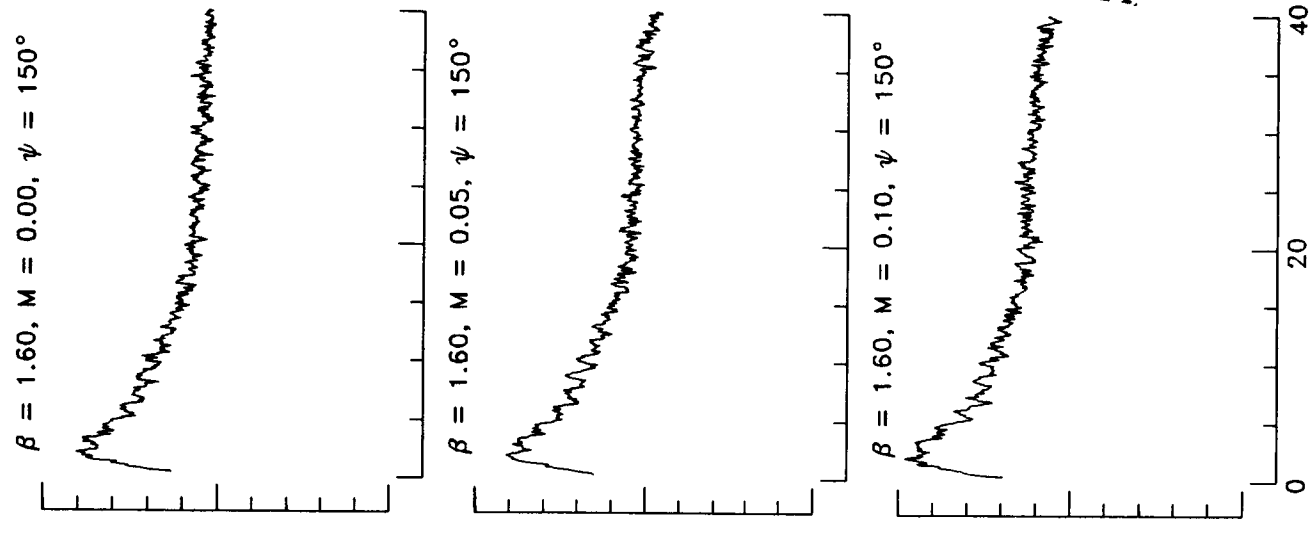
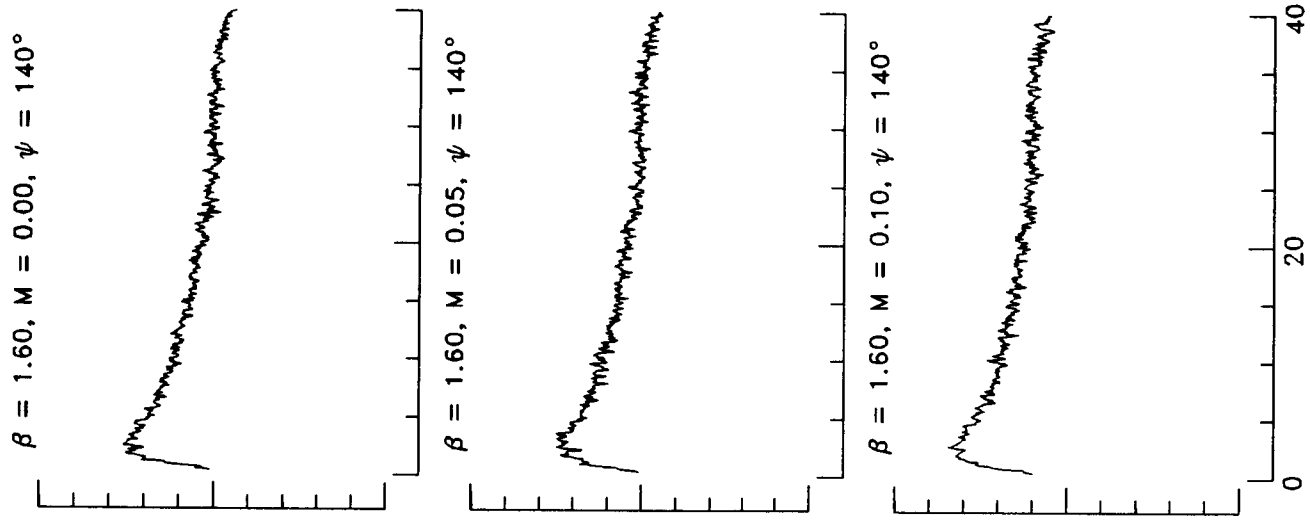
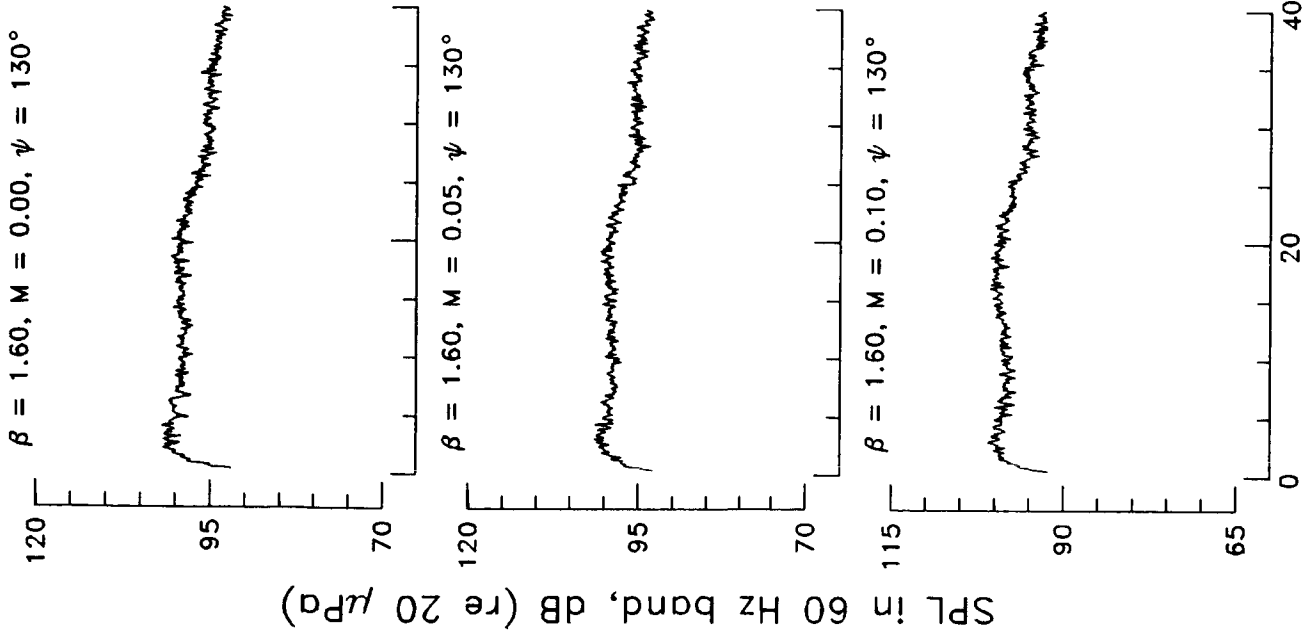
SPL in 60 Hz band, dB (re 20 μ Pa)





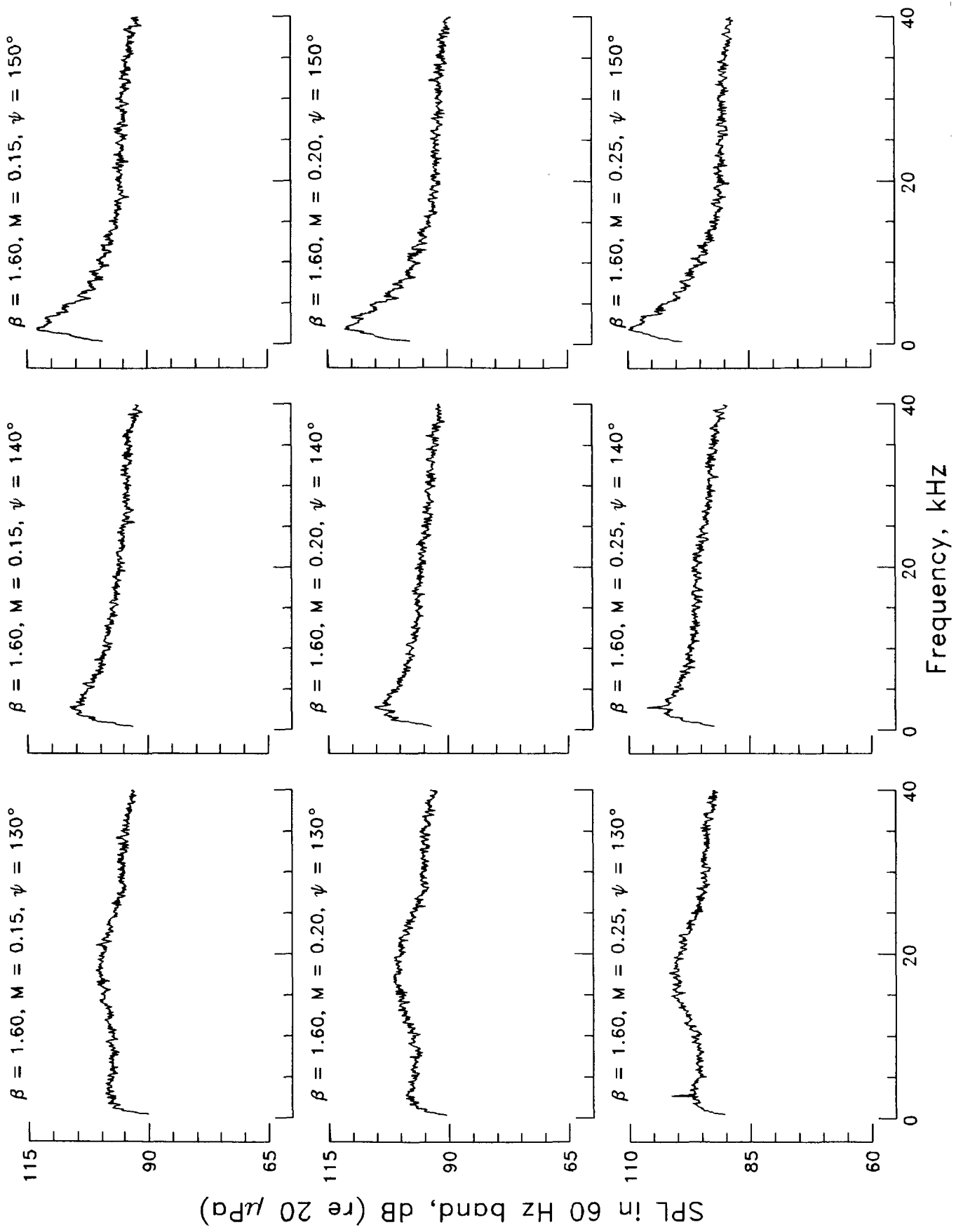




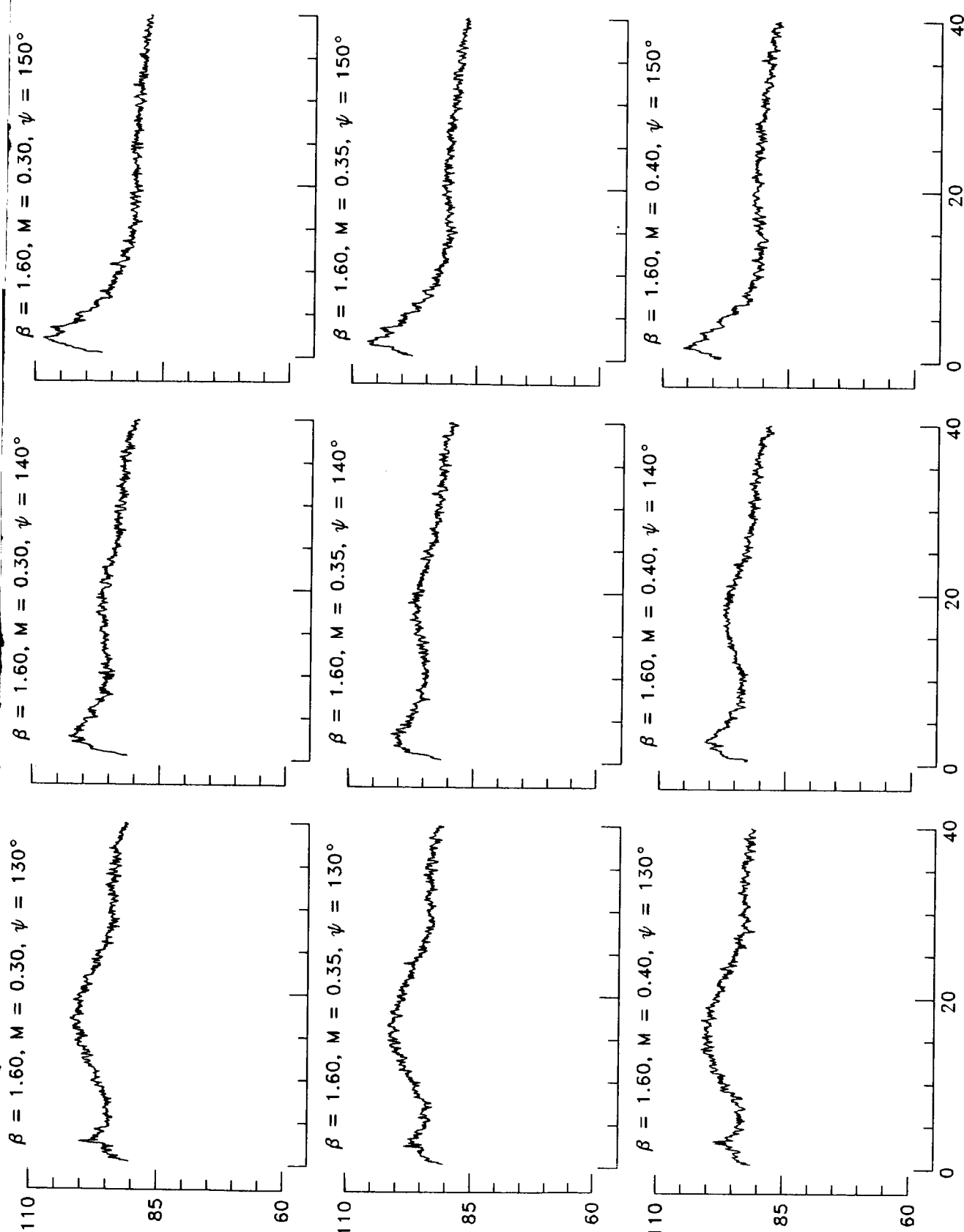


Frequency, kHz

SPL in 60 Hz band, dB (re 20 μ Pa)



SPL in 60 Hz band, dB (re 20 μ Pa)



Frequency, kHz

References

1. Powell, Alan: On the Noise Emanating From a Two-Dimensional Jet Above the Critical Pressure. *Aeronaut. Q.*, vol. IV, pt. 2, Feb. 1953, pp. 103-122.
2. Harper-Bourne, M.; and Fisher, M. J.: The Noise From Shock Waves in Supersonic Jets. *Noise Mechanisms*, AGARD-CP-131, Mar. 1974, pp. 11-1-11-13.
3. Tam, C. K. W.; and Tanna, H. K.: Shock Associated Noise of Supersonic Jets From Convergent-Divergent Nozzles. *J. Sound & Vib.*, vol. 81, no. 3, Apr. 8, 1982, pp. 337-358.
4. Tam, Christopher K. W.: *Effects of Forward Flight on Broadband Shock Associated Noise of Supersonic Jets*. Eng. Rep. No. LG84ERO 120, Lockheed-Georgia Co., Aug. 1, 1984.
5. Bryce, W. D.; and Pinker, R. A.: The Noise From Unheated Supersonic Jets in Simulated Flight. AIAA Paper 77-1327, Oct. 1977.
6. Yamamoto, K.; Brausch, J. F.; Balsa, T. F.; Janardan, B. A.; and Knott, P. R.: *Experimental Investigation of Shock-Cell Noise Reduction for Single Stream Nozzles in Simulated Flight*. NASA CR-3845, 1984.
7. Norum, Thomas D.; and Shearin, John G.: *Effects of Simulated Flight on the Structure and Noise of Under-expanded Jets*. NASA TP-2308, 1984.
8. Norum, Thomas D.; and Shearin, John G.: Shock Noise From Supersonic Jets in Simulated Flight to Mach 0.4. AIAA-86-1945, July 1986.
9. Norum, Thomas D.; and Seiner, John M.: *Measurements of Mean Static Pressure and Far-Field Acoustics of Shock-Containing Supersonic Jets*. NASA TM-84521, 1982.
10. Schlinker, Robert H.; and Amiet, Roy K.: *Refraction and Scattering of Sound by a Shear Layer*. NASA CR-3371, 1980.

ORIGINAL PAGE IS
OF POOR QUALITY

ORIGINAL PAGE IS
OF POOR QUALITY.



L-83-1,624

Figure 1. Nozzles and microphones mounted in anechoic chamber during the first phase acoustic experiments.

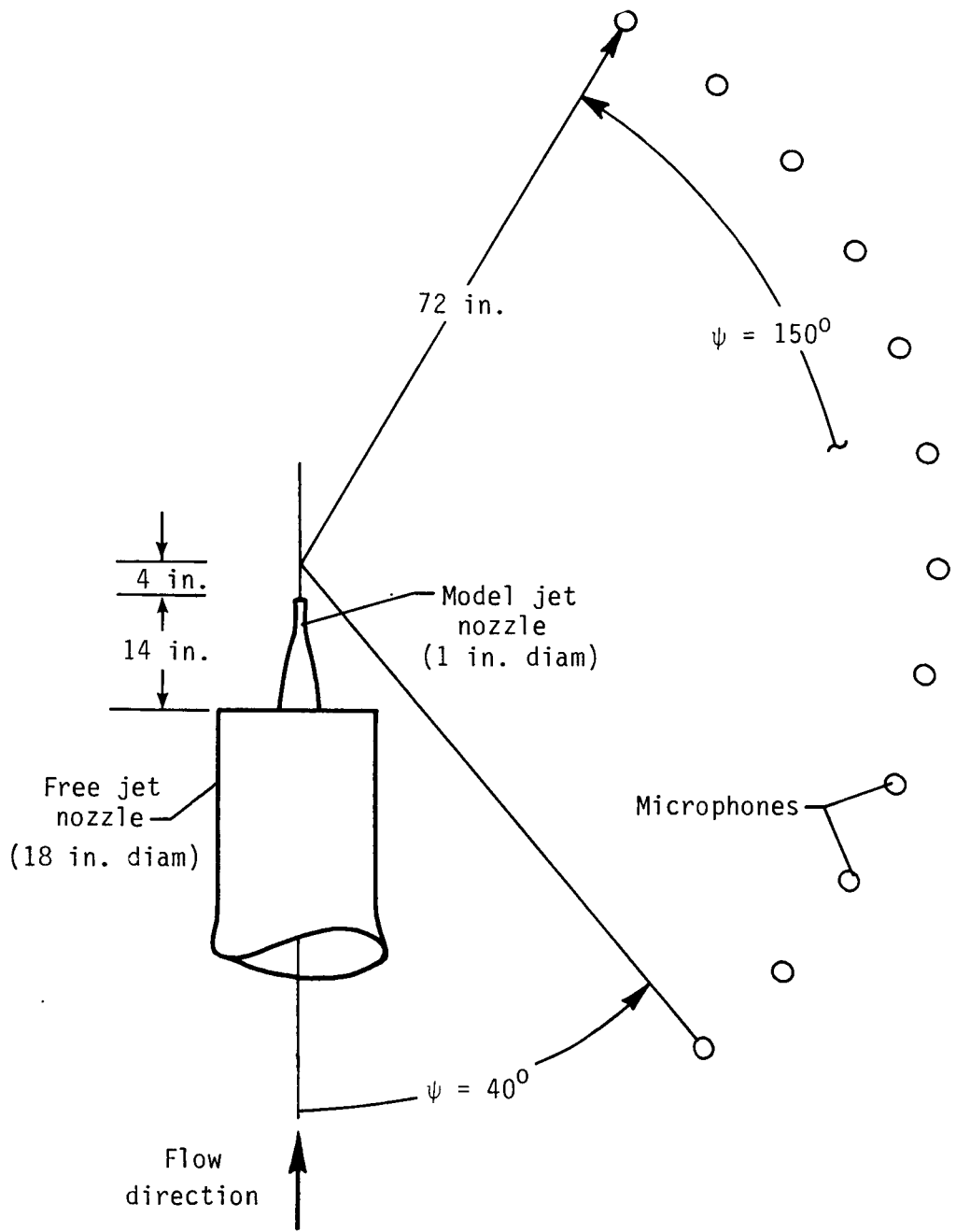


Figure 2. Microphone geometry for the acoustic experiments.

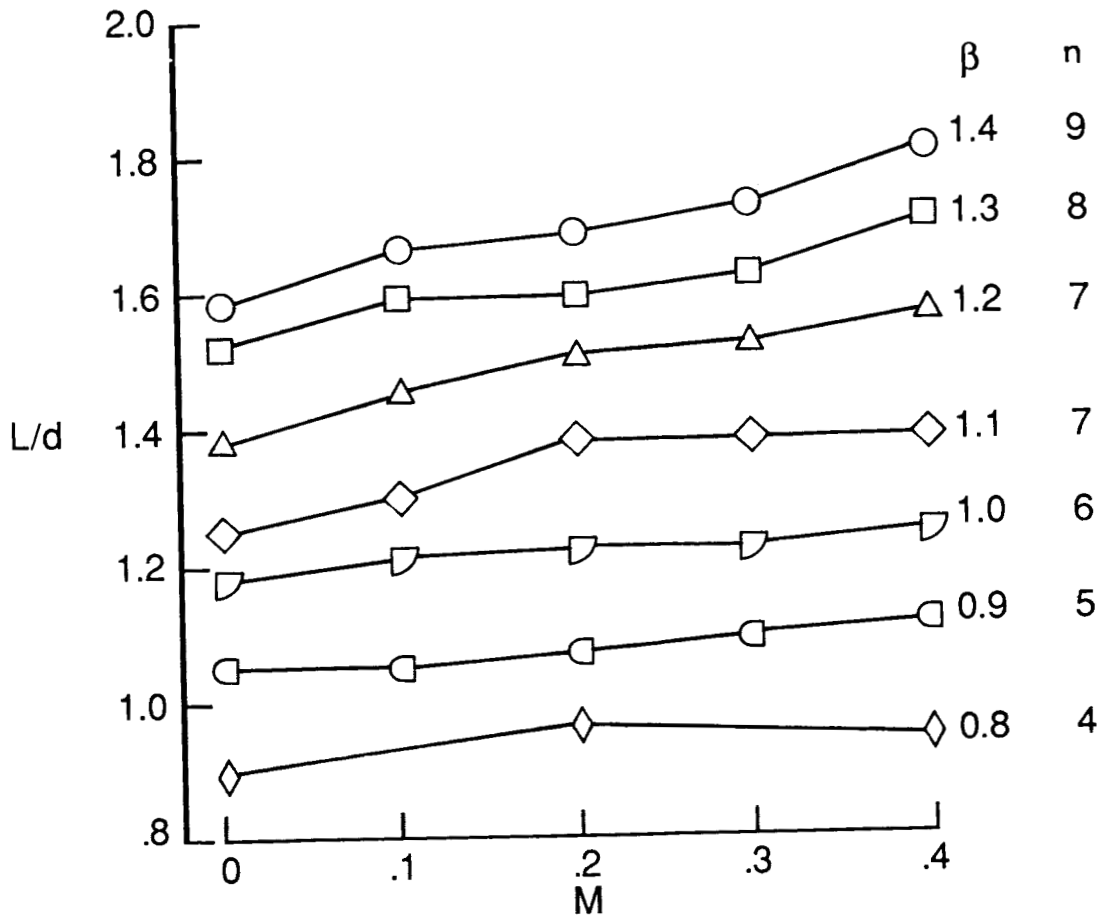


Figure 3. Variation of average shock cell spacing with flight Mach number.

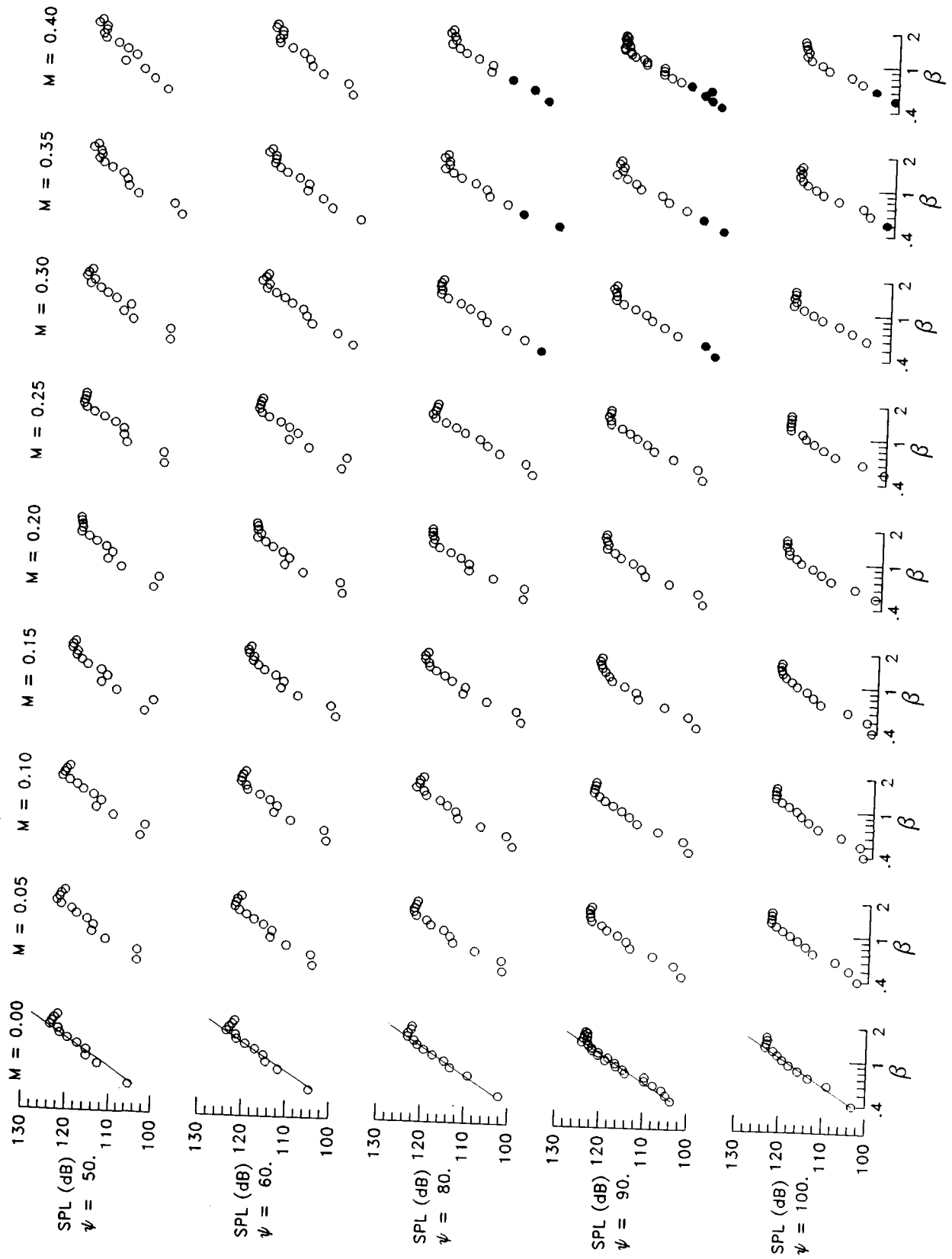


Figure 4. Variation of screech-removed overall sound pressure level with β . ψ is measured in degrees; filled symbols indicate contamination by background noise.

ORIGINAL PAGE IS
OF POOR QUALITY

ORIGINAL PAGE IS
OF POOR QUALITY

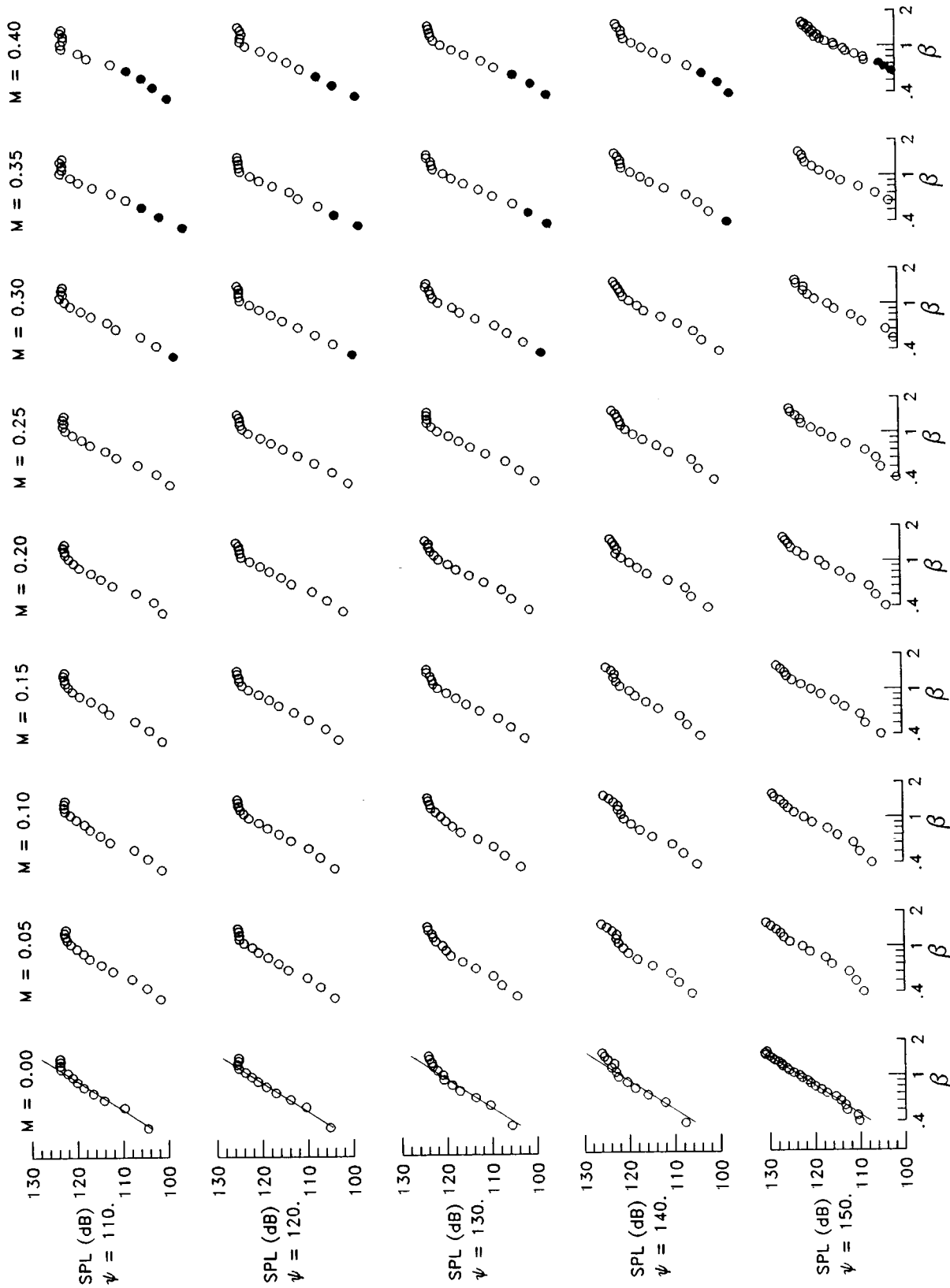


Figure 4. Concluded.

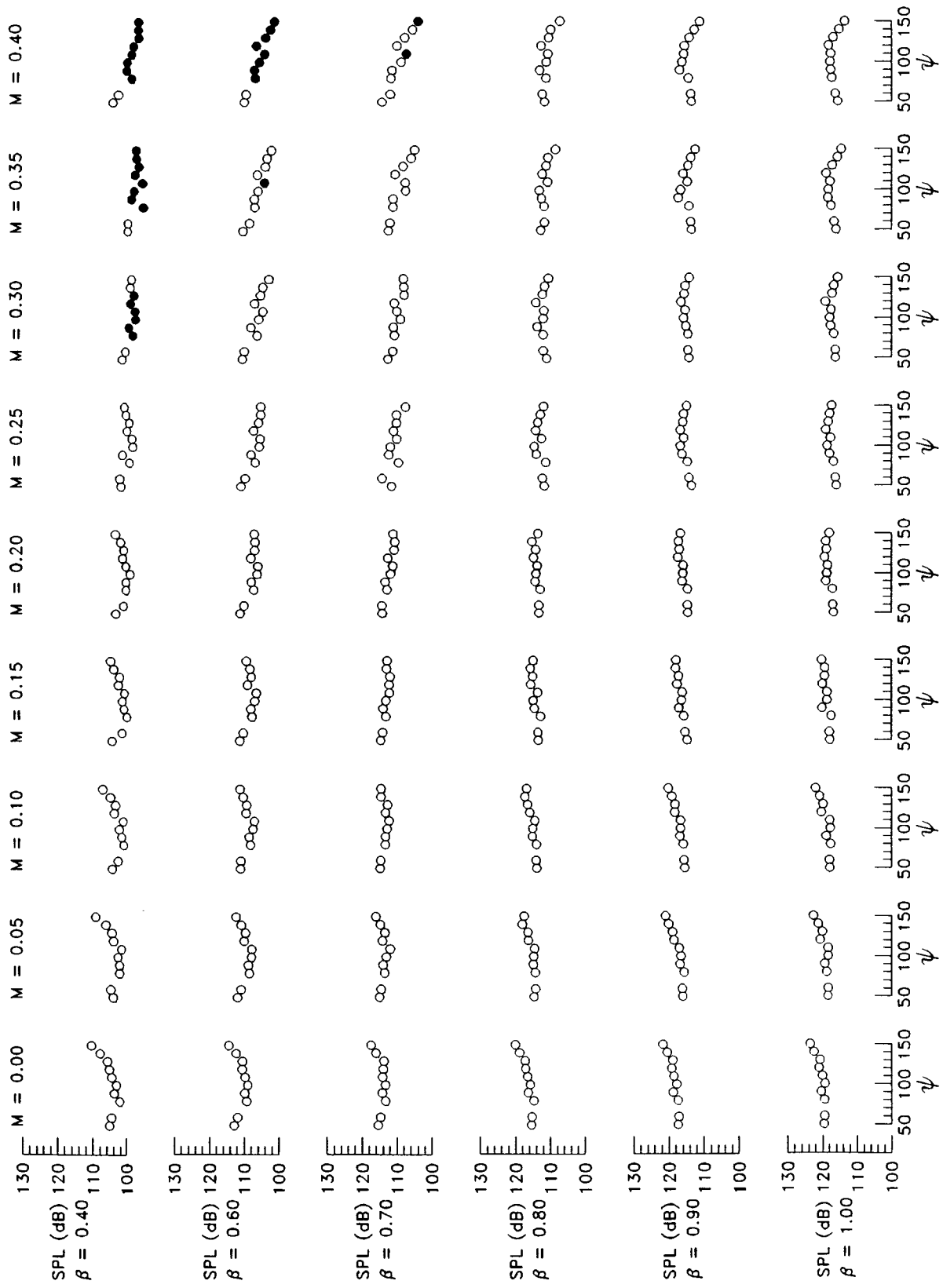


Figure 5. Variation of screech-removed overall sound pressure level with microphone angle. ψ is measured in degrees; filled symbols indicate contamination by background noise.

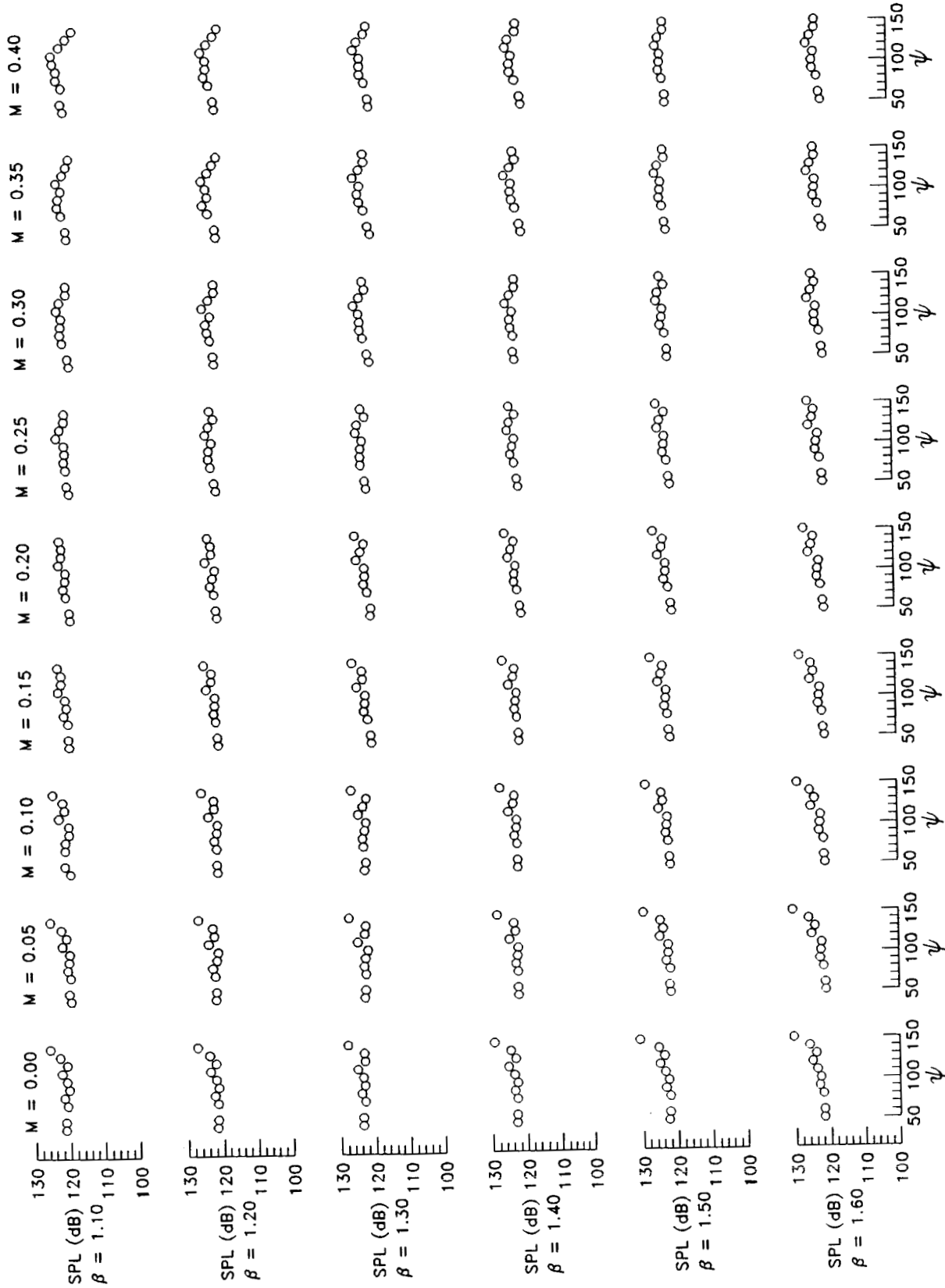


Figure 5. Concluded.

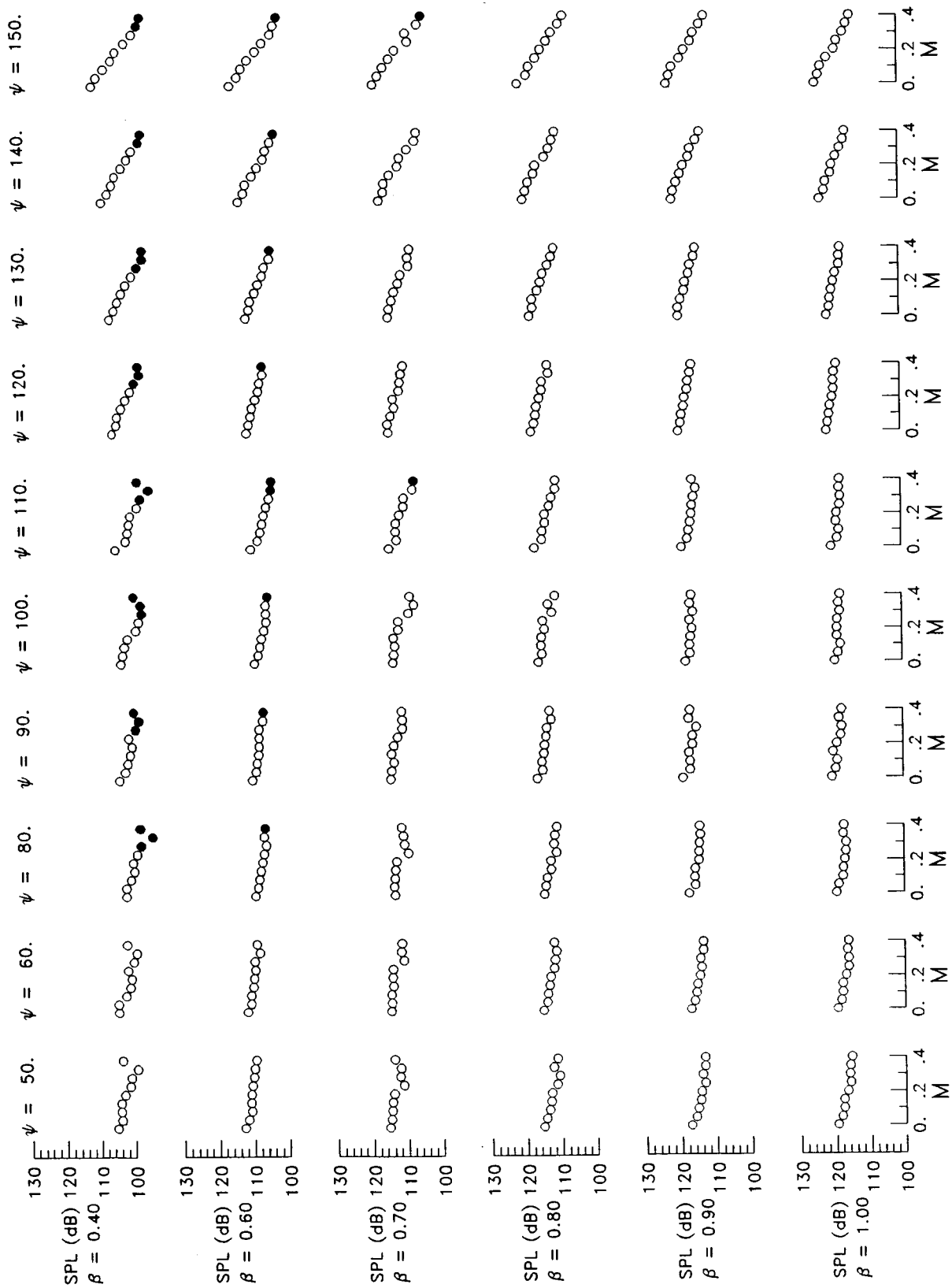


Figure 6. Variation of screech-removed overall sound pressure level with flight Mach number. ψ is measured in degrees; filled symbols indicate contamination by background noise.

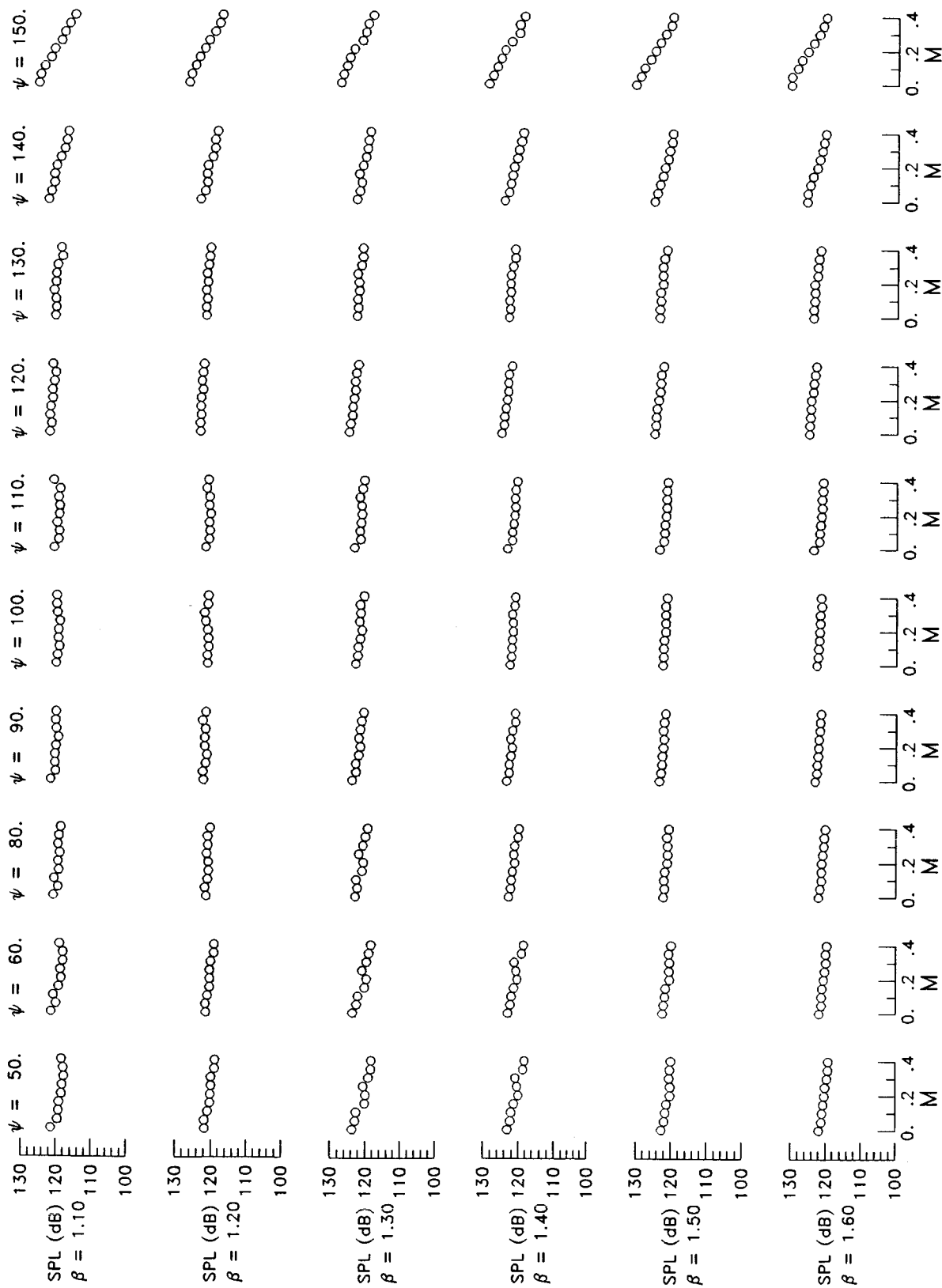
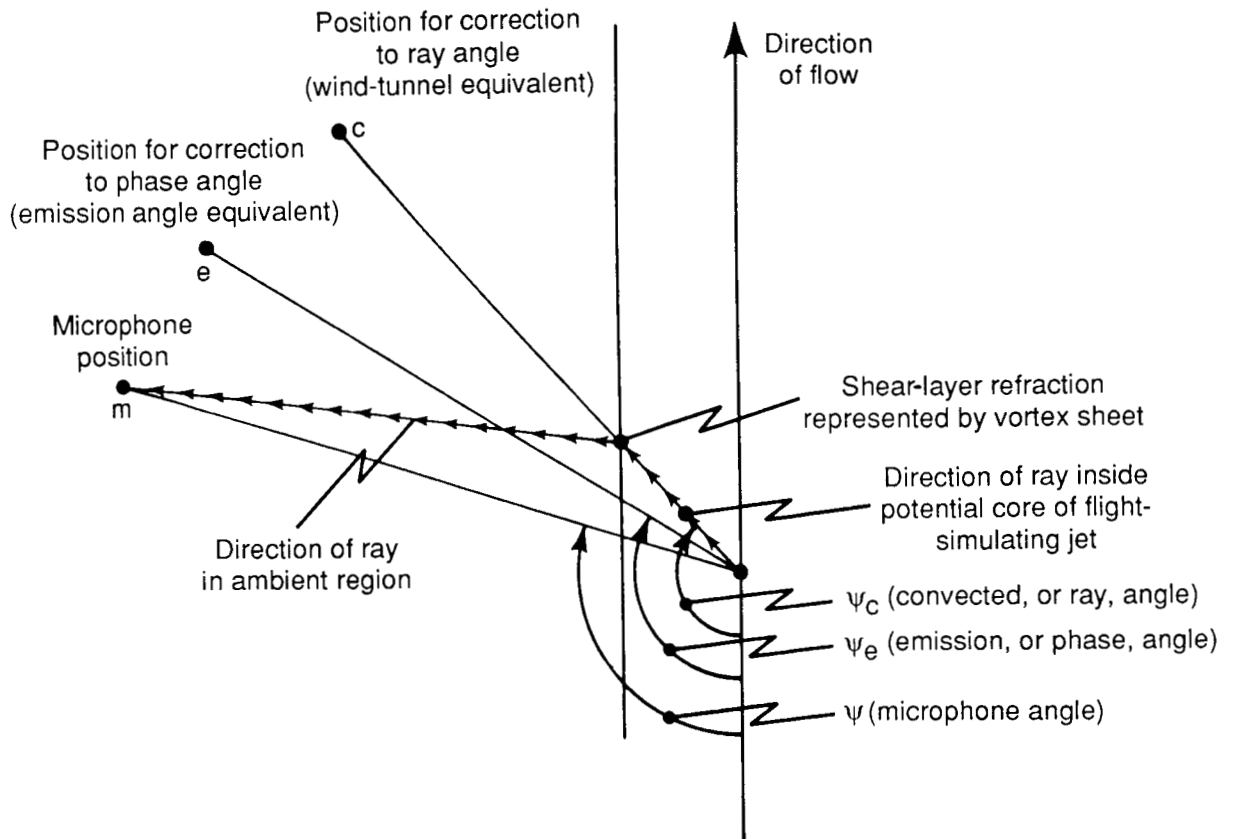


Figure 6. Concluded.



Velocity diagram inside flight-simulating jet

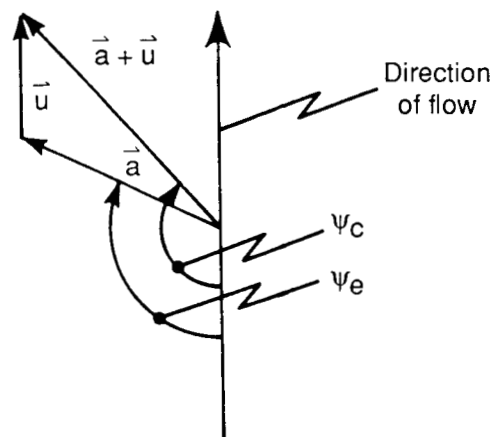


Figure 7. Schematic of the free jet shear layer refraction phenomenon.

ORIGINAL PAGE IS
OF POOR QUALITY

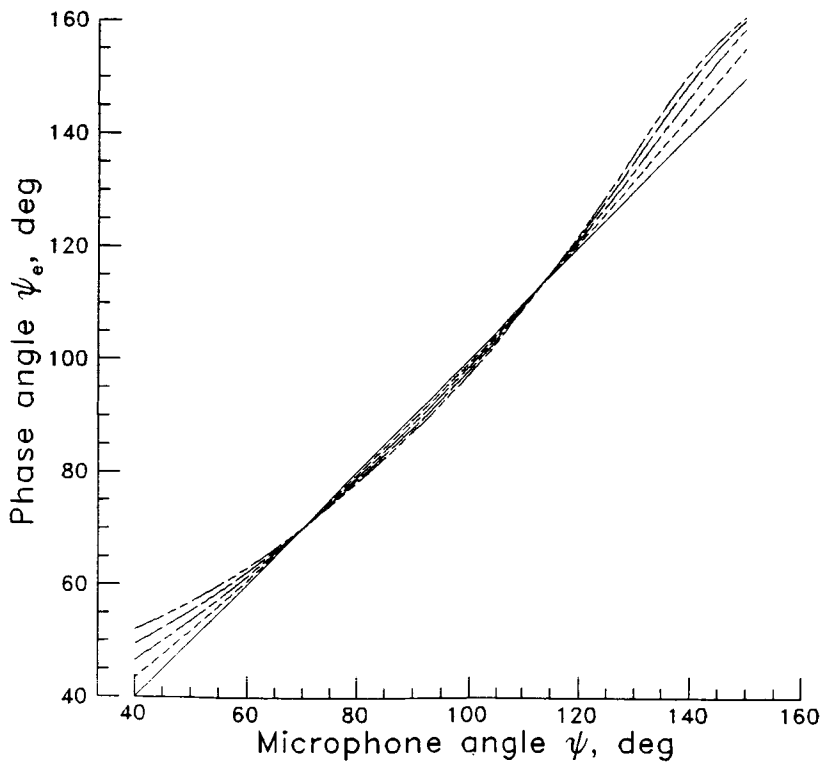
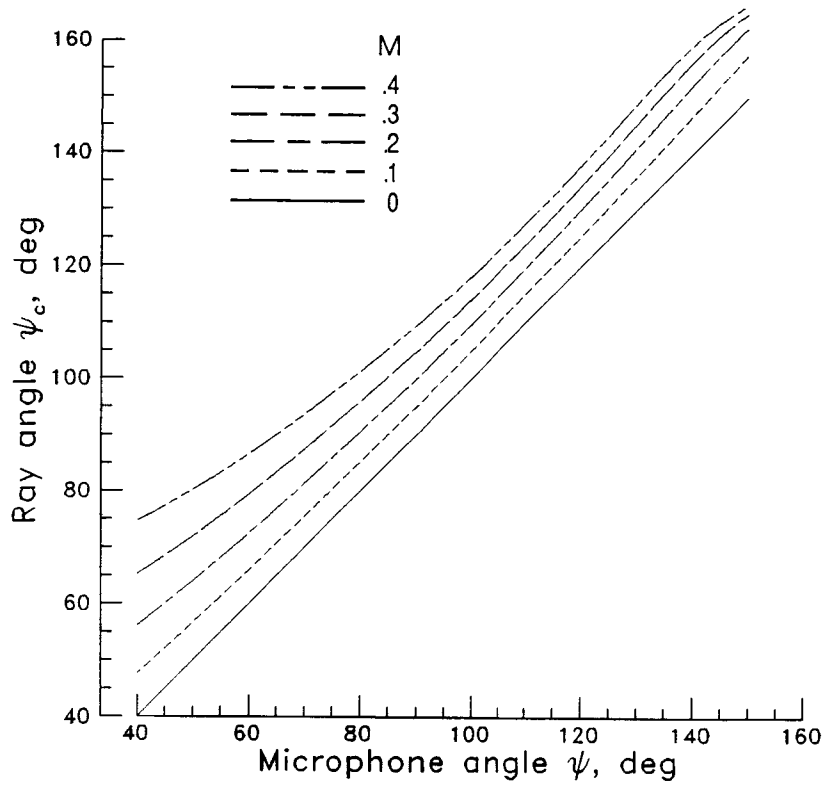


Figure 8. Variation of phase angle and ray angle with microphone angle.

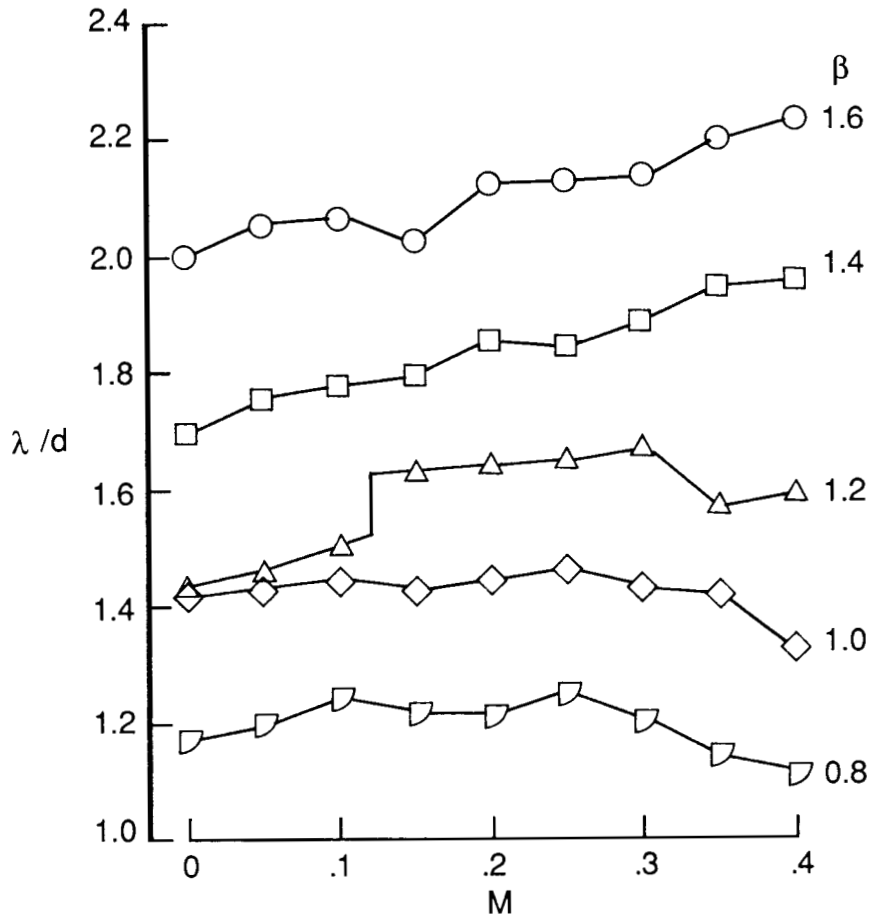


Figure 9. Variation of peak broadband shock noise wavelength at constant emission angle of 90° with flight Mach number.

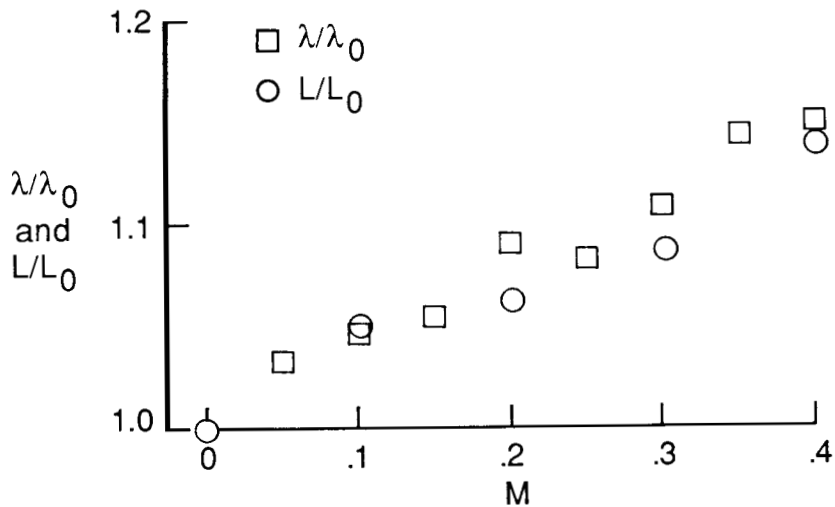


Figure 10. Correlation between broadband shock noise wavelength changes and average shock cell length changes with flight Mach number at $\beta = 1.4$.



Report Documentation Page

1. Report No. NASA TP-2785	2. Government Accession No.	3. Recipient's Catalog No.	
4. Title and Subtitle Shock Structure and Noise of Supersonic Jets in Simulated Flight to Mach 0.4		5. Report Date February 1988	
		6. Performing Organization Code	
7. Author(s) Thomas D. Norum and John G. Shearin		8. Performing Organization Report No. L-16341	
		10. Work Unit No. 505-61-11-01	
9. Performing Organization Name and Address NASA Langley Research Center Hampton, VA 23665-5225		11. Contract or Grant No.	
		13. Type of Report and Period Covered Technical Paper	
12. Sponsoring Agency Name and Address National Aeronautics and Space Administration Washington, DC 20546-0001		14. Sponsoring Agency Code	
		15. Supplementary Notes	
16. Abstract Measured jet plume static pressure distributions and far-field acoustic spectra are presented for underexpanded jets in simulated flight up to a Mach number of 0.4. A gradual stretching of the downstream shock cells is found as the Mach number increases, with no perceptible change in the shock strength. There appears to be little effect of flight on the amplitude of the broadband shock noise, and the small changes in its peak frequency for the same emission angle are correlated with the slightly longer shock cells in flight. The larger changes in the broadband peak frequency found at the same angle in wind-tunnel coordinates are attributable to convection. Jet mixing noise production decreases significantly with increasing flight speed.			
17. Key Words (Suggested by Authors(s)) Supersonic jet noise Jet plume pressure distributions Jet shock noise in flight		18. Distribution Statement Unclassified—Unlimited Subject Category 71	
19. Security Classif.(of this report) Unclassified	20. Security Classif.(of this page) Unclassified	21. No. of Pages 185	22. Price A09